Functional and structural studies of a C-terminally extended YidC

Dissertation zur Erlangung des Doktorgrades

der Naturwissenschaften (Dr. rer. nat.)

Fakultät Naturwissenschaften

Universität Hohenheim

Institut für Mikrobiologie

vorgelegt von

Ines Seitl

aus Esslingen a.N.

2015

Dekan:	Prof. Dr. Heinz Breer
1. berichtende Person:	Prof. Dr. Andreas Kuhn
2. berichtende Person:	Prof. Dr. Heinz Breer

Eingereicht am:	30.09.2015
Mündliche Prüfung am:	18.02.2016

Die vorliegende Arbeit wurde am 26.11.2015 von der Fakultät Naturwissenschaften der Universität Hohenheim als „Dissertation zur Erlangung des Doktorgrades der Naturwissenschaften“ angenommen.

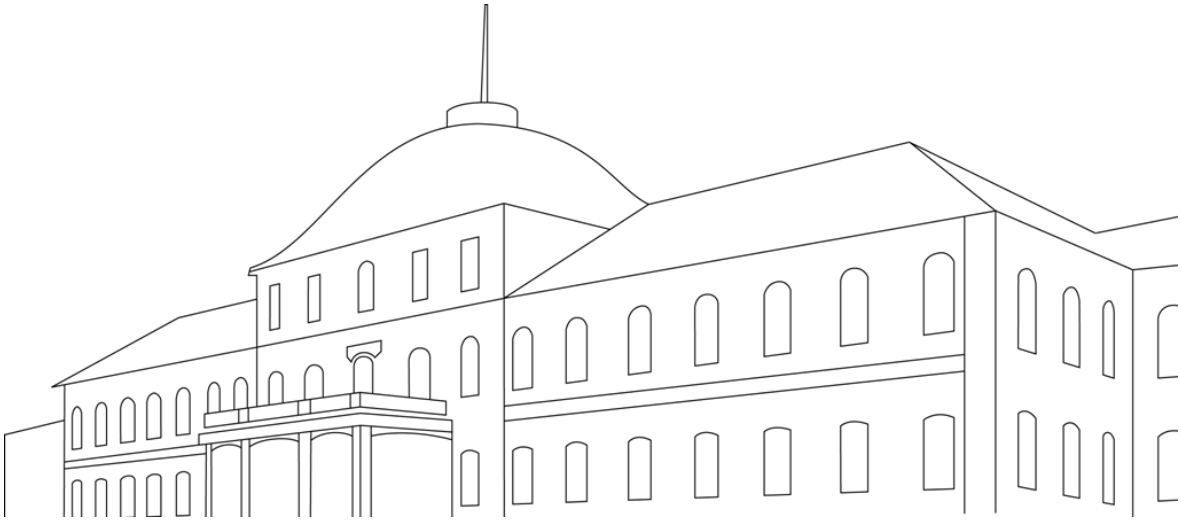

Parts of this thesis have been published in

Seitl I., Wickles S., Beckmann R., Kuhn A. and Kiefer D. (2014) The C-terminal regions of YidC from Rhodopirellula baltica and Oceanicaulis alexandrii bind to ribosomes and partially substitute for SRP receptor function in Escherichia coli. ***Mol Microbiol*** 91(2):408-421

Parts of this thesis have been presented at national and international conferences

Symposium Goethe University Frankfurt, 2010: Evolution of protein translocation systems Poster presentation *"The positively charged C-terminal extensions of marine YidC-homologs are crucial for interaction with E. coli ribosomes"*

Gordon Conference, Galveston USA 2012: Protein transport across cell membranes Poster presentation incl. young investigator talk *"Functional analysis of the C-terminal extensions of marine YidC homologs in the SRP-dependent membrane insertion"*

EMBO Conference, Dubrovnik 2013: From structure to function of translocation machines Poster presentation "*Characterization of the interaction between the C-terminal domain of a planctomycete YidC homolog and the bacterial ribosome*"

TABLE OF CONTENT

1 INTRODUCTION

1.1 The prokaryotic ribosome

In all living cells, proteins are constantly being rearranged and degraded, and a steady production of cellular proteins is therefore required. Hence, typical mammalian cells contain more than a million ribosomes and even bacterial cells contain ~ 100 000 ribosomes. Ribosomes are nanomachines which translate the genetic DNA-code into proteins. Prokaryotic ribosomes are constituted of two unequal subunits, the small ribosomal subunit 30S and the large 50S subunit, which assemble during the initiation step of protein biosynthesis to form the active 70S ribosome. The 30S subunit contains an RNA chain (16S rRNA) of about 1540 nucleotides decorated with 20-21 different proteins, whereas the large subunit has two RNA chains (23S and 5S rRNA) of about 2904 nt and 120 nt, respectively, packed with 31 different ribosomal proteins. In bacteria, ribosomes synthesize proteins on a continuous basis at an incredible speed of > 15 peptide bonds formed per second. Despite their size difference (prokaryotic: 70S, ~ 2.5 MDa; eukaryotic: 80S, ~ 4 MDa), ribosomes in all kingdoms of life are functionally conserved, with the highest level of sequence conservation appearing in the functional domains. The central core contains the ribosomal active site within a highly conserved symmetrical region in which 98 % of the nucleotides are found in > 95 % of sequences from 930 different species in all three domains of life (Agmon *et al*., 2006).

Due to the recent scientific and technical progress in elucidating ribosome biochemistry and performing macromolecular crystallography, complete atomic-resolution structures for both subunits of archaeal and bacterial ribosomes were solved in 2000 (Ban *et al*., 2000; Schluenzen *et al*., 2000; Wimberly *et al*., 2000). Finally, in 2001 the first structure of the complete 70S ribosome from *Thermus thermophilus* was published (Yusupov *et al*., 2001). High resolution structures from various ribosomes and ribosomal complexes, both in eukaryotic and prokaryotic, followed (Jenner *et al*., 2012; Demeshkina *et al*., 2012; Yusupova and Yusupov, 2014). A high-resolution structure of the *Escherichia coli* ribosome was solved this year and reveals unprecedented views of solvation as well as post-transcriptional and post-translational modifications of the ribosome in key functional and antibiotic-binding sites (Noeske *et al*., 2015). Recent reviews demonstrate the current understanding of the ribosomal function, based on the correlation between functional data and their high resolution crystal structures (Bashan and Yonath, 2008). Deep understanding of the ribosomal assembly process and its protein synthesis machinery

reveals detailed views also into antibiotic action as many of the clinically relevant antibiotics target the bacterial ribosome (Jenner *et al.*, 2013).

1.1.1 The duty cycle of the bacterial ribosome

This chapter highlights the ribosomes' roles in protein translation and summarizes what is known today about the biochemistry of eubacterial protein synthesis. Ribosomes comprise two ribonucleoprotein subunits, 30S and 50S, that associate to form the functional 70S ribosome. The small subunit contains the decoding center and mediates the base-pairing interactions between the codon triplets of the mRNAs (messenger RNAs) and the appropriate tRNAs (transfer RNAs) that determine the amino acid sequences of the originating proteins (Nirenberg, 1964). The large subunit includes the peptidyl transferase center (PTC) that catalyzes peptide bond formation (Monro, 1967) by transferring the C-terminal carboxylate group of a nascent polypeptide still bound to a tRNA to the α-amino group of an amino acid esterified to a second tRNA molecule. The site on the ribosome occupied by peptidyl tRNAs just before peptide bond transfer occurs is called the P site. The site occupied by aminoacyl tRNAs is called the A site (Monro *et al.*, 1969). The third major site is called E site through which deacylated tRNA molecules pass on their way out of the ribosome to get recycled and reloaded with amino acids (Rheinberger and Nierhaus, 1983). Hence, the protein synthesis cycle of ribosomes can be separated into three parts, the initiation, the elongation and the termination step (Fig. 1.1), whereupon several additional protein factors are required.

The initiation of protein synthesis begins with recruitment of ribosomal subunits from the cellular pool by the three initiation factors IF-1, IF-2 and IF-3 (Gualerzi and Pon, 1990), followed by the binding of an mRNA. The initiation phase ends with an aminoacylated initiator tRNA molecule (fMet tRNA) residing in the P-site of the ribosome, while the A-site is empty. The subsequent elongation step starts with an incoming tRNA complexed with elongation factor Tu (EF-Tu) which is delivered to the A-site driven by GTP hydrolysis: Peptide bond formation then occurs between the aminoacyl tRNA in the A-site and the adjacent peptidyl tRNA bound to the P-site. To reinitialize the ribosome during the so called translocation process that is facilitated by the elongation factor G (EF-G), the deacetylated tRNA in the P site first leaves the ribosome via the E site. This makes the peptidyl tRNA in the A site now move to the empty P site. Thus, the ribosome moves along its mRNA in the 3´direction by one codon so that the next aminoacyl tRNA can be delivered to the empty A site.

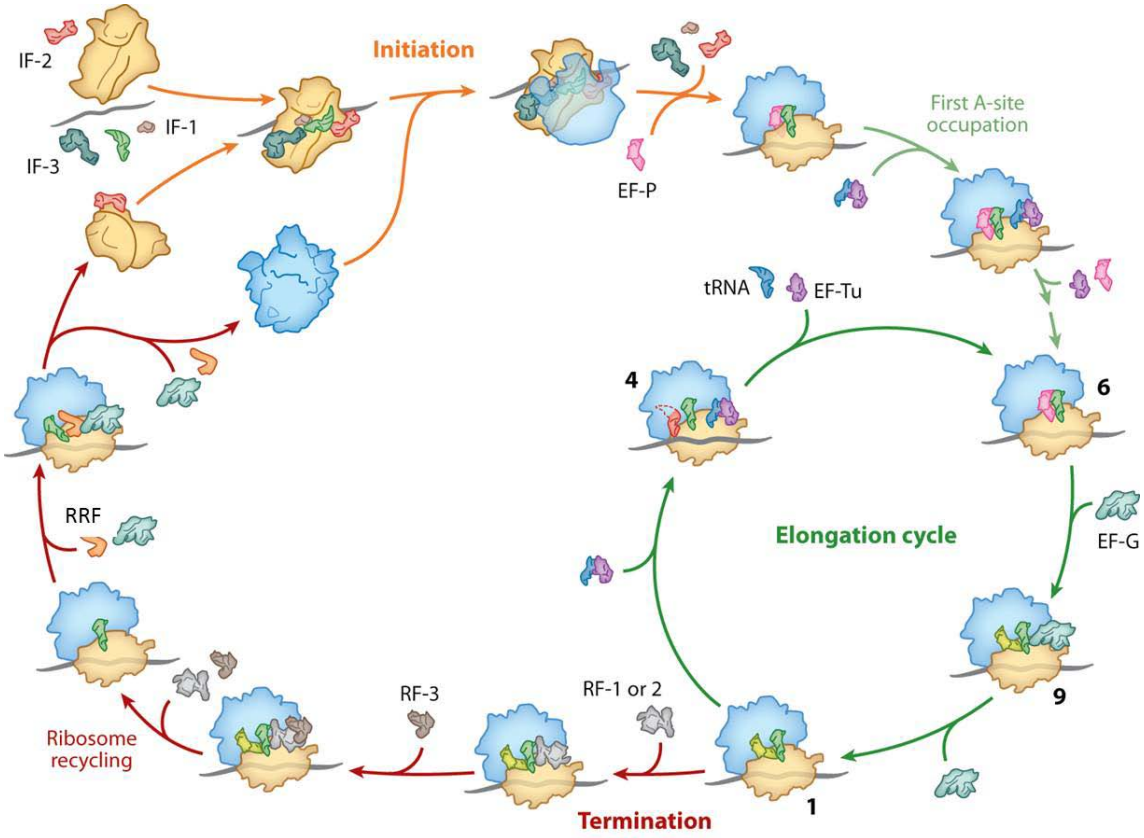

Fig. 1.1 ***The ribosomal protein synthesis cycle.*** *Initiation occurs by two ribosomal subunits being assembled at the start codon of an mRNA molecule together with a loaded tRNA molecule and three initiation factors (IF), and the first peptide bond is formed. The sequence of events that results in the addition of one amino acid residue to a growing peptide chain is called the elongation cycle, and is repeated several times depending on the protein size. When the translating ribosome encounters a stop codon, the nascent polypeptide is released from the ribosome and the two subunits return to the cellular pool, called termination and ribosome recycling. In vivo, the ribosome functions needs the assistance of several protein factors. The most important are elongation factor G (EF-G) and elongation factor Tu (EF-Tu). The small ribosomal subunit is shown in gold, and the large subunit in blue. tRNAs and protein factors are consistently color coded, and the shapes assigned to them resemble their 3-dimensional structures. Abbreviations: EF, elongation factor; IF, initiation factor; RF, release factor; RRF, ribosomal recycling factor (Moore, 2012).*

At the end of the elongation cycle when the stop codon (UAA, UAG or UGA) in the mRNA has been positioned into the A site, one of two release factors (RF1 or RF2) binds to the A site and promotes the deacylation of the last peptidyl tRNA. RF1 recognizes UAG and RF2 is specific for UGA, but both factors recognize UAA (Youngman *et al*., 2008). RF3 accelerates the dissociation of RF1 or RF2 from the ribosome. In order to prepare the ribosome for a new synthesis cycle, the ribosome recycling factor (RRF) binds together with EF-G to the ribosome and, driven by GTP hydrolysis, causes the release of the mRNA, removal of the deacylated tRNA from the P-site (Ramakrishnan, 2002) and the dissociation of the two ribosomal subunits (Karimi *et al*., 1999). However, the exact mechanism of factor-assisted elongation remains unclear since the observation was made

that ribosomes can elongate peptide chains in the absence of both EF-G and EF-TU (Pestka, 1968). Thus we still do not understand how the system uses the free energy released by the GTP hydrolysis that accompanies the process. Single-molecule experiments may provide the data needed to understand not only the details of the mechanism of elongation, but also its design philosophy (Moore, 2012).

1.1.2 The ribosomal exit tunnel: a flexible binding platform

Since its identification in the early 1980s by EM images of Unwin and co-workers (Milligan and Unwin, 1982), the polypeptide exit tunnel has been a subject of extensive study but also speculation concerning its function. The tunnel is located adjacent to the PTC in the large ribosomal subunit (Ban *et al.*, 2000; Harms *et al.,* 2001) and is surrounded mainly by rRNA and only a few ribosomal proteins. This tunnel has a length of 80 - 100 Å with a varying diameter of 10 – 20 Å (Fig. 1.2 B) and possesses the flexibility and dynamics required for interacting with the nascent protein progressing through the tunnel (Fedyukina and Cavagnero, 2011). The tunnel resembles a tube that is able to accommodate a peptide stretch of ~ 30 amino acid residues in extended or up to 40 amino acid residues in an α-helical conformation (Voss *et al*., 2006; Picking *et al*., 1992; Malkin and Rich, 1967). In bacteria, the tunnel wall is formed predominantly by 23S rRNA and looped-out segments of the ribosomal proteins L4, L22 and L23 (Fig. 1.2 C). At its distal end, the rim of the exit point at the large ribosomal subunit is composed of RNA, a ring of the four ubiquitously conserved ribosomal proteins L22, L23, L24 and L29 and additional kingdom-specific proteins (Kramer *et al.,* 2009).

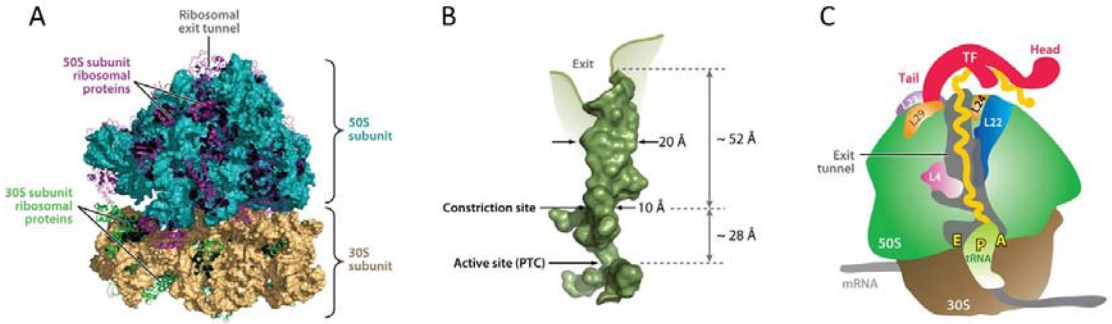

Fig. 1.2 ***The ribosomal environment for nascent polypeptides. (A)*** *Crystal structure of the E. coli ribosome at 3.5 Å resolution (PDB IDs: 2AVY and 2AW4). The ribosomal RNA of the 50S subunit (23S and 5S rRNA) are shown in turquoise and the 16S rRNA of the small subunit in beige. Ribosomal proteins are shown as ribbons (50S subunit proteins in purple, 30S subunit proteins in green).* ***(B)*** *Structure of the ribosomal exit tunnel (Voss et al., 2006). There is a constriction in the tunnel about 30 Å away from the PTC where loops of L4 and L22 come in close proximity. At the distal end, the ribosomal exit tunnel widens up.* ***(C)*** *Schematic representation of a vertical section of the prokaryotic ribosome, highlighting the ribosomal proteins facing or located near the exit tunnel. The ribosome-associated trigger factor (TF) is shown in pink (adapted from Fedyukina and Cavagnero, 2011).*

During protein biosynthesis, the nascent peptide chains on translating ribosomes are scanned by a number of additional proteins, called ribosome-associated protein biogenesis factors (RPBs), such as the chaperone trigger factor (TF), the signal recognition particle (SRP) and the processing enzymes peptide deformylase (PDF) and methionine aminopeptidase (MAP). These RPBs use six ribosomal proteins surrounding the tunnel exit as a confined binding platform of the bacterial 50S ribosomal subunit (Fig. 1.3). The bacterial enzyme peptide deformylase (PDF) is an essential protein that co-translationally removes the formyl group of nascent chains, a step required for subsequent action of the methionine aminopeptidase (MAP) to excise the N-terminal methionine residue (Fry and Lamborg, 1967; Pine, 1969; Adams, 1968). *E. coli* PDF binds to a groove between ribosomal proteins L22 and L32, located next to the exit tunnel, thus positioning the active site for interaction with the emerging nascent polypeptides (Bingel-Erlenmeyer *et al*., 2008), adjacent to the trigger factor binding site (Kramer *et al*. 2002). The ribosomal protein L17 was identified as the major interaction partner of MAP (Sandikci *et al*., 2013).

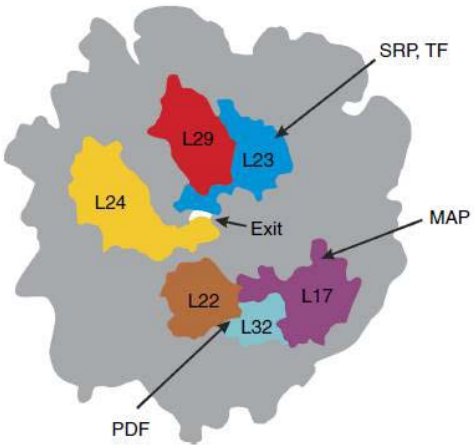

Fig. 1.3 ***Flexible binding platform at the ribosomal exit tunnel.*** *The ribosomal proteins L23, L24 and L29 surround the tunnel exit and provide binding sites for diverse factors, involved in co-translational processing, folding, targeting and insertion of the nascent peptide chain. L23 is the main contact site for both SRP and TF, offering the possibility to influence the binding affinity of each other. Binding of MAP to L17 does not compete with TF or SRP, but strongly competes with PDF binding to a groove between L22 and L32. Grey outline: 50S subunit (Bornemann et al., 2014).*

The ribosome-associated signal recognition particle (SRP) is involved in co-translational targeting of nascent inner membrane proteins to the protein-conducting channel (translocon) in the bacterial plasma membrane (Luirink *et al*., 2005; Bibi, 2011; Grudnik *et al*., 2009), whereas nascent cytoplasmic, periplasmic and outer membrane proteins interact with the chaperon trigger factor (TF), which transiently associates with the large ribosomal subunit (Oh *et al*., 2011). Trigger factor forms an arch above the tunnel (Fig. 1.2 C) and thus protects the nascent chain from misfolding and aggregation. It also assists early folding events (Agashe *et al*., 2004; Hoffmann *et al*., 2012; Deuerling *et al*., 1999; Teter *et al*., 1999; Kramer *et al*., 2002). Later folding steps often are supported by the

DnaK and GroEL chaperon systems that act independently of the ribosome. SRP and TF both bind to the ribosomal protein L23 (Ferbitz *et al*., 2004; Kramer *et al*., 2002; Merz *et al*., 2008; Gu *et al*., 2003; Halic *et al*., 2004) at the peptide exit site (Fig. 1.3). This concurrent binding is accompanied by rearrangements of the complex (Buskiewicz *et al*., 2004; Ullers et al., 2003). Qualitative and quantitative analyses indicate concurrent binding also of TF and PDF or SRP and PDF to ribosomes (Bornemann *et al*., 2014; Sandikci *et al*., 2013), indicating non-competitive binding. Based on these observations a working model was generated for the co-translational processes at the tunnel exit of ribosomes (Fig. 1.4). Fast ribosome binding kinetics facilitates early ribosomal recruitment of SRP at nascent chain lengths of about 30 amino acid residues (Holtkamp *et al.,* 2012; Bornemann *et al*., 2008). The complex is further stabilized by the emergence of a signal anchor sequence, which finally results in SRP receptor recruitment and targeting the translating ribosomal complex to the translocon. Since SRP does not exclude PDF binding, it is assumed that deformylation of the initiator f-met methionine residue and co-translational targeting can occur simultaneously which is consistent with the almost complete absence of native formylated proteins in *E. coli* (Solbiati *et al*., 1999; Milligan and Koshland, 1990). However, around 5 % of the complete proteome stay formylated. Interestingly, nearly all the formylated proteins are proteins of the inner membrane or proteins involved in protein synthesis and early co-translational events (Bienvenut *et al*., 2015). It was suggested that the charge of the N-terminus could have influence on the transmembrane topology of some specific proteins (von Heijne, 1989). In this context, the retention of the N-formyl group changes the protein N-terminus charge and might favor transmembrane inclusion. In mitochondria for example, it was shown that COX1 requires an N-terminal formyl methionine for the assembly of cytochrome c oxidase (Hinttala *et al*., 2015). However, the vast majority of SRP substrates are deformylated, but retain the N-terminal methionine and therefore do not require MAP-mediated processing (Huber *et al*., 2005). For all other nascent chains, the fast ribosome interaction kinetics of PDF and MAP ensure that N-terminal methionine excision (NME) is completed before trigger factor is recruited to translating ribosomes with much slower kinetics (Rutkowska *et al*., 2008) and only after 100 residues on average have been synthesized on the growing peptide (Fig. 1.4; Oh *et al*., 2011).

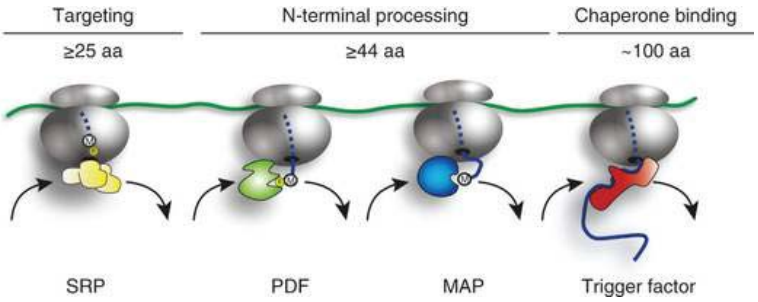

Fig. 1.4 ***Dynamic enzyme docking at the ribosomal exit tunnel.*** *SRP contacts the ribosome while the growing peptide is still buried in the ribosomal tunnel (~ 25-30 aa). Once the nascent chain emerges, its N-terminus is deformylated by the ribosome-bound PDF. Then MAP binds at a site overlapping the PDF binding position to excise the methionine of the polypeptide chain. Both co-translational processing procedures are completed once the nascent chains have reached a length of ~ 44-48 residues and trigger factor is recruited as a chaperone to the translating ribosome when the nascent chain has reached an average length of approx. 100 residues (Sandikci et al., 2013).*

Recent studies propose that during the interplay of TF and SRP, concurrent binding of both factors to RNCs presenting the respective specific nascent chain for a SRP-dependent or TF-dependent protein leads to weakening of the binding of the respective other ligand. This partial competitive binding behavior of TF and SRP increases therefore the specificity of the small amount of SRP present in the cell in promoting co-translational membrane targeting of those RNCs that synthesize membrane proteins (Bornemann *et al*., 2014).

In addition to the early processes of RPBs binding, the proteins building the tunnel rim constitute major interaction sites for various factors involved in nascent chain folding, targeting and insertion. Interestingly one of them, the ribosomal protein L23, is involved in almost all interactions of the ribosome with ribosome-associated factors investigated so far, including the translocon SecYEG (Mitra *et al*., 2005; Frauenfeld *et al*., 2011) as well as the soluble ATPase SecA (Singh *et al*., 2014). SecA mediates translocation of periplasmic and outer membrane proteins and channels newly synthesized polypeptides into the post-translational Sec-translocation pathway (Huber *et al*., 2011; Driessen and Nouwen, 2008). A specific interaction with L23 was also described for the insertases Oxa1 in mitochondria (Jia *et al*., 2003) and the bacterial YidC (Kohler *et al*., 2009; Seitl *et al*., 2014) as well as for the targeting factor SRP (Schaffitzel *et al*., 2006) and the chaperone trigger factor (Ferbitz *et al*., 2004; Kramer *et al*., 2002). It is known that ribosomes can transmit information about the presence of a nascent chain from their interior to the surface, to control the interaction for example with SRP. In *E. coli*, SRP shows a 100-fold increased affinity for translating ribosomes (Bornemann *et al*., 2008), whereupon the signal transfer from the inside of the tunnel to the ribosomal surface occurs via a loop structure in L23 that reaches into the exit tunnel (Kramer *et al*., 2009). Thus, L23 seems to

constitute a general docking platform for various factors that transiently associate with ribosomes to act on nascent chains and could be used for the coordination of these factors in time and space. This even holds for the homologous ribosomal proteins and the ribosome-associated chaperone counterparts in yeast and mammals (Preissler and Deuerling, 2012).

1.1.3 Ribosome nascent chain complexes

Protein synthesis proceeds at variable rates and with different velocities depending on environments and organisms (Zhang and Ignatova, 2010). Since translation rates are faster in prokaryotes (15 – 20 aa / sec) than in eukaryotes (3 – 4 aa / sec) the recombinant expression of eukaryotic proteins in *E. coli* often does not work proper, indicated by misfolding of the recombinantly expressed heterologous protein. An average timescale for the production of a small or medium sized protein in prokaryotes of ~ 10 s is similar to chaperone binding/release times and longer than folding/unfolding timescales of small proteins (Fedyukina and Cavagnero, 2011) suggesting that nascent chains encoding only small proteins may have sufficient time to adopt the proper conformation during synthesis. In contrast, large proteins take much longer and need multiple folding-unfolding rounds to fold properly. In addition, the co-translational folding in *E. coli* seems to be highly protein- and codon-dependent. Rare codon clusters (Clarke and Clark, 2008) seem to be an important feature for an orchestrated translational pausing in order to facilitate co-translational domain folding before synthesis of the following domain is initiated (Zhang *et al*., 2009). For instance, mutant ribosomes displaying slower translation than wild-type *E. coli* ribosomes enhance the production of active mutli-domain proteins of eukaryotic origin in bacteria (Siller *et al.,* 2010).

Characterizing the nature and properties of RNCs exhibits a significant challenge structural and cellular biology experiments. One strategy for defining the structural and dynamic properties of a nascent chain during co-translational folding and targeting up to its interaction with translocons or insertases is the generation of translation arrested RNCs, resulting in the nascent peptide chain being retained on the ribosome. Several nascent peptides stall ribosomes using specific leader peptides during their own translation in both prokaryotes and eukaryotes and can regulate downstream gene expression. Two well characterized leader peptides from *E. coli* cause ribosome stalling and increase the expression of a gene further downstream on the same mRNA. SecM, for example acts as a secretion monitor peptide that regulates *secA* in response to changes in protein translocation activity (Oliver *et al*., 1998). The 17 residues long SecM arrest peptide corresponds to the intrinsic class of stalling sequences which stalls without any

inducing molecule until the arrest is released as the nascent chain interacts with specific cellular machineries, in this particular case with the Sec translocon. SecM-stalled ribosomes can be rescued by mechanical force generated by the translocon (Goldman *et al*., 2015). On the other hand, the 24 residues long TnaC leader peptide corresponds to the inducible class of arresting peptides that only stalls in the presence of a specific effector, such as an antibiotic or a metabolite (Ito *et al*., 2010). TnaC is the regulatory peptide of the tryptophanase *tnaCAB* operon in *E. coli* (Gong and Yanofsky, 2002) using a feedback loop requiring the small molecule L-tryptophan (L-Trp). The respective DNA sequence is localized on the *E. coli* chromosome upstream of the L-Trp catabolizing tryptophanase (TnaA) gene and the tryptophan-specific permease (TnaB) gene. In the presence of inducing levels of free L-Trp, peptide release by RF2 is inhibited (Gong and Yanofsky, 2001) and the ribosome stalls on the TnaC mRNA carrying the Tna leader peptide. As a consequence, the transcription termination factor Rho is blocked from binding to the mRNA region between *tnaC* and *tnaA* and, thus, allows the transcription and subsequent translation of TnaB and TnaA (Gong and Yanofsky, 2002) (Fig. 1.5 A). A previous cryo-EM structure of a TnaC-stalled ribosome complex demonstrated that TnaC stalls the ribosome with a peptidyl-tRNA remaining in the ribosomal P-site. The nascent peptide adopts a defined conformation within the ribosomal exit tunnel, and close contacts between TnaC and components of the tunnel wall were identified (Seidelt *et al*., 2009). A highly resolved cryo-EM structure (Fig. 1.5 B) revealed the formation of two composite binding pockets by the nascent chain and the tunnel wall (Fig. 1.5 C), turning the translating ribosome into an efficient sensor for L-Trp (Bischoff *et al*., 2014-2).

The observation that only the sequence of the stalling peptide (e.g. for SecM: 17 aa of the 170 residues full length protein) is necessary for proper ribosome stalling, unrelated of downstream sequences (Nakatogawa and Ito, 2002), offers new possibilities to analyze the interaction of substrate-specific RNCs with factors involved in folding, targeting and translocation or insertion of the nascent protein. The SecM and TnaC approaches are preferentially used when RNCs are generated *in vivo* and purified by affinity chromatography (Bischoff *et al*., 2014-1).

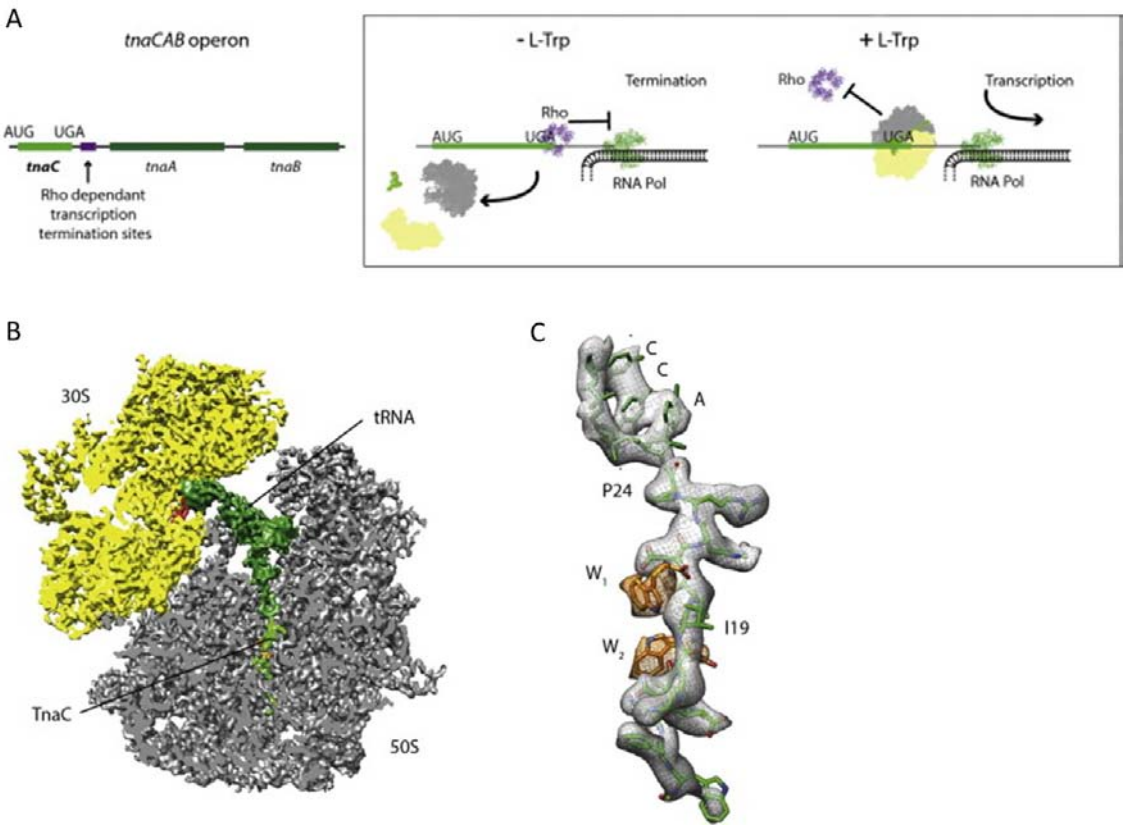

Fig. 1.5 ***Cryo-EM structure of a TnaC-stalled ribosome nascent chain complex. (A)*** *Model for TnaCAB operon regulation in E. coli. In the absence of L-Trp the TnaC translation reaches the stop codon UGA, RF2 promotes termination and the ribosome dissociates. Therefore, Rho can bind to its transcription termination site, prior to synthesis of the tnaAB mRNA. If free L-Trp is present, it interacts with two binding pockets in the nascent chain and in the tunnel wall and thus prevents peptide release by RF2. Rho binding is blocked and transcription of tnaAB occurs.* ***(B)****Cross-section through the cryo-EM density of the TnaC-RNC. Displaying the 30S (yellow) and 50S (grey) subunit of the E. coli ribosome, carrying a tRNA in the P-site (dark green) and the nascent chain (light green) with free tryptophan molecules (orange) in the ribosomal exit tunnel.* ***(C)*** *Directly within the ribosomal tunnel, 15-20 Å from the PTC, a density for two free L-Trp molecules (W1 and W2) was observed. (Adapted from Bischoff et al., 2014-2)*

Taken together, the understanding of the stalling mechanism of RNCs in *E. coli* and new methods for their synthesis and purification provided the visualization of RNCs in complex with SRP/FtsY (von Loeffelholz *et al*., 2015), SecA (Singh *et al*., 2014), SecYEG (Frauenfeld *et al*., 2011; Bischoff et al., 2014-1) and YidC (Kohler *et al*., 2009; Seitl *et al*., 2014; Wickles *et al*., 2014) by cryo-EM reconstruction and brought new insights into the mechanism of co-translational protein biogenesis.

1.2 Protein targeting in bacteria

The proper biogenesis and homeostasis of proteins are essential to all living cells and require the correct folding, localization, maturation, and quality control of all newly synthesized proteins (Hartl *et al*., 2011; Powers *et al*., 2009). As described in the previous chapter, the mechanisms that ensure proper protein homeostasis already begin at the ribosome, where a variety of proteins meet and compete for access to nascent polypeptides. A new era in cell biology was spawned in the 1970s by Günter Blobel`s "signal hypothesis" proposing that newly synthesized proteins carry intrinsic signals, the so called signal sequences, that encode information about their cellular localization (Blobel and Sabatini, 1971; Blobel, 1980). In the subsequent years, the signal sequences and respective targeting factors were identified and characterized for various organelles particularly those mediating the delivery of proteins to the membranes of the endoplasmic reticulum (ER), nucleus, mitochondria and chloroplasts (Dalbey and von Heijne, 2002). Bacterial cells also contain distinct compartments and specified sites to which newly synthesized proteins must be correctly transported and located, including the inner and outer membranes as well as the periplasmic and the extracellular space. The major protein trafficking route involves the transport of newly synthesized membrane and secretory proteins from the cytosol to the plasma membrane and multiple pathways have evolved for the delivery and sorting of these proteins (Fekkes and Driessen, 1999; Cross *et al*., 2009).

Protein targeting in bacteria can be divided into two major routes (Fig. 1.6): (a) post-translational delivery after the complete synthesis and release of the protein from the ribosome prior to targeting; (b) the co-translational pathway, in which the targeting and translocation is coupled to the ongoing synthesis by RNCs. In contrast to higher eukaryotes, where the co-translational delivery is the major pathway for secretory proteins, most secretory proteins in bacteria are post-translationally targeted to the plasma membrane. This is, presumably due to most efficiently utilizing the limited number of SecYEG translocation channels, a major translocon in the bacterial inner membrane, since the rate of protein synthesis might be higher than the delivery step (Hegde and Bernstein, 2006). During post-translational delivery, the primary challenge is to keep polypeptides in a translocation-competent state that can be transported into or across the target membrane. Hence, a major function of post-translational delivery factors is to bind the hydrophobic regions of the substrate polypeptide to inhibit misfolding, aggregation and inappropriate interaction with other cytosolic proteins. This task is fulfilled by several molecular chaperones that mostly depend on ATP hydrolysis. For both, the post- and the

co-translational pathway, a cycling mode of action is characteristic for most cellular factors. They can be distinguished by either using regulatory ATP binding components, such as SecA (Fig. 1.6 a) or alternatively by using the highly conserved GTPases of the SRP cycle (Fig. 1.6 b).

The homotetrameric SecB chaperone binds with high affinity to nascent secretory precursor proteins with a typical N-terminal cleavable signal sequence (Baars *et al*., 2006), whereas the export sequence is not bound directly but its presence might extend the time frame for interaction with SecB (Hardy and Randall, 1991). SecB captures and keeps the secretory proteins in a translocation-competent state and mediates the post-translational targeting to the translocation ATPase SecA. SecA tightly associates with the membrane-embedded SecYEG translocon and pushes unfolded substrate protein across it using ATP-driven highly dynamic conformational changes (Fig. 1.6 a) (Cabelli *et al*., 1988; Gold *et al*., 2013; Denks *et al*., 2014). Recent structural analysis of SecA bound to the SecYEG complex reveals the two helix finger domain (Zimmer *et al*., 2008) driving the substrate through the SecYEG translocation channel by acting as a translocation piston to push the substrate into the periplasmic space (Erlandson *et al*., 2008). Several reports suggest that a distinct cytosolic pool of SecA can also associate with ribosomes and with the nascent signal sequence of secretory proteins, raising the intriguing possibility that post-translational targeting machineries could also exert some of their actions co-translationally (Eisner *et al*., 2003; Karamyshev and Johnson, 2005; Huber *et al*., 2011). Other general chaperones, such as the trigger factor (TF), GroEL or DnaK, may also be involved in maintaining the nascent polypeptides in a translocation-competent unfolded state (Hoffmann *et al*., 2012).

In an alternative targeting route to the post-translation delivery, a subset of bacterial secretory proteins are translocated in a tightly folded state, in particular cofactor-containing membrane-located redox enzymes (Sargent F., 2007). Substrates for this pathway exhibits a characteristic twin arginine motif in their signal sequences and are translocated via the Tat (twin Arg translocation) complex, a translocon composed of the TatA, TatB and TatC subunits (Palmer and Berks, 2012). The DnaK and DnaJ proteins are cytosolic molecular chaperones of the Hsp70 family that carry important roles in general protein folding and assembly (Genevaux *et al*., 2007). Despite its role in the export of some SecB-independent substrates (Wild *et al*., 1992; Qi *et al*., 2002), DnaK might also play a role in the Tat-pathway. DnaK probably interacts with Tat substrates and promotes their export by sheltering the signal sequence from premature engagement with the TatABC translocon (Graubner *et al*., 2007; Perez-Rodriguez *et al*., 2007).

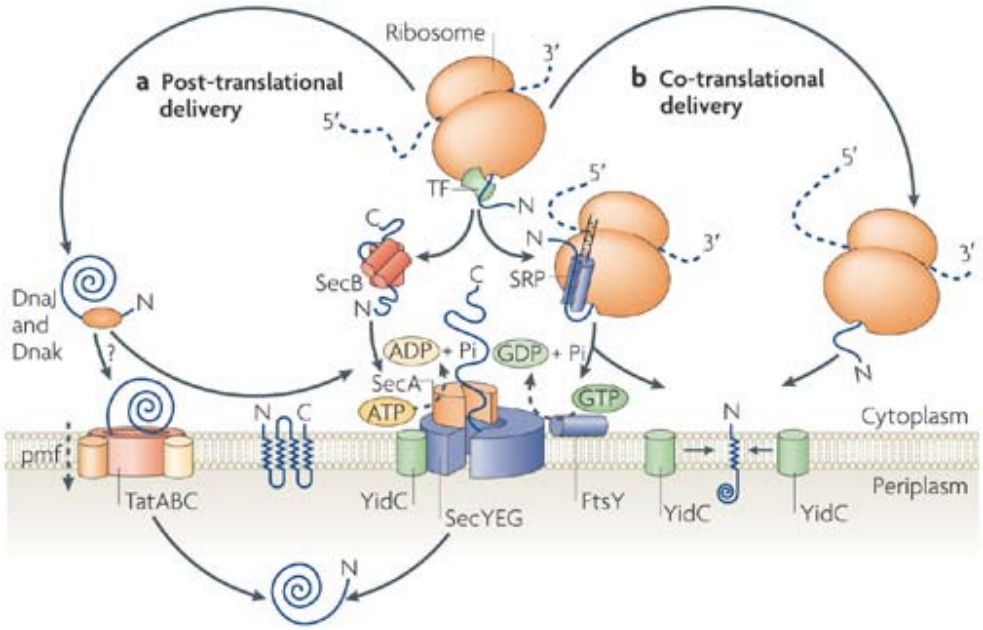

Fig. 1.6 ***Protein targeting and export pathways in prokaryotes.*** *Depending on the specific protein and its final destination, the delivery of proteins from the cytosol to the membrane occurs through distinct routes.* ***(a)*** *Post-translational delivery of secretory proteins is mainly mediated by SecB and driven by ATP hydrolysis cycles of SecA into the translocon, which comprises the conserved SecYEG channel together with YidC. YidC is an essential insertase required for the membrane insertion and assembly of a subset of integral inner membrane proteins. The TatABC translocon in cooperation with the chaperones DnaJ and DnaK mediates the export of folded proteins containing a twin arginine motif in their signal sequence.* ***(b)*** *The co-translational targeting to SecYEG occurs via SRP and its receptor FtsY in a GTP-dependent manner. For YidC, acting here as an independent insertase without SecYEG, the targeting might occur either following SRP-mediated delivery or through direct binding of the ribosome to YidC. (Cross et al., 2009)*

An alternative strategy to maintain the translocation competence of proteins destined for export, instead of using chaperones, is to intimately couple protein synthesis to membrane translocation by delivering the nascent polypeptide on the ribosome to the membrane during translation. This co-translational delivery strategy (Fig. 1.6 b) also prevents the potential and fatal exposure of multiple hydrophobic transmembrane segments of integral membrane proteins to the aqueous cytosolic environment and ensures their coordinated insertion and correct assembly at the membrane. The co-translational targeting starts with the partial competitive exclusion of trigger factor from the ribosomal exit site by the highly conserved ribonucleoprotein complex, the Signal Recognition Particle (SRP) which specifically guides the RNCs translating integral membrane proteins (Ulbrandt *et al*., 1997; Valent *et al*., 1997) and some secretory proteins (Emanuelsson and von Heijne, 2001) to the membrane, mainly to the Sec translocon (Keenan *et al*., 2001). The recruitment of the SRP-RNC to the inner membrane is mediated by the interaction of SRP with its membrane-associated receptor FtsY and driven by GTP hydrolysis (Yang and Zhang, 2011).

The heterotrimeric SecYEG translocon is the primary protein export channel in *E. coli* and it is used for both, post- and co-translationally delivered proteins. The crystal structure from the homologous *Methanocaldococcus jannaschii* SecYEβ provided the first high-resolution insight into the organization and structure of the translocation channel (Fig. 1.7; van den Berg *et al*., 2004).

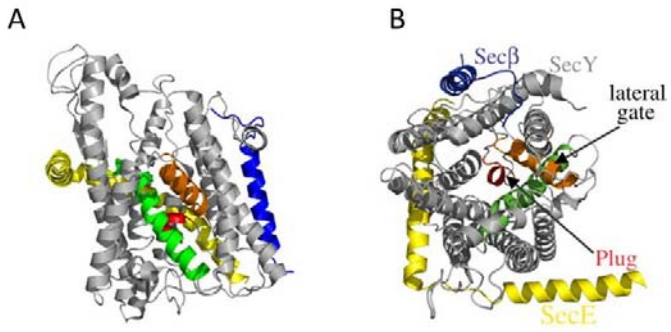

Fig. 1.7 ***Crystal structure of the M. jannaschii SecYEβ complex. (A)*** *Side and* ***(B)*** *top view from the cytoplasm. SecY (grey) is indicated with the plug (red). The lateral gate helices 2b and 7 are shown in orange and green, respectively. SecE is colored yellow and Secβ is shown in blue. PDB code: 1RH; adapted from Lycklama et al., 2012.*

The SecY protein forms the channel pore by its 10 α-helical transmembrane domains (TMDs) through which proteins might traverse the membrane. TMDs 1-5 and TMDs 6-10 of SecY are pseudo-symmetrically aligned resembling a bivalent shell that forms a lateral gate for the release of hydrophobic domains into the membrane, hinged by SecE (Fig. 1.7). The channel is intrinsically sealed by a plug domain formed by a subregion within the second TMD of SecY (Lycklama *et al*., 2012). While SecYEG is the main site for protein insertion and translocation, the essential insertase YidC was found to act in conjunction with the translocon in integral membrane protein insertion in bacteria (Zhu *et al*., 2013). YidC appears to exist in two pools (Fig. 1.6 b): one that is tightly associated with SecYEG and assists in the integration of polytopic membrane proteins (Scotti *et al*., 2000; Nouwen and Driessen, 2002; Plessis *et al*., 2006; Kol *et al*., 2009), and another species that acts independently of SecYEG to mediate the integration of, mainly small, membrane proteins of *E. coli* (Samuelson *et al*., 2000; van der Laan *et al*., 2003 & 2004; Serek *et al*., 2004). The targeting to YidC is thought to mainly occur via the SRP pathway (Facey *et al*., 2007), although SRP-independent mechanisms have also been described (Gerken *et al*., 2008; Welte *et al*., 2012). The direct interaction of YidC with translating ribosomes was elucidated in several studies during the recent years (Kohler *et al.*, 2009; Funes *et al*., 2011; Kedrov *et al*., 2013; Seitl *et al*., 2014; Wickles *et al*., 2014; Geng *et al*., 2015). The functionality and role of this interaction in the targeting and insertion of YidC-only substrates is one main focus of this work. Despite the diversity of trafficking pathways, protein targeting can be divided into three key steps that are common to all pathways: 1.

substrate recognition in the cytosol, 2. targeting and delivery to the respective membrane and 3. passage through or insertion into the membrane lipid bilayer. The SRP pathway comprises these general principles and serves as a paradigm for understanding the molecular basis of protein localization and sorting in all cells.

1.2.1 The Signal Recognition Particle and its RNA

SRP is an ancient and essential ribonucleoprotein particle conserved across all kingdoms of life (Walter and Johnson, 1994; Keenan *et al*., 2001; Akopian *et al*., 2013-1). The evolutionary conservation of this pathway was demonstrated experimentally *in vitro* by the substitution of the eukaryotic homolog with the highly simplified bacterial SRP system. The latter could efficiently mediate the targeting of mammalian substrates to ER microsomes (Bernstein *et al*., 1993; Powers and Walter, 1997). This allows the bacterial SRP to serve as a universal model system for understanding the fundamental molecular mechanisms of this targeting machine in prokaryotic and eukaryotic cells.

The *E. coli* SRP is comprised of the protein component Ffh (SRP54 in eukaryotes) and the 4.5S RNA (7S RNA in eukaryotes) (Poritz *et al*., 1988). The SRP RNA binds with picomolar affinity to the methionine-rich M-domain of SRP (Batey *et al*., 2000; Jagath *et al*., 2001; Siu *et al*., 2007). The M-domain, together with the SRP RNA facilitates the signal sequence recognition and binding (Keenan *et al*., 1998; Batey *et al*., 2000; Janda *et al*., 2010; Hainzl *et al*., 2011). Besides the C-terminal M-domain, the second structurally and functionally distinct domain of SRP is the NG-domain (Fig. 1.8) composed of an N-terminal helical N-subunit and a centrally located GTPase subunit, the so called G-domain (Freymann *et al*., 1997; Montoya *et al*., 1997). The N-domain mediates interactions with the ribosome via binding to the ribosomal protein L23 at the ribosomal tunnel exit site (Pool *et al*., 2002; Gu *et al*., 2003; Halic *et al*., 2006; Schaffitzel *et al*., 2006), and the G-domain mediates GTP binding and hydrolysis. Collectively, the NG-domain of Ffh interacts directly with the highly conserved NG-domain of the SRP receptor protein FtsY, forming a heterodimeric GTPase core of the SRP targeting complex (Egea *et al*., 2004; Focia *et al*., 2004) (Fig. 1.8). In addition to the NG-domain, FtsY contains an N-terminal acidic A-domain, which mediates the peripheral association of the receptor with the phospholipid membrane and with the SecYEG translocon (Parlitz *et al*., 2007; Weiche *et al*., 2008).

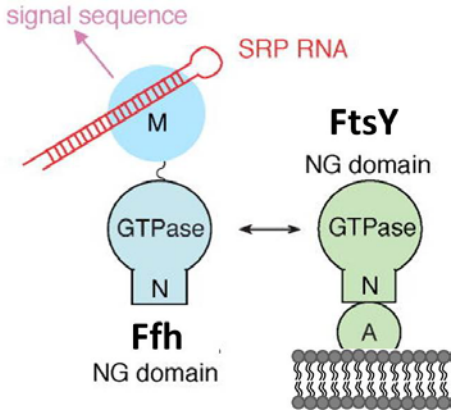

Fig. 1.8 ***Domain structure of SRP and FtsY****. Cargo recognition of SRP occurs via the M-domain with bound 4.5S RNA, whereas the N-domain interacts with the ribosome. By their NG-domains, SRP and FtsY merge to form a heterodimeric GTPase core complex that is associated to the membrane and the translocases via the acidic A-domain of FtsY. (adapted from Zhang and Shan, 2014)*

The discovery of the bacterial SRP RNA (Poritz *et al*., 1988 &1990), years later after the discovery of the mammalian SRP RNA by Peter Walter, challenged the view of the RNA component to be a passive scaffold necessary for the correct assembly of the six mammalian SRP protein subunits (Walter and Blobel, 1982). Recent biochemical and structural studies have demonstrated that indeed, the SRP RNA actively mediates domain rearrangement of SRP upon cargo recognition (Buskiewicz *et al*., 2005), thus allowing also proper interaction with its receptor FtsY (Peluso *et al*., 2000; Jagath *et al*., 2001) as well as activating and stimulating the GTPase function of the SRP-receptor complex (Siu *et al*., 2007). Bacterial SRP shows high homologies to the domain IV of the eukaryotic SRP RNA, a region of ~ 50 nucleotides, whose highly conserved secondary structure consists of two internal loops that include noncanoncial base pairings and unpaired nucleotides (Fig. 1.9 A) and a second hairpin structure that is capped by a highly conserved GGAA tetraloop. Domain IV in bacterial and human SRP stabilizes the ribonucleoparticle and its interaction with the signal peptide (Gowda and Zwieb, 1997; Zheng and Gierasch, 1997). The 4.5S RNA of *E.* coli binds with picomolar affinity to the M-domain of Ffh (Fig. 1.9 C) via its two internal loops (Fig. 1.9 B) adjacent to the GGAA tetraloop (Batey *et al*., 2000). The orientation of the M-domain/RNA complex relative to the Ffh NG domain exhibits a high degree of flexibility. At least 4 different structures were found by crystallographic analysis and structural mapping studies, each exhibiting a distinct interdomain arrangement (Keenan *et al*., 1998; Rosendal *et al*., 2003; Buskiewicz *et al*., 2005 1&2; Mainprize *et al*., 2006; Hainzl *et al*., 2007). These observations suggest that free SRP is a highly dynamic particle that can undergo substantial structural rearrangements, likely due to the 30 amino acid residues long flexible linker within the Ffh protein, connecting its M- and the NG-domains.

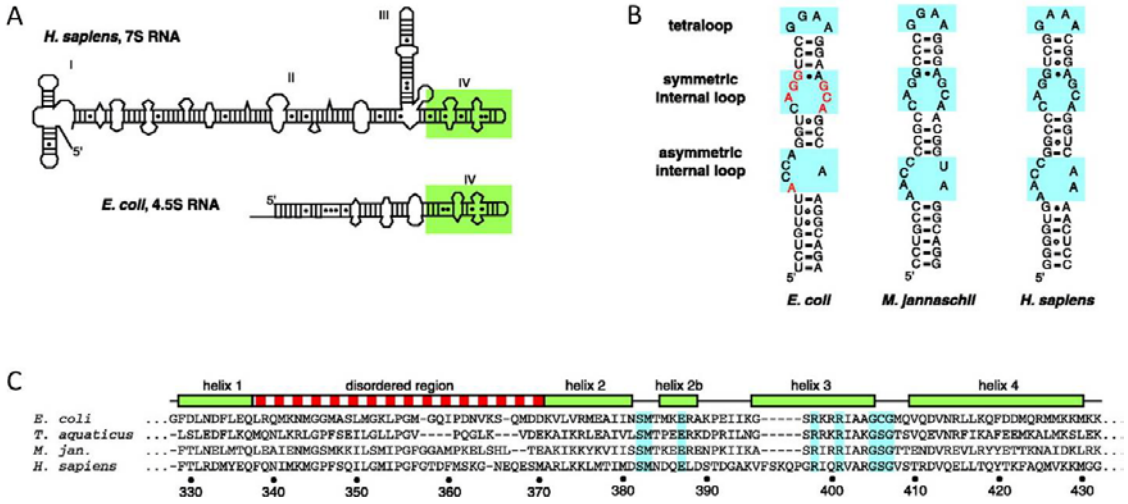

Fig. 1.9 ***Overview of the highly conserved SRP ribonucleoprotein core. (A)****Secondary structure of the 7S RNA from humans and the 4.5S RNA from E. coli. The universally conserved domain IV of the RNA is highlighted in green.* ***(B)*** *Domain IV nucleotide sequences of SRP RNA from organisms of the three kingdoms of life, representing the three conserved features: the distal GGAA-tetraloop, the symmetric internal loop and the asymmetric internal loop (cyan boxes). Nucleotides highlighted in red in the E. coli SRP RNA domain IV are important for in vivo function (Wood et al., 1992) and Ffh binding (Lentzen et al., 1996).* ***(C)*** *Sequence alignment of the SRP54/Ffh M-domains from various organisms (Escherichia coli, Thermus aquaticus, Methanocaldococcus jannaschii, Homo sapiens), with the numbering consistent with that of the E. coli Ffh. Cyan boxed residues are invariant in the RNA binding region of the protein. (adapted from Batey et al., 2000)*

Exempt from domain IV, the sizes, sequences, and secondary structures of SRP RNAs vary widely, even among bacterial species (Samuelsson and Zwieb, 1999), and it is unclear whether these regions of the RNA are essential for SRP function. A recently published crystal structure of the SRP-FtsY/receptor complex provided a possible function for the distal end of the SRP RNA, which trapped the SRP-FtsY GTPase complex ~ 100 Å away from the tetraloop domain (Ataide *et al*., 2011). Together with biochemical studies and single molecule fluorescence measurements, these results suggest a model in which the SRP-FtsY NG domains, after initial assembly at the tetraloop end of the RNA, relocalize to its distal end where GTP hydrolysis is activated (Shen *et al*., 2012). The movement of the NG domains to the distal RNA end is negatively regulated by the translating ribosome and restored by the SecYEG complex, providing the first experimental support for a concerted mechanism of cargo handover from SRP to the SecYEG complex by vacating the ribosomal protein L23. This hypothesis provides an attractive mechanism of coupling unloading of the SRP substrate protein cargo to GTP hydrolysis (Shen *et al*., 2012; Akopian *et al*., 2013-b). In addition, a recent study showed that the 6S RNA of the SRP from the Gram-positive bacterium *Bacillus subtilis* facilitates elongation slowdown similarly to the eukaryotic translational arrest by the Alu domain of

SRP (Beckert *et al*., 2015). Thus the SRP RNA is an active molecular scaffold, mediating protein rearrangements and exchange of distinct factors via multiple protein interaction sites, therefore allowing effective coordination of a complex cellular pathway.

1.2.2 Signal sequence recognition by SRP

In general, N-terminal signal sequences that are recognized by SRP are characterized by a positively charged n-region, an h-region containing the hydrophobic core (8-20 aa) and a polar c-region, preferentially adopting an α-helical structure (von Heijne, 1985; Gierasch, 1989). The unifying characteristic of all signal sequences, and apparently the only essential feature for binding SRP, is an uninterrupted stretch of at least seven hydrophobic residues surpassing a threshold level of hydrophobicity (Lee and Bernstein, 2001). Thus the first transmembrane domain often serves as a signal sequence for SRP. One fundamental question is, how SRP recognizes these signals that are highly divergent in sequence, length and amino acid composition without any known consensus motif (Zheng and Gierasch, 1996; Hegde and Bernstein, 2006). To test the specificity during the cargo recognition step by SRP, several research groups have compared the binding affinities of SRP for RNCs bearing SRP-dependent and SRP-independent substrates (Flanagan *et al*., 2003; Bornemann *et al*., 2008; Zhang *et al*., 2010; Saraogi *et al*., 2011; Holtkamp *et al*., 2012). Depending mainly on the hydrophobicity of the signal peptide, SRP tightly binds RNCs displaying an SRP signal sequence with equilibrium dissociation constants (K_d) in the nanomolar range (1 – 10 nM). However, yet the weakest cargo or even empty ribosomes bind SRP with significant K_d values in the 50 – 100 nM range (Flanagan *et al*., 2003; Bornemann *et al*., 2008; Zhang *et al*., 2010; Holtkamp *et al*., 2012). This suggests that SRP can bind rapidly to RNCs bearing both SRP-dependent and -independent substrates, but its dissociation occurs much more slowly from the RNCs displaying a proper cargo. Since the binding of isolated signal peptides to SRP is much weaker, with a dissociation constant in the micromolar range (~ 1,5 µM; Bradshaw *et al*., 2009), the interaction with the ribosome obviously contributes significantly to the RNC-SRP binding energy and provides an important driving force for SRP-recruitment to nascent polypeptide chains. Regarding the cellular concentrations of SRP (~ 400 nM in bacteria) and ribosomes (40 - 50 µM), it is unlikely that the different affinities in the initial cargo-binding step are sufficient to discriminate against incorrect cargos and to ensure the accurate substrate selection by SRP. Thus, additional fidelity and quality checkpoints are provided by the SRP- and FtsY-GTPases, described in the following chapter. Cross-linking studies (Pool *et al*., 2002; Gu *et al*., 2003) and cryo-EM reconstruction data revealed the ribosomal protein L23 as a major contact site for the Ffh N-domain on the ribosome and to a lesser extend L29 in the vicinity of the ribosomal exit tunnel, in both

eukaryotic and bacterial systems (Halic *et al*., 2004 & 2006; Schaffitzel *et al*., 2006). The crystal structures of SRP-signal peptide fusions (Janda *et al*., 2010; Hainzl *et al*., 2011) clearly showed that the signal sequence binds into a deep, hydrophobic groove in the M-domain. However, different docking modes of the signal peptide arose, highlighting the flexibility of the signal sequence-M domain interaction. Compared to the structures of the respective free SRP (Fig. 1.10 A), without bound signal sequence, it became obvious that upon binding of a signal sequence, huge structural changes in the SRP core are induced (Fig. 1.10 B).

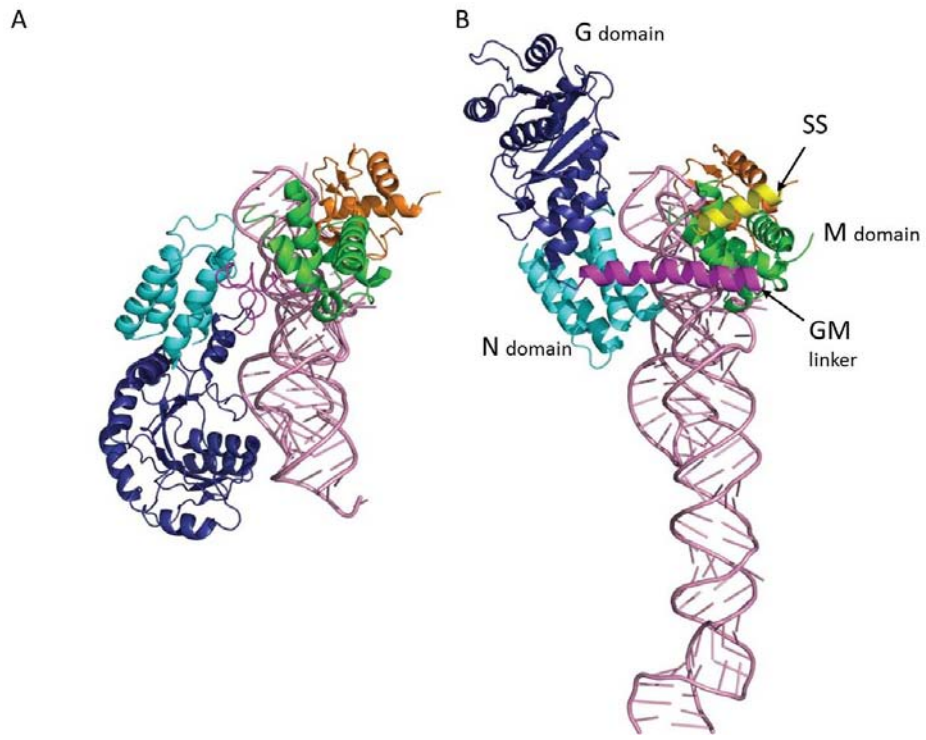

Fig. 1.10 ***Domain rearrangement of the SRP core upon signal sequence binding. (A)*** *Free form of the M. jannaschii SRP54-SRP19-S domain RNA complex (Hainzl et al., 2011).* ***(B)*** *Signal-sequence (SS) bound form of (A) reveals an SRP54 domain rearrangement in the SRP core generated by a 90° rotation and a 180° flip of the NG domain. Additionally, the GM-linker forms a continuous helix compared to an extended conformation in the free SRP core. Ribbon representations of the SRP / SRP-signal sequence complex with the color code as follows: M domain, green; N domain, cyan; G domain, dark blue; SRP19, orange; signal sequence, yellow and the GM linker in magenta. (adapted from Hainzl et al., 2011)*

The two distinct structures of free SRP and SRP bound to a signal sequence suggest that the binding of a signal sequence triggers the local restructuring and an α-helical formation of the, until then disordered, GM-linker (compare Fig. 1.10 A and B), causing the repositioning of the NG domain in an RNA dependent manner (Fig. 1.10 B). This brings

the GTPase domain into proximity of the universally conserved tetraloop, preparing the NG-domain for receptor (FtsY) interaction (Hainzl *et al*., 2011).

1.2.3 Co-translational targeting: SRP-FtsY assembly

The SRP receptor, called FtsY in bacteria mediates the membrane targeting of cargo-bound SRP via interaction through their GTPase modules. The acidic A domain of FtsY is supposed to anchor the targeting complex to the membrane (Parlitz *et al*., 2007; Weiche *et al*., 2008) in a dynamic mode (Luirink *et al*., 1994; Rubio *et al*., 2005; Mircheva *et al*., 2009) also involving membrane lipids, preferentially anionic phospholipids (phosphatidyl glycerol (PG) and cardiolipin (CL)) (de Leeuw *et al*., 2000; Parlitz *et al*., 2007; Lam *et al*., 2010). In addition, to entail the targeting complex into the vicinity of the translocon, a direct interaction of FtsY with the SecYEG translocon was found (Angelini *et al*., 2005 & 2006; Kuhn *et al*., 2011). The GTPase domains of SRP and FtsY contain the four conserved sequence motifs of the GTPase superfamily and share the classic P-loop GTPase-fold. Two additional structural features were identified, comprising a flexible insertion box domain (IBD) loop with multiple catalytic residues and the N-domain, which is a four-helix bundle that packs tightly against the G-domain to form the structural and functional NG-domain unit (Freymann *et al*., 1997; Montoya *et al*., 1997). Compared to classic signaling GTPases which are regulated by specific G-protein activating factors (GAPs, GEFs), the SRP and FtsY proteins belong to a new class of GTPases which are activated by nucleotide-dependent dimerization (GADs) (Gasper *et al*., 2009).

Free SRP and FtsY have their GTPase domains, even with bound GTP, in an inactive open conformation exhibiting low nucleotide binding affinity as their nucleotide-binding pocket is wide open, allowing free exchange of nucleotides (Montoya *et al*., 1997; Freymann *et al*., 1997 & 1999). In this state their catalytic IBD loops are not correctly positioned provoking only a low basal GTPase activity (Peluso *et al*., 2001). Driven by dimerization, the GTPase cycles of SRP and its receptor are initiated by a series of discrete conformational changes that causes activation. SRP and FtsY can initially associate to form a transient 'early' intermediate (Fig. 1.11 [2]) independently of GTP (K_d ~ 4-10 µM), primarily driven by electrostatic interaction of the N-domains without stable contacts between their G-domains (Estrozi *et al*., 2011; Zhang *et al*., 2011). A stable closed complex (Fig. 1.11 [3]) with extensive interactions between the G-domains (~ 16-30 nM) is formed by GTP dependent rearrangements, primarily involving readjustment of the NG-domain interface (Shan and Walter 2003; Egea *et al*., 2004; Focia *et al*., 2004; Shan *et al*., 2004) and repositioning of the inhibitory N-terminal helix N1 of FtsY (Shepotinovskaya and Freymann 2002; Gawronski-Salerno and Freymann 2007; Neher *et*

al., 2008). The final rearrangement in the GTPase cycle involves repositioning of the catalytic residues in the IBD loops at the active site and results in an activated complex (Fig. 1.11 [4]) that triggers efficient GTP hydrolysis (Egea *et al*., 2004; Focia *et al*., 2004; Shan *et al*., 2004). This, in turn completes the cycle by causing the disassembly and release of the SRP-FtsY complex (Fig. 1.11 [5]) (Connolly *et al*., 1991; Peluso *et al*., 2001). The conformational changes during the GTPase cycle are versatilely regulated both by the cargo protein and the target membrane (Zhang *et al*., 2009; Lam *et al*., 2010; Akopian *et al*., 2013-b) to enhance the targeting efficiency and to provide multiple fidelity checkpoints to reject incorrect cargos (Fig. 1.11 red arrows).

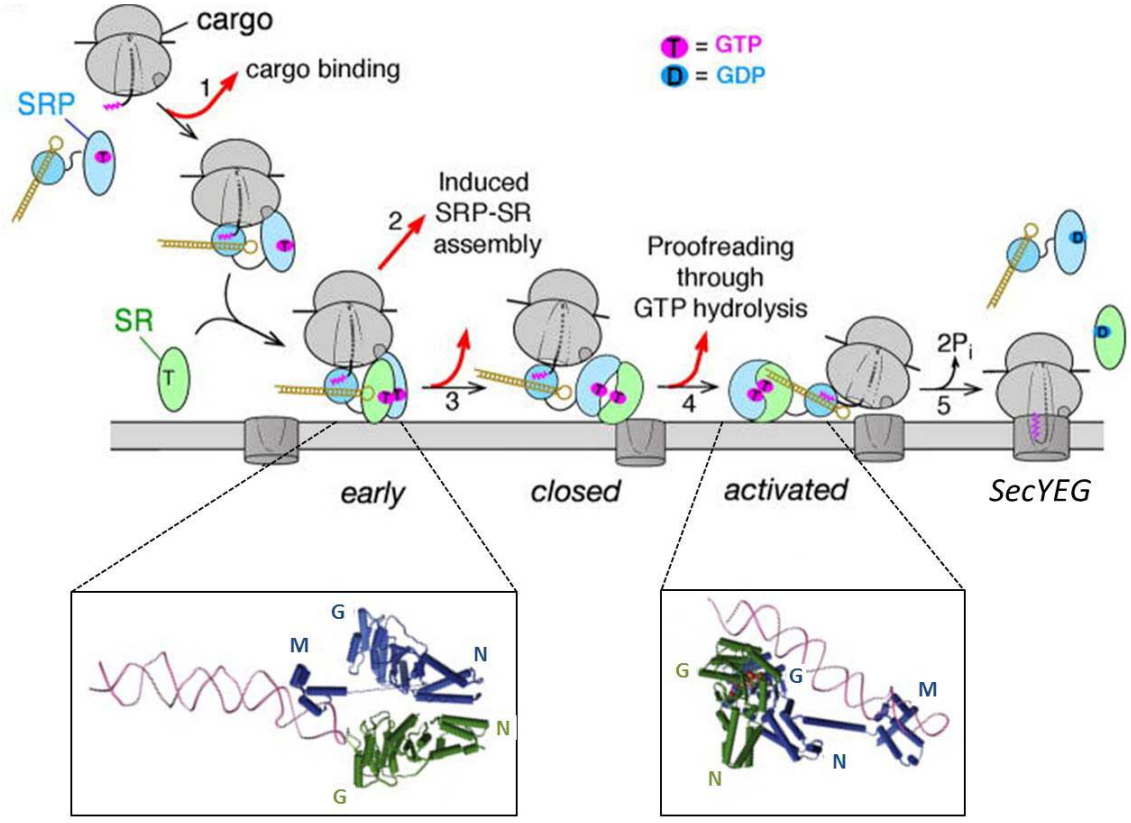

Fig. 1.11 ***Conformational changes in SRP and FtsY GTPase domains are coupled to incorrect cargo rejection.*** *[1] The binding of an RNC exposing a proper signal sequence (purple) to SRP (blue) positions the NG domain onto the top of the SRP RNA tetraloop. [2] The cargo bound SRP forms a stabilized early intermediate with FtsY (SR; green) due to interaction between their N-domains. [3] FtsY association to anionic phospholipids in the membrane strongly accelerates the rearrangement of the early targeting complex to the closed state. [4] Interaction with the SecYEG translocon (dark grey) induces the formation of the activated state in which the NG-domain complex relocalizes to the distal end of SRP RNA. [5] Hydrolysis of GTP triggers disassembly of the SRP-GTPase complex while the cargo is transferred from SRP to the Sec translocon. At each step it is possible to retain (black arrows) or reject (red arrows) the cargo from the SRP pathway (Zhang and Shan, 2014). The lower panels show molecular models of the SRP (blue) – FtsY (green) complex in the early (left) and activated (right) state (adapted from Saraogi and Shan, 2013).*

The first quality checkpoint in the SRP targeting cycle is the binding of SRP to RNCs displaying a correct cargo. This results in a stabilization of the early intermediate by more than 100-fold (Zhang *et al*., 2009), allowing the SRP-RNC-FtsY complex to be sufficiently stable to accumulate under physiological conditions (Fig. 1.11 [1]). Thereby, the assembly of the closed SRP-FtsY state is accelerated by 1000-fold (Zhang *et al*., 2009), accomplishing the rapid delivery to the target membrane once a correct cargo is loaded on SRP. In contrast, the less stable targeting complexes formed with incorrect cargos are much more likely to disassemble before they arrive at the membrane (Fig. 1.11 [2+3]). Another important step is the timing and regulation of GTP hydrolysis to avoid abortive targeting reactions before the complex successfully transfers the cargo to the Sec-translocation machinery. The so called kinetic proofreading by GTP hydrolysis solves this problem since a correct cargo delays the conformational rearrangement that leads to GTPase activation (Fig. 1.11 [4]). This retards the GTP hydrolysis rate by 6-8 fold (Zhang *et al*., 2009) and consequently extends the lifetime of the targeting complex from < 1 s to ~ 5 s. However, the delayed GTPase activation can be reversed by anionic phospholipids (Lam *et al*., 2010; Braig *et al*., 2011) and the interaction with the SecYEG complex (Akopian *et al*., 2013-b), indicating that GTP hydrolysis is tightly coupled to the unload of cargo at the target membrane (Fig. 1.11 [5]). In the last step of co-translational protein targeting the loaded ribosome has to be transferred to the SecYEG translocon without abortive loss of cargo. This challenging task is solved by the use of overlapping binding sites of SRP and SecYEG on the ribosome. Biochemical and genetic studies (Cheng *et al*., 2005; Ménétret *et al*., 2007) together with cryo-EM reconstitutions of the SecYEG-RNC-translocon complex (Beckmann *et al*., 2001; Mitra *et al*., 2005; Becker *et al*., 2009; Frauenfeld *et al*., 2011), showed that highly conserved basic residues in the cytosolic loops C4 and C5 of SecY interact with the ribosomal protein L23. Thus, the binding of SRP and SecYEG to RNCs is expected to be mutually exclusive and SRP has to detach from the RNC prior to its stable engagement with the translocon, involving a coordinated mechanism of cargo transfer. This process occurs via formation of a quaternary complex of RNC-SRP-FtsY-SecYEG (Akopian *et al*., 2013-b) and the movement of the NG dimer to the RNA distal end (Shen *et al*., 2012; Akopian *et al*., 2013-a,b) that vacates the ribosomal protein L23, thereby making it accessible for SecYEG.

There are first evidences that this could also hold for other translocation and insertion machineries since similar specific binding sites on the ribosome were found for the YidC insertase (Kohler *et al.*, 2009; Funes *et al*., 2011; Kedrov *et al*., 2013; Seitl *et al*., 2014; Wickles *et al*., 2014; Geng *et al*., 2015), suggesting a general mechanism for the cargo handover of SRP dependent substrates to their final insertase or translocase.

1.3 The YidC/Oxa1/Alb3 insertase family

In all living cells, biological membranes form hydrophobic, though semipermeable, barriers that separate the intracellular compartment from the extracellular environment. These membranes contain numerous intrinsic proteins that play vital roles for the cell and make up approximately 30 % of the proteome in an organism (Poetsch and Wolters, 2008). In eukaryotic cells, proteins are sorted from their source of origin in the cytoplasm to membrane-enclosed organelles such as the nucleus, endoplasmic reticulum, peroxisomes, mitochondria and chloroplasts. In prokaryotes, membrane proteins are also transported from the cytoplasm into or across the inner phospholipid bilayer. Due to the prokaryotic origin of mitochondria and chloroplasts, specialized membrane protein translocation systems have evolved that are exclusively found in these organelles and in bacteria. One of those unique protein families is the YidC/Oxa1/Alb3 insertase family which promotes membrane protein integration into bacterial inner membranes as well as into mitochondrial and plastid membranes, utilizing an evolutionarily conserved pathway for protein insertion.

1.3.1 Functional specialization in bacteria, mitochondria and chloroplasts

The YidC/Oxa1/Alb3 protein family is widely spread throughout all three domains of life (Yen *et al*., 2001; Zhang *et al*., 2009) and its members direct the insertion of integral membrane proteins into the lipid bilayer of the bacterial plasma membrane, the inner mitochondrial membrane, and the chloroplast thylakoid membrane (Saller *et al*., 2012; Dalbey *et al*., 2014). Insertase-dependent membrane proteins mainly consist of components of the respiratory chain or other energy transducing protein complexes (Luirink *et al*., 2001). Most bacteria contain only one YidC insertase gene copy, but some Gram-positive bacteria such as *Bacilli*, *Lactobacilli*, *Actinobacteria* and some *Clostridia*, often harbor two YidC homologs (Zhang *et al*., 2009; Funes *et al*., 2009 & 2011). The number of YidC homologs in eukaryotic organelles varies between different organisms with a maximum number of six in the plant *Arabidopsis thaliana* (Alb chloroplast proteins). This is probably caused by separate gene duplication and / or secondary losses of Oxa/Alb3 proteins leading to a rich diversity and to the distinct number of homologs found in each organism. The existence of YidC homologs in archaea has been proposed based on phylogenetic analysis within the *Euryarchaeota* but not in *Nanoarchaeota* and *Crenarchaeota* (Pohlschröder *et al*., 2005; Zhang *et al*., 2009). Recently, the first crystal structure of a YidC-like protein (DUF) from the archaeal plasma membrane of *Methanocaldococcus jannaschii* was solved and provided first experimental evidence for a structural and functional homology to YidC/Oxa1/Alb3 family members (Borowska *et al*.,

2015). Unlike eukaryotic insertases, the archaeal YidC-like protein could not complement for YidC insertases in eubacteria, suggesting an only distantly related homology of the DUF proteins.

The YidC/Oxa1/Alb3 proteins are thought to share a conserved core domain of approximately 250-300 residues in length comprising five transmembrane (TM) domains (Saaf *et al*., 1998; Luirink *et al*., 2001; Kuhn *et al*., 2003; Kumazaki *et al*., 2014-a & -b) exhibiting the insertase activity of the proteins (Fig. 1.12). However, the conserved transmembrane core found in the shorter archaeal proteins of the DUF106 family is predicted to contain only three TM helices (Borowska *et al*., 2015). Extensive studies showed that those hydrophobic core domains can be functionally exchanged between different non-archaeal members of this family (Jiang *et al*., 2002; Funes *et al*., 2004-2; Preuss *et al*., 2005; van Bloois *et al*., 2007; Dong *et al*., 2008). Noticeably, the homology within this insertase family is mainly a kind of functional conservation rather than mere sequence homology. The YidC/Oxa1/Alb3 proteins only share a low level of primary sequence similarity and their lengths vary over a four-fold range (~ 200 – 800 amino acid residues; Yen *et al*., 2001; Jiang *et al*., 2003). The highest homology is found in the core TM domains 1, 2 and 5 (corresponding to TM 2,3 and 6 in *E. coli* and other Gram-negative bacteria) (Yen *et al*., 2001), whereas the N- and C-terminal flanking regions of the core domain exhibit a huge variety in length, composition and structure (Fig. 1.12). Unique to the YidC proteins of Gram-negative bacteria is an additional N-terminal TM domain connected via a large periplasmic loop to TM2, indicating an organism-specific function (Oliver and Paetzel, 2008; Ravaud *et al*., 2008). On the other hand, Oxa1, Alb3, Alb4 from organelles and YidC2 from the Gram-positive bacterium *Streptococcus mutans* contain elongated, highly positively charged C-terminal tails mediating specialized functions during protein insertion in the respective organism (Fig. 1.12).

Mitochondria of animals, fungi and plants consistently contain two insertase homologs, Oxa1 and Cox18 (Funes *et al*., 2004-1). Oxa1 facilitates the insertion of the mitochondrial-encoded inner membrane proteins of the respiratory chain complex as well as of the ATP synthase subunits ATP6, 4 and 9, related to the bacterial subunits F_Oa, F_Ob and F_Oc, respectively (Bonnefoy *et al*., 1994; Bauer *et al*., 1994; Hell *et al*., 2001; Jia *et al*., 2007). Also some nuclear encoded proteins like the ABC-transporter Mdl1 depend on Oxa1 for their correct membrane assembly (Bohnert *et al*., 2010; Hildenbeutel *et al*., 2012). The membrane insertion of mitochondrial translation products occurs in a co-translational process (Hell *et al*., 1997 & 1998), mediated by Oxa1 with its C-terminal α-helical region binding mitochondrial ribosomes at the exit tunnel via the ribosomal proteins Mrp20 and Mrp40. These are homologs of the bacterial L23 and L24 ribosomal proteins, respectively

(Jia *et al*., 2003 & 2009; Szyrach *et al*., 2003; Kohler *et al*., 2009; Gruschke *et al*., 2010). Electrophysiological measurements with purified Oxa1 showed an ability to form substrate-gated pores in lipid bilayers (Krueger *et al*., 2012). The second insertase in mitochondria, Cox18, is an essential assembly factor of cytochrome c oxidase (Souza *et al*., 2000). Compared to Oxa1 (Fig. 1.12), Cox18 lacks a C-terminal ribosome binding domain and presumably functions exclusively in a post-translational manner (Funes *et al*., 2004-1) downstream of Oxa1 (Saracco and Fox, 2002).

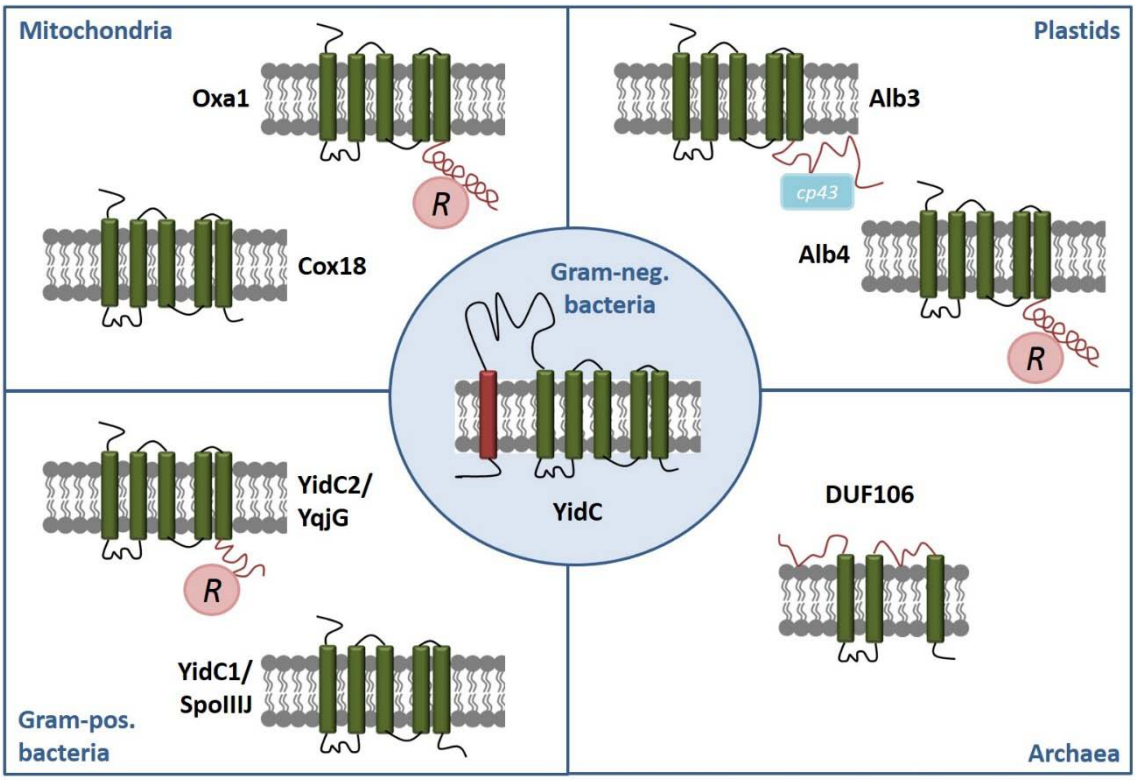

Fig. 1.12 ***Functional specialization of the YidC/Oxa1/Alb3 family members.*** *All insertase homologs are comprised of a core region of 5 TM domains (green) with flanking N- and C-terminal regions of variable lengths and functions (red). The smaller archaeal homolog contains a catalytically active domain of only 3 TM domains (DUF106) and possesses 1 paralog like in Gram-negative bacteria, shown in the center. The Gram-negative YidC is characterized by an additional N-terminal domain and a large periplasmic loop. Gram-positive bacteria, mitochondria and plastids contain two different paralogs, each being functionally and structurally distinct. These additional features are for example a direct interaction with ribosomes (R) or the chloroplast SRP (cp43). Independent gene duplications in Gram-positive bacteria and in organelles have led to specialized co- and posttranslational functions of YidC/Oxa1/Alb3 proteins, presumably developed from a common ancestor with similarities to YidC found in Gram-negative bacteria (Funes et al., 2011).*

Plastids of *Arabidopsis thaliana* and other plants contain also two paralogs, Alb3 and Alb4, which differ in their function (Sundberg *et al*., 1997; Gerdes *et al*., 2006). Alb3 is critical for the post-translational insertion of LHCP (light-harvesting chlorophyll-binding

proteins) into the thylakoids (Moore *et al*., 2000; Bellafiore *et al*., 2002), the most abundant membrane protein system on earth. The nuclear-encoded LHCP-precursors are synthesized in the plant cell cytosol and subsequently targeted and imported into the chloroplast stroma where they bind to the plastid SRP (cpSRP) (Schuenemann *et al*., 1998). Instead of an SRP RNA, the plant cpSRP contains a specialized subunit, cpSRP43, mediating the interaction with the extended C-terminal domain of Alb3 (Fig. 1.12). Consequently, the C-terminal domain of Alb3 is crucial for the targeting of LHCPs to the thylakoid membrane (Moore *et al*., 2003; Falk *et al*., 2010), representing a plant-specific factor for the biogenesis of LHCPs. Alb4 does not interact with cpSRP43 and therefore cannot compensate for the loss of Alb3. Interestingly, however upon expression in mitochondria, Alb4 can functionally replace Oxa1 (Funes *et al*., 2004-1) indicating that its C-terminal extended domain can facilitate ribosome binding (Fig. 1. 12). In plastids, Alb4 interacts with subunits of the CF_OCF_1-ATPase (Benz *et al*., 2009), similar to YidC and Oxa1 mediating the membrane assembly of the F_OF_1-ATPase.

The genomes of most Gram-positive bacteria encode two slightly different YidC proteins (Fig. 1.12) (Yen *et al*., 2001; Funes *et al*., 2009) with obviously overlapping activities, since only the simultaneous deletion of both leads to a lethal phenotype (Murakami *et al*., 2002; Tjalsma *et al*., 2003; Saller *et al*., 2009). In *Bacillus subtilis* the YidC proteins are termed SpoIIIJ, a protein that was found to be essential for sporulation, and YqjG that is upregulated under conditions at which the levels of SpoIIIJ are not sufficient to fully promote protein insertion (Chiba *et al*., 2009). *Streptococcus mutans* exhibits two functional orthologs of *E. coli* YidC, YidC1 (SpoIIIJ) and YidC2 (YqjG) (Hasona *et al*., 2005), each complementing multiple defects of YidC depletion in *E. coli.* The *S. mutans* YidC1 and 2 proteins can mediate insertion of both, Sec-dependent and -independent YidC substrates (Dong *et al*., 2008). However, deletion of YidC1 alone has only little obvious effect, whereas the phenotype of a YidC2 deletion is strikingly similar to that of SRP pathway mutants, suggesting that YidC1 and YidC2 are functionally distinct (Hasona *et al*., 2005). One reason for these differences is probably the C-terminal ribosome binding domain of YidC2 which is similar to that of Oxa1. This domain is lacking in YidC1 (Dong *et al*., 2008). Interestingly, deletion of SRP is not lethal in *S. mutans* until simultaneous deletion of YidC2, suggesting that YidC2 supports a co-translational insertion pathway in Gram-positive bacteria that does not solely rely on the SRP pathway. This hypothesis was supported by the observation that YidC2 expression in yeast mitochondria promotes co-translational integration of proteins into the mitochondrial inner membrane in the absence of Oxa1 (Funes *et al*., 2009). Thus, a gene duplication of YidC

proteins in Gram-positive bacteria obviously allowed the specialization of one paralog for a co-translational protein insertion route (Funes *et al*., 2009).

Gram-negative bacteria usually compromise only one YidC protein with a short C-terminal tail and no essential function could yet be ascribed to this domain (Jiang *et al*., 2003) (Fig. 1.12). However, genomic analyses and sequence comparisons show that YidC homologs in many marine and extremophilic eubacteria have C-terminal hydrophilic and often highly charged extensions comparable to the eukaryotic organellar YidC-like proteins (Kiefer and Kuhn, 2007). In this work, evidence is presented for a possible (ancestral) function of these extended tails by analyzing the function of the YidC C-tail regions of two marine prokaryotes in membrane targeting. One of those bacteria, the marine planctomycete *Rhodopirellula baltica* was first isolated from the Baltic Sea (Schlesner *et al*., 2004) as a unique bacterium which can anaerobically oxidize ammonium in specialized cellular compartments, the anammoxomes. *Rhodopirellulas* genome of 7.15 Mbp is one of the largest found in bacteria (Glöckner *et al*., 2003). The YidC homolog of *R. baltica* has a size of 90 kDa and a hydrophilic C-terminal tail region of 80 amino acid residues with a predicted isoelectric point (pI) of 10.45. *Oceanicaulis alexandrii,* the second marine bacterium used in this study, is a stalked, aerobic α-proteobacterium, isolated originally as a symbiont from the dinoflagellate *Alexandrium tamarense* (Strömpl *et al*., 2003). Its YidC homolog is 83 kDa in size and has a large, positively charged C-terminal tail of 99 residues with an estimated pI of 9.85. In comparison, *E. coli* YidC is 61 kDa in size and its C-terminal region is only 16 amino acid residues long. Marine prokaryotic organisms are, in many cases, unique in their genomic organization (Serres *et al.,* 2009). Particularly in the planctomycete group, several gene duplications and protein motifs are found that only have counterparts in archaeal or even eukaryotic phyla (Studholme *et al.,* 2004). Thus, studying marine bacterial groups may be a key to understand how complex cellular processes like protein translocation and membrane targeting may have evolved and spread over the whole organismic world.

Taken together, the gene duplications broaden the physiological range of substrates using YidC members during cell evolution and revealed a phylogenetic tree of YidC/Oxa1/Alb3 membrane insertases with 6 subbranches that evolved from a common ancestor (Funes *et al*., 2011). In this phylogenetic analysis two main bacterial branches exist (YidC, YidC1, SpoIIIJ and YidC2, YqjG) where the YidC gene first arose in proteobacteria and only later in Gram-positive bacteria where it was duplicated in the firmicutes subphylum to form the YidC1 and YidC2 subbranches (Zhang *et al*., 2009). Since the proteobacteria and cyanobacteria, being most closely related to mitochondria and chloroplasts respectively,

have only a single copy of the YidC gene, gene duplications must have occurred after the endosymbiotic event that leads to mitochondria and chloroplasts. This resulted in two mitochondrial branches (Oxa1 and Cox18) and two chloroplast branches (Alb3 and Alb4). The YidC/Oxa1/Alb3 homologs of eubacteria and eukaryotes are more closely related to each other than to the highly diverged archaeal DUF106 proteins (Luirink *et al*., 2001; Zhang *et al*., 2009). Their lack of two of the five TMs present in the other YidC homologs may reflect differences in substrate specificity or in the mechanism of action in the archaeal DUF insertases (Borowska *et al*., 2015). This is consistent with the finding that many of the YidC/Oxa1/Alb3 paralogues, particularly the various insertase proteins in organelles and in Gram-positive bacteria, differ in their substrate preference and therefore differ in their distinct function (Saller *et al*., 2009; Benz *et al*., 2009 & 2013) representing organism specific, specialized membrane insertases.

1.3.2 The bacterial membrane insertase YidC

In 1994 it was discovered that the mitochondrial Oxa1 has homologous genes in Gram-negative and Gram-positive bacteria (Bonnefoy *et al*., 1994). Six years later the function of the bacterial Oxa1 homolog, termed YidC, as an essential membrane insertase in *E. coli* was shown by Samuelson *et al*., (Samuelson *et al*., 2000). Its Sec-dependent membrane protein inserting function was discovered by Scotti *et al*. (Scotti *et al*., 2000) in the same year. Since then, the membrane insertase YidC of *E. coli* was the focus of many structural and functional studies to understand the new membrane insertion mechanism and is one of the best-studied YidC/Oxa1/Alb3 family members. The 548 amino acid residues comprising YidC of *E. coli* is a six-spanning membrane protein with 61 kDa in size and is integrated into the inner membrane by the SecYEG/SecA translocase as well as in an SRP dependent manner. This suggests that YidC, in contrast to its mitochondrial orthologue Oxa1, cannot engage a SecYEG-independent protein conducting channel (Koch *et al*., 2002).

A large number of substrate proteins was identified that are inserted by the bacterial YidC alone or in cooperation with the Sec translocase. This results in a much broader substrate spectrum of YidC compared to the rather limited number of substrates inserted by Oxa1 or Alb3 in organelles. In cooperation with the Sec translocon, YidC promotes the insertion of the F_1F_O ATP synthase subunits F_OA and F_OB, the NADH-quinone oxidoreductase subunit K NuoK, and CyoA, the subunit 2 of the cytochrome *bo* oxidase (Yi *et al*., 2004; du Plessis *et al*., 2006; van Bloois *et al*., 2006; Celebi *et al*., 2006; Kol *et al*., 2009; Price and Driessen 2010). In addition to its insertase function, YidC is also required for the folding of LacY (Nagamori *et al*., 2004; Zhu *et al*., 2013) and MalF (Wagner *et al*., 2008) in the

membrane bilayer as well as for the membrane assembly of the oligomeric maltose transporter MalFGK (Wagner *et al*., 2008). As part of the holo-translocon (HTL) SecYEG-SecDF-YajC-YidC (Scotti *et al*., 2000; Schulze *et al*., 2014), YidC interacts directly with SecY involving the residues Gly 355 in TM2 and Met 471 in TM4 of *E. coli* YidC (Li *et al*., 2014). Supposedly, by this interaction YidC promotes the dislodge of the transmembrane segments of inserting membrane proteins from the Sec channel through its lateral gate (Zhu *et al*., 2012), facilitating their integration into the lipid bilayer (Urbanus *et al*., 2001), thus serving as an assembly site for multi-spanning membrane proteins (Beck *et al*., 2001). With approximately 2500 to 3000 copies per cell, YidC is much more abundant than the SecYEG complex (Urbanus *et al*., 2002), and therefore probably only a portion of the YidC protein pool forms a constituent of the HTL. Recently, the isolation of a stable holo-translocon revealed two distinct versions of the HTL. One containing a single copy of SecYEG, YidC, SecDF and YajC each, that functions preferably in membrane protein insertion, while the second HTL species is comprised of a SecYEG dimer only which functions in protein export (Schulze *et al*., 2014).

As an independent insertase, YidC facilitates the insertion of F_Oc, the subunit c of F_1F_O ATP synthase, the mechanosensitive channel protein MscL, the phage proteins M13 procoat and Pf3 coat, and the tail anchored membrane protein TssL (Samuelson *et al*., 2000 & 2001; Chen *et al*., 2002; Yi *et al*., 2003; van Bloois *et al*., 2004; Facey *et al*., 2007; Aschtgen *et al*., 2012). Interestingly, all these substrate proteins comprise less than 200 amino acid residues and have only short periplasmic loops (< 30 residues). The region of the five conserved TM domains 2 - 6 of *E. coli* YidC is crucial for its insertase function, whereas the unique features of Gram-negative YidC homologs, the additional TM1 and the large periplasmic loop 1 (P1), are dispensable (Jiang *et al*., 2003). However, the additional N-terminal TM helix serves as a signal sequence for inserting YidC correctly into the inner membrane. The P1 domain interacts with multiple components of the Sec machinery and is considered to facilitate stable complex formation particularly through binding to the SecF-subunit (Xie *et al*., 2006; Sachelaru *et al*., 2013). The large periplasmic P1 loop was the first domain of the *E. coli* YidC whose structure was solved. It revealed a β-super sandwich fold with short α-helical domains in the interior as well as at the edge of the sandwich. A flexible linker of two α-helices at the very C-terminus connects the P1 loop to the downstream core domain (Oliver and Paetzel, 2008).

In the year 2014, Kumazaki *et al.* reported the first crystal structure of a bacterial YidC protein. The molecular structure from *Bacillus halodurans* YidC1 was solved to 2.4 Å resolution (Kumazaki *et al*., 2014-a), contributing a landmark to the membrane biology

field. In late 2014, the X-ray structure of *E. coli* YidC was also solved to 3.2 Å by Kumazaki *et al*. (Kumazaki *et al*., 2014-b), providing new insight into the mechanism by which YidC inserts proteins into the bacterial inner membrane. Recently, Borowska *et al*., (2015) reported the crystal structure and provide experimental evidence that the DUF106 (Mj0480) protein from *M. jannaschii* represents a YidC-like archaeal membrane insertase. This provides the evidence that those membrane insertases are present in all three domains of life. All of these structures show closed topologies towards the periplasmic / extracellular space and form a hydrophilic groove that is open to the cytoplasm and also to the lipids of the membrane (Fig. 1.13), providing a new mechanism of membrane protein insertion. In contrast to the Sec translocase, YidC has no channel that is controlled by a hydrophobic pore ring and a periplasmic lid, but rather provides a platform to bind small proteins in an amphiphilic groove and reduces the required translocation energy to cross the membrane (Dalbey and Kuhn, 2014). Both bacterial YidC structures showed that the five conserved TM domains are tightly packed in the periplasmically exposed half of the membrane and spread out in the cytoplasmic half. Strikingly, the three TMs of the much smaller (23 kDa) Mj0480 DUF-like protein form a structure similarly folded as parts of the YidC hydrophilic groove of *B. halodurans* YidC1 and the *E. coli* YidC (Fig. 1.13). Another feature that is conserved in all family members is the accumulation of methionine residues at the cytoplasmic surface region of the YidC proteins, similar to the methionine rich M-domain of SRP which facilitates the binding of the signal peptide (Bernstein *et al*., 1989). This suggests that these methionine residues might also play a role in binding the inserting TM segments of the substrate proteins (Borowska *et al*., 2015). This methionine rich region includes the first cytoplasmic loop (C1) which contains a dynamic coiled coil motif (CH1+2 Fig. 1.13) being located near the cytosolic entrance of the hydrophilic groove and was shown to be essential for YidC function *in vivo* (Chen *et al*., 2014; Kumazaki *et al*., 2014-a). The corresponding region in Mj0480 is predicted to form also a coiled coil but is disordered and therefore not shown in the crystal structure (Fig. 1.13).

Despite the similarities of the membrane-embedded core regions, the insertases from the archaeon *M. jannaschii*, the Gram-positive *B. halodurans*, and the Gram-negative *E. coli* show an increasing complexity having gained additional features like the large periplasmic domain (P1 Fig. 1.13) of the *E. coli* YidC. The archaeal version of YidC possibly describes the minimal core motif forming the insertase domain. A subsequent step in characterizing the role of the DUF106 protein in the archaeal membrane-protein biogenesis is to find an endogenous substrate and test the ability to cooperate with the Sec translocase.

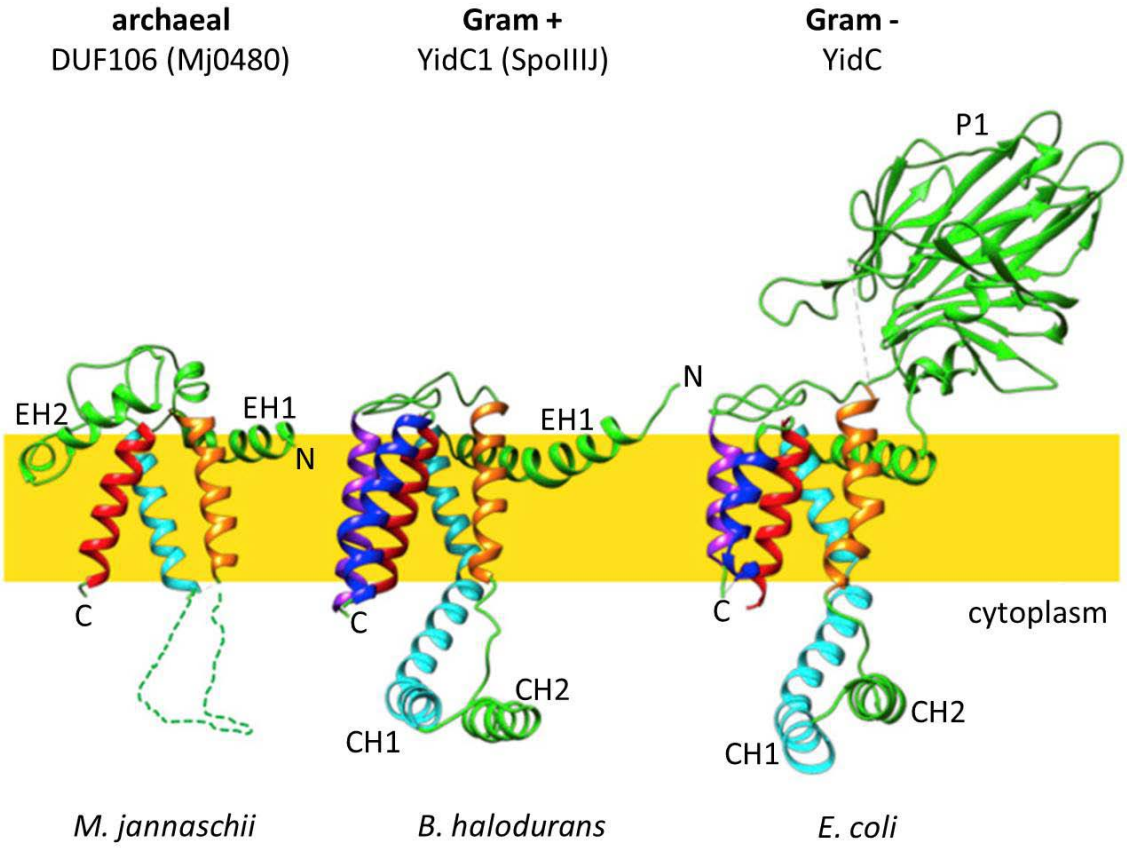

Fig. 1.13 ***Structures of the archaeal, Gram-positive and Gram-negative membrane insertases from M. jannaschii, B. halodurans and E. coli.*** *Cartoon representation of the homologous YidC proteins depicting a transverse profile through the membrane. The respective homologous TM domains are displayed in the same color code and cytosolic and periplasmic / extracellular domains in green, respectively. CH1+2: cytoplasmic helix 1 and 2; EH1+2: extracellular helix 1 and 2; P1: periplasmic loop 1. The coiled-coil C1 region of the M. jannaschii YidC, as well as TM1 and the N-terminal part of the P1 domain of the E. coli YidC are not visible in the crystal structure due to their high flexibility (Kumazaki et al., 2014-b; Borowska et al., 2015).The three structures of YidC insertases demonstrate the conservation of the basic structural elements of the membrane-embedded core domain, as well as the additional features that were added on or were lost during evolution (adapted from Dalbey and Kuhn, 2015).*

Several substrate contacts were previously reported for the *E. coli* YidC to Sec-dependent and -independent substrate proteins in *in vivo* and *in vitro* cross-linking assays (Yu *et al*., 2008; Klenner and Kuhn, 2012). Combined with the new insights of the *E. coli* YidC crystal structure, they are located in the groove between TM3 and TM5, on the exterior region of the TM as well as in the hydrophilic groove (Kumazaki *et al*., 2014-b). This leads to the assumption that residues facing the hydrophilic cavity contact the translocated, hydrophilic regions of the substrate proteins while those facing the membrane bilayer assist the insertion and lateral integration of the substrate's hydrophobic segments into the membrane (Hennon *et al*., 2015). Recently it was shown that the evolutionarily conserved positively charged arginine residue in the hydrophilic groove of YidC is crucial only in

some members of the YidC/Oxa1/Alb3 family, suggesting that there are different insertion requirements based on the characteristics of the substrates (Chen *et al*., 2014). Finally, the crystal structures of YidC provide a first insight into the unique mechanism by which YidC is inserting proteins into the membrane lipid bilayer as an independent, monomeric insertase (Kumazaki *et al.,* 2014-a). In the initial step, a single spanning membrane protein with an acidic N-terminal extracellular region, such as the Pf3 coat protein, binds electrostatically to the membrane inner surface and contacts the flexible C1 region of YidC (Fig. 1.14 A). Subsequently, the negatively charged residues in the N-tail interact, in some cases, with the conserved positively charged arginine residue in the hydrophilic groove of YidC and is then transiently captured in its aqueous cavity (Fig. 1.14 B). This binding step can induce structural changes in the hydrophilic groove to accommodate the various substrate proteins. Catalyzed by electrophoretic attraction of the positively charged membrane potential side in the periplasmic space on the negatively charged residues in the translocated region of the substrate (Chen *et al*., 2002; Zhu *et al*., 2013) and hydrophobic interaction between the substrate TM segment and YidC (Fig. 1.14 C), the N-tail is then released from the groove and crosses the outer leaflet of the membrane lipid bilayer (Fig. 1.14 D).

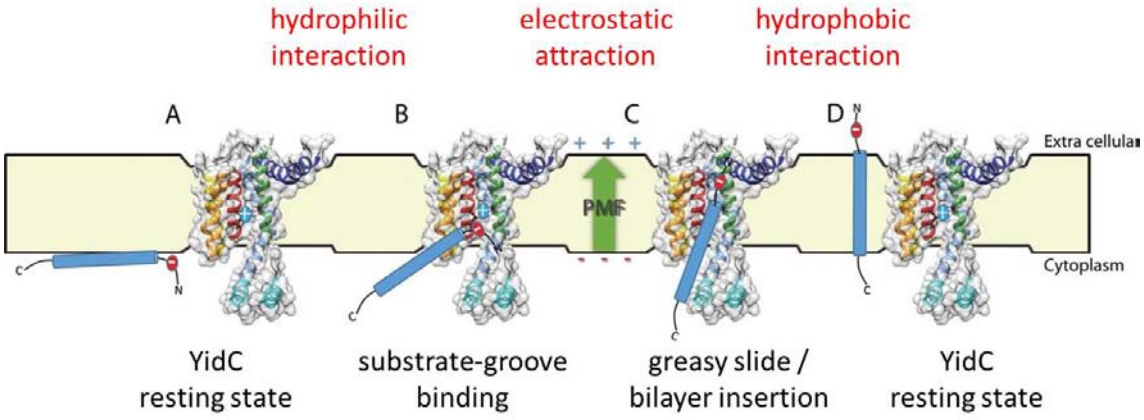

Fig. 1.14 ***Model for the insertion of a single-spanning membrane protein via YidC. (A)*** *Prior to the interaction with YidC in the resting state, the substrate protein is peripherally associated with the membrane.* ***(B)*** *The hydrophilic N-terminal region of the substrate would then be transiently captured in the hydrophilic substrate groove of YidC, possibly mediated by interaction with a cytoplasmic loop (C1) and hydrophilic interaction, resulting in the substrate-bound state of YidC.* ***(C)*** *Substrate insertion is believed to be facilitated by the proton motive force, hydrophobic interaction between the TM regions and the aliphatic chains, as well as possibly thinning of the membrane by YidC.* ***(D)*** *After successful translocation and insertion into the bilayer via a greasy slide, the substrate protein is laterally released from YidC and YidC returns to the resting state. (adapted from Kumazaki et al., 2014-a and Hennon et al., 2015)*

It is proposed that the inserting substrate TM segment moves along a greasy slide formed by TM3 and TM5 of the *E. coli* YidC in order to form a proper transmembrane configuration (Dalbey and Kuhn, 2014). To which extent this mechanism holds also true for the insertion of other YidC substrate classes like double-spanning membrane proteins, remains to be elucidated. In addition, further biological and structural studies are required to understand how the individual YidC homologs differ in their insertion mechanism and in their determinants of substrate properties that govern the YidC-dependent integration into the membrane.

In *E. coli*, the conserved arginine residue in TM2 is not essential for insertion or cell survival (Jiang *et al*., 2003), whereas the substitution of the conserved arginine residue R73 in *B. halodurans* YidC1 abolished the insertion activity of the endogenous substrate protein MifM (Kumazaki *et al*., 2014-a). As already mentioned, this underlines the fact that the conserved positively charged residue in the hydrophilic groove is critical for the insertase function only in certain YidC homologs (Chen *et al*., 2014) and some YidC substrates may use a different combination of specific structural features for insertion. Two recent studies analyzed the influence of TM segment composition and charge distribution of the translocated regions in guidance of the substrate membrane proteins into the YidC, SecYEG or YidC/SecYEG insertion pathway, respectively. Zhu *et al*. (2013) and Soman *et al*. (2014) proposed that increasing hydrophobicity in TM segments and decreasing polarity and number of charges in the translocated loop or tail region lowers the requirement of YidC or SecYEG for insertion. In addition, they showed that a positive charge in a translocated loop requires YidC and SecYEG, while a negative charge in the loop region only required YidC. These findings are in good agreement with the proposed insertion mechanism by Kumazaki *et al*. (2014-a) (Fig. 1.14). Earlier, it had been shown that Oxa1 in mitochondria was important for the insertion of proteins with highly charged domains and negative charges in the translocated region (Herrmann and Bonnefoy, 2004), proposing a conserved and specialized insertion mechanism of the YidC/Oxa1/Alb3 insertase family as respiratory proteins, their major substrates often have negatively charged residues that are essential for function (Price and Driessen, 2010). Although it was shown that charge-unbalanced TM segments more likely depend on YidC for insertion (Gray *et al*., 2011), many of the identified YidC-dependent proteins did not have unbalanced TM segments and other features obviously also influence the recruitment to and insertion via YidC.

1.3.3 YidC and the ribosome

Despite recent structural insights, our understanding of how ribosomes associate with the components of the insertion machinery, especially with YidC, is still relative scarce. Hence, further investigation of the coupling of co-translational targeting to YidC-mediated insertion might be an important step forward to understand the exact molecular mechanism of YidC-mediated membrane protein biogenesis. Due to the hydrophobic nature of the YidC substrate proteins, those nascent membrane proteins have a high risk to form insoluble, nonfunctional and non-translocation-competent aggregates. Thus, a tight coupling of the synthesis to the insertion of membrane proteins appears to be crucial. The C-terminal regions of the mitochondrial Oxa1 (89 residues; total charge +24) and *S. mutants* YidC2 (64 residues; +14) proteins have been shown to be pivotal for direct ribosome interaction (Szyrach *et al*., 2003; Jia *et al*., 2003; Wu *et al*., 2013), and deletions within these domains compromised the protein insertion efficiency. In mitochondria it is known that the C-terminal tail of Oxa1 tethers the mitochondrial ribosomes permanently to the membrane, presumably as an evolutionary consequence of the elimination of genes in the mitochondrial genome that code for hydrophilic proteins (Szyrach *et al*., 2003; Jia *et al*., 2003). Moreover this spurred the loss of an SRP-like pathway (Funes *et al*., 2009). In *E. coli,* the hydrophilic, C-terminal segment of YidC is moderately positively charged and substantially shorter (16 residues; +8) than the mitochondrial counterpart. Its role in facilitating ribosome binding was analyzed in several studies (Kohler *et al.,* 2009; Funes *et al*., 2009; Kedrov *et al*., 2013; Seitl *et al*., 2014; Geng *et al*., 2015) and is also an important scope of this work.

Cross-linking studies indicated that during membrane protein synthesis, YidC and bacterial ribosomes are in close contact (de Gier and Luirink 2003; Welte *et al*., 2012) and binding of a detergent-solubilized *E. coli* YidC dimer to translating ribosomes was visualized by cryo-EM for the first time in 2009 (Kohler *et al*., 2009), proposing an Oxa1-like insertase-ribosome complex. However, subsequent studies revealed that the addition of just six histidine residues to the C-terminus of *E. coli* YidC, as was used for the cryo-EM studies by Kohler *et al*., is sufficient to bind YidC to ribosomes (Kedrov *et al*., 2013). Moreover, Kedrov *et al.* showed that YidC binds only to ribosomes if they expose a YidC substrate from their exit tunnel and that the C-terminal domain of YidC is involved but not essential for ribosome recruitment in *E. coli*. In contrast to the data published by Kohler *et al*. (2009) describing a YidC dimer binding to ribosomes, it was shown that a single YidC copy is sufficient to bind a substrate-translating ribosome, thus being the minimal functional unit (Kedrov *et al*., 2013; Seitl *et al*., 2014). This suggests that *E. coli* ribosomes do not intrinsically associate with YidC but only when synthesizing YidC substrates or

when additional interacting sequences are added to its C-terminus (Kohler *et al*., 2009; Seitl *et al.*, 2014). Other supplementary factors, particularly the bacterial SRP and its receptor, might further contribute to this interaction *in vivo.* Since the C-terminal tail of the *E. coli* YidC was thought not to be the only determinant for its interaction with the ribosome, the positively charged cytosolic loops (C1 and C2) were suggested as potential binding partners (Kedrov *et al*., 2009; Wickles *et al*., 2014). Geng *et al*. (2015) applied both *in vivo* and *in vitro* analyses to investigate the roles played by these two cytosolic domains of *E. coli* YidC. They demonstrate that the cytosolic loop C2 and the C-terminal tail of YidC may determine binding to RNCs, while the C1 loop is essential for cell viability but not for ribosome interaction. The approximately 10 amino acid residues long C2 loop of YidC is proposed to be flexible, since the conformation of this region could not be resolved in the crystal structures of YidC (Kumazaki *et al*., 2014-a & 2014-b). The C2 loop bears one conserved charged residue (Asp488) which is essential in this position for cell viability (Wickles *et al*., 2014), and is proposed to ensures the stable docking of a translating ribosome to YidC. Further studies will be necessary to elucidate the precise interplay between YidC, SRP and the ribosome nascent chain complexes in *E. coli*.

1.4 Aims of the study

For the insertion of inner membrane proteins in *E. coli*, the membrane translocase SecYEG and the membrane insertase YidC, as well as the signal recognition particle (SRP) targeting system are of central importance. Insertion of integral membrane proteins into the lipid bilayer takes place co-translationally at membrane-associated ribosomes (Luirink and Sinning, 2004; Egea *et al*., 2005; Halic and Beckmann, 2005). Not fully clear, however, is how SRP recognizes the specific features of nascent chains of hydrophobic proteins and how the ribosome nascent chain (RNC) complexes are transferred to the respective translocase or insertase, especially in the YidC-only insertion pathway.

The primary subject of this work was to characterize and analyze in detail the function of a C-terminal ribosome-binding domain on YidC and its role in SRP mediated membrane insertion in Gram-negative bacteria. Therefore, the C-terminal ribosome-binding domains of YidC homologs from the marine Gram-negative bacteria *Rhodopirellula baltica* and *Oceanicaulis alexandrii* were fused to the short C-terminal region of the *E. coli* YidC. In order to understand the mechanism by which the YidC insertase is coupled to translating ribosomes, the determination of a cryo-EM structure of RNCs in complex with the C-terminally extended YidC was one aim of this study. Despite the structural analysis, different biochemical approaches were performed to identify the interaction mode of the C-terminal ribosome binding domains with particular ribosomal proteins of the polypeptide exit tunnel. Furthermore, *in vivo* studies in *E. coli* were performed to investigate a possible role of the C-terminally extended YidC in SRP-mediated co-translational membrane insertion of the YidC-dependent MscL protein.

The second part focuses on the interaction of the signal recognition particle with SRP signal sequences to determine the specificity of SRP recognition in proteins. The interaction studies were established in an *in vitro* system and binding affinities were determined by microscale thermophoresis (MST), a new approach that enables immobilization-free, in-solution kinetic measurements of biomolecular interactions.

Taken together, this study contributes to the understanding of the molecular mechanisms of co-translational membrane protein biogenesis in bacteria and also highlights evolutionary aspects of this complex vital cellular process.

2 MATERIALS AND METHODS

2.1 Culture media and additives

2.1.1 LB medium (Luria-Bertani)

10 g/l tryptone, 5 g/l yeast extract, 5 g/l NaCl

The pH was adjusted to 7.5 with NaOH. For the preparation of LB-agar plates, 15 g/l Agar No1 were added prior to autoclaving. Antibiotics and other additives are added after autoclaving when the medium has cooled down to approximately 50 °C.

2.1.2 Antibiotics

antibiotic	stock solution	working concentration
ampicillin	200 mg/ml ($_{dd}H_2O$)	200 µg/ml
chloramphenicol	25 mg/ml (EtOH)	25 µg/ml
kanamycin	25 mg/ml ($_{dd}H_2O$)	25 µg/ml
streptomycin	10 mg/ml ($_{dd}H_2O$)	10 µg/ml

2.1.3 Sugars

arabinose	20 %	0,2 %
glucose	40 %	0,4 %

2.2 Bacterial strains

2.2.1 *Escherichia coli* XL1-Blue

*lac thi*1 *gyrA*96 *endA*1 *hsdR*17 *relA*1 *supE*44 *recA*1 [*F' proAB lacI9 lacZ* ΔM15 Tn10]

E. coli XL1-Blue is a cloning strain with recombination deficiency, used for the amplification and subsequent isolation of plasmid DNA. The mutated lacZ gene in this strain allows blue-white screening with appropriate vectors.

2.2.2 *Escherichia coli* BL21 (DE3)

E. coli B F^- *dcm ompT hsdS* (r_B^- m_B^-) *gal λ* (DE3)

E. coli BL21 contains an integrated bacteriophage λ DE3 on its chromosome, carrying the T7 RNA-polymerase gene under the control of the *lac* promoter. This strain is used for

intense overexpression of genes which are cloned into expression vectors under the control of the bacteriophage T7 promoter. The gene expression is induced by the addition of IPTG.

2.2.3 *Escherichia coli* C41 (DE3) (Miroux and Walker, 1996)

E. coli B F$^-$ *dcm ompT hsdS* ($r_B^- m_B^-$) *gal λ* (DE3); additional uncharacterized mutations

E. coli C41 (DE3) is a derivative of *E. coli* BL21 (DE3), discovered by Miroux and Walker during screening studies of BL21 to find mutants that allow overexpression of proteins which are toxic to BL21 cells.

2.2.4 *Escherichia coli* C43 (DE3) (Miroux and Walker, 1996)

E. coli B F$^-$ *dcm ompT hsdS* ($r_B^- m_B^-$) *gal λ* (DE3); additional uncharacterized mutations

E. coli C43 (DE3) is developed from C41 during further screening studies. This strain allows over expression of particular heterologous membrane proteins which are toxic to *E. coli* C41 (DE3) cells.

2.2.5 *Escherichia coli* MK6S (Klenner *et al*., 2008)

E. coli F- *araD*139 Δ(*ara-leu*) 7696 *galE*15 *galK*16 Δ(*lac*) *X*74 *rpsL* (Str^r) *hsdR*2 ($r_k^- m_k^-$) *mcrA mcrB*1 p_{ara} YidC

MK6S is a derivative of the *E. coli* strain MC1061 (Casadaban and Cohen, 1980). In this strain the promoter region of *yidc* on the chromosome was replaced by an *araC-araBAD* promoter cassette. This allows regulation of the YidC expression by the addition of arabinose (YidC expression) or glucose (YidC depletion).

2.2.6 *Escherichia coli* MC-Ffh (Seitl *et al*., 2014)

MC1061-Kan-AraCP-ffh

The Ffh depletion strain MC-Ffh was derived from *E. coli* MC1061 by homologous recombination of the *araC-araBAD* operator region, containing a kan resistance cassette for screening, into the chromosome upstream of the *ffh* gene (2.6.11).

2.2.7 *Escherichia coli* IY26

BW25113-Kan-AraCP-ftsY

The FtsY depletion strain IY26 was obtained from E. Bibi. FtsY is under the control of the *araBAD* promoter and operator.

2.3 Plasmids

2.3.1 Complementation assay (A)

Nr. A	Vector	Gene	Modification	Cloning
1	pGZ119 EH	*Escherichia coli* YidC	-	Diploma thesis; Sandra Grenz, 2009
2	pGZ119 EH	*Rhodopirellula baltica* YidC	-	EcoR1 fragment from pGEM-Teasy
3	pGZ119 EH	Oceanicaulis YidC	-	Nde fragment from pGEM-T (diploma thesis; Ines Seitl, 2010)
4	pGZ119 EH N-His (from pET16b)	*Saccharomyces cerevisiae* mOxa1	mature Oxa1, without mitochondrial targeting sequence	Nde / BamH1 from pUC18
5	pGZ119 EH	YidC-Rb	*E. coli* YidC 1-540 and *R. baltica* YidC 748-827	Nde (diploma thesis Ines Seitl, 2010)
6	pGZ119 EH	YidC-Oa	*E. coli* YidC 1-540 and *O. alexandrii* YidC 575-673	
7	pGZ119 EH	YidC-Oxa	*E. coli* YidC 1-540 and *S. cerevisiae* Oxa1 272-360	Nde

Genomic DNA from *R. baltica* and *O. alexandrii* was used to amplify the homologous *yidC* genes with an Nde restriction site, serving as start codon. The second Nde site was

obtained by cloning the PCR product into pGEM-T / pGEM-T easy vectors. Based on this constructs, the *yidC* genes can be cloned by Nde restriction in several other vectors.

Three chimeric proteins of the *E. coli* YidC were constructed (YidC-Rb, YidC-Oa, YidC-Oxa) with the C-terminal region of YidC replaced. First, an NsiI restriction site at the codon representing the amino acid position 539 of the *E. coli* YidC was introduced using site-directed mutagenesis. The C-terminal extensions of both marine YidC homologs and Oxa1 were amplified with flanking Nsi sites. The resulting PCR products were digested with Nsi and cloned into *E. coli yidC* resulting in YidC-Rb, YidC-Oa and YidC-Oxa fusion proteins.

2.3.2 Protein overexpression and purification (B)

Nr. B	Vector	Gene	Modification	Cloning
1	pET16b	*Escherichia coli* YidC (Ec-YidC)	N-terminal His_{10} Tag	Nde
2	pET16b	*Oceanicaulis alexandrii* YidC (Oa-YidC)	N-terminal His_{10} Tag	Nde from pGEM-T
3	pET16b	YidC-Rb; chimeric gene EcYidC-RbCT	N-terminal His_{10} Tag	Nde from pGZ 119 EH
4	pET 16b	YidC-Oa; chimeric gene EcYidC-OaCT	N-terminal His_{10} Tag	Nde from pGEM-T
5	pET 16b	RbCT	*R. baltica* YidC 748-827 N-terminal His_{10} Tag	Nde-Xho (PCR)
6	pET 16b	OaCT	*O. alexandrii* YidC 575-673 N-terminal His_{10} Tag	Nde-Xho (PCR)

7	pET 22b	A3CT	*A. thaliana* Alb3 349-462 C-terminal His_6 Tag	Nde-Xho (PCR)
8	pET 16b	O1CT no signal seq. no target seq.	*S. cerevisiae* Oxa1 272-360 N-terminal His_{10} Tag	Nde-Xho (PCR)
9	pET 16b	*Escherichia coli* L23; ribosomal protein	N-terminal Strep-Tag	Nco-BamH1 (PCR)
10	pET 16b	*Escherichia coli* L24; ribosomal protein	N-terminal Strep-Tag	Nco-BamH1 (PCR)
11	pET 16b	*Escherichia coli* L29; ribosomal protein	N-terminal Strep-Tag	Nco-BamH1 (PCR)
12	pMS119-Nco	*Escherichia coli* Ffh	N-terminal Strep-Tag	Nco-EcoR1 (PCR)
13	pMS 119-Nco	*Escherichia coli* Ffh	C-terminal Strep-Tag	Nco-EcoR1 (PCR)
14	pMS 119-Nco	*Escherichia coli* Ffh C406S / M423C; single cys mutant	C-terminal Strep-Tag	Quick-change (Nr. B 13)

The PCR primers for the generation of the C-terminal YidC peptides from *R. baltica* YidC (RbCT), *O. alexandrii* YidC (OaCT), *A. thaliana* Alb3 (A3CT) and *S. cerevisiae* Oxa1 (O1CT) contained flanking Nde and Xho restriction sites. This allowed direct cloning into the respective expression vectors (pET16b and pET22b).

The ribosomal proteins L23, L24 and L29 from *E. coli* were cloned by Emmanuelle Mboubi Kouaga during her Master thesis work in this lab (Strukturelle Dynamik der ribosomalen Proteine L23, L24 und L29 bei der Interaktion mit Membraninsertasen, 2013).

2.3.3 Pulse chase assay (C)

Nr. C	Vector	Gene	Modification	Cloning
1	pGZ119 HE	*Oceanicaulis alexandrii* YidC	N-terminal His_{10} Tag	Xba-EcoR1 from pET16b
2	pGZ119 HE	*Escherichia coli* YidC	N-terminal His_{10} Tag	Nde from pET16b into pGZ119 HE *Oceanicaulis alexandrii* YidC
3		YidC-Rb		
4		YidC-Oa		
5		YidC-Oxa		
6	pGZ119 HE	*Escherichia coli* Ffh	N-terminal His_{10} Tag	Nde from pGEM-T into pGZ119 HE *Oceanicaulis alexandrii* YidC
7	pMS119 EH	*Escherichia coli* MscL I68C; single cys mutant	N-terminal His_{10} Tag	Facey *et al*., 2007 (pSF147)

For the pulse chase analyses (2.9) the YidC constructs were cloned into the pGZ119 HE vector by Nde restriction. In this vector the *yidC* genes are under the control of the *tac* promoter and the ColD replicon allowed coexpression of the proteins with pMS119EH-MscLI68C.

2.3.4 Fluorescence microscopy (D)

Nr. D	Vector	Gene	Modification	Cloning
1	pMS 119 EH	*E. coli* MscL	C-terminal GFP fusion ; N-terminal His_{10} Tag	Xba-HindIII from pSF195 into pSF147 (Facey *et al*., 2007)

2.3.5 *In vitro* transcription (E)

Nr. E	Vector	Gene	Modification	Cloning
1	pUC18	4.5S RNA of *E. coli* SRP	T7 promoter sequence	I. Sinning group; BZH

2.4 PCR primer

Primers for cloning of ***Rhodopirellula baltica* YidC** (Rb-YidC)

Rhoba*Nde*: [5`- 3`]: A GGA GGT TGA *CAT ATG* GCC GAC AGT TCA GTG GAA CGC CGA C

Rhoba*Chistag*(Hind) [5`- 3`]: C GAA AAG CTT CTA *ATG GTG ATG GTG ATG GTG ATG GTG ATG GT*G ACC **GCG GCG TTT CTT GTT GCC GGG**

Template DNA: Rb-YidC in pGEM-T

Primers for cloning of **YidC-Rb**

Ribo*Nsi*-fw: [5`- 3`]: GGC GGC CGC *ATG CAT* CCAT CGA AGC CTC ACT TC

Ribo*Nsi*-rv: [5`- 3`]: C GCG GCC GCA TGC *ATG CAT* GCG GCG TTT CTT GTT G

Template DNA: Rb-YidC in pGEM-T

Primers for cloning of ***Oceanicaulis alexandrii* YidC** (Oa-YidC)

1) Ocean-fw: [5`- 3`]: CGC CCT CAA AAC CGT AAG GGA CCG

Ocean-rev: [5`-3`]: CCT GGG CTT CGG GAG AGG GCT C

Template DNA: chromosomal DNA from *O. alexandrii*

2) Ocean- *Nde*-fw: [5`-3`]: *CAT ATG* GGT GAG AAC CGC AAT TTC CTG

Ocean-*TAG*-rev: [5`-3`]: *CTA* TTT CTT CTT GCC GCC GCG

Template DNA: Oa-YidC from 1) in pGEM-T

Primers for cloning of **YidC-Oa**

Ocean-Rib-fw (*Nsi*): [5`- 3`]: GGC GGC CGC *ATG CAT* CGT CAG GGC GTG GTG ACC

Ocean-Rib-rev (*Nsi*): [5`- 3`]: CGC GGC CGC *ATG CAT* CTA TTT CTT CTT GCC GCC

Template DNA: Oa-YidC from 1) in pGEM-T

Primers for cloning of **YidC-Oxa**

O1CT-*Nsi* fw: [5`- 3`]: GA TAC *ATG CAT* ATG ATT TTG AGA AAC AAA TGG

O1CT-*Nsi* rev: [5`- 3`]: GC ACG *ATG CAT* TCA TTT TTT GTT ATT AAT GAA G

Template DNA: *Saccharomyces cerevisiae* mOxa1 in pUC18

Primers for cloning of **RbCT N-His$_{10}$**

Rhoba-*Nde*: [5`- 3`]: GG AAA AAA CGT *CAT ATG* CAT CCA TCG AAG

Rhoba-*Xho*-**Stop:** [5`- 3`]: G ATA TTC *CTC GAG* **CTA** GCG GCG TTT C

Template DNA: YidC-Rb in pGZ119EH

Primers for cloning of **RbCT C-His$_6$**

Rhoba-*Nde*: [5`- 3`]: GG AAA AAA CGT *CAT ATG* CAT CCA TCG AAG

Rhoba-*Xho*-2: [5`- 3`]: G ATA TTC *CTC GAG* GCG GCG TTT C

Template DNA: YidC-Rb in pGZ119EH

Primers for cloning of **OaCT N-His$_{10}$**

Ocean-*Nde*: [5`- 3`]: G GAA AAA CGT *CAT ATG* CAT CGT CAG GG

Ocean-*Xho*-**Stop**: [5`- 3`]: GAT ATC *CTC GAG* **CTA** TTT CTT CTT GCC G

Template DNA: YidC-Oa in pGZ119EH

Primers for cloning of **OaCT C-His$_6$**

Ocean-*Nde*: [5`- 3`]: G GAA AAA CGT *CAT ATG* CAT CGT CAG GG

Ocean-*Xho*-2: [5`- 3`]: GAT ATC *CTC GAG* TTT CTT CTT GCC G

Template DNA: YidC-Oa in pGZ119EH

Primers for cloning of **A3CT N-His$_{10}$**

Alb-*Nde*: [5`- 3`]: GAT ATC *CAT ATG* AAT AAT GTA CTT AGT ACC GCC

Alb-*Xho*-**Stop**: [5`- 3`]: GAT ATC *CTC GAG* **CTA** TAC AGT GCG TTT CCG

Template DNA: Alb3CT in pET21d provided by I. Sinning, University of Heidelberg

Primers for cloning of **A3CT C-His$_6$**

Alb-*Nde*: [5`- 3`]: GAT ATC *CAT ATG* AAT AAT GTA CTT AGT ACC GCC

Alb-*Xho*-2: [5`- 3`]: GAT ATC *CTC GAG* TAC AGT GCG TTT CCG

Template DNA: Alb3CT in pET21d provided by I. Sinning, University of Heidelberg

Primers for cloning of **O1CT N-His$_{10}$**

Oxa1-*Nde*: [5`- 3`]: GAT ATC *CAT ATG* ATT TTG AGA AAC AAA TGG

Oxa1-*Xho*-**Stop**: [5`- 3`]: GCA TGC *CTC GAG* **TCA** TTT TTT GTT ATT AAT G

Template DNA: *Saccharomyces cerevisiae* mOxa1 in pUC18

Primers for cloning of **Ffh N-Strep**

Ffh *Nco* **Strep** fw: [5`- 3`]: *CC ATG G*CA AGC **TGG AGC CAC CCG CAG TTC GAA AAG** GGT TTT GAT AAT TTA ACC GAT CG

Ffh *Eco*-**Bam** rev: [5`- 3`]: **GGA TCC** *GAA TTC* TTA GCG ACC AGG GAA GCC TGG

Template DNA: Ffh N_{His} in pGZ119HE

Primers for cloning of **L23, L24 and L29**

Master thesis MSc Emmanuelle Mboubi, 2013; University of Hohenheim

Primers for cloning of **Ffh C-Strep / Ffh C-His_{10} Prescission**

Ffh *Nco* fw: [5`- 3`]: *CC ATG G*CA TTT GAT AAT TTA ACC

Ffh *Mun*-**Strep**-Eco rev: [5`- 3`]: GAA TTC TTA **CTT TTC GAA CTG CGG GTG GCT C*CA*** *ATT G*CC GCG ACC AGG GAA GCC TGG

Template DNA: Ffh N_{His} in pGZ119HE

2.5 Peptide synthesis

The N-terminal KdpD-peptides for SRP binding studies via Microscale Thermophoresis (2.17) were synthesized by the Custom peptide synthesis services from GENOSPHERE Biotechnologies (France).

The 27 amino acid residues long peptides were synthesized with N-terminal acetylation and C-terminal amidation and a purity of > 95 %.

The following three synthesized peptides were shipped and stored in lyophilized form at -80 °C:

$N22\text{-}48_{pep}$: $_{N\text{-acetyl}}$RGKLKVFFGACAGVGKTWAMLAEAQRL $_{C\text{-amid}}$

$W3A_{pep}$: $_{N\text{-acetyl}}$RGKLKVFFAACAAVAKTWAMLAEAQRL $_{C\text{-amid}}$

$3Q_{pep}$: $_{N\text{-acetyl}}$QGQLQVFFGACAGVGKTWAMLAEAQRL $_{C\text{-amid}}$

Solution conditions: 3 mg/ml in ddH_2O

Molecular Weight: ~ 2 951 Da

Ɛ = 5 500 approx.

2.6 Methods in molecular biology

2.6.1 Polymerase chain reaction (PCR)

Polymerase chain reaction was used to amplify DNA fragments for cloning *in vitro* using the GoTaq polymerase (Promega) from *Thermus aquaticus* according to the manufacturer´s protocol.

The cycle of denaturation (95 °C), annealing (X °C) and elongation (72 °C) is repeated for 30 steps. The annealing temperature varies according to the melting temperatures (T_m) of the used primer pair (approximately 5°C below the calculated melting point of the primer with the lowest T_m). The duration of the elongation step depends on the DNA polymerase and on the length of the DNA fragment to be amplified.

Reaction mixture:

Component	**Final Volume**	**Final Concentration**
5X Green GoTaq reaction buffer	10 µl	1X (1,5 mM $MgCl_2$)[2]
dNTP Mix (10 mM each)	1 µl	0,2 mM each dNTP
upstream primer (10 µM)	3 µl	0,6 µM
downstream primer (10 µM)	3 µl	0,6 µM
GoTaq Polymerase (5 u/µl)	0,25 µl	1,25 u
template DNA	X µl	<0,5 µg / 50µl
nuclease-free water to	50 µl	

Thermal cycling conditions:

Step	**Temperature**	**Time**	**Number of Cycles**
Initial Denaturation	95 °C	2 min	1
Denaturation	95 °C	30 sec	
Annealing	X °C	30 sec	30
Elongation	72 °C	1 min/kb	
Final Elongation	72 °C	5 min	1
Soak	7 °C	∞	1

The PCR products were then separated by agarose gel electrophoresis in the presence of EtBr under UV light. Reactions performed with the 5X Green GoTaq reaction buffer were loaded onto the gel directly after amplification.

2.6.2 Agarose gel electrophoresis

The concentration used for gels in this work was between 0,7 % and 1 % (w/v) agarose (Biozym) in 1X TAE buffer (40 mM Tris base, 20 mM acetic acid, 1 mM EDTA) and 2 µl of an ethidium bromide solution (Sigma, 10 mg/ml). DNA samples were mixed 5:1 with 6X loading dye (0,25 % bromophenol blue, 0,25 % Xylene cyanol, 15 % Pharmacia Ficoll400, 60 mM EDTA) prior to loading into the wells of the gel and run for 60-90 min at a constant voltage of 70 V. DNA bands were visualized at a wavelength of 302 nm and documented using the UV light documentation system Diana v1.6 (raytest, Straubenhardt).

2.6.3 Restriction digest of DNA

For cloning of defined DNA fragments into vectors it is necessary to digest the DNA with restriction endonucleases (Fermentas). These enzymes cleave DNA strands near or at specific recognition sequences and create blunt or sticky ends.

In general, an 20 µl restriction mixture was composed of 18 µl DNA, 1 µl conventional (10 U/µl) or FastDigest restriction enzyme (1 FDU/µl) and 1 µl of the appropriate 10x reaction buffer. The restriction digest was incubated at 37 °C for 30 min using FastDigest enzymes or 2 h using conventional endonucleases.

The restriction reactions were subjected to agarose gel electrophoresis and the DNA fragments of interest were cut out from the gel. For the isolation of DNA from agarose gels, the GeneJET^{TM} Gel Extraction Kit (Thermo Fisher Scientific) was used according to the manufacturer´s protocol.

2.6.4 Ligation of DNA fragments

Ligation of digested DNA fragments after isolation from an agarose gel was performed with T4 DNA ligase (Fermentas). For a standard 10 µl ligation reaction, a threefold molar excess of the insert DNA-fragment was added to the linearized vector and mixed with 1 µl 10x ligation buffer and 1 µl T4 DNA ligase. The ligation reaction was incubated for 2 hours at 22 °C or overnight at 4°C and transformed into chemically competent *E. coli* XL1 cells (5 µl ligation mixture / 50 µl XL1).

2.6.5 Transformation of chemically competent *E. coli* cells

For transformation of chemically competent *E. coli* cells (2.2) 1 µl of plasmid DNA or 5 µl of ligation mixture (2.6.4) was incubated with 50 µl thawed cells for 20 min on ice. A heat shock at 42 °C for 90 sec allows the DNA to enter the bacterial cells. After incubation for 5 min on ice, 1 ml LB medium was added and incubated for 1 h at 37 °C on a shaker. Prior to centrifugation (2 min; 3000 rpm) 100 µl of the sample was directly plated onto an antibiotic containing LB agar plate. The cell pellet was resuspended in 100 µl LB medium and also plated for overnight growth at 37 °C.

2.6.6 Preparation of chemically (RbCl) competent *E. coli* cells

The rubidium chloride (RbCl) method was used to prepare competent cloning and expression strains of *E. coli*, since this method allows long term storage of the competent cells at -80 °C without significant loss of competence.

100 ml LB medium was inoculated 1:100 from an overnight culture of the respective strain and grown to an OD_{600} of 0.6 at 37 °C. The cells were harvested in a sterile JLA14.500 tube for 15 min at 3000 g and 4 °C. The cell pellet was carefully resuspended in 10 ml ice cold TFB1 buffer (100 mM RbCl, 50 mM $MnCl_2$, 30 mM KAc, 10 mM $CaCl_2$, 15 % glycerol; pH 5.8) on ice and incubated for 90 min. After a second centrifugation (15 min, 3000 g, 4 °C) in a sterile JA25.50 tube, the cell pellet was resuspended in 2,5 ml ice cold TFB2 buffer (10 mM MOPS, 10 mM RbCl, 75 mM $CaCl_2$, 15 % glycerol; pH 8). The competent cells were aliquoted and shock frosted in liquid nitrogen for storage at -80 °C.

2.6.7 Isolation of plasmid DNA from bacterial cultures

The Zyppy^{TM} Plasmid Miniprep Kit (Zymo Research) was used to isolate the plasmid DNA according to the manufacturer´s protocol with a few modifications.

2 ml LB medium containing the appropriate antibiotics was inoculated with a single colony picked from the transformation plate and incubated overnight at 37 °C. The cells were pelleted (1 min, 13 000 rpm), resuspended by vortexing in 600 µl 1x TE buffer (10 mM Tris-HCl pH 7.5, 1 mM EDTA) and mixed carefully with lysis buffer and neutralization buffer. After two washing steps, a centrifugation step of the empty column was performed to remove the ethanol contained in the second wash buffer completely from the column. The DNA was eluted by 50 µl preheated $_{dd}H_2O$ (56 °C).

2.6.8 DNA sequencing (Sanger *et al*., 1977)

The Thermo Sequenase™ Cycle Sequencing kit from USB was used to sequence DNA by a modified dideoxy chain termination method according to Sanger with fluorescently labeled primers.

The sample was divided into four separate amplification reactions, containing all of the deoxynucleotides (dNTPs). Additionally each reaction contained one of the four dideoxynucleotides (ddATP, ddCTP, ddGTP, ddTTP) which causes the chain termination when incorporated into the extending DNA strand (termination mix). This resulted in a mixture of different elongated DNA fragments which were separated by polyacrylamide-urea gel electrophoresis and detected by an infrared laser at 700 nm or 800 nm, respectively (primer dependent).

Four PCR tubes were prepared by adding 4 µl of the respective termination mix and 4 µl of the master mix (13 µl template DNA, 2 µl reaction buffer, 1 µl primer [2 pMol], 1,5 µl thermosequenase [4 U/µl]).

Thermal cycling conditions:

Step	Temperature	Time	Number of Cycles
Initial Denaturation	95 °C	2 min	1
Denaturation	95 °C	30 sec	
Annealing	X °C	30 sec	40
Elongation	72 °C	1 min	
Final Elongation	72 °C	3 min	1
Soak	7 °C	∞	1

The sequencing reaction was terminated by adding 3 µl of stopping buffer (95 % formamide, 10 mM EDTA, 0,1 % Basic Fuchsin, 0,01 % Bromophenol Blue, pH 9). The samples were heated to 72 °C for 2 min and 1,7 µl of each reaction was loaded onto the sequencing gel (1X TBE [89 mM Tris-HCl pH 8, 89 mM boric acid, 2 mM EDTA], 6 % acrylamide [Long Ranger], 7 M Urea, 0,05 % APS, 0,05 % TEMED).

2.6.9 Site-directed mutagenesis (Quikchange)

The Quikchange mutagenesis is a method that allows the introduction of site-specific mutations into plasmid DNA. Two complementary primers, containing the desired

mutation in the middle, are used to linearly amplify the entire plasmid with a non-strand-displacing DNA polymerase (Pfu-Ultra II, Stratagene).

This method was used to create the single cysteine mutant of Ffh (2.3 plasmid B14) with the following primers (the respective complementary primer is not shown):

- *Ffh C406**S***: removal of the wildtype cysteine residue at position 406
  5`CGT ATT GCT GCC GGT **TCC** GGT ATG CAG GTG CAG G 3`

- *Ffh M423**C***: introduction of a cysteine residue at position 423
  5` CAG TTC GAC GAC **TGC** CAG CGC ATG ATG 3`

To mutate both amino acid residues at once, a double mutagenesis with both primer pairs Ffh C406S and Ffh M423C in one PCR reaction, was performed.

Reaction mixture:

Component	**Final Volume**	**Final Concentration**
Pfu Ultra II buffer (10x)	5 µl	1X
dNTP Mix (10 mM each)	1 µl	0,2 mM each dNTP
each primer (10 µM)	0,5 µl	0,1 µM
Pfu Ultra II Polymerase	1 µl	
template DNA	X µl	200 ng / 50µl
Nuclease-Free Water to	50 µl	

Thermal cycling conditions:

Step	**Temperature**	**Time**	**Number of Cycles**
Initial Denaturation	95 °C	3 min	1
Denaturation	95 °C	1 min	
Annealing	56 °C	1 min	20
Elongation	68 °C	15 min	
Final Elongation	68 °C	10 min	1
Soak	12 °C	∞	1

The methylated template plasmid DNA was digested by adding 1 µl DpnI and incubating for 2 h or overnight at 37 °C. Immediately, 10 µl of the reaction were transformed into 100 µl competent XL-1 cells, while the rest the sample was precipitated with EtOH (2.6.10).

2.6.10 EtOH precipitation of plasmid DNA

The DNA sample was transferred into a 1,5 ml Eppendorf tube and 1/10 Vol. 3M Na acetate pH 5.2 and 2,5 Vol. EtOH (100 %) were added. The precipitate was incubated at -20 °C for at least 1 h or overnight, centrifuged for 20 min at 17 000 g, 4 °C and dried in the speedvac for 30 min. The precipitated DNA was solved in 10 µl 1x TE (10 mM Tris-HCl pH 7.5, 1 mM EDTA) and transformed into 100 µl competent XL-1 cells.

2.6.11 Homologous recombination to generate the *E. coli* strain MC-Ffh

The Ffh depletion strain MC-Ffh (2.2.6) was derived from *E. coli* strain MC1061 (Casadaban and Cohen, 1980) by homologous recombination of the *araC-araBAD* operator region together with a kanamycin cassette as a selective marker into the chromosome upstream of the *ffh* gene (Datsenko and Wanner, 2000).

1. Preparation of $P1_{wt}$-phage lysate

For the preparation of the $P1_{wt}$-lysate an overnight culture of MC 4100 was used to inoculate 2,5 ml LB medium 1:100. The culture was grown to an OD_{600} of 0.4 then 10 mM $CaCl_2$ and 10 µl $P1_{wt}$ ($P1_{vir}$) lysate were added. Continuing growth for about 2,5 h at 37 °C led to the complete lysis of the cells. To isolate the phages the lysed culture was mixed with a few drops of chloroform and stood still for 10 min until the chloroform separated. 2 ml from the supernatant was transferred to an Eppendorf tube and centrifuged for 5 min at 17 000 g. The supernatant contained the $P1_{wt}$ –lysate and was transferred to a new Eppendorf tube. The lysate was stored at 4 °C.

2. Amplification of the *kan-ara* cassette for promoter exchange of *ffh*

To integrate the araC-araBAD operator region into the chromosomal *ffh* promoter region of the *E. coli* strain DY330 by homologous recombination, a PCR reaction was performed to amplify the *kan-ara* cassette with primers containing flanking regions of the upstream *ffh* promoter sequence and the start region of the *ffh* gene.

The *ffh* gene is monocistronic so that no other genes are affected by the promoter exchange (Fig. 2.1).

Fig. 2.1 ***Vicinity of ffh on the E. coli chromosome.*** *The upstream gene of ffh (ypjD) does not reach into the promoter region of ffh. The ffh gene is located in an antisense direction on the complementary strand of the DNA.*

The following primers were used for the amplification of the *kan-ara* cassette:

ffh-prom (fw): T_m match 66 °C

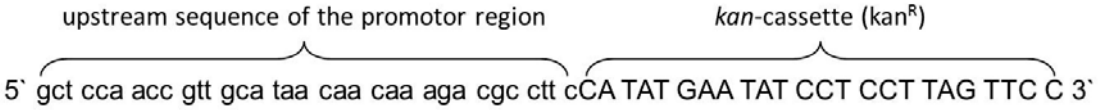

ffh-start (rev): T_m match 64 °C

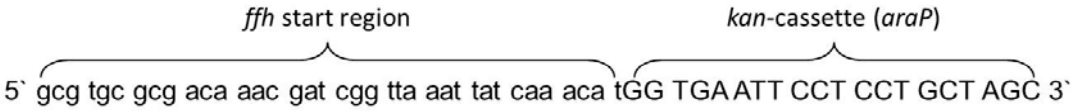

The PCR reaction was performed according to the standard protocol (2.6.1) with additional 1 mM $MgCl_2$. The annealing temperature was set to 62 °C and as template DNA an isolated *kan-ara*-cassette fragment from IY26 was used. The expected PCR fragment had a size of 2500 bp, including the *kan-ara-cassette* (~2400 bp) with flanking regions of the upstream promoter sequence and the start region of *ffh* (2.2).

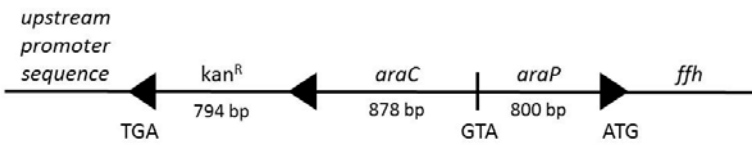

Fig. 2.2 ***PCR fragment of the kan-ara-cassette with flanking ffh regions****. The kan-ara-cassette consists of the coding regions for a kanamycin resistance (kan^R), the regulator gene araC and the structural genes of araP (araBAD). The genes araC and araBAD are transcribed in opposite directions.*

3. Preparation of electro competent DY330 cells

The linear *ffh-kan-ara* fragment was transformed by electroporation into the DY330 strain. This strains allows temperature induced (42 °C) expression of the Rec proteins, which are necessary for homologous recombination. The electro competent DY330 cells were always prepared freshly before use.

100 ml LB were inoculated 1:100 with an overnight culture of DY330 and grown at 30 °C (no expression of Rec proteins) to an OD of 0.8. The culture was divided into halves, one was grown at 30 °C and the other one at 42 °C (expression of Rec proteins) for 15 min. The cells were cooled down on ice for 15 min and harvested in sterile JA 25.50 tubes for 8 min at 7 000 rpm, 4 °C. After two washing steps with 4 ml $_{dd}H_2O$ and one step with 1,5 ml $_{dd}H_2O$ in an Eppendorf tube, the cell pellets were resuspended in 400 µl $_{dd}H_2O$ and immediately used for electroporation. It is possible to store the electro competent cells at -80 °C in a 20% glycerol solution, but then the transformation efficiency is strongly reduced.

4. Electroporation of DY330 with the *ffh- kan-ara* cassette

For the transformation of the linear DNA fragment 40 µl electro competent DY330 cells (42 °C, rec+) were incubated with 2 µl *ffh-kan-ara* cassette (Fig. 2.2) for 1 min on ice. As a negative control the same was performed with DY330 cells grown at 30 °C (rec -). The approaches were transferred into an Epo-cuvette and pulsed according to the manufacturer's protocol. Immediately after electroporation, 1ml SOC-Ara media (2,5 % tryptone, 0,5 % yeast, 10 mM NaCl, 2,5 mM KCl, 10 mM $MgCl_2$, 10 mM $MgSO_4$, 0,2% arabinose) was given to the cells, then transferred into a sterile plastic tube and incubated at 42 °C for 15 min in the shaker. Subsequently, the cells were grown for 1,5 more hours at 30 °C and then plated on LB-kanamycin (25 µg/ml) + arabinose (0,2 %) plates. The candidates were patched on LB-kan-arabinose and LB-kan-glucose (0,4 %) plates, respectively. Colonies which showed growth on arabinose plates, but not on glucose plates have the *ffh-kan-ara* cassette integrated in their chromosome by homologous recombination and were used to inoculate 2 ml LB-kan-ara media for the following P1-DY330 kan ara-lysate preparation.

5. Preparation of the $P1_{DY330\ kan\ ara}$ lysate

The overnight cultures of each candidate were used to inoculate 2,5 ml LB-kan-ara media and were grown to an OD of 0.3 at 30 °C. At this point 10 mM $CaCl_2$ and 20 µl $P1_{wt}$-lysate were added and incubated on the shaker for 3 h at 30 °C. To isolate the phages the lysed culture was mixed with 50 – 100 µl chloroform and stood on ice for 5 min until the

chloroform separated. 2 ml from the supernatant was transferred to an Eppendorf tube and centrifuged for 2 min at 16 000 g. The supernatant contained the $P1_{DY330\ kan\ ara}$ lysate and was transferred to a new Eppendorf tube. The lysate was used to transduce the target strain MC1061.

6. Transduction of MC1061 with the $P1_{DY330\ kan\ ara}$ lysate

An overnight culture of the recipient strain (MC1061) in 2 ml LB was used to inoculate (1:100) 4 ml LB media. The cells were grown at 37 °C to an OD_{600} of 0.8 and 10 mM $CaCl_2$ was added. Three reactions were set up, each consisting of 1 ml recipient mixture and 100 µl $P1_{DY330\ kan\ ara}$ lysate, mixed and incubated for 20 min, 30 min and 40 min at room temperature, respectively. To each reaction 100 µl 1 M sodium citrate was added to avoid additional phage adsorption, incubated for 1 h at 37 °C in the shaker and plated on LB plates with kanamycin, arabinose and sodium citrate. After an incubation over night at 37 °C the colonies were plated for another three times on LB-kan-ara-Na-citrate plates to remove the P1 phages completely. Finally, single colonies were patched on LB-ara and LB-glc plates and candidates who showed only growth on the arabinose plates were used for chromosomal control PCRs.

7. Control PCRs of the MC-Ffh candidates

To analyze whether the kan-ara cassette was correctly integrated into the chromosomal region downstream of *ffh,* four control PCRs were performed. Therefore chromosomal DNA of the respective MC-Ffh candidates was isolated and used as template for the PCR reaction with the following primers:

PCR 1: ypjD-stop / ffh-rev

ypjD-stop: 5` GGA CAA TTC GGC TGC CGA AGT AGG 3`

ffh-rev: 5` CGG TGC CAA AAT GGC AAA CAA GCC 3`

expected fragment length: 4622 bp

PCR 2: kan / ffh rev

kan: 5` CCC AAT AGC AGC CAG TCC CTT CC 3`

expected fragment length: 3030 bp

PCR 3: araC / ffh rev

araC: 5` GTA CCC GAT TAT CCA TCG GTG GAT GG 3`

expected fragment length: 2241 bp

PCR 4: ffh-fw / ffh-rev

ffh-fw: 5` GGC CAA CCG TTT CCA CCC CAG G 3`

expected fragment length: no fragment

➔ ffh-fw binds to the wild type promoter region of *ffh* which should be deleted in the correct candidate

As a negative control, the same PCR reactions were performed with chromosomal DNA from the MC1061 parent strain. The expected fragment sizes were 2154 bp (ypjD-stop / ffh-rev), 1362 bp (ffh-fw / ffh-rev) and no fragments for the kan and araC / ffh-rev PCRs.

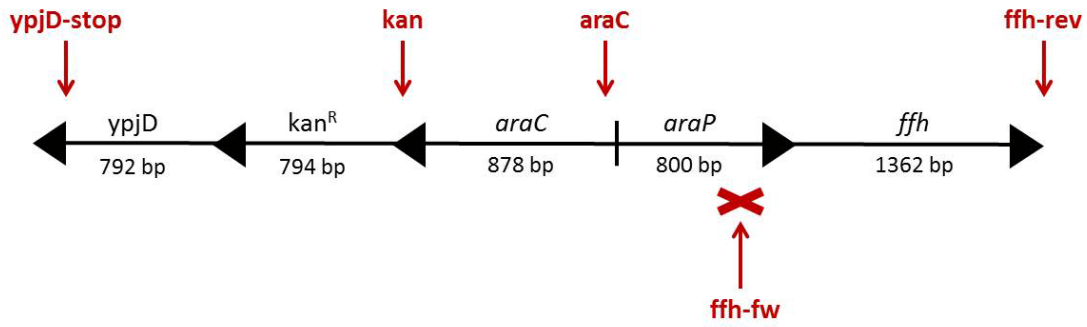

Fig. 2.3 ***Overview of the chromosomal control PCRs.*** *Four control PCRs were performed to check the correct localization of the kan-ara-cassette downstream of ffh. Each reaction contained the ffh-rev primer and one of the primers ypjD-stop, kan, araC and ffh-fw, respectively. The PCR reaction with ffh-fw should not give a PCR fragment, since the respective binding site is lost during the homologous recombination.*

The depletion of Ffh in the MC-Ffh candidates that showed correct PCR fragments was tested via an expression test in LB-ara and LB-glc media and the Ffh level was detected with an antibody against the Ffh protein. The strain has to be grown for at least 3 h in glucose media to deplete Ffh completely. The expression of a plasmid encoded *ffh* rescued the lethal phenotype of MC-Ffh on LB-glc-IPTG plates in the complementation assay (2.7).

2.6.12 *In vitro* transcription

To synthesize the 4.5S RNA of the *E. coli* SRP the Thermo Scientific™ TranscriptAid™ T7 High Yield Transcription Kit was used.

1. DNA template preparation for *in vitro* transcription

Linearized plasmid DNA can be used as template for transcription if it contains a double-stranded RNA polymerase promoter region in the correct orientation. For the transcription of the 4.5S RNA the pUC18 plasmid (2.3 E1) was used with the integrated consensus promoter sequence for the T7 RNA polymerase (TAATACGACTCACTATAGGG). G will be the first base (+1) of the RNA transcript. The 4.5S RNA sequence was placed downstream of the promoter to synthesize sense RNA. To produce RNA transcripts of a defined length, the plasmid DNA has to be linearized by restriction digestion downstream of the insert prior to *in vitro* transcription. The pUC18-4.5S RNA plasmid was linearized by BamHI and gel purified with a DNA Gel Extraction Kit (GeneJet™, Thermo Fisher Scientific).

2. Phenol / chloroform extraction

The template DNA should have an A260/280 ratio of 1.8 - 2.0. Otherwise it is recommended to purify the DNA template by phenol/chloroform extraction using the following protocol:

- Add 1/10 volume of 3 M Sodium Acetate Solution to the DNA.
- Mix thoroughly.
- Extract with an equal volume of a 1:1 phenol/chloroform mixture, and then twice with an equal volume of chloroform. Collect the aqueous phase and transfer to a new tube.
- Precipitate the DNA by adding 2 volumes of ethanol. Incubate at – 20 °C for at least 30 min and collect the pellet by centrifugation.
- Remove the supernatant and rinse the pellet with 500 µl of cold 70 % ethanol.
- Resuspend the DNA in 20 µl of DEPC-treated Water (0,1 % (v/v) DEPC incubated overnight and autoclaved).

3. *In vitro* transcription protocol

The following reaction components were combined at room temperature in the given order:

Component	Amount
DEPC-treated water	to 20 µl
5X TranscriptionAid Reaction Buffer	4 µl
ATP/CTP/GTP/UTP mix	8 µl
Template DNA	1 µg
TranscriptAid Enzyme Mix	2 µl

The reaction was mixed thoroughly, spun briefly to collect all drops and incubated at 37 °C for 3 h. Immediately after the *in vitro* transcription the RNA was purified by the RNA Clean & Concentrator^{TM} -25 Kit from Zymo Research and analyzed on a 2 % native agarose gel in 1X Tris-borate-EDTA buffer from Sigma Aldrich. For sample loading, 0,5 – 1 µg RNA were mixed with 2-fold RNA loading dye and incubated for 10 min at 70 °C and cooled down on ice for 3 min prior to loading. 0,5 mg/ml ethidium bromide was added to the gel and the running buffer, respectively. The gel was run for 2,5 h at a constant voltage of 40 V.

2.7 *in vivo* complementation assay

To analyze the functionality of the YidC homologs and the chimera (2.3.1), *in vivo* complementation assays in the YidC depletion strain MK6S (2.2.5) were performed. *E. coli* MK6S cells bearing the respective pGZ119EH plasmids expressing the protein of interest (2.3.1) were grown in LB medium with 0,2 % arabinose and 0,4 % glucose to an OD_{600} of 1.0. Cells were washed once with LB, serially diluted in LB (10^{-2}, 10^{-4}, 10^{-6}) and spotted (5 µl) on LB plates containing 0,2 % arabinose to allow chromosomal YidC expression or 0,4 % glucose to repress chromosomal YidC expression. In the presence of 1 mM IPTG, the plasmid-encoded YidC proteins were expressed. The plates were incubated overnight at 37 °C.

2.8 Fluorescence microscopy – *GFP localization*

For the localization studies, an MscL-GFP fusion protein (2.3.4) was expressed from a pMS119 derivative. The strains IY26 (2.2.7) and MC-Ffh (2.2.6) were transformed with the MscL-GFP encoding plasmid and pGZ119EH derivatives encoding the YidC homologs or

YidC chimera (2.3.3), respectively. Strains were grown overnight at 37 °C in LB medium with 0,2 % arabinose and 0,4 % glucose, washed twice in LB and diluted 1/150 into fresh LB medium with arabinose (0,2 %) to allow normal membrane insertion or in glucose (0,4 %) to deplete FtsY or Ffh, respectively. Cells were grown at least 3 h to an OD_{600} of 0.6 and protein expression was then induced with 1 mM IPTG for 2 h at 30 °C. Cells were collected by centrifugation, washed twice in LB medium, resuspended in 2 mM EDTA, 50 mM Tris-HCl pH 8.0 and incubated overnight at 4 °C. The cell suspension (corresponding to 50 µl cells) was applied to a polylysine-coated slide (Sigma-Aldrich) and examined by a Zeiss AXIO Imager M1 fluorescence microscope. Emission was detected with a filter set specific for GFP.

2.9 AMS derivatization – *pulse chase & immuno-precipitation*

In vivo AMS derivatization studies were used to analyze the proper insertion and topology of the MscL protein during the rescue experiments without a functional SRP system, while coexpressing the YidC proteins.

2.9.1 Depletion of SRP-pathway components

For the AMS (4 – acetamido- 4´- maleimidylstilbene- 2,2´- disulfonic acid, sodium salt) derivatization studies, *E. coli* MC-Ffh (Ffh depletion) and IY26 (FtsY depletion) were transformed with pMS-MscLI68C and one of the pGZ-YidC plasmids (2.3.3), respectively. The MscL mutant and the YidC proteins were coexpressed by induction of IPTG. To deplete cells of Ffh or FtsY, the cells of overnight cultures were washed twice in LB to remove the arabinose and back diluted 1/150 into fresh LB medium containing 0,4 % glucose (w/v). Cells were grown for at least 3 h in glucose to an OD_{600} of 0.5. 1,2 ml cells were washed 2 times (3 min, 6000 x *g*) in 1 ml 1x M9-salt medium (34 mM Na_2HPO_4, 22 mM KH_2PO_4, 18,7 mM NH_4Cl, 8,6 mM NaCl) and resuspended in 1 ml M9-minimal medium (1x M9-salt medium, 1 mM $MgSO_4$, 0,1 mM $CaCl_2$, 5 µg/ml Thiamin, 0,0005 % iron (II) citrate, 0,1 mM amino acid mix (19 aa -met)) supplemented with 0,2 % arabinose or 0,2 % glucose, respectively. For the AMS control (+/- AMS) the sample was divided in two 500 µl portions and incubated for another 60 min at 37 °C prior to pulse chase labelling.

2.9.2 Pulse chase

Cells coexpressing the MscL mutant and the YidC proteins were induced for 10 min with 1 mM IPTG. Cells were radiolabeled with [^{35}S] Met (10 µCi ml^{-1} culture) for 2 min. After labelling, cells were incubated with AMS (2,5 mM final concentration; Molecular Probes)

and non-radioactive L-methionine was added (final concentration, 500 µg/ml) for 10 min and then combined with 20 mM DTT for 10 min to quench the AMS reaction.

2.9.3 Immuno-precipitation

After quenching, samples were acid-precipitated and incubated overnight at 4 °C. Prior to immuno-precipitation the samples were washed with 1 ml acetone (10 min, 14 000 rpm, 4 °C) and the dried pellets (5 min, 95°C) were resuspended in 10 mM Tris pH 8, 2 % SDS (5 min, 95 °C shaker). The samples were mixed with 1 ml TEN-TX buffer (10 mM Tris pH 8, 1 mM EDTA, 150 mM NaCl, 2 % Triton X-100) and 15 µl Staph A (*Staphylococcus aureus* Protein A) and incubated for 1 h at 4 °C on a rotary wheel. After incubation the Staph A matrix was pelleted (10 min, 14 000 rpm, 4 °C) and the supernatant transferred to a new tube, mixed with 2 µl His antibody (monoclonal from Sigma, 1:10 dilution) and incubated overnight on a rotary wheel at 4 °C. Then 20 µl Staph A, binding the antigen-antibody complex, were added and incubated for another hour on the rotary wheel. The Staph A complex was washed two times (30 s, 8000 rpm, 4 °C) with 1 ml TEN-TX buffer and once (2 min, 11 000 rpm) with 1ml TEN buffer (10 mM Tris pH 8, 1 mM EDTA, 150 mM NaCl). The supernatant was discarded and the Staph A pellet resuspended in 50 µl 1x SDS sample buffer (5 parts solution 1 [200 mM Tris base, 20 mM EDTA] + 4 parts solution 2 [83,3 mM Tris base, 8,3 % SDS, 29 % glycerol, 0,15 % bromophenol blue] + 1 part 1 M DTT] by vortexing and boiling for 5 min at 95 °C.

2.9.4 Phosphorimaging and quantification

The samples were then analyzed in 14 % SDS-polyacrylamide gels. Therefor the samples were centrifuged immediately before loading for 2 min at 14 000 rpm and 30 µl of the supernatant was loaded on the SDS-polyacrylamide gel. For a good resolution of the AMS shift, the gel was run at 22 mA for 3,5 h. Then the gel was retained in a fixing solution (40 % MeOH, 7 % acetic acid) for 30 min, dried on a Whatman filter paper for 2 h at 80 °C and finally examined by phosphorimaging (Dürr Medical CR 35 bio). The imaging plate (Fujifilm BAS-IP) was incubated between 1 – 3 days and the samples were quantified with ImageJ (Schneider *et al*., 2012).

2.10 Protein purification

2.10.1 Purification of *E. coli* YidC$_{NHis10}$

Recombinant protein expression & membrane preparation

E. coli C43 cells (2.2.4) were transformed (2.6.5) with pET16b-EcYidC (2.3.2, B1) and grown in 6 L LB containing 100 µg/ml ampicillin at 37 °C. Induction was initiated at an OD_{600} of 0.6 with 0,5 mM IPTG for 3 h. The cells were pelleted, resuspended in 2 ml/g cells buffer A_{EY} (20 mM Tris pH 7.5, 300 mM NaCl, 10 % glycerol) and lysed using a One Shot cell disruption instrument (Constant Systems $_{LTD}$) at 1,3 kbar. Before cell disruption 1 mM DTT, 0,1 mM PMSF (phenylmethanesulfonyl fluoride) and 1 mM EDTA were added. The lysate was centrifuged for 12 min at 24 000 *g* to spin down the unbroken cells and centrifuged a second time under the same conditions to clear the supernatant from remaining cell debris. The membranes were pelleted by centrifugation for 1 h at 140 000 *g*, resuspended and homogenized in 20 ml buffer A_{EY} and centrifuged a second time. Membranes containing the YidC protein were homogenized in 25 ml buffer A_{EY} and extracted by the addition of 1 % n-dodecyl β-D maltoside (DDM; 10 % w/v stock solution) overnight at 4 °C on a rotary wheel.

Immobilized metal ion affinity chromatography (IMAC)

The YidC protein was purified by Ni chelating chromatography. To this end, the approach was filled up to 50 ml with buffer A_{EY} including the addition of 20 mM imidazole, 0,1 mM PMSF and 2 ml cV Ni-NTA agarose (Quiagen). After 2 h incubation at 4 °C on a rotary wheel, the batch was filled into an empty 10 ml column (90 µm filter, MoBiTec) by gravity flow and the matrix was washed with 20 ml buffer A_{EY} + 30 mM imidazole and 0,05 % DDM. The protein was eluted from the matrix with 20 ml buffer A_{EY} + 300 mM imidazole + 0,05 % DDM (10 x 2 ml fractions). The elution fractions (10 µl sample + 5 µl 5x sample buffer [4 parts solution 2 + 1 part 1M DTT) were analyzed on 12 % SDS acrylamide gels and visualized by Coomassie staining (0,4 % Coomassie R250 [Serva], 45 % methanol puriss. [Sigma-Aldrich], 10 % acetic acid puriss. [Sigma-Aldrich]).

Size exclusion chromatography (SEC)

The main YidC-containing IMAC-fractions were further purified on a Superdex 200 16/60 column (GE Healthcare) with the Äkta-purifier System (GE Healthcare). The protein fractions from the IMAC were concentrated to 5 ml with Amicon® Ultra 15 ml Filters (Merck Millipore) and filtered prior to loading (Ultrafree® Durapore – PVDF 0.22 µm, Merck Millipore). The size exclusion chromatography (SEC) of *E. coli* YidC was performed

at room temperature in buffer GF_{EY} (20 mM Tris pH 7.5, 300 mM NaCl, 10 % glycerol, 0.05 % DDM, 1 mM DTT) at a flow rate of 0,5 ml / min. 2 ml fractions were collected and the peak fractions were analyzed on 12 % SDS acrylamide gels (10 µl sample) and visualized by Coomassie staining. The purified protein was stored at 4 °C. Typical YidC protein concentrations were ~ 0,5 mg/ml (Fig. 3.5 B).

2.10.2 Purification of YidC-Rb $_{NHis10}$

Recombinant protein expression & inner membrane vesicle (IMV) preparation

E. coli C43 cells (2.2.4) were transformed (2.6.5) with pET16b-YidC-Rb (2.3.2, B3) and grown in 6 L LB containing 100 µg/ml ampicillin at 37 °C. Induction was initiated at an OD_{600} of 0.6 by 0,5 mM IPTG for 2 h. The cells were pelleted, resuspended in 2 ml/g cells buffer A_{ER} (50 mM Tris pH 7.5, 10 % sucrose, 1 mM EDTA) and lysed using a One Shot cell disruption instrument (Constant Systems $_{LTD}$) at 1,3 kbar. Before cell disruption, 0,1 mM PMSF (phenylmethanesulfonyl fluoride) was added. The lysate was centrifuged for 15 min at 10 000 *g* to spin down the unbroken cells and cell debris. The membranes were pelleted by centrifugation for 2 h at 140 000 *g*, resuspended and homogenized in 5 ml buffer A_{ER}. To isolate inner membrane vesicles containing the YidC-Rb protein, the resuspended membrane pellet was loaded onto a three step sucrose gradient (1 – 1.5 ml crude membrane suspension / gradient). The sucrose gradient consists of 3 sucrose steps (770 mM, 1440 mM and 2020 mM sucrose) in 20 mM Tris pH 8 and 1 mM EDTA. First, 12 ml of the 770 mM sucrose solution were filled into a SW28 centrifuge tube (Polyallomer 25 x 89 mm, Beckman) then 12 ml of the 1440 mM solution and finally 10 ml of the 2020 mM solution were underlayed. Prior to loading the gradient was incubated for 1 h at 4 °C. After centrifugation (SW28 rotor; 113 000 *g*, 16 h, 4 °C), the inner membrane vesicles accumulate at the boundary between 770 mM and 1140 mM sucrose. The IMV bands were pooled, diluted 1:5 with 50 mM Tris pH 7.5 and centrifuged for 2 h at 180 000 *g*. The IMV pellet was resuspended in 5 ml storage buffer (50 mM Tris pH 7.5, 10 % glycerol, 0,1 mM PMSF) and stored at - 80 °C or directly solubilized over night at 4 °C on a rotary wheel. For the solubilization 1,5 % LDAO (lauryldimethylamine-oxide), 500 mM NaCl, 1 mM DTT were added and filled-up to 10 ml with storage buffer. After the solubilization, the sample was centrifuged for 1 h at 100 000 *g* to remove aggregated or non-solubilized material.

Immobilized metal ion affinity chromatography (IMAC)

For the IMAC, the supernatant from the LDAO-solubilization (= load) was filled-up to 25 ml with buffer B_{ER} (50 mM Tris pH 9, 400 mM NaCl, 5 % glycerol) and 20 mM imidazole + 1

mM DTT were added. 2 ml (cV) NiNTA agarose (Quiagen) were equilibrated in buffer B_{ER} with 20 mM imidazole, 1mM DTT and 0,1 % LDAO and combined with the diluted load (= batch). The batch was incubated for 2 h at 4 °C on a rotary wheel and then filled into an empty 10 ml column (90 µm filter, MoBiTec) by gravity flow. The matrix was washed with 35 ml buffer W_{ER} (50 mM Tris pH 9, 500 mM NaCl, 15 % glycerol, 50 mM imidazole, 1 mM DTT, 0,1 % LDAO) and the protein was eluted from the matrix with 20 ml buffer E_{ER} (50 mM Tris pH 7.5, 300 mM NaCl, 5 % glycerol, 500 mM imidazole, 1 mM DTT, 0,2 % LDAO) in 10 x 2 ml fractions. The elution fractions (10 µl sample + 5 µl 5x sample buffer [4 parts solution 2 + 1 part 1M DTT]) were analyzed on 12 % SDS acrylamide gels and visualized by Coomassie staining (0,4 % Coomassie R250 [Serva], 45 % methanol puriss. [Sigma-Aldrich], 10 % acetic acid puriss. [Sigma-Aldrich]).

Size exclusion chromatography (SEC)

The main fractions from the IMAC were further purified on a Superdex 200 16/60 column (GE Healthcare) with the Äkta-purifier System (GE Healthcare). The protein fractions were concentrated to 5 ml with Amicon® Ultra 15 ml Filters (Merck Millipore) and filtered prior to loading (Ultrafree® Durapore – PVDF 0.22 µm, Merck Millipore). The size exclusion chromatography (SEC) of YidC-Rb was performed at room temperature in buffer GF_{ER} (50 mM Tris pH 7.5, 300 mM NaCl, 5 % glycerol, 0,2 % LDAO, 1 mM DTT) at a flow rate of 0,5 ml / min. 2 ml fractions were collected and the peak fractions were analyzed on 12 % SDS acrylamide gels (10 µl sample) and visualized by Coomassie staining. The purified protein was stored at 4 °C. Typical protein concentrations were 1,5 mg/ml (Fig. 3.7 B).

The YidC homolog from *Oceanicaulis alexandrii* and the respective hybrid protein YidC-Oa (2.3.2 B2 & B4) were purified as described for YidC-Rb with typical protein concentrations of ~ 0,5 mg/ml.

2.10.3 Purification of *E. coli* Ffh & Ffh C406S / M423C

Recombinant protein expression

Both, the wild type Ffh and the single cysteine mutant C406S / M423C were expressed in BL21 cells (2.2.2) and purified via a Strep-tag at the C-terminus of the protein (2.3.2, B12 & B14). The expression was done in 4 L LB medium by induction at an OD_{600} of 0.6 with 0,5 mM IPTG for 3 h at 37°C. The cells were pelleted, resuspended in 60 ml buffer A_{Ffh} (20 mM Hepes pH 8, 350 mM NaCl, 10 mM $MgCl_2$, 10 mM KCl, 10 % glycerol) and lysed using a One Shot cell disruptor (Constant Systems $_{LTD}$) at 1,3 kbar. Before cell disruption, 0,1 mM PMSF (phenylmethanesulfonyl fluoride) was added. The lysate was centrifuged

for 30 min at 20 000 *g* for two times to spin down the unbroken cells and cell debris. The supernatant, containing the soluble Ffh protein, was stored at - 80 °C.

Strep-tag affinity chromatography

The *Strep*-tag® II is a short peptide (8 amino acids, WSHPQFEK), which binds to *Strep*-Tactin® with a high selectivity. In this work, the *Strep*-Tactin matrix, an engineered streptavidin, from IBA was used.

The supernatant was loaded onto 4 ml *Strep*-Tactin matrix in a 10 ml column by gravity flow directly. The matrix was washed with 50 ml buffer W_{Ffh} (20 mM Hepes pH 8, 500 mM NaCl, 10 mM $MgCl_2$, 100 mM KCl) and the protein was eluted from the matrix with 20 ml buffer E_{Ffh} (20 mM Hepes pH 8, 350 mM NaCl, 10 mM $MgCl_2$, 10 mM KCl, 10 % glycerol, 2.5 mM desthiobiotin [Sigma]) in 10 x 2 ml fractions. The elution fractions (10 µl sample + 5 µl 5x sample buffer) were analyzed on 12 % SDS acrylamide gels and visualized by Coomassie staining. After the elution of the Ffh protein, the matrix was washed 3 times with 5 cV regeneration buffer (IBA, 100 mM Tris-HCl, 150 mM NaCl, 1 mM EDTA, 1 mM HABA (hydroxy-azophenyl-benzoic acid, pH 8.0) to displace desthiobiotin from the binding pocket. The regeneration buffer was removed from the matrix by extensive washing with buffer W (IBA, 100 mM Tris-HCl, 150 mM NaCl, 1 mM EDTA, pH 8.0). Once the red color of the regeneration buffer has disappeared, the column can be reused and was stored in buffer W at 4 °C.

Size exclusion chromatography (SEC)

The main Strep-tag elution fractions were further purified on a Superdex 75 16/60 column (GE Healthcare) with the Äkta-purifier System (GE Healthcare). The protein fractions were concentrated up to 5 ml with Amicon® Ultra 15 ml Filters (Merck Millipore) and filtered prior to loading (Ultrafree® Durapore – PVDF 0.22 µm, Merck Millipore). The size exclusion chromatography (SEC) of Ffh was performed at room temperature in buffer GF_{Ffh} (20 mM Hepes pH 8, 200 mM NaCl, 10 mM $MgCl_2$, 10 mM KCl, 10 % glycerol) at a flow rate of 0,5 ml / min. 2 ml fractions were collected and the peak fractions were analyzed on 12 % SDS acrylamide gels (10 µl sample) and visualized by Coomassie staining. The purified protein was stored at - 80 °C with typical concentrations of ~ 1 mg/ml without further concentration (Fig. 3.31 A).

2.10.4 Purification of ribosomal proteins L24 and L29

Recombinant protein expression

The ribosomal proteins L24 and L29 were expressed from pET16b vectors (2.3.2, B10 & B11) in BL21 cells and purified via a Strep-tag at the N-terminus of the protein. The expression was performed in 2 L LB media and the cells were induced at an OD_{600} of 0.6 with 0,5 mM IPTG for 3 h at 30°C. The cells were pelleted, resuspended in 2 ml/g buffer A_{Rib} (100 mM Tris pH 8, 150 mM NaCl, 1mM EDTA, 10 % glycerol) and lysed using an One Shot cell disruptor (Constant Systems $_{LTD}$) at 1,3 kbar. Before cell disruption, 0,1 mM PMSF was added. The lysate was centrifuged for 20 min at 10 000 *g* to spin down the unbroken cells and cell debris. Then the supernatant was centrifuged for 1 h at 150 000 *g* to pellet the membranes. The cleared supernatant, containing the soluble ribosomal proteins, was stored at - 80 °C.

Strep-tag affinity chromatography

The supernatant was loaded onto a 2 ml *Strep*-Tactin column matrix by gravity flow. The matrix was washed with 5 cV buffer W_{Rib} (100 mM Tris pH 8, 150 mM NaCl, 1mM EDTA) and the protein was eluted from the matrix with buffer E_{Rib} (100 mM Tris pH 8, 150 mM NaCl, 1mM EDTA, 2,5 mM desthiobiotin) in 6 x 1 ml fractions. The elution fractions (10 µl sample + 5 µl 5x sample buffer) were analyzed on 18 % SDS acrylamide gels and visualized by Coomassie staining. After the elution of the ribosomal proteins, the matrix was washed 3 times with 5 cV regeneration buffer (IBA, 100 mM Tris-HCl, 150 mM NaCl, 1 mM EDTA, 1 mM HABA (hydroxy-azophenyl-benzoic acid, pH 8.0) to displace desthiobiotin from the binding pocket. The regeneration buffer was removed by extensive washing with buffer W (IBA, 100 mM Tris-HCl, 150 mM NaCl, 1 mM EDTA, pH 8.0). Once the red color of the regeneration buffer has disappeared the column can be reused and was stored in buffer W at 4 °C.

Ion exchange chromatography (IEC)

For further purification of the ribosomal proteins, a cation exchange chromatography (CEX) with a SP Sepharose FastFlow matrix (4 cV) followed.

First the main strep-tag elution fractions were pooled, concentrated to 1 ml with Amicon® Ultra 15 ml Filters (MWCO 3 kDa, Merck Millipore) and a buffer exchange was performed to reduce the Tris and NaCl concentration in the sample for better binding to the SP Sepharose matrix. The concentrated sample was loaded onto a 5 ml HiTrap desalting

column and eluted with 2 cV SP-buffer$_{Rib}$ A (50 mM Tris-HCl pH 8, 100 mM NaCl, 1 mM EDTA, 1mM DTT) at 2 ml/min in 0,5 ml fractions using again the Äkta-purifier system.

The main fractions of the desalting step were pooled and loaded onto the SP Sepharose FastFlow column (0,5 ml/min), followed by a washing step with 5 cV SP-buffer$_{Rib}$ A to remove unbound proteins. Then the ribosomal proteins were eluted by a linear salt gradient from 100 mM NaCl to 1 M NaCl over 20 cV (0 % - 100 % SP-buffer$_{Rib}$ B: 50 mM Tris-HCl pH 8, 1 M NaCl, 1 mM EDTA, 1mM DTT). Flow through, washing step and the elutions were collected in 1 ml fractions and were analyzed by detecting the absorption at 280 nm and 260 nm. The SP-fractions of the ribosomal proteins were dialyzed against an appropriate buffer depending on the assay that will be performed (2.15 and 2.16).

2.10.5 Purification of the C-terminal insertase domains RbCT, OaCT, O1CT and A3CT

The C-terminal domains (CTDs) of the YidC homologs from *R. baltica* (RbCT) and *O. alexandrii* (OaCT), as well as the CTDs of the eukaryotic insertase homologs Oxa1 from *S. cerevisiae* (O1CT) and Alb3 from *A. thaliana* (A3CT) were cloned with an N- or C-terminal His$_{10}$-Tag in pET16b or pET22b, respectively. In a pilot experiment the expression of all constructs was tested in C43, C41 and Bl21 cells for the N- or C-terminal tagged versions of the proteins. The results are summarized in table 2.1.

CTD	Plasmid	HisTag	Strain	Induction [h]
RbCT	2.3.2 B5	N-terminal	C41	3h
OaCT	2.3.2 B6	N-terminal	C41	3h
A3CT	2.3.2 B7	C-terminal	BL21	3h
O2CT	2.3.2 B8	N-terminal	BL21	3h

Table 2.1 ***Summary of the best expression conditions of the CTDs***

Recombinant protein expression

The CTDs were expressed according to the best conditions described in table 2.1. The expression was performed in 1l LB amp medium and the cells were induced at an OD_{600}

of 0.6 with 0,5 mM IPTG for 3 h at 37°C. The cells were pelleted and resuspended in 2 ml/g buffer A_{CT1} (50 mM Tris pH 9, 300 mM NaCl, 5 mg $MgCl_2$, 10 % (w/v) glycerol) for RbCT and OaCT. A3CT and O1CT were resuspended in buffer A_{CT2} (100 mM Hepes pH 7.5, 300 mM NaCl, 5 mM $MgCl_2$, 10 % (w/v) glycerol, 1 mM DTT). All cell suspensions were lysed using an One Shot cell disruptor (Constant Systems $_{LTD}$) at 1,3 kbar. Before cell disruption, 0,1 mM PMSF was added. The lysate was centrifuged for 30 min at 50 000 *g* to spin down the unbroken cells and cell debris. The cleared supernatant, containing the soluble CTDs, was stored at - 80 °C.

Immobilized metal ion affinity chromatography (IMAC)

2 ml (cV) NiNTA agarose (Quiagen) were equilibrated in the appropriate buffer A_{CT}, supplemented with 10 mM imidazole and combined with the cleared supernatant. The batch was incubated for 2 h at 4 °C on a rotary wheel and then filled into an empty 10 ml column (90 µm filter, MoBiTec) by gravity flow. The matrix of the bound RbCT and OaCT purification step was washed with 20 ml buffer W_1 (50 mM Tris pH 9, 600 mM NaCl, 5 mM $MgCl_2$, 10 % (w/v) glycerol, 50 mM imidazole). For the A3CT and O1CT purification, three washing steps were performed each with 5 ml buffer W_2 (50 mM Hepes pH 7.5, 300 mM NaCl, 5 % (w/v) glycerol, 1 mM DTT) supplemented with 0 mM, 10 mM, 50 mM imidazole, respectively.

Then the CTDs were eluted from the matrix with 10 ml buffer E_{Rb} (50 mM Tris pH 8, 150 mM NaCl, 5 % (w/v) glycerol, 400 mM imidazole, 1 mM DTT) for RbCT, with 10 ml buffer E_{Oa} (50 mM Tris pH 7, 150 mM NaCl, 5 % (w/v) glycerol, 400 mM imidazole, 1 mM DTT) for OaCT and with 10 ml buffer $E_{A3/O1}$ (50 mM Hepes pH 7.5, 150 mM NaCl, 5 % (w/v) glycerol, 1 mM DTT,300 mM imidazole) for the C-terminal domains of Alb3 (A3CT) and Oxa1 (O1CT). The proteins were collected in 5 x 2 ml fractions and analyzed on 15 % SDS acrylamide gels with subsequent Coomassie staining.

Ion exchange chromatography (IEC)

For further purification of the CTDs a cation exchange chromatography (CEX) with a SP Sepharose FastFlow matrix (4 cV) followed.

The main elution fractions were pooled and concentrated to 2 ml with Amicon® Ultra 15 ml Filters (MWCO 5 kDa, Merck Millipore). The concentrated sample was loaded onto the SP Sepharose FastFlow column (0,3 ml/min), followed by a washing step with 5 cV SP-buffer A_{CT} to remove unbound proteins. For the different CTDs, different SP-buffers were used:

RbCT: 50 mM Tris pH 8, 150 mM NaCl, 5 % (w/v) glycerol, 1 mM DTT

OaCT: 50 mM Tris pH 7, 150 mM NaCl, 5 % (w/v) glycerol, 1 mM DTT

A3CT & O1CT: 50 mM Hepes pH 7.5, 150 mM NaCl, 5 % (w/v) glycerol, 1 mM DTT

Then the CTD proteins were eluted with a linear salt gradient from 150 mM NaCl to 1 M NaCl over 20 cV (0 % - 100 %) SP-buffer B_{CT} (1 M NaCl in the respective SP-buffer$_{CT}$). Flow through, washing step and the elution were collected in 1 ml fractions and analyzed by detecting the UV-absorption at 280 nm and 260 nm and Coomassie staining in SDS-gels.

The main fractions were pooled and concentrated to 1 ml for buffer exchange on a HiTrap desalting column (GE Healthcare) with the Äkta-purifier System (GE Healthcare) and filtered prior to loading (Ultrafree® Durapore – PVDF 0,22 µm, Merck Millipore). The buffer exchange of the CTDs was performed at room temperature in the respective CTD-buffer (20 mM Hepes pH 8 (RbCT) / pH 7 (OaCT) / pH 7.5 (A3CT + O1CT), 150 mM NaCl, 2 mM $MgCl_2$, 1 mM EDTA, 1 mM DTT) at a flow rate of 2 ml / min. 0,5 ml fractions were collected and the peak fractions were analyzed on 15 % SDS acrylamide gels (10 µl sample) and subsequent Coomassie staining. The purified protein was stored at - 80 °C. For CD spectroscopy studies, the CTDs were dialyzed in Micro Float-A-Lyzer (MWCO 0,5 – 1 kDa; Spectra/Por®) to 20 mM K_3PO_4 pH 8 / 7.5 / 7, respectively.

2.11 Protein concentration determination according to Scopes

This method was used to determine the concentration of the small ribosomal proteins L24, L29 and the C-terminal YidC peptides RbCT, OaCT, O1CT and A3CT since they do not contain enough aromatic amino acid residues (Trp, Tyr) for the absorbance measurements at 280 nm. At a wavelength of 205 nm, the absorbance of the peptide bondage of the protein backbone is measured. First, the extinction coefficient (ε_{205}) was determined according to the empirical formula proposed by Scopes (Scopes, 1974):

ε_{205} [mg/ml] = 27 + 120 x A_{280}/A_{205}

Then, the protein concentration was calculated according to the Lambert-Beer law:

c [mg/ml] = A_{205} / (d x ε_{205})

2.12 *in vitro* ribosome binding assay

The ribosomes were isolated from a soluble cell extract of the *E. coli* strain MRE600 according to Maguire *et al*. (2008). The isolated ribosomes and the purified YidC proteins

were incubated on ice for 1 h (100 nM ribosomes; 500 nM protein) in ribosome-binding buffer (20 mM Tris-HCl pH 7.4, 25 mM $MgOAc_2$, 100 mM NaCl, 0,1 % DDM, 1 mM DTT), with a total reaction volume of 500 µl. Then the samples were centrifuged for 3 h at 200 000 *g* in a TLA 100.3 rotor. The pellet was directly resuspended in SDS-PAGE loading buffer, whereas the supernatant was precipitated with 10 % trichloroacetic acid (TCA) overnight and then subjected to SDS-PAGE analysis and subsequent Coomassie staining or immunoblotting and detection with antibodies against the His_{10}tag. For quantification, the total amount of applied protein in the assay (input) was loaded on the gel separately.

2.13 Reconstitution of an RNC-YidC complex

The purification of the ribosome nascent chain complexes (RNCs) was carried out as described (Seidelt *et al*., 2009) by our collaboration partner from the Roland Beckmann laboratory at the Ludwig-Maximillian's-University in Munich, Germany. The translation system was programmed with an mRNA coding for an N-terminal His-tag followed by amino acid residues 1 – 115 of MscL and the TnaC stalling sequence at the C-terminus. This results in the first two transmembrane helices of MscL being fully emerged from the ribosomal exit tunnel. The sample complex was reconstituted by incubating 10 pMol MscL-RNCs with 50 pMol freshly purified YidC-Rb from our lab (2.10.2) in a final volume of 50 µL grid buffer (20 mM Hepes pH 7.2, 100 mM KOAc, 10 mM $MgOAc_2$, 0,1 % Cymal 6) for 30 min at 37 °C.

2.14 Electron microscopy and image processing

The here described electron microscopy and image processing was established and carried out by our collaboration partners from the Roland Beckmann laboratory at the Ludwig-Maximillian's-University in Munich, Germany.

The reconstituted RNC-YidC-Rb (2.10.2) complex was vitrified on 2 mm pre-coated Quantifoil R3/3 holey carbon supported grids using a Vitrobot Mark IV (FEI Company). For automated data collection on the Titan Krios TEM (FEI Company) under low dose conditions (~ 20 e/Å^2) the magnification was set to nominal 75.000x with a defocus range between -1 µm and -3.5 µm. The microscope was operated at 200 keV and a magnification of 148.721x at the plane of the CCD using a 4k x 4k TemCam-F416 CMOS camera (TVIPS GmbH) resulting in an image pixel size of 1.12 Å (object scale).

A total of 14 165 micrographs were collected of which 4 488 were selected manually for further processing based on the information content of the power spectra and particle density on the grid. The data processing was performed using the SPIDER software

package (Frank *et al*., 1996). The defocus of each micrograph was determined using the TF ED command in SPIDER and particles were automatically selected using SIGNATURE (Chen and Grigorieff, 2007). The complete data sets of 140 266 particles was aligned to the structure of an empty 70S ribosome that was generated using the crystal structure of an *E. coli* ribosome (Schuwirth *et al*., 2005). Using semi-supervised classification (Penczek *et al*., 2006) it was possible to sort for subpopulations showing distinct ribosomal conformations and ligands (+/- E-site tRNA, +/- ligand at tunnel exit). A final dataset of 51 903 particles resulted in a density map refined to 8.6 Å resolution according to a Fourier Shell Correlation (FSC at 0.5 cut-off) showing P-site tRNA and high occupancy of YidC at the ribosomal exit site.

2.15 *in vitro* pull down assays

For the *in vitro* pull down assays 120 µg of purified *E. coli* $YidC_{NHis}$ (2.10.1) or YidC-Rb_{NHis} protein was prebound to 50 µl cV NiNTA resin (Quiagen), respectively. Immobilization of the YidC proteins was performed in 1 ml binding buffer containing 50 mM Tris pH 7, 150 mM NaCl, 1 mM DTT and 0,05 % DDM (*E.coli* YidC) or 0,1 % LDAO (YidC-Rb) for 2 h at 4°C on a rotary wheel. Unbound protein was then collected by gravity flow. The ribosomal proteins L24 and L29 (2.10.4; ~ 500 µg) were loaded onto preloaded His-YidC columns. After 3 washing steps with 200 µl wash buffer (50 mM Tris pH 7, 100 mM NaCl, 1 mM DTT), all bound proteins were eluted by wash buffer supplemented with 500 mM imidazole by centrifugation.

2.16 Circular dichroism (CD) - spectroscopy

To analyze the secondary structure of the C-terminal domains RbCT and OaCT, a spectropolarimeter (J-715; Jasco, Tokyo, Japan) was used for CD measurements with 1 mm path-length quartz cuvettes (Hellma AG, Müllheim, Germany). All experiments were performed in 20 mM potassium phosphate buffer, pH 7 for OaCT or pH 8 for RbCT with a protein concentration of ~ 200 µg/ml. Background-corrected CD-spectra were recorded in the 190 - 260 nm range with a scan speed of 50 nm/min and a step size of 1 nm at 25 °C.

To facilitate the comparison of spectra from different samples, all spectra were normalized to mean residue weight ellipticity (θ_{MRW}) [deg cm^2/dmol], according to the formula:

$$\theta_{MRW} = \frac{MW \times \theta \mathrm{mdeg}}{N \times c \times d \times 10000}$$

θ_{mdeg} is the recorded ellipticity in millidegrees for a given wavelength, *MW* is the molecular weight of the protein in Da, *d* is the path length of the cuvette in cm, *N* is the number of amino acid residues in the peptide and *c* is the sample concentration in mg/ml.

Secondary structure predictions were performed on the DICHROWEB server (Whitmore and Wallace, 2004 & 2008) using the data set 4 (Sreerama and Woody, 2000) computed by the CDSSTR algorithm (Johnson, 1999).

Folding experiments of the C-terminal YidC domains upon titration of the ribosomal proteins L24 and L29 were performed by Emmanuelle Mboubi Kouaga and are described in detail in her Master thesis (Mboubi Kouaga, University of Hohenheim 2013).

2.17 Microscale thermophoresis (MST) measurements

MST measurements were performed to calculate the binding affinity of the isolated *E. coli* SRP to different purified internal signal peptides of KdpD (N22-48, W3A and 3Q).

2.17.1 Labeling of Ffh_{M423C}

Ffh_{M423C} (2.10.3) was labeled using the NT-647-MALEIMIDE fluorescent dye and the RED-Maleimide Labeling kit (NanoTemper Technologies). The labeling reaction was performed according to the manufacturer´s instructions. Prior to labeling, a buffer exchange was performed to remove the glycerin from the protein sample (20 mM Hepes pH 8, 200 mM NaCl, 10 mM $MgCl_2$, 10 mM KCl) using the column provided in the kit. The protein concentration was adjusted to 10 µM and two labeling reactions were prepared with a 6 fold molar excess of the dye. After incubation for 30 min at room temperature both labeling reactions were combined, followed by the purification step to remove unreacted “free” dye. Therefore, the supplied dye removal columns were equilibrated with Ffh_{GF}-buffer (20 mM Hepes pH 8, 200 mM NaCl, 10 mM $MgCl_2$, 10 mM KCl, 10 % glycerin). The degree of labeling (DOL, dye:protein ratio) was determined using an UV-Vis Spectrophotometer (NanoDrop 2000, ThermoScientific) at 650 and 280 nm. The DOL was calculated with:

$$DOL = \frac{A650 \times \varepsilon\, Ffh}{(A280 - A650 \times CF280) \times \varepsilon\, dye}$$

ε_{Ffh} = 8480

ε_{dye} = 250 000

$CF280_{647mal}$ = 0.05

Thereby, a DOL of ~ 50 % was typically achieved. The labeled Ffh_{647NT} protein was stored in aliquots at – 80°C and protected from light.

2.17.2 Reconstitution of SRP

To get a functional SRP it is necessary to reconstitute the labeled Ffh_{647NT} protein with the *in vitro* synthesized 4.5S RNA (2.6.12). The Ffh_{647NT} protein was adjusted to 40 nM with MST_{RNA} buffer (20 mM Hepes-KOH pH 7.5, 100 mM KCl, 10 mM $MgCl_2$, 0,5 mM EDTA, 0,05% Tween-20). Prior to use, the 4.5S RNA was 5-fold diluted, also in MST_{RNA} buffer, to a final concentration of 9,48 µM. For refolding of the RNA, the diluted stock solution was heated to 75 °C for 2 min, and then cooled on ice for 1 min. Ffh_{647NT} and 1.5 fold molar excess of 4.5S RNA (40 nM Ffh + 60 nM 4.5S RNA in 200 µl RNA buffer) were incubated together at 20 °C for 10 min and centrifuged for 10 min at 14 000 rpm, 4°C. The reconstituted SRP was kept on ice until start of the MST measurements.

2.17.3 MST measurement 1: Reconstitution of SRP

To analyze the correct assembly of SRP, the reconstitution and binding of Ffh to the 4.5S RNA was tested via MST measurement.

The labeled Ffh_{647NT} protein was adjusted to 8 nM in MST_{RNA} buffer (20 mM Hepes-KOH pH 7.5, 100 mM KCl, 10 mM $MgCl_2$, 0,5 mM EDTA, 0,05% Tween-20). The *in vitro* synthesized 4.5S RNA was diluted to a concentration of 400 nM in MST_{RNA} buffer and a series of 16 1:1 dilutions was prepared in the same buffer, producing ligand concentrations ranging from 12,2 pM to 400 nM. For thermophoresis, each ligand dilution was mixed with one volume of labeled Ffh_{647NT}, which leads to a final concentration of fluorescently labeled Ffh_{647NT} of 4 nM and a final ligand concentrations ranging from 6,1 pM to 200 nM. After 10 min incubation at room temperature, approximately 4 µl of each solution was filled into Monolith NT Premium Treated Capillaries (NanoTemper Technologies GmbH). Thermophoresis was measured using a Monolith NT.115 instrument at a temperature of 25 °C with 5 s/30 s/5 s laser off/on/off times, respectively. Instrument parameters were adjusted to 95 % LED power and 20 % MST power. Data of two independently pipetted measurements were analyzed (NT Affinity Analysis v2.0.1334, NanoTemper Technologies) using the signal from Thermophoresis + T-Jump.

2.17.4 MST measurement 2: Binding of SRP to signal peptides

To study the interaction of SRP to the putative SRP signal sequence at the very N-terminus of the KdpD protein different KdpD peptides (2.5), encompassing amino acid 22 - 48 of KdpD, were tested of their ability to bind to SRP via MST.

Therefore, the labeled SRP protein was reconstituted as described in 2.17.2 and adjusted to 40 nM in MST_{RNA} buffer. The *in vitro* synthesized peptides were dissolved in MST_{opt} buffer (50 mM Tris pH 7.4, 150 mM NaCl, 10 mM $MgCl_2$, 0,05 % Tween-20) and series of 16 1:1 dilutions were prepared in the same buffer, producing ligand concentrations ranging from 80 µM to 2,4 nM, respectively. For thermophoresis, each ligand dilution was mixed with one volume of labeled SRP, which leads to a final concentration of fluorescently labeled SRP of 20 nM and final ligand concentrations ranging from 1,2 nM to 40 µM. After 20 min incubation on ice, approximately 4 µl of each solution was filled into Monolith NT Premium Treated Capillaries (NanoTemper Technologies GmbH). Thermophoresis was measured using a Monolith NT.115 instrument at temperature of 23 °C with 5 s/30 s/5 s laser off/on/off times, respectively. Instrument parameters were adjusted to 50 % LED power and 20 % MST power. Data of 2 - 3 independently pipetted measurements were analyzed (NT Affinity Analysis v2.0.1334, NanoTemper Technologies) using the signal from Thermophoresis + T-Jump or manual evaluation settings (Cold region start / end: -1 s / 0 s; Hot region start / end: 4.51 s / 5.51 s).

2.17.5 K_d Model: standard MST curve fitting mode

The K_d Model is the standard fitting mode derived from law of mass action:

$$f\,(Concentration) = Unbound + \frac{(Bound - Unbound)x\,(concentration + TargetConc + Kd - \sqrt{(Concentration + TargetConc + Kd)^2 - 4xConcentrationxTargetConc}\,)}{2\,x\,TargetConc}$$

Unbound: response value of unbound state

Bound: response value of bound state

TargetConc: final concentration of fluorescent molecule

Fit quality was checked with the following parameters:

Response Amplitude = absolute difference between bound and unbound

K_d Confidence = with a confidence of 68%, K_d is within the given range. The lower this number, the better the experimental data is represented by the fitted curve.

Standard Error of Regression = root mean square error (RMSE) of experimental data to fitted curve. The lower this number, the better the experimental data is represented by the fitted curve.

The measured data in this work were evalutated and presented as baseline-corrected normalized fluorescence (ΔF_{norm} in [‰]). To obtain ΔF_{norm}, the baseline F_{norm} value (unbound molecule) is subtracted from all data points. Thus, by definition, ΔF_{norm} is 0 in the unbound state and can adopt positive or negative values, depending on an increase or decrease in F_{norm} relative to the unbound state. This allows comparing both, amplitude of the binding curve as well as the K_d of multiple experiments in one graph.

3 RESULTS

3.1 Chimera of the membrane insertase YidC with altered C-terminal regions

In comparison to the *E. coli* YidC (Ec-YidC), that has a charged C-terminal domain (CTD) of 16 aa only, the marine Gram-negative bacteria *Rhodopirellula baltica* and *Oceanicaulis alexandrii* feature membrane insertases with extended and highly positively charged C-terminal regions similar to the YidC homologs in mitochondria (Oxa1; CTD of 89 aa), chloroplasts (Alb3; CTD of 114 aa) and Gram-positive bacteria (YidC2; CTD of 64 aa). The YidC homolog of the planctomycete *R. baltica* (Rb-YidC) has a size of 90 kDa and a hydrophilic C-terminal region of 80 amino acid residues. The α-proteobacterium *O. alexandrii* YidC homolog (Oa-YidC) is 83 kDa in size and has a positively charged C-terminal tail of 99 residues (Fig. 3.1).

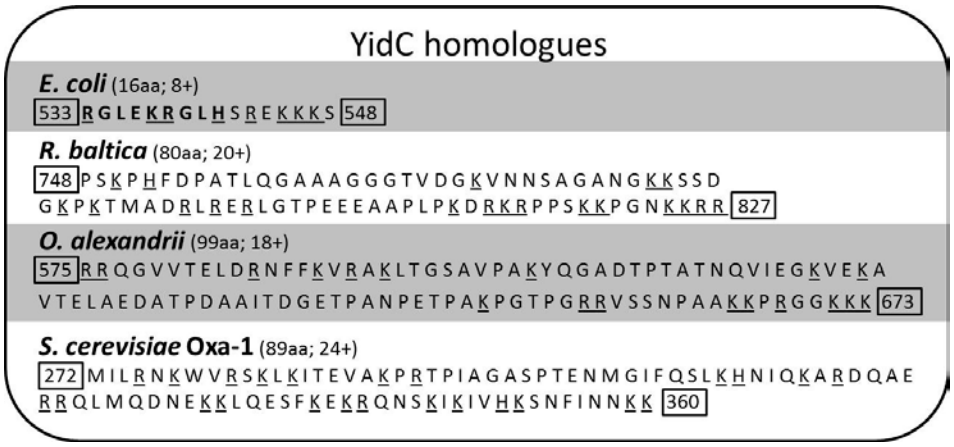

Fig.3.1 ***Diversity of the C- terminal regions of YidC homologs****. The sequence after TM segment 6 is shown for E. coli, the marine bacteria R. baltica, O. alexandrii and, for comparison, the corresponding sequence of S. cerevisiae Oxa1. The length of the tail regions and the number of positively charged amino acid residues are indicated.*

To analyze the role of the extended C-terminal tails, chimeric forms of *E. coli* YidC were constructed where the C-terminal region of YidC was replaced by the C-terminal tail of *R. baltica* (YidC-Rb), *O. alexandrii* (YidC-Oa) and *S. cerevisiae* (YidC-Oxa) (Fig. 3.2), respectively.

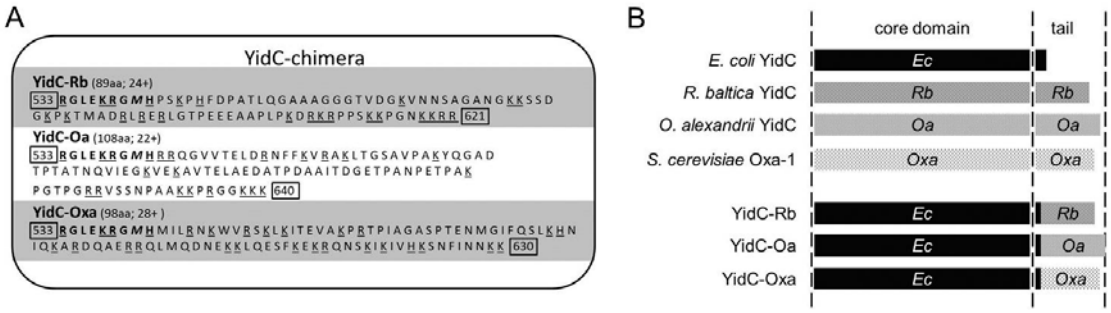

Fig. 3.2 ***Chimeric proteins of E. coli YidC with elongated C-terminal tails. (A)*** *The respective sequence of the chimeric protein tails of Ec-YidC with the C-terminal tails of R. baltica (YidC-Rb), of O. alexandrii (YidC-Oa) and of S. cerevisiae (YidC-Oxa) is shown.* ***(B)*** *Schematic representation of the YidC proteins. The core domain of each YidC consists of 6 transmembrane segments and a large P1 domain, except Oxa1 from S. cerevisiae (TM 2-6).*

Genetic construction of the YidC-chimera is described in Seitl, 2010 (University of Hohenheim). A brief summary of the cloning steps is listed in chapter 2.3.

3.1.1 Complementation of *E. coli* YidC

To analyze whether the YidC homologs and the chimera were functional, they were studied in the YidC depletion strain MK6S (2.2.5). In this strain, the *yidc* promoter is replaced by an *araC-araBAD* promoter on the chromosome. Growth in the presence of glucose for more than 2 h results in the depletion of YidC and finally to cell death, whereas the presence of arabinose allowed normal growth (Fig. 3.3 A and B). When the respective agar-plate contained 0,4 % glucose and 1 mM IPTG (Fig. 3.3 C) the plasmid-derived expression of Ec-YidC, Oa-YidC, YidC-Rb, YidC-Oa and YidC-Oxa promoted growth.

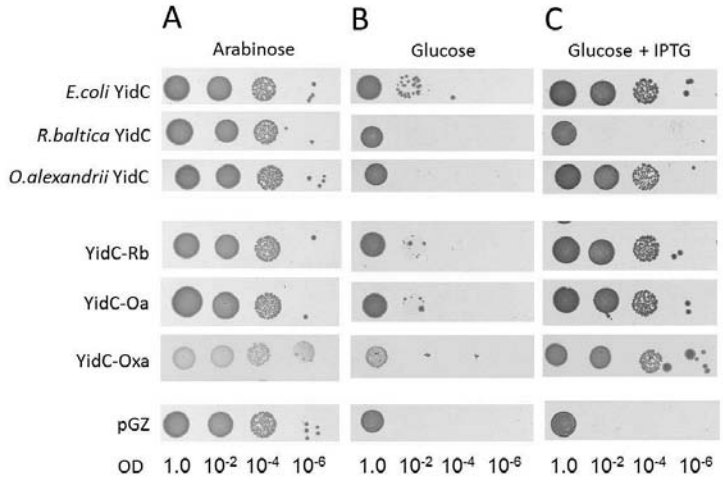

Fig. 3.3 ***Complementation of YidC in E. coli MK6.*** *Serial dilutions of the E. coli MK6 YidC depletion strain cultures, bearing the plasmid-encoded YidC from the marine bacteria and the YidC chimera, were prepared. The cells were spotted onto agar-plates containing 0,2 % arabinose* ***(A)*** *to allow chromosomal YidC expression, 0,4 % glucose* ***(B)*** *to repress chromosomal YidC expression and 0,4 % glucose and 1 mM IPTG* ***(C)*** *to allow the sole plasmid-derived expression of YidC.*

This clearly shows that the YidC homolog of *O. alexandrii* (Oa-YidC) and also the chimeric proteins YidC-Rb, YidC-Oa and YidC-Oxa are fully functional and can complement the wild-type YidC in *E. coli*, whereas the YidC homolog from *R. baltica* cannot. Therefore, only the three chimeras and the Oa-YidC homolog were used for the further studies.

3.1.2 Purification of the YidC proteins

For the *in vitro* assays and the cryo-EM studies it was necessary to purify N-terminally histidine-tagged versions of the YidC proteins in sufficient amounts. In the following chapter the purification of the Ec-YidC and the YidC-Rb chimera is shown.

1. Purification of *E. coli* $YidC_{NHis10}$ (2.10.1)

The recombinant expression of the *E. coli* YidC from a pET16b vector (2.3.2 B1) was performed in a 6 L LB culture of *E. coli* C43 cells for 3 h at 37 °C. After the preparation of crude membranes, the Ec-YidC protein was solubilized by 1 % DDM and purified by Ni chelating chromatography (IMAC). The protein was eluted in 10 x 2 ml fractions with buffer E_{EY} (20 mM Tris pH 7.5, 300 mM NaCl, 10 % glycerol, 0,05 % DDM, 1 mM DTT, 300 mM imidazole). 10 µl samples of elution fractions 1 – 7 were analyzed on a 12 % SDS acrylamide gel and Coomassie staining (Fig. 3.4).

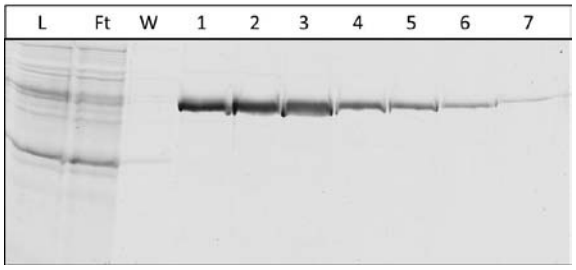

Fig. 3.4 ***IMAC elution fractions of Ec-$YidC_{NHis}$.*** *Samples, corresponding to the amount of protein of 1 ml cell culture, from the IMAC load (L), flow through (Ft) and the washing step (W), as well as 10 µl of each of the Ec-YidC elution fractions (1-7) were analyzed on a 12 % SDS gel by Coomassie staining.*

Although the IMAC elutions were quite pure, the main fractions (Fig. 3.4 1-3) were further purified on a Superdex 200 16/60 column, especially to separate aggregates and higher oligomers of the Ec-YidC from the monomeric form to get a homogeneous protein sample. Additionally, the quick removal of imidazole from the sample is important for protein stability, since the Ec-YidC tends to aggregate in high imidazole concentrations. The size exclusion chromatography (SEC) of *E. coli* YidC was performed with a Superdex 200 16/60 column at room temperature in buffer GF_{EY} (20 mM Tris pH 7.5, 300 mM NaCl, 10 % glycerol, 0,05 % DDM, 1 mM DTT) at a flow rate of 0,5 ml / min. The elution profile of Ec-YidC was monitored using the UV absorbance at 280 nm (Fig. 3.5 A). 2 ml fractions were collected and samples of the three main peaks were analyzed (10 µl) on a

Coomassie stained 12 % SDS gel (Fig. 3.5 B). All samples showed a single Ec-YidC band. However, implicating the elution profile of the SEC, there were huge differences in homogeneity for the different fractions. The first peak, represented by fraction 2 with an elution volume at ~ 44 ml, corresponds to the void volume (V_0) with a molecular weight (MW) of > 2000 kDa, presumably containing aggregated Ec-YidC. Ec-YidC from fraction 5 of the second peak that is not completely separated from peak 1, has a high oligomeric form since the elution volume at ~ 51 ml corresponds to a MW of about 440 kDa. The third peak around an elution volume of 65 ml presumably contains the dimeric form of Ec-YidC with a MW of ~ 158 kDa. This calculated size matched perfectly for the 60 kDa Ec-YidC being a dimer in a DDM micelle with a theoretical MW of ~ 40 kDa. However, since the peak had a wide range from fractions 11 – 17, corresponding to a MW of 200 – 100 kDa, it is difficult to estimate if there are only dimers or a mixture of monomeric (later fractions around 70 ml) and dimeric (earlier fractions around 65 ml) forms of Ec-YidC.

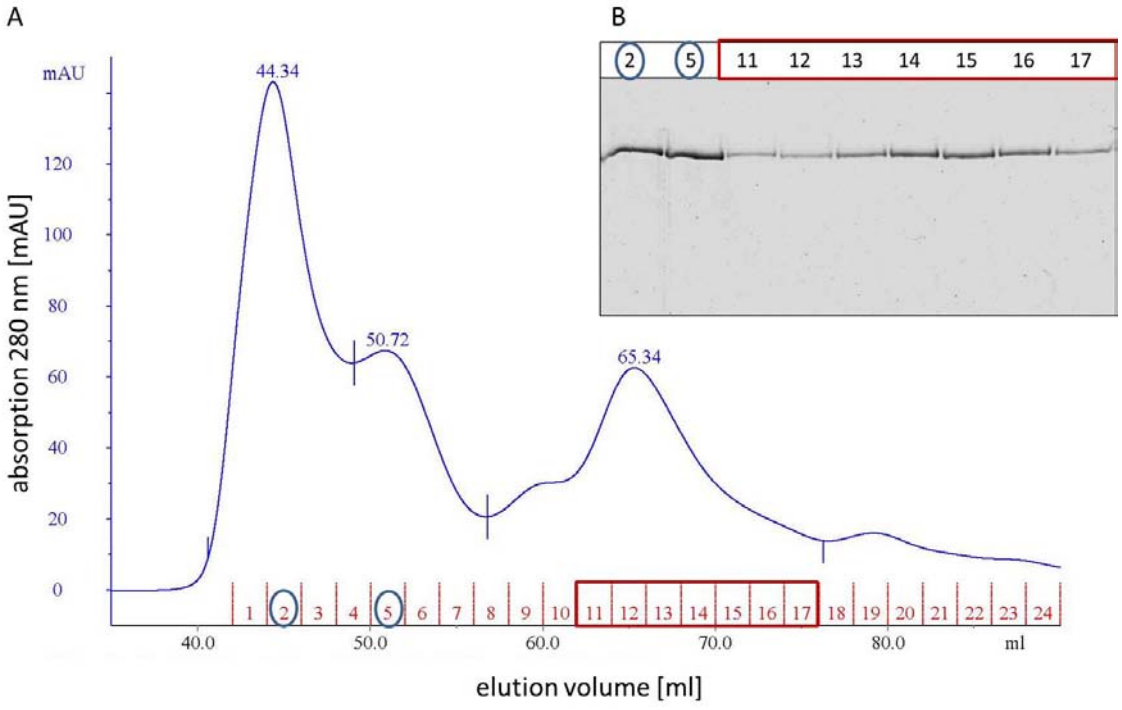

Fig. 3.5 ***SEC elution profile of Ec-YidC on a Superdex 200 16/60 column.*** **(A***) Pooled Ec-YidC IMAC elution fractions (5 ml; Fig. 3.4) were loaded on the Superdex 200 16/60 column to separate aggregated (1. peak at 44.34 ml; > 2000 kDa) and higher oligomers (2. peak at 50.72 ml; ~ 440 kDa) from the dimeric or monomeric (3. peak at 65.34 ml; ~ 158 kDa) form of the protein. Flow rate: 0.5 ml/min System: Äkta purifier Detection: absorbance at 280 nm Fractionation: 2 ml* ***(B)*** *SEC fractions of Ec-YidC, corresponding to the three main peaks were analyzed on 12 % SDS gels (10 µl of each fraction) and Coomassie staining. Blue circles: fraction 2 from peak 1; fraction 5 from peak 2. Red box: fractions 11 – 17 of the third dimer / monomer Ec-YidC peak. All fractions showed pure Ec-YidC, but in putatively different oligomeric states.*

Fractions 14 – 16 (Fig. 3.5 B) were concentrated by an Amicon® Ultra centrifugal unit 15 ml (MWCO 30 kDa) to a concentration of 0,641 mg/ml (= 10,6 µM). The concentration was determined by measurement of the absorbance at 280 nm with the NanoDrop 2000 UV-Vis spectrophotometer and calculated using the following parameters: ε_{YidC} = 93310; MW = 60 kDa. The concentrated Ec-YidC sample was stored in aliquots at 4 °C and used for further *in vitro* assays (3.2.2 & 3.3.2).

2. Purification of the YidC-Rb$_{NHis}$ chimera (2.10.2)

High effort was made to optimize the YidC-Rb purification, mainly for the cryo-EM structure (3.3.1). For the reconstitution of YidC-Rb with RNCs for the cryo-EM studies it was necessary to get a very pure and homogeneous protein sample of 1 ml with concentrations between 1 – 2 mg/ml.

The recombinant expression of the YidC-Rb from a pET16b vector (2.3.2 B3) was performed in a 6 L LB culture of *E. coli* C43 cells for 2 h at 37 °C. After the preparation of inner membrane vesicles (IMV), the YidC-Rb protein was solubilized with 1,5 % LDAO and purified by Ni chelating chromatography (IMAC). The protein was eluted in 10 x 2 ml fractions with buffer E_{ER} (50 mM Tris pH 7.5, 300 mM NaCl, 5 % glycerol, 0,2 % LDAO, 1 mM DTT, 500 mM imidazole). 10 µl sample of fractions 1 – 8 were analyzed on a 12 % SDS acrylamide gel and Coomassie staining (Fig. 3.6).

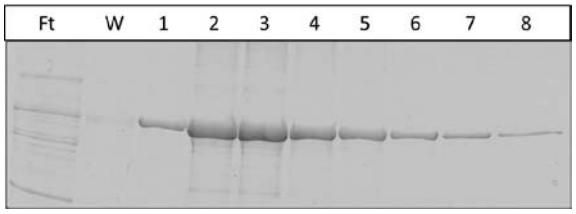

Fig. 3.6 ***IMAC elution fractions of YidC-Rb$_{NHis}$.*** *Samples, corresponding to the amount of protein of 1 ml cell culture, from the IMAC flow through (Ft) and the washing step (W), as well as 10 µl of each of the YidC-Rb elution fractions (1-8) were analyzed on a 12 % SDS gel by Coomassie staining.*

For further purification, the main elution fractions (Fig. 3.6 1-7) were pooled, concentrated (Amicon® Ultra 15 ml; MWCO 30 kDa) to 5 ml and loaded onto a Superdex 200 16/60 column. The SEC of YidC-Rb was performed in buffer GF_{Rb} (50 mM Tris pH 7.5, 300 mM NaCl, 5 % glycerol, 1 mM DTT, 0,2 % LDAO) at a flow rate of 0,75 ml/min at room temperature. The elution profile of YidC-Rb was monitored using UV absorbance at 280 nm (Fig. 3.7 A). 1 ml fractions were collected and samples of the main peaks were analyzed (10 µl each) on a Coomassie stained 12 % SDS gel (Fig. 3.7 B). All samples of the different fractions at the various retention times showed a single YidC-Rb band, indicating that the YidC-Rb load (Fig. 3.7 B load$_{SEC}$) contained inhomogeneous oligomeric states of the protein. This became obvious by analyzing the elution profile of the SEC (Fig.

3.7 A) and calculating the respective molecular weights. YidC-Rb started eluting from the beginning of the void volume (= 43 ml) up to the end of the main elution peak (= 70 ml). However, there was a dominant peak with a maximum at 63,25 ml (fractions 22 – 25), corresponding to a MW of ~ 180 kDa. This leads to the assumption that the dimeric form of YidC-Rb, with a calculated monomeric mass of ~ 70 kDa and a LDAO micelle with the theoretical MW of ~13 kDa, was present in the second main elution peak. Again it cannot be excluded that in the later fractions (28 – 33) of the second peak monomeric YidC-Rb was present.

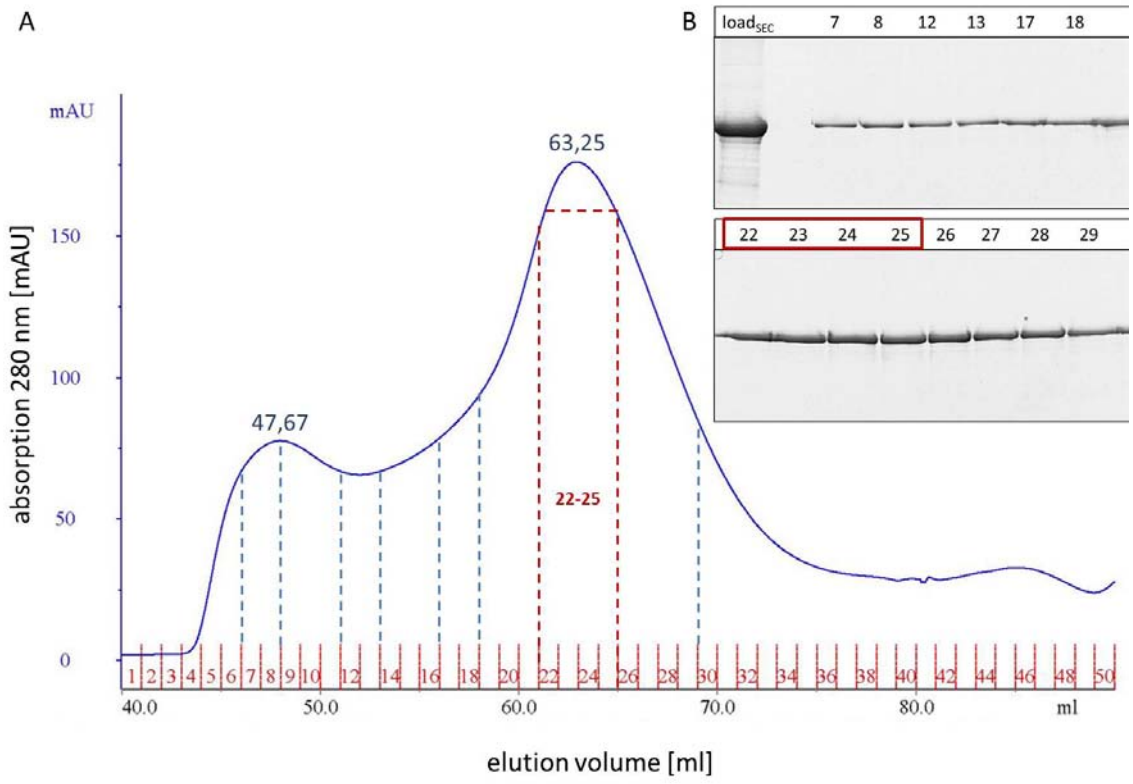

Fig. 3.7 ***SEC elution profile of YidC-Rb on a Superdex 200 16/60 comlumn.*** **(A)** *Pooled YidC-Rb IMAC elution fractions (5 ml concentrated) were loaded on the Superdex 200 16/60 column to separate aggregated (1. peak at 47,67 ml; > 2000 kDa) and higher oligomers (fraction 12 - 18) from the dimeric or monomeric (2. peak at 63,25 ml; ~ 158 kDa) active form of the protein. Flow rate: 0,75 ml/min System: Äkta purifier Detection: UV absorbance at 280 nm Fractionation: 1 ml* ***(B)*** *SEC fractions of YidC-Rb, corresponding to the main peaks were analyzed on 12 % SDS gels (10 µl of each fraction) and Coomassie staining. Load$_{SEC}$: 10 µl sample of 5 ml concentrated YidC-Rb IMAC elution. Dashed lines blue: fraction 7+8 from peak 1; fraction 12+13, 17+18 from the shoulder between peaks 1+2; fraction 22 – 29 of the main dimer / monomer YidC-Rb peak. Dashed lines red: dimeric YidC-Rb fractions 22-25. All fractions showed pure YidC-Rb, but in different oligomeric states.*

The main peak fractions 22 – 25 (Fig. 3.7; red dashed lines) were concentrated to 1,5 mg/ml (= 23,07 µM). The concentration was determined by measurement of the UV

absorbance at 280 nm and calculated using the following parameters: $\varepsilon_{YidC\text{-}Rb}$ = 96260; MW = 70 kDa. The concentrated YidC-Rb sample was stored in aliquots at 4 °C and used for the cryo-EM studies (3.3.1) and for further *in vitro* assays (3.2.2 & 3.3.2).

3.1.3 Ribosome binding of YidC is improved by the extended C-terminal tails

Since ribosome binding of the C-terminal region of the mitochondrial Oxa1 protein has been documented (Jia *et al*., 2003), it would be interesting to see whether the extended C-tails of YidC homologs from Gram-negative marine bacteria have a similar function.

The ribosome binding assays were mainly established within the scope of my diploma thesis (Seitl, 2010) and therefore will be discussed just briefly in this work. Ribosomes were isolated from *E. coli* MRE600 cells using a special chromatography system (Maguire *et al*., 2008) and incubated with the purified YidC proteins (Fig. 3.2) on ice. The ribosome-bound YidC proteins were separated by centrifugation and the pellet and supernatant fractions were analyzed by SDS-PAGE (Fig. 3.8). Whereas YidC-Rb and YidC-Oa fusion proteins readily bound to the 70S ribosomes and consequently were found in the pellet fraction (Fig. 3.8 A and C), YidC from *E.coli* was found in the supernatant (Fig. 3.8 A). Likewise, Oa-YidC, the insertase homolog from *O. alexandrii*, was found associated with the *E. coli* ribosomes in the pellet fraction (Fig. 3.8 D). When no ribosomes were present, virtually the bulk of all YidC versions was found in the supernatant.

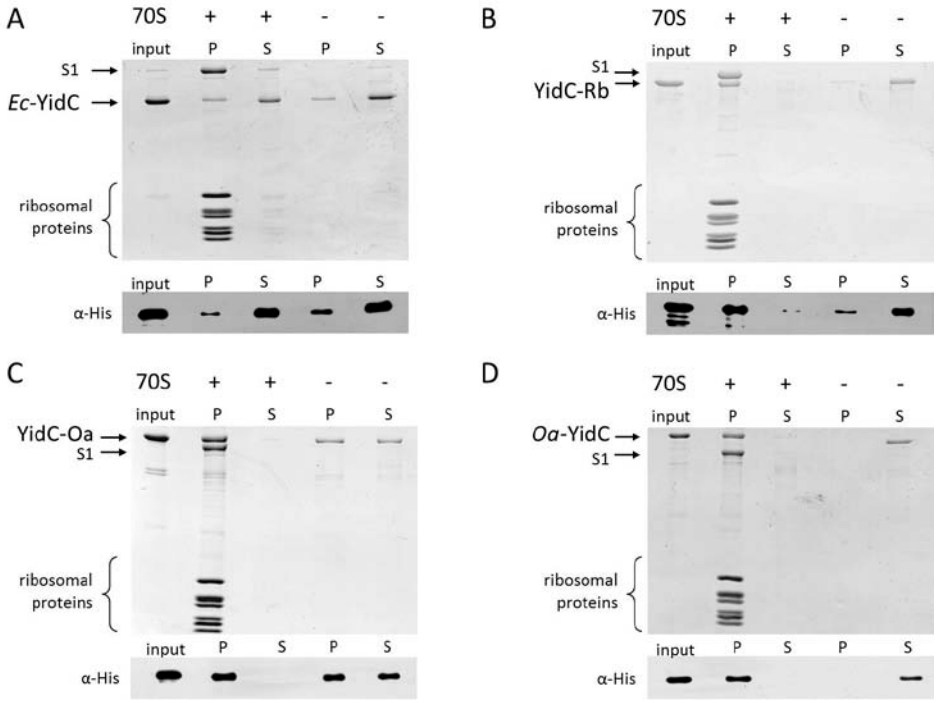

Fig. 3.8 ***Ribosome binding of YidC by the extended C-tails.*** *The N-terminally his-tagged, purified YidC proteins were incubated with isolated E. coli ribosomes and binding was analyzed by centrifugation. Pellet (P) and supernatant (S) were collected and analyzed by SDS-PAGE, stained with Coomassie blue (upper panels) or analyzed by Western blot using an anti-His antibody (lower panels). Ec-YidC* ***(A)****, YidC-Rb* ***(B)****, YidC-Oa* ***(C)*** *and Oa-YidC* ***(D)*** *were analyzed. As a control, the distribution of the YidC proteins was monitored in the absence of ribosomes. S1: ribosomal protein S1 of the 30S subunit.*

The binding of the YidC proteins with the extended C-terminal tails to the ribosomes was salt sensitive, indicating that binding is mediated by ionic interactions (Fig. 3.9).

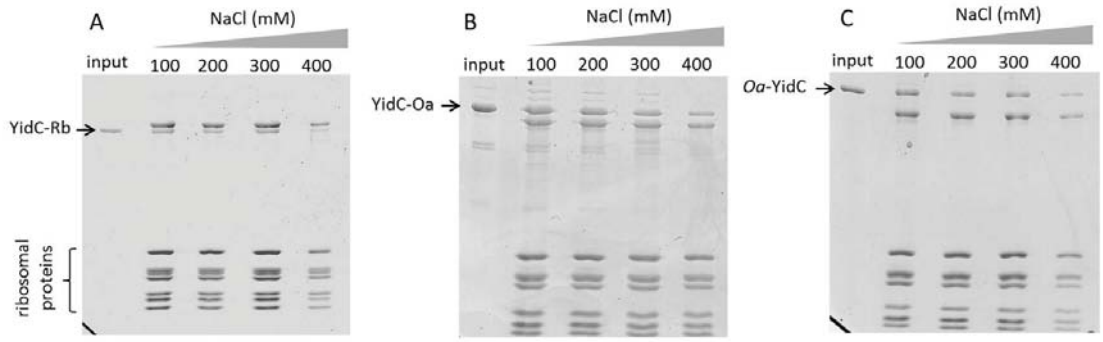

Fig. 3.9 ***Binding of the YidC variants to E. coli 70S ribosomes is mediated by ionic interactions.*** *To test the salt-sensitivity of the interaction, the in vitro ribosome binding assay was performed with increasing concentrations of NaCl. In the presence of up to 300 mM NaCl constant amounts of YidC-Rb* ***(A)****, YidC-Oa* ***(B)*** *and Oa-YidC* ***(C)*** *was found in the ribosome containing pellet. In the presence of 400 mM NaCl binding was significantly reduced for all three YidC proteins.*

These data demonstrate that the charged C-terminal extensions are crucial for efficient binding of the ribosome to YidC. Therefore, the C-terminal tails of the marine YidC homologs most likely function as ribosome binding domains.

3.2 Structural studies of the $YidC_{Rb}$ - ribosome complex

Since the obtained results demonstrate increased ribosome affinity of the YidC derivatives with an extended hydrophilic C-terminal domain, we performed a structural analysis of YidC-ribosome complexes using cryo-EM and CD-spectroscopy.

3.2.1 Cryo-EM structure of the $YidC_{Rb}$ – RNC complex

In order to get high resolution cryo-EM structures of a $YidC_{Rb}$ – RNC complex, the preparation of a homogeneous sample was a prerequisite. The homogeneously purified YidC-Rb protein (3.1.2) was provided from our laboratory. The ribosome nascent chain (RNC) formation and purification, as well as the cryo-EM and 3D reconstruction was carried out by our collaboration partner Stephan Wickles from the Roland Beckmann laboratory (Gene Center and Department of Biochemistry) of the Ludwig-Maximillian's-University in Munich, Germany.

In addition to the C-terminal ribosome binding domain of the YidC-Rb chimera, the use of RNCs instead of empty ribosomes stabilizes the insertase-ribosome complex (Kedrov *et al*., 2013). Therefore we used a TnaC stalled (Seidelt *et al*., 2009) nascent peptide chain of the mechanosensitive channel protein MscL, that is known to be a native substrate protein of the *E. coli* YidC. MscL is targeted to the membrane of *E. coli* by SRP and is then inserted by YidC into the inner membrane (Facey *et al*., 2007). The MscL protein consists of 136 amino acid residues and possesses two transmembrane helices (aa 17-45 and 75-94). In addition, there is a cytoplasmic amphipathic helix in the C-terminal segment (aa 105-119; Fig. 3.10 A). The *in vitro* translation system was programmed with an mRNA coding for an N-terminal His-tag followed by amino acid residues 1 – 115 of MscL and the TnaC stalling sequence at the C-terminus (Fig. 3.10 B). This results in a ribosome-coupled nascent protein chain bearing the first two transmembrane helices of MscL being fully emerged from the ribosomal exit tunnel. The RNCs were synthesized in a coupled *in vitro* transcription-translation reaction and purified as described (Seidelt *et al*., 2009), using the His_6-tag for affinity purification.

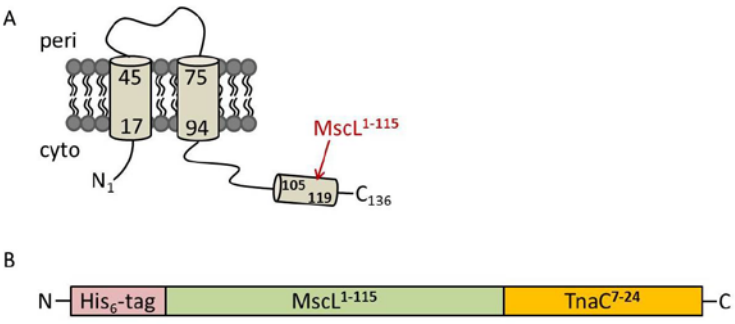

Fig. 3.10 ***Schematic representation of MscL and the MscL - nascent chain construct. (A)*** *Topology model of the E. coli MscL protein with its two TM domains and the characteristic C-terminal helix.* ***(B)*** *The MscL$^{1-115}$ nascent chain construct was stalled by the TnaC$^{7-24}$ sequence and contains an N-terminal his-tag for purification.*

For the cryo-EM analyses, isolated MscL-RNCs were reconstituted with the purified YidC-Rb (3.1.2) for 30 min at 37 °C. We determined the 3D structure of a complex consisting of a single YidC-Rb bound to a translating ribosome carrying the MscL protein with its first two TM segments as a nascent chain stalled by a C-terminally fused TnaC sequence (Fig. 3.11). The position of the extra density accounting for YidC-Rb agreed well with the density pattern observed in an earlier study of ribosome-bound *E. coli* YidC (Kohler *et al*., 2009). Moreover, we observed a similar interaction pattern between our C-terminally extended YidC-Rb and the ribosome. Ribosomal rRNA helix H59 and the ribosomal protein L24 appear to be the main contact sites with both types of YidC. Thus, the presence of the C-terminal extension increases the affinity of YidC to the ribosome without changing its overall interaction mode. An additional contact to the ribosomal protein L29 was observed for the bound YidC-Rb protein (Fig. 3.11 D).

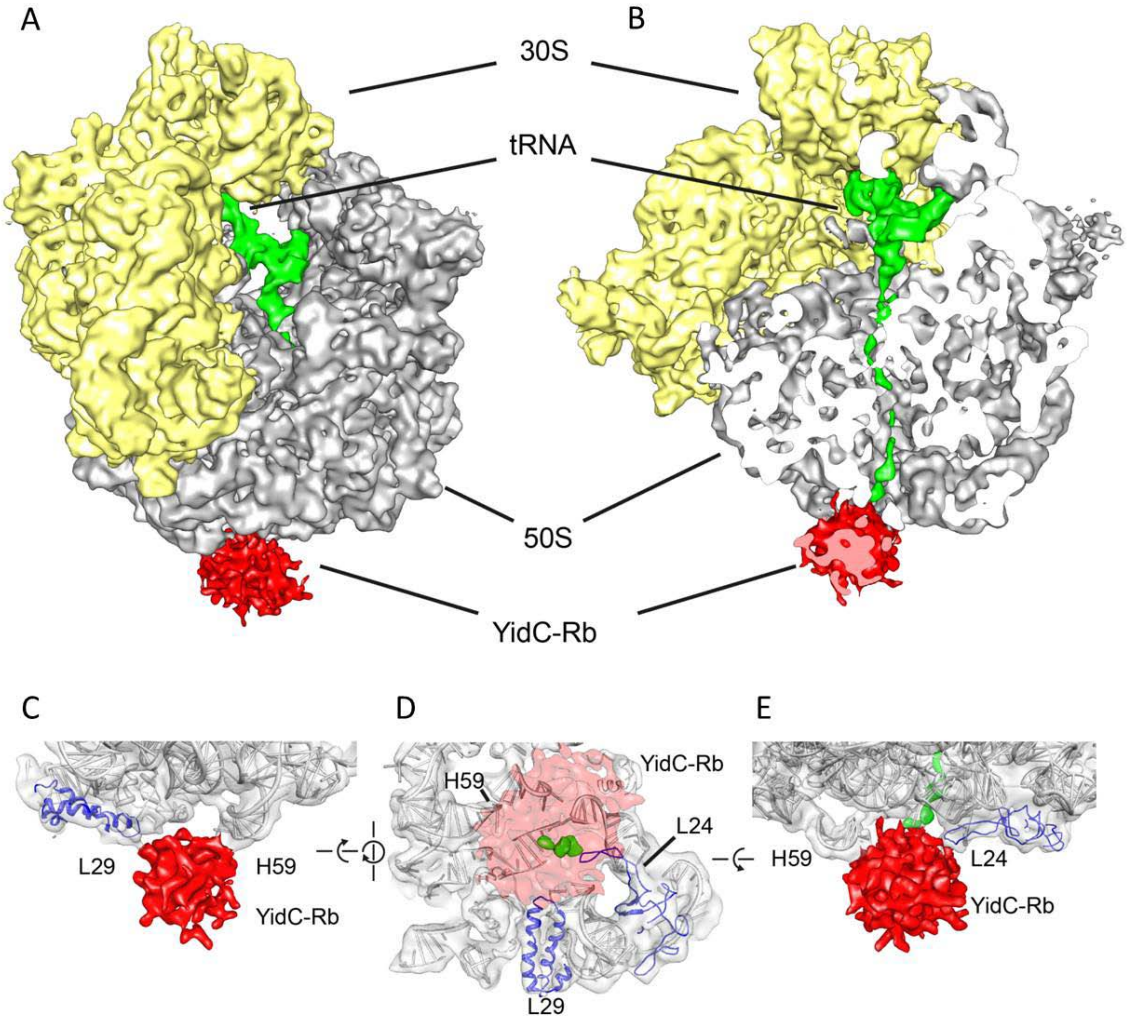

Fig. 3.11 ***Cryo-EM reconstruction of an RNC-YidC-Rb complex****. **(A)** The 30S and 50S ribosomal subunits are shown in yellow and grey, respectively; tRNA is shown in green and additional density accounting for YidC-Rb in red. **(B)** Cut through of the density to view the ribosomal tunnel and fragmented nascent chain density in green. **(C** and **E)** Close up view with the fitted molecular model of a 70S ribosome. L24 and L29 are shown in blue. YidC-Rb shows defined contacts to the ribosomal proteins L24, L29 and the helix H59. **(D)** Close up bottom view of the interaction area with a transparent density for YidC-Rb and the nascent MscL chain (green) surrounded by the YidC-Rb density.*

For the 3D reconstruction a total of 14 165 micrographs were collected. 4 488 were selected manually for further processing based on the information content of the power spectra and particle density on the grid. The complete data sets of 140 266 particles was aligned to the structure of an empty ribosome that was generated using the crystal structure of an *E. coli* ribosome (Schuwirth *et al*., 2005). Using semi-supervised classification (Penczek *et al*., 2006) it was possible to sort for subpopulations showing distinct ribosomal conformations and ligands (+/- E-site tRNA, +/- ligand at tunnel exit). A final data set of 51 903 particles resulted in a density map refined to 8.6 Å resolution

according to a Fourier Shell Correlation (FCS at 0.5 cut-off) showing P-site tRNA and high occupancy of YidC-Rb at the ribosomal exit site.

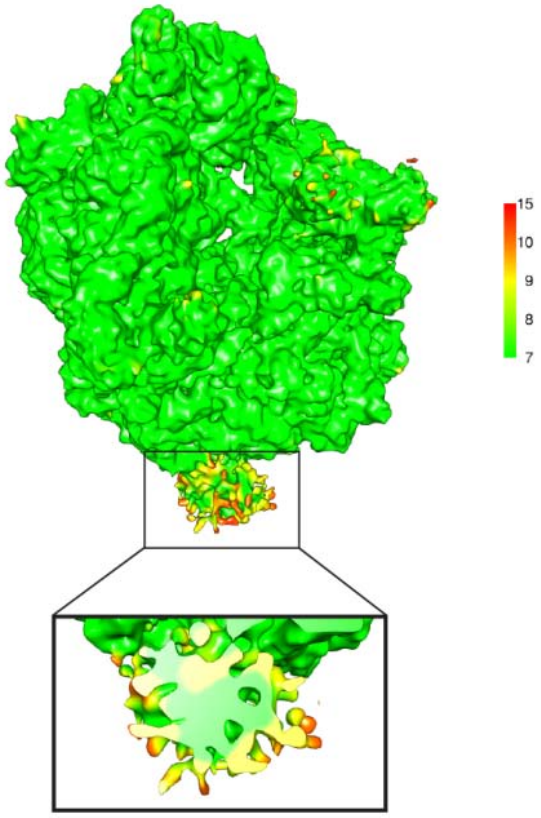

Fig. 3.12 ***Local resolution of the RNC-YidC-Rb map.*** *Surface and cross-section of the electron density map colored according to the local resolution. A reconstitution of the complex could be refined to 8.6 Å resolution after semi-supervised classification using competitive projection matching.*

The TnaC-stalled ribosome has a strong density for a tRNA molecule located in the P-site indicating a high percentage of programmed RNCs in the final dataset. The path of the nascent chain can be traced from the peptidyl transferase center (PTC) through the ribosomal tunnel into an extra density at the tunnel exit representing YidC-Rb (Fig. 3.13).

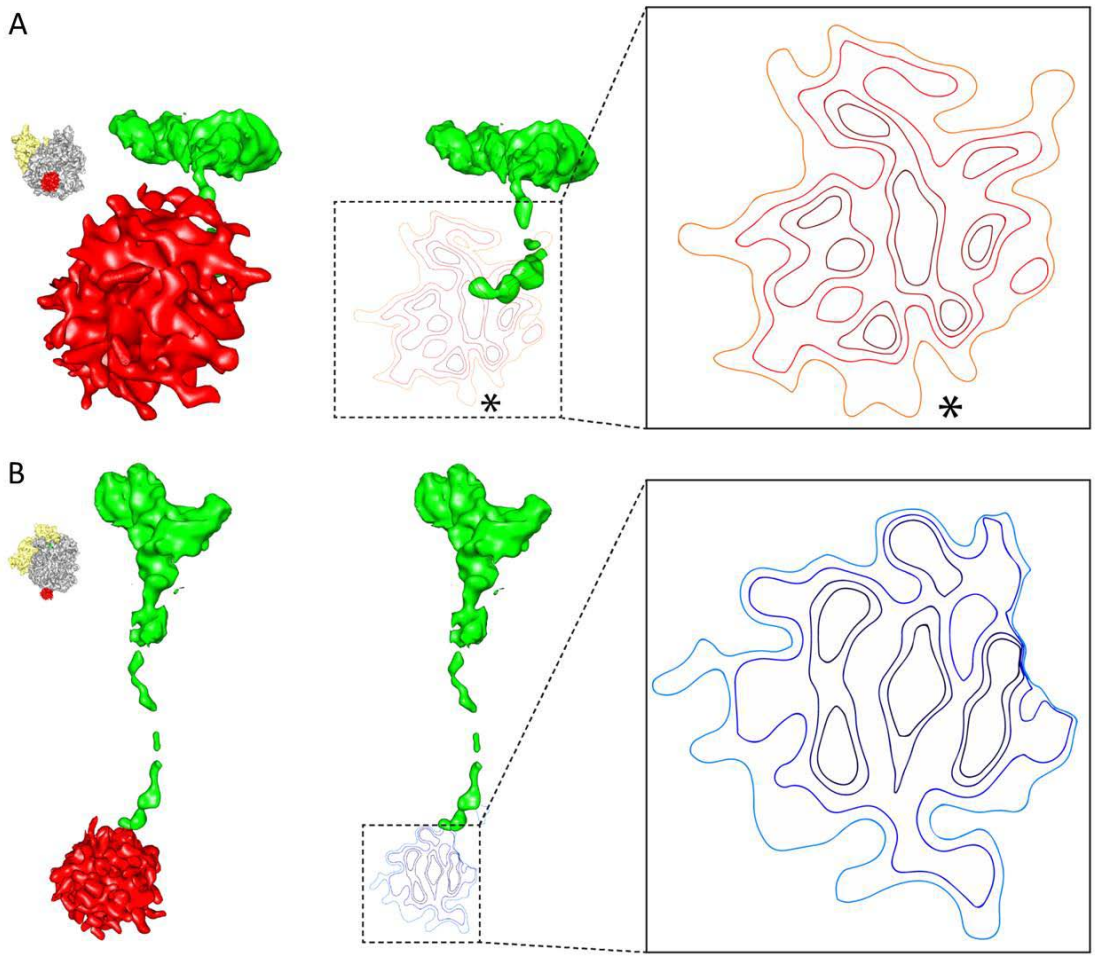

Fig. 3.13 ***3D structure of the isolated density for the nascent chain – YidC-Rb complex at 8.6 Å. (A)*** *Bottom view of the isolated YidC-Rb density. Density blot of YidC-Rb shows entering of the nascent MscL chain (green) in the center of the YidC-Rb density (red). The asterisks mark the position of the ribosomal protein L29.* ***(B)*** *Side view of the translating ribosome carrying the MscL protein with its first 2 TM segments as a nascent chain stalled with an introduced TnaC sequence.*

Notably, the presence and size of the detergent micelle (LDAO) surrounding the solubilized YidC-Rb was difficult to estimate at this resolution. Also, the large periplasmic loop of YidC-Rb between TM1 and TM2 is not resolved in the cryo-EM structures probably due to its dynamic motions relative to the membrane-embedded domains. The size of the density indicates the presence of only one copy of YidC-Rb under our conditions (Fig. 3.11). Even when assuming the presence of a minimal micelle, a YidC homodimer, as had been suggested in a previous study (Kohler *et al*., 2009) could not be accommodated. This suggests that a single copy of YidC is stably bound to the ribosome and may be sufficient to act as a ribosome-bound insertase complex for MscL as proposed by Kedrov *et al*., 2013.

3.2.2 The ribosomal protein L29 binds to the C-terminal tail of YidC-Rb

To investigate whether the observed contact between YidC-Rb and L29 is caused by the extended C-tail of the protein, the ribosomal proteins L24 and L29 were purified and their interaction with YidC-Rb was analyzed in pull-down experiments. The purified L24 protein was kindly provided by my master student Emmanuelle Mboubi. Since both ribosomal proteins were purified similarly (2.10.4), only the purification of L29 is shown here.

The ribosomal proteins were expressed in *E. coli* BL21 cell cultures and purified via a Strep-tag fused to the N-terminus of the protein. Because both proteins, L24 as well as L29, were soluble, the cleared supernatant after the cell disruption was directly applied to strep-tag affinity chromatography. $L29_{strep}$ was eluted from the matrix with buffer E_{Rib} (100 mM Tris pH 8, 150 mM NaCl, 1mM EDTA, 2,5 mM desthiobiotin) and 10 µl of each fraction were analyzed on an 18 % SDS gel (Fig. 3.14). The L29 protein was isolated and ran on the gel at a height, corresponding to a molecular weight of ~ 10 kDa. Notably, the contaminating proteins in the elution fractions showed the typical pattern of 70S ribosomal proteins (Fig. 3.14). Therefore it seems that the recombinantly expressed $L29_{strep}$ protein was present in a complex with the endogenous *E. coli* ribosomes, so that the ribosomes co-eluted with $L29_{strep}$ from the matrix.

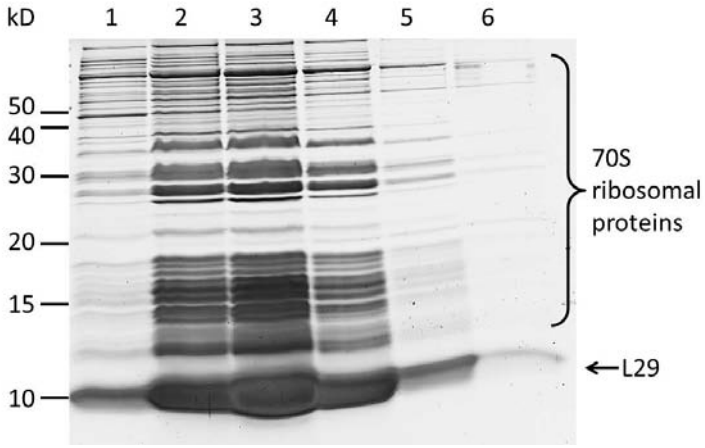

Fig. 3.14 ***Strep elution fractions of L29.*** *10 µl of $L29_{strep}$ elution fractions 1-6 were analyzed on an 18 % SDS gel and Coomassie staining. 70S ribosomes co-elute with L29.*

To separate the strep-tagged L29 from the endogenous ribosomal proteins and other contaminants, an ion exchange chromatography (IEC) followed. Since L29, as well as L24, has a rather basic isoelectric point (pI) of ~ 10, a cation exchange chromatography (CEX) using a SP Sepharose Fastflow column was performed. Prior CEX, the salt concentration of the L29 sample has to be reduced to ensure proper binding to the SP Sepharose matrix. The main fractions from the Strep-tag affinity purification (Fig. 3.14; fractions 2-4) were concentrated (Amicon® Ultra, MWCO 3 kDa) to 1 ml and a buffer

exchange with SP-buffer$_A$ (50 mM Tris pH 8, 100 mM NaCl, 1 mM EDTA, 1 mM DTT) on a HiTrap desalting column using the Äkta-purifier system was performed. The resulting HiTrap elution fractions were pooled and immediately loaded onto the SP Sepharose column for CEX (maximal load: 5 ml), followed by a washing step with SP-buffer$_A$ to remove unbound proteins. Subsequently, the L29 protein was eluted by a linear salt gradient from 100 mM (0% B) to 1 M NaCl (100% B) over 20 cV. L29 eluted at the beginning of the NaCl gradient between 5 – 10 % buffer B (Fig. 3.15 A), showing a defined peak including the fractions 3 - 8 that were analyzed on a 18 % SDS gel (Fig. 3.15 B).

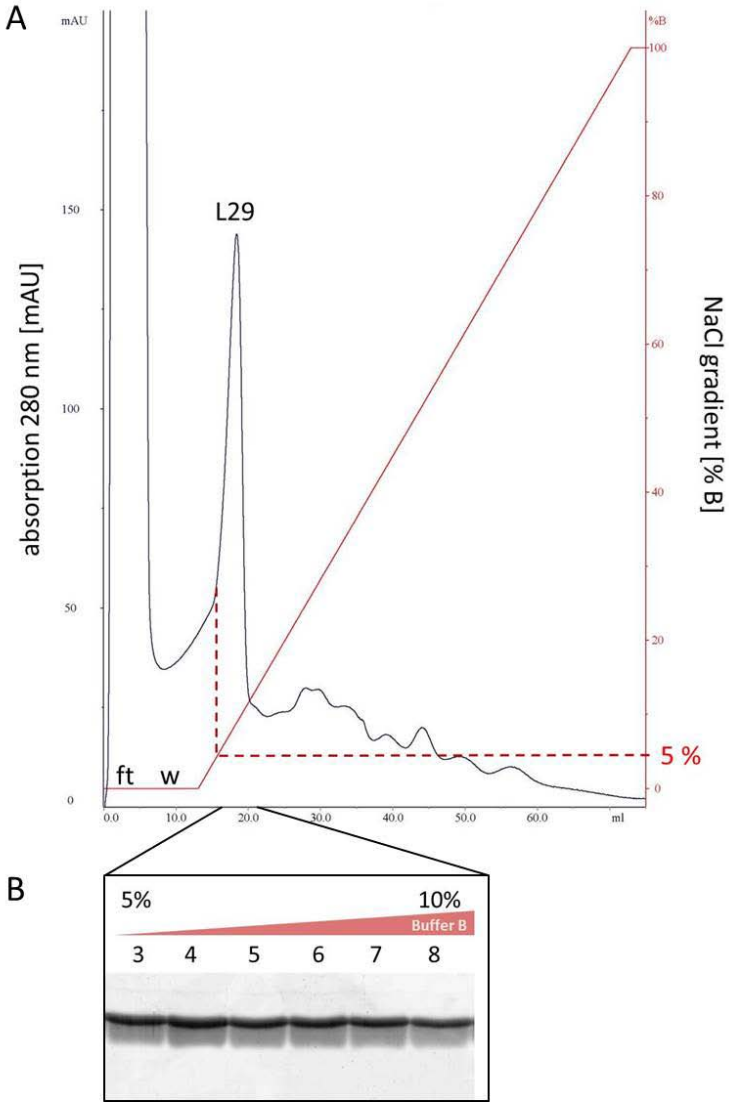

Fig. 3. 15 ***CEX elution profile of L29 with SP Sepharose Fast flow. (A)*** *The ribosomal protein L29 started eluting from the CEX-matrix at 5 % buffer B of the NaCl gradient. ft: flow through (5 ml; peak > 2000 mAU) w: washing step (2 cV).* ***(B)*** *10 µl samples of the fractions 3-8 of the L29 peak were analyzed on an 18 % SDS gel and visualized by Coomassie staining, showing that the L29 protein eluted between 5 – 10 % buffer B.*

The early elution point (5 – 10 % buffer B) suggests a weak binding of L29 to the cation exchange matrix, probably due to still too high salt concentration in the loaded sample and

in the SP-buffer$_{A}$ (100 mM NaCl). However the peak fractions showed pure L29 protein in sufficient amounts and hence were used for the further pull down assays.

To study the interaction of the ribosomal proteins with the YidC insertases, the purified ribosomal proteins were loaded on Ni-NTA agarose matrix-immobilized YidC-Rb$_{NHis}$ and Ec-YidC$_{NHis}$, respectively (3.1.2). The L24 as well as the L29 protein co-eluted from the resin together with the His-tagged YidC-Rb protein (Fig. 3.16 A; lane 4), demonstrating that both ribosomal proteins physically interact with YidC-Rb. In contrast, L29 was unable to bind and therefore did not co-elute from the resin together with the His-tagged wild type Ec-YidC (Fig. 3.16 B lane 4, lower panel), whereas L24 co-eluted in similar amounts as for YidC-Rb (Fig. 3.16 A and B lane 4, upper panels).

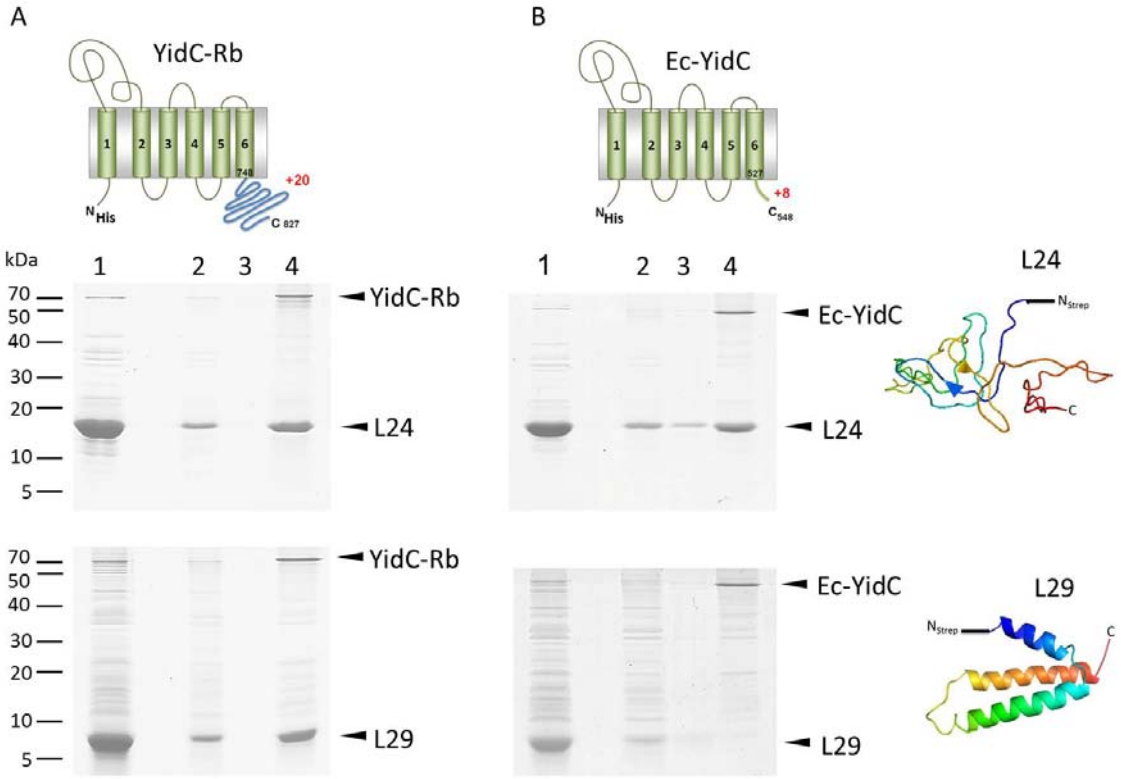

Fig. 3. 16 ***Interaction of the ribosomal proteins L24 and L29 with YidC-Rb and Ec-YidC.*** *Pull down assays of L24 (upper panels) and L29 (lower panels) were performed with immobilized YidC-Rb* ***(A)*** *and Ec-YidC* ***(B)****, respectively****.*** *About 120 µg of the respective YidC$_{His}$ proteins were attached to the NiNTA resin. Purified L24$_{Strep}$ or L29$_{Strep}$ (~ 500 µg) proteins were then loaded onto the immobilized YidC proteins. Lanes 1 show the total amount of added L24 and L29, respectively (input). Unbound protein was collected by gravity flow (lanes 2). After three washes (lanes 3 show the last washing steps), bound proteins were eluted with 500 mM imidazole by centrifugation (lanes 4). The proteins were acid-precipitated and analyzed by SDS-page and Coomassie staining.*

These results show that the enhanced affinity of YidC-Rb to the ribosome is at least partially caused by the interaction of the C-terminal domain of the *R. baltica* YidC homolog

with the ribosomal protein L29. But also features of the wild type Ec-YidC may contribute to the binding as suggested by the interaction of Ec-YidC with the ribosomal protein L24.

3.2.3 Structure of the YidC/Oxa1/Alb3 C-terminal domains (CTDs)

To further investigate the native architecture of the C-terminal domains of the diverse YidC homologs, the CTDs of both marine YidC homologs (RbCT, OaCT) as well as of Alb3 (A3CT) and Oxa1 (O1CT) were isolated as peptides without the insertase core domain and inspected by far-UV CD-spectroscopy and binding assays. The most important facts of the CTDs are summarized in Fig. 3.17 A. The amino acid sequence alignment of the CTDs showed no significant homology (Fig. 3.17 B). Therefore, it is assumed that the functional similarities are caused by shared structural features in the C-terminal extended domains, like the huge number of positively charged amino acid residues, the highly basic theoretical pI and probably a specific folding mechanism upon binding.

A

CTD	organism	number of amino acids (aa)	positively charged aa	theoretical pI	MW [kD]
RbCT	*R. baltica*	80	19	10.44	8.4
OaCT	*O. alexandrii*	99	17	9.52	10.4
O1CT	*S. cerevisiae*	91	22	10.73	10.7
A3CT	*A. thaliana*	114	26	9.39	12.7

B

```
RbCT_1    --------------------------------PSKPH----------FDPATL----QGA    14
OaCT_1    ------------------------RQGVVTELDRNFFKVRAKLTGSAVPAKY----QGE    31
O1CT_1    QTMILRNKWVRSKLKITEVAKPRTPIAGASPTENMGIFQS-------LKHNIQKARDQAE    53
A3CT_1    ------QVYLR-------------KLGGAKPNMDENASKIIS--AGRAKRSIAQPDDAGE    39
                                                .                .

RbCT_15   A---AGGGTVDGKVNNSA---------GANGK------KSSDGKPKTMADRLRERLGT--P    55
OaCT_32   DTPTATNQVIEGKVEKAV---------TELAEDANADAAITDGETPA-NPETPAKPGT--P    80
O1CT_54   RRQLMQDN--EKKLQESFKEKRQNSKIKIVHKSNF-----------INN-----------    89
A3CT_40   RFRQLKEQEKRSKKNKAVA----KDTVELVEESQS--ESEEGSD---DEEEEAREGALAS    90
                    * :::          .

RbCT_56   EEEAAPLPKDRKRPPSKKPGNKKRR--                                    80
OaCT_81   GRR------VSSNPAAKKPRGGKKK--                                    99
O1CT_90   ---------------------KK----                                    91
A3CT_91   STTSKPLPEVGQRRSK---RSKRKRTV                                   114
                              :
```

Fig. 3.17 ***Comparison of the CTDs of diverse members of the YidC/Oxa1/Alb3 family. (A)*** *All compared CTDs have in common that the elongated C-terminal domain (from 80 – 114 aa) contains a huge number of positively charged aa (from 19 – 26) and a basic theoretical isoelectric point (pI) of about 10. All parameters were calculated using the ExPASy ProtParam tool.* ***(B)*** *Sequence alignment of the C-terminal amino acid residues of RbCT, OaCT, O1CT and A3CT. There is no striking sequence homology within the CTDs. Only 1 lysine residue shows an identical*

position in all 4 domains (asterisk). Two points indicate position of residues with very similar characteristics and one point indicates residues with minor similarities. Positively charged residues are shaded green. The alignment was performed using UniProt (UniProt Consortium, 2015).

The CTDs of RbCT, OaCT and O1CT were amplified by PCR using the YidC-chimera plasmids as template DNAs and cloned as fusion with either an N- or C-terminal His tag in pET16b or pET22b, respectively (2.3.2 B5, B6 + B8). The A3CT (2.3.2 B7) construct was kindly provided by the Irmgard Sinning group, Heidelberg (Falk *et al.,* 2010). The CTDs were expressed according to the best conditions described in Table 2.1 and purified from 1 L cultures as described in the method section (2.10.5). The IMAC elution fractions of the CTDs showed a good yield of RbCT, OaCT and A3CT (Fig. 3.18 A, B and D), whereas the purification of O1CT could not be achieved with satisfying amounts (Fig. 3. 18 C).

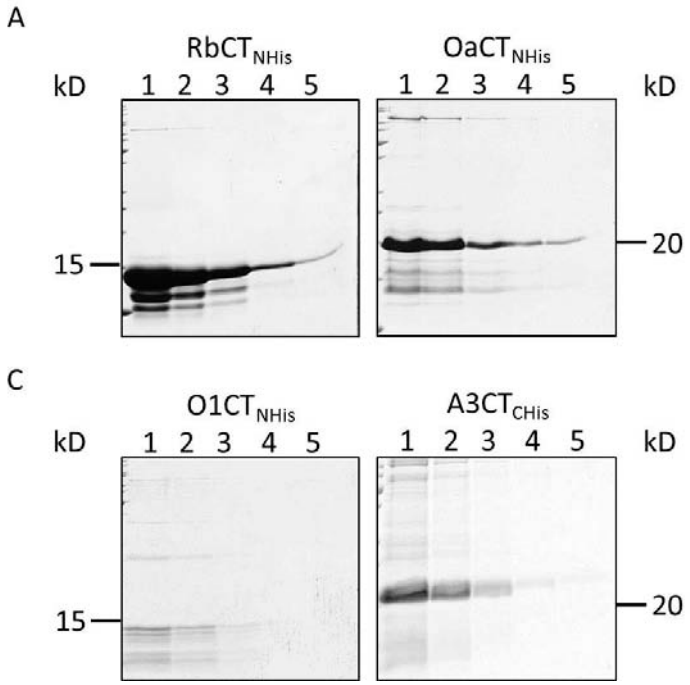

Fig. 3.18 ***IMAC elution fractions of the C-terminal YidC/Oxa1/Alb3 domains.*** *10 µl of each RbCT* ***(A)****, OaCT* ***(B)****, O1CT* ***(C)*** *and A3CT* ***(D)*** *fractions 1-5 were analyzed on 15 % SDS-gels and Coomassie staining. A3CT was purified using a C-terminal His tag, the others as N-terminally tagged versions.*

For further purification of the CTDs, a cation exchange chromatography (CEX) using a SP Sepharose FastFlow matrix was performed. The salt concentration of the CTD elution buffer from the IMAC (50 mM Tris, 150 mM NaCl) was low enough to bind the proteins to the CEX matrix and no buffer exchange has to be performed prior to the IEC. The main fractions of the IMAC elutions were concentrated to 2 ml and loaded onto the SP matrix, followed by a washing step with low salt (150 mM NaCl) buffer A (see method section 2.10.5 for buffer details). Finally, the CTDs were eluted by a linear gradient from 0 % - 100 % of high salt buffer B (1 M NaCl) over 20 cV (Fig. 3.19 A-D). RbCT started eluting from

the matrix at ~ 40 % buffer B (≈ 490 mM NaCl), indicating proper binding to the cation exchange matrix (Fig. 3.19 A). RbCT also eluted in a second peak at higher NaCl concentration (fractions 48 + 49), but only with a low protein yield compared to the main elution peak of fractions 38 – 43. Additionally, the first RbCT peak showed an increased UV absorption at 260 nm (Fig. 3.19 A, red curve), probably due to bound ribosomal RNA of co-eluting ribosomes (Fig. 3.20). The RNA possibly caused earlier elution of RbCT from the negatively charged matrix than the pure RbCT protein without bound RNA in the second peak. The elution of OaCT (Fig. 3.19 B) started at 20 % buffer B (≈ 320 mM NaCl) in a symmetric peak, including the fractions 18 – 24. Similar to RbCT, a second elution peak of OaCT was obtained (fraction 34 – 46), but without changes in the 260 nm absorption. O1CT (Fig. 3.19 C) and A3CT (Fig. 3.19 D) eluted at 22 % and 30 % buffer B, respectively, without a second elution peak at higher NaCl concentrations.

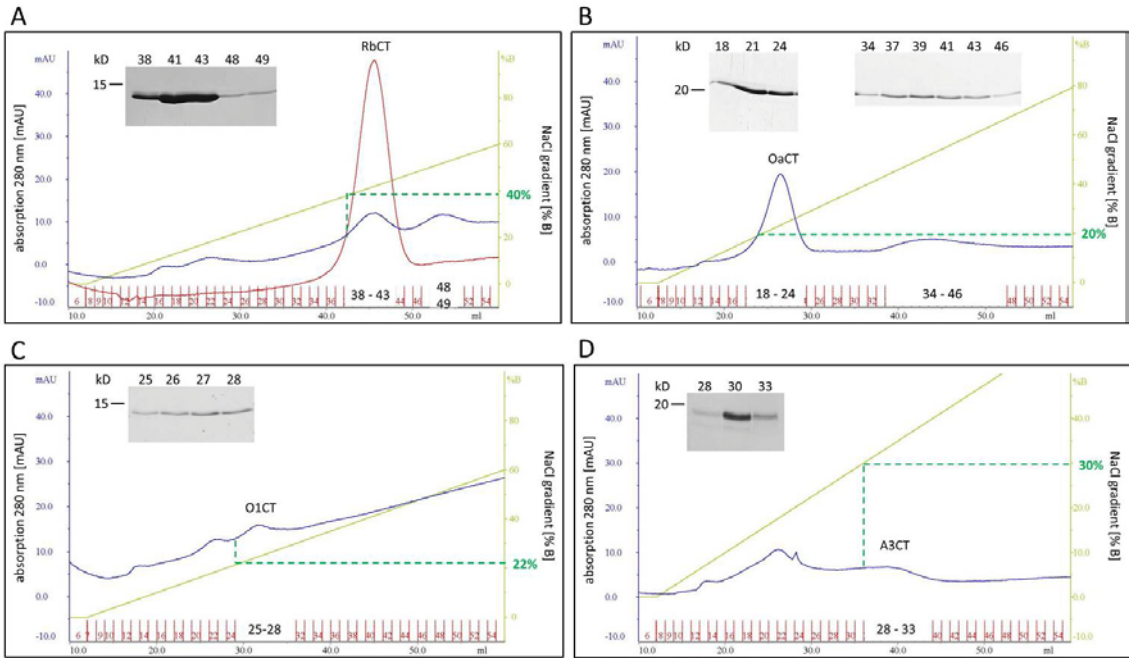

Fig. 3.19 ***IEC elution profiles of the C-terminal YidC/Oxa1/Alb3 domains.*** *The cation exchange profiles show the close up view of the main elution peaks and the respective fractions, analyzed on 15 % SDS-gels by Coomassie staining (insets).* ***(A)*** *RbCT showed the best binding on the SP Sepharose matrix and started eluting at ~ 40 % buffer B. Interestingly, the RbCT peak had an extended absorption at 260 nm (red curve). OaCT* ***(B)*** *and O1CT* ***(C)*** *eluted around 22 % of the salt gradient and the full length A3CT* ***(D)*** *at ~ 30 %. RbCT and OaCT showed two distinct elution peaks. The first (RbCT fractions 38-43; OaCT fractions 18-24) with higher protein amounts than the second peak (RbCT 48-49; OaCT 34-46).*

In general, the CTD peptides showed only small peaks with heights between 10 – 20 mAU for the absorption at 280 nm. This is not surprising since the C-terminal domains are small

proteins with nearly no aromatic amino acid residues. RbCT for example contains no tryptophan (trp), tyrosine (tyr) or cysteine (cys) residues and is therefore expected to be barely visible. Only O1CT contains 1 tryptophan residue and A3CT, as well as OaCT, one tyrosine residue, respectively. Therefore, the protein concentration was not determined by UV absorption at 280 nm, but the peptide backbone was used to calculate the concentration of the CTDs by measuring the UV absorption at 205 nm and estimation of the value according to the empirical formula proposed by Scopes (Scopes, 1974) (2.11).

To highlight the strong binding affinity of the C-terminal tails to ribosomes, $RbCT_{NHis}$ was expressed in *E. coli* and the IMAC of RbCT was performed under low salt conditions, namely 150 mM NaCl instead of 600 mM in the washing step. Within this purification procedure native ribosomes co-purified with his-tagged RbCT resulting in a complex which is stable during SEC (Fig. 3.20).

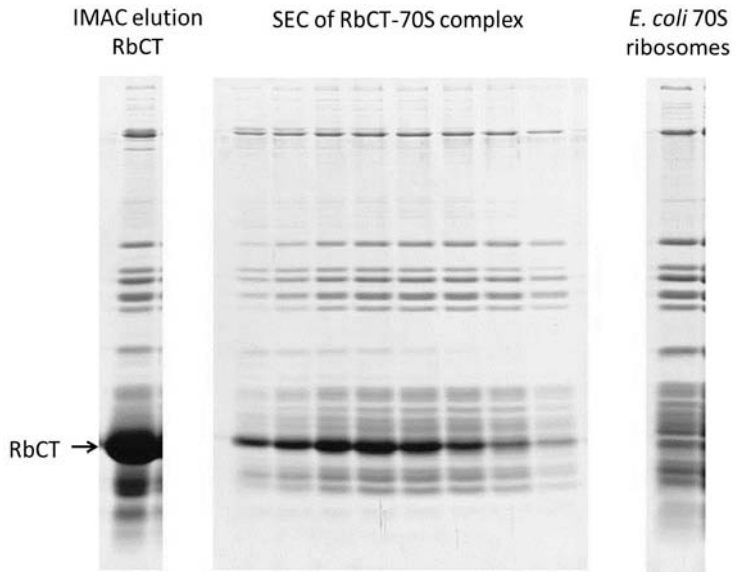

Fig. 3.20 ***RbCT forms a stable complex with E.coli 70S ribosomes.*** *Native 70S ribosomes from E.coli were co-purified with $RbCT_{NHis}$ under low salt IMAC conditions (left panel). The RbCT-70S complex was stable during SEC with a SD75 16/60 column and eluted in a large void peak (middle panel). For comparison, the protein pattern of isolated 70S ribosomes from E. coli is shown (right panel).*

As known from the aforementioned studies of this work (3.2 Fig. 3.9) the binding of the C-terminal domains to ribosomes is mediated by ionic interactions and therefore is salt-sensitive. To avoid the massive co-elution of ribosomes during CTD purification, a high salt washing step of 600 mM NaCl was performed, resulting in separation of the CTD-ribosome complexes as shown in Fig. 3.18.

In previous studies it was shown that the C-terminal domain of the chloroplast Alb3 protein is intrinsically disordered and folds upon interaction with the chaperone cpSRP43, its native binding partner (Falk *et al*., 2010). To test if a ligand-triggered folding also holds for the C-terminal domains of the marine YidC homologs and for Oxa1, potential intrinsic

disorder of the CTDs was analyzed by theoretical structure predictors (PONDR) suited to identify unstructured regions in proteins (Fig. 3.21). RbCT and OaCT are similar to A3CT, their structure being predicted as intrinsically disordered regions for the last 70 amino acid residues (Fig. 3.21 A and B). In contrast to that, O1CT showed two distinct, shorter unfolded regions that were separated by a clearly folded region encompassing the amino acid residues 30 – 35. Also the very C-terminal region (aa 75 – 90) is predicted to be folded.

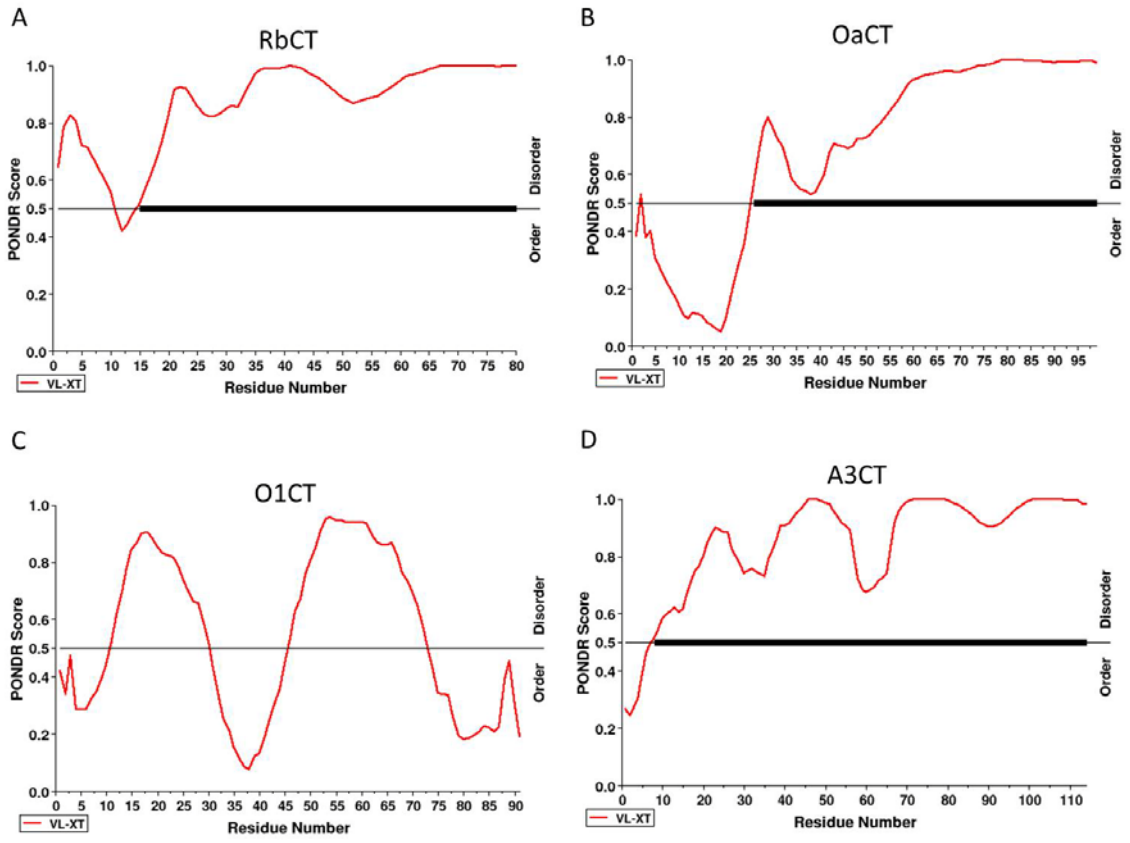

Fig. 3.21 ***PONDR Predictions of naturally disordered regions in the C-terminal domains of YidC/Oxa1/Alb3 family members.*** *RbCT, OaCT and A3CT are clearly predicted as intrinsically disordered regions with an overall percentage of disordered portions of 95, 76 and 94, respectively. However, O1CT with only 53 % overall disorder has two regions (aa 30-45 and 75-90) that were predicted to be folded. Large segments of predicted disorder are indicated by horizontal black bars.*

The potential intrinsic disorder of the isolated C-terminal domains was then experimentally analyzed by far UV CD-spectroscopy. For these purposes, the purified proteins (Fig. 3.19 A-D) were dialyzed against 20 mM K_3PO_4 CD-buffer and the protein concentration was then determined. Unfortunately, O1CT and A3CT were not stable in the CD-buffer and it was not possible to record a proper CD-spectrum. For RbCT and OaCT, far-UV CD-spectra could be measured in the range of 260 nm – 180 nm with 4 accumulations and a

speed of 50 nm/min (2.16), respectively. The far-UV spectra of RbCT (Fig. 3.22 A, blue curve) and OaCT (Fig. 3.22 B, blue curve) exhibited minima around 200 nm and only weak ellipticity above 210 nm, typical for unfolded proteins. However, the formation of an α-helical conformation of RbCT and OaCT was induced by the addition of trifluoroethanol (TFE), resulting in changed CD spectra of RbCT and OaCT with shifted minima to 207 nm, stronger ellipticity around 222 nm and positive maxima at 185 nm, respectively (Fig. 3.22 A and B, red curves). Secondary structure predictions confirmed the presence of regions in both CTDs that could possibly form α-helices (Fig. 3.22 C and D), whereas for OaCT, larger α-helical regions were predicted. This may be a reason for the extended α-helical signal of the OaCT spectrum after the addition of TFE compared to the RbCT-TFE curve.

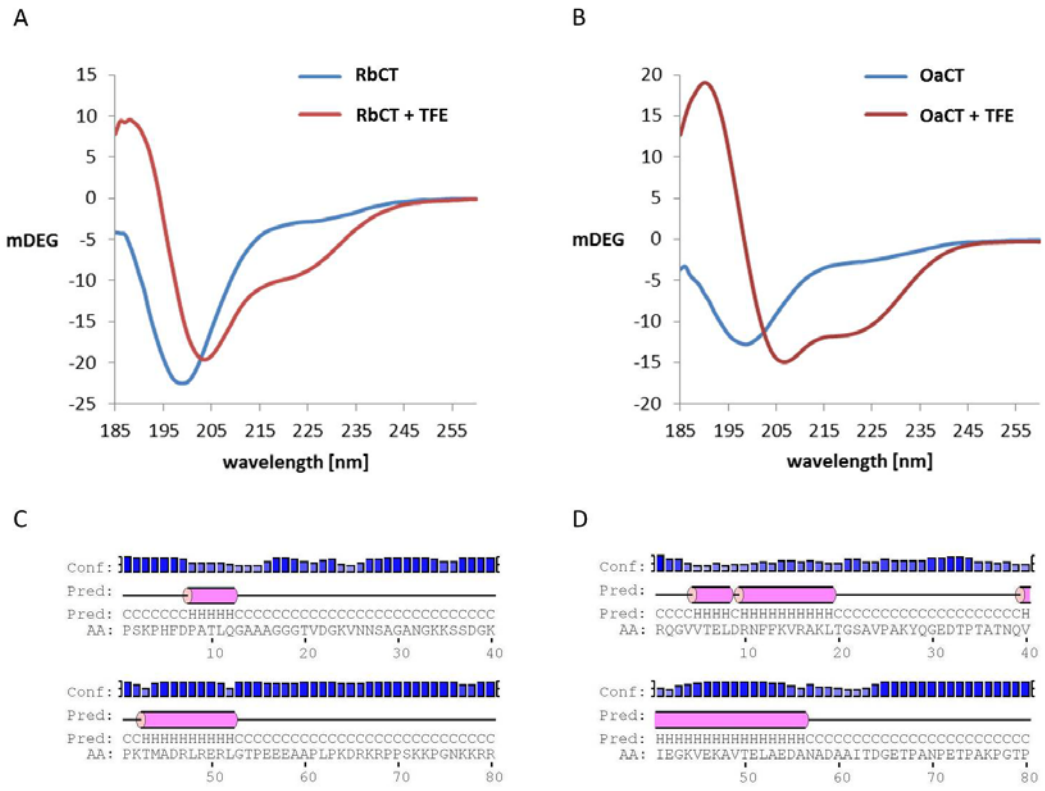

Fig. 3.22 ***RbCT and OaCT are intrinsically disordered and fold upon addition of TFE.*** *Analyses of RbCT and OaCT secondary structures using CD spectroscopy indicates that both C-terminal domains are unfolded in solution. Addition of TFE changed their conformation and induced the formation of α-helices in both proteins. Far-UV CD spectra of* ***(A)*** *RbCT and OaCT* ***(B)*** *in the absence of TFE (blue lines) or in the presence of 50 % TFE (red lines). Secondary structure prediction for RbCT* ***(C)*** *and OaCT* ***(D)*** *was generated using the PSIPRED server (McGuffin, 2000). Helices are symbolized by purple cylinders. Two shorter helices were predicted for RbCT and two longer helices for OaCT.*

Although it was shown that RbCT and OaCT are intrinsically disordered in solution (Fig. 3.21 A and B; Fig. 3.22 A and B *blue curves*), the helices predicted in Fig. 3.22 C and D are likely to form upon interaction with their respective binding partner, namely the ribosome. In the context of the full length insertase proteins, membrane interaction might also influence the structure of the C-terminal domains.

As a direct interaction of the ribosomal protein L29 with the C-terminal domain of YidC-Rb was shown in the previous pull-down experiments (Fig. 3.16 A), we tested whether RbCT folds upon binding to L29. CD-spectra of the two individual binding partners were compared to a CD spectrum of the RbCT-L29 complex (Fig. 3.23 A). L29 shows a typical CD-spectrum of an α-helical conformation (red line), whereas RbCT is in a disordered formation as mentioned (3.22 A). The equimolar mixture of RbCT and L29 did not show a significant conformational change of the sum spectrum (green line) compared to the native RbCT spectrum (blue line). Accordingly, the difference spectrum obtained by subtracting the CD spectrum of L29 from the spectrum of the RbCT-L29 mixture revealed the unchanged minima around 200 nm of a disordered conformation (Fig. 3.23 B).

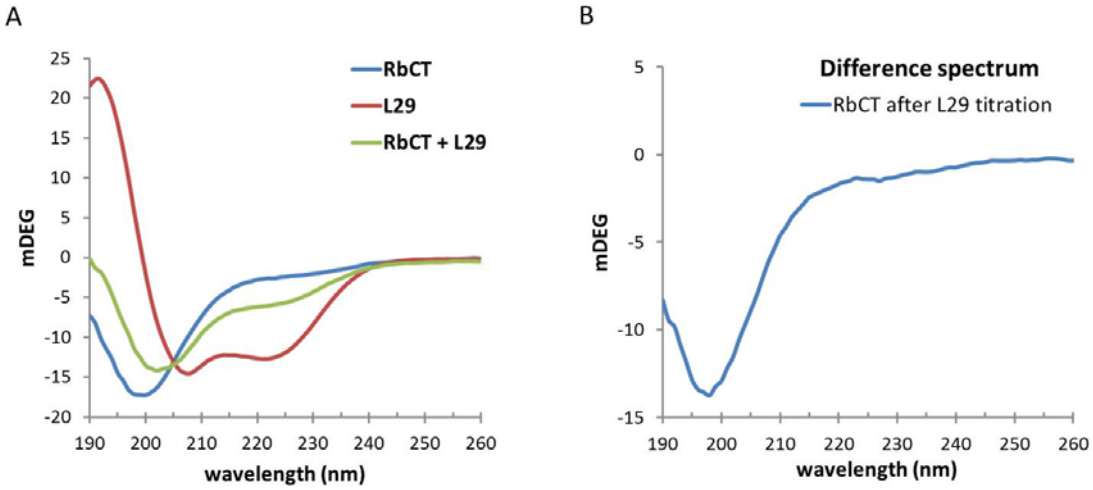

Fig. 3.23 ***RbCT shows no conformational change upon L29 titration. (A)*** *CD spectra of RbCT (blue, unfolded), L29 (red, α-helical) and RbCT+L29 mixture (green).* ***(B)*** *The difference spectrum obtained by subtracting the CD spectrum of L29 from the RbCT+L29 mixture shows the typical minima of an unfolded structure. This assay was performed in cooperation with E. Kouaga Mboubi during her master thesis (2013).*

Taken together, these data show that similar to Alb3 the isolated C-terminal domains of the marine YidC homologs are intrinsically disordered in solution, but no conformational change could be detected upon addition of the putative ribosomal binding partner L29.

3.3 *In vivo* studies: function of the C-terminal YidC regions

The discovery of YidC isoforms with a C-terminal extension in mitochondria (Oxa1) and Gram-positive bacteria (YidC2) suggested that they play a role in facilitating the co-translational membrane targeting activity independent of the SRP pathway (Funes *et al*., 2009). This might also hold true for the C-terminal extensions of the marine YidC homologs of Gram-negative bacteria. To analyze the cellular function of the C-terminally extended YidC proteins during the co-translational protein targeting and insertion, depletion strains of the SRP components were used for the *in vivo* studies. For depletion of Ffh, the protein component of the signal recognition particle, the depletion strain MC-Ffh was constructed (2.6.11). In this strain, the promoter of the chromosomal *ffh* gene has been exchanged with the *araC-araBAD* promoter cassette. Depletion of the chromosomally encoded Ffh was thus achieved by growth of MC-Ffh in the presence of 0,4 % glucose. For depletion of the SRP receptor protein FtsY, the strain IY26 (2.2.7) was obtained from E. Bibi, depleting the chromosomal FtsY expression also under glucose conditions (0,4 %).

3.3.1 Insertion of MscL via YidC-Rb in the absence of a functional SRP system

The C-terminally extended YidC proteins are not able to compensate completely for the loss of the SRP components in whole cells (data not shown). However, it is conceivable that the C-terminal domains may replace particularly the ribosome-assisted targeting function of components of the SRP system. Therefore, the ability of the C-tail modified YidC proteins to rescue either the targeting function or the insertion step mediated by SRP and its receptor FtsY was tested. The YidC substrate protein MscL that is known to be targeted via SRP to the membrane of *E. coli* and is then inserted by YidC into the inner membrane (Facey *et al*., 2007) was analyzed. To investigate whether an extended C-terminal region of YidC can compensate for a loss of distinct SRP functions, the FtsY depletion strain IY26 and the Ffh depletion strain MC-Ffh were transformed with pGZ119HE-N-his encoding the various YidC proteins (2.3.3 C1-6) and a second plasmid pSF147 encoding a single cysteine mutant (I68C) of the MscL protein (2.3.2 C7). The cells were grown in glucose media to deplete the SRP receptor protein FtsY or the Ffh protein component of SRP, respectively (2.9.1). Membrane insertion of MscL was monitored by chemical modification of the single cysteine residue at position 68 in the periplasmic loop of MscL with AMS (2.9), a membrane impermeable sulfhydryl-reagent that shifts the protein mobility on SDS-gels. Addition of AMS during the radioactive pulse chase experiments leads to a derivatization of the translocated cysteine residue at

position 68 of MscL and results in a shift in molecular size of ~ 0.5 kDa of the MscL cysteine mutant, indicating its proper membrane insertion (Facey *et al*., 2007).

It was tested whether the expression of Oa-YidC, YidC-Rb, YidC-Oa or YidC-Oxa can compensate for a loss of Ffh in the membrane targeting efficiency of MscL. Therefore, MC-Ffh cells coexpressing the MscL-68C single cysteine mutant and the respective YidC variant were pulse-labelled with [^{35}S]-Met, chased with non-radioactive methionine and then incubated with AMS (2.9.2). After treatment with AMS, total proteins were acid-precipitated and immuno-precipitated to visualize MscL (2.9.3). Derivatized and underivatized proteins were separated by SDS-PAGE and examined by phosphorimaging (2.9.4). In the absence of Ffh, AMS derivatization of MscL is reduced by about 40 % (Fig. 3.24 B; left column). As expected, this corroborates that the insertion process of MscL is affected by Ffh depletion (Facey *et al*., 2007). Coexpression of the YidC proteins did not significantly restore membrane insertion of MscL under Ffh depletion conditions (Fig. 3.24 A; lanes 3-12), in contrast to the control cells where Ffh was coexpressed from a plasmid (Fig. 3.24 A lane 14; Fig. 3.24 B right column).

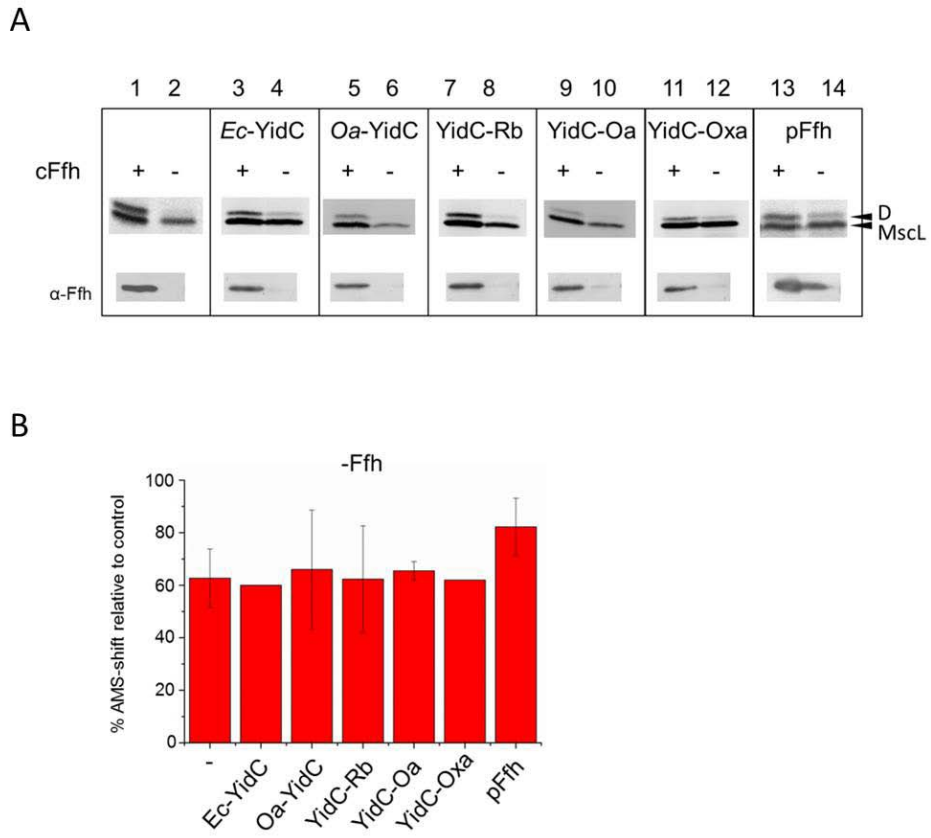

Fig. 3.24 ***Ffh is indispensable for the proper membrane insertion of MscL and not replaceable by C-terminally tailed YidC proteins.*** *The coexpression of the YidC variants could*

not maintain the correct insertion of MscL in the absence of Ffh. The membrane insertion of MscL was monitored by AMS reactivity of a single cysteine residue (C68) in the periplasmic loop of MscL. ***(A)*** *E. coli strain MC-Ffh expressing the MscL cysteine mutant was grown in M9 minimal medium containing arabinose (cFfh+, lane 1). For depletion of Ffh (cFfh-, lane 2), the cells were grown in the presence of glucose. IPTG (1 mM) was added for 10 min to induce expression. Cells were incubated in the presence of AMS, pulse-labeled with [^{35}S] Met for 2 min and chased with non-radioactive Met for 10 min. After quenching with 20 mM DTT, the radiolabeled samples were acid-precipitated and immune-precipitated with an anti-His antibody and then subjected to SDS-PAGE and phosphorimaging. The arrowhead D denotes the AMS-derivatized MscL protein. Parallel experiments were performed with cells coexpressing Ec-YidC (lanes 3 and 4), Oa-YidC (lanes 5 and 6), YidC-Rb (lanes 7 and 8), YidC-Oa (lanes 9 and 10) or YidC-Oxa (lanes 11 and 12). As a control, the derivatization of MscL was monitored in MC-Ffh cells coexpressing plasmid-encoded Ffh (pFfh) in the absence of chromosomal Ffh (cFfh) (lane 14). The lower panels show immunoblots of the Ffh level under arabinose (+) and glucose (-) conditions, respectively.* ***(B)*** *The AMS-shift assay was quantified with ImageJ. In each experiment the amount of derivatized MscL in the presence of Ffh was set to 100 % (control). The relative amount of the derivatized MscL in the absence of Ffh (red columns) was calculated after coexpression of the indicated YidC protein from plasmid. Cells without coexpression are shown in the very left bar (-). The data for the control cells with coexpression of plasmid-encoded Ffh protein are shown in the right column (pFfh). For several repeated experiments the standard deviations (error bars) were calculated.*

Subsequently, it was analyzed whether the C-terminal extensions of the YidC proteins could replace the function of the SRP receptor protein FtsY. To assess the ability of YidC-Rb, YidC-Oa or YidC-Oxa to mediate membrane targeting and insertion of MscL in the absence of FtsY, the same experiment as described above for Ffh, was performed in the FtsY depletion strain IY26. When FtsY was present, about 50 % of the MscL protein was shifted during the pulse time indicating that it was correctly inserted into the inner membrane (Fig. 3.25 A, lane 1). However, when cells were grown in the absence of arabinose to deplete FtsY, a much lower proportion of MscL was derivatized by AMS (lane 2), showing that the targeting of MscL to the membrane and the insertion process is inhibited, somewhat stronger than after Ffh depletion. To investigate whether coexpression of the YidC proteins can compensate for the loss of FtsY and promote membrane insertion of MscL, a parallel experiment was performed with IY26 cells that express MscL together with Ec-YidC, Oa-YidC, YidC-Rb, YidC-Oa or YidC-Oxa, respectively (Fig. 3.25, lanes 3-12). In the absence of FtsY, coexpression of the YidC-Rb and YidC-Oxa proteins with the C-terminal extensions allowed substantial AMS derivatization of MscL (lanes 8 and 12). In contrast, the coexpression of YidC-Oa or Oa-YidC showed no significant improvement of the membrane insertion of MscL in the absence of FtsY (lanes 6 and 10). To exclude that the overexpression of a functional YidC protein causes an enhanced MscL insertion under FtsY depletion conditions, wild type Ec-YidC was coexpressed (Fig. 3.25 A, lanes 3 and 4) and no improved MscL derivatization was observed (Fig. 3.25 B, second left column).

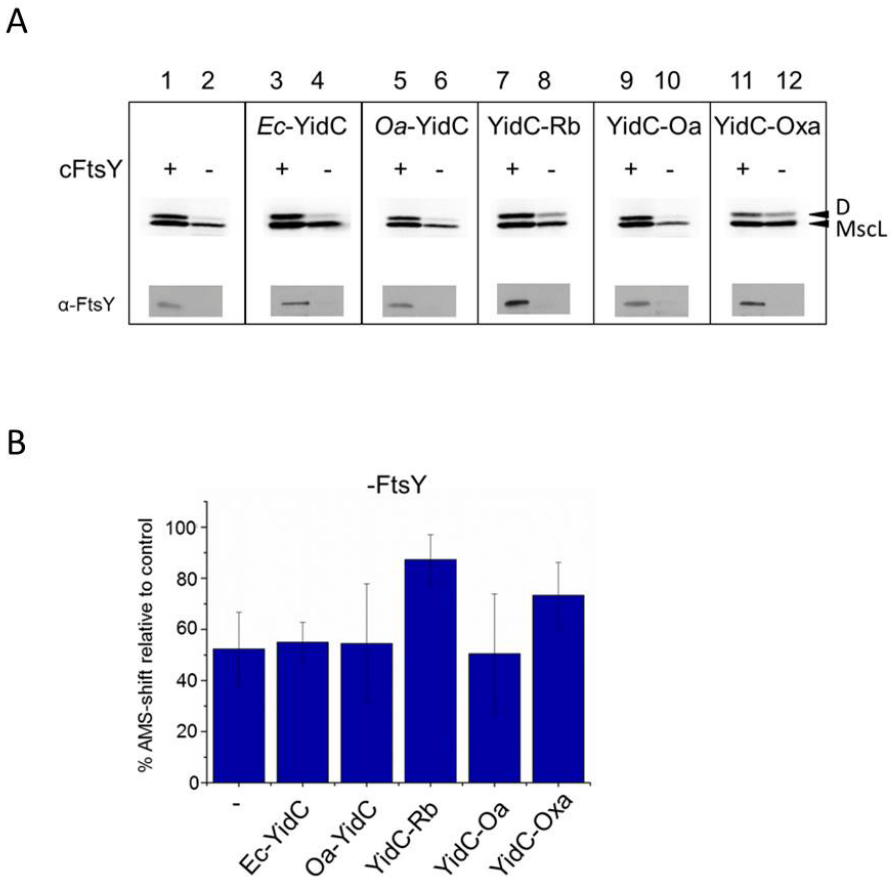

Fig. 3.25 ***The C-terminal extensions of YidC-Rb and YidC-Oxa can mediate the membrane targeting of MscL in the absence of the SRP receptor protein FtsY.*** *MscL is inserted into the membrane in the absence of FtsY when YidC-Rb or YidC-Oxa is coexpressed. Samples and AMS derivatization assays were prepared and processed as described for MC-Ffh (Fig. 3.24).* ***(A)*** *The FtsY depletion strain IY26 bearing the MscL I68C cysteine mutant was grown under either FtsY depletion (lane 2) or FtsY expression conditions (lane 1). Parallel experiments were performed with cells coexpressing Ec-YidC (lanes 3 and 4), Oa-YidC (lanes 5 and 6), YidC-Rb (lanes 7 and 8), YidC-Oa (lanes 9 and 10) and YidC-Oxa (lanes 11 and 12). The lower panels show immunoblots of the FtsY level under arabinose (+) and glucose (-) conditions, respectively.* ***(B)*** *The quantified AMS-shift assay (ImageJ) showed that the relative amount of derivatized MscL in the absence of FtsY is enhanced by 30 % when YidC-Rb was coexpressed and by 20 % for the YidC-Oxa coexpression, compared to cells without coexpression (left column -) or coexpressing Ec-YidC (second left column). The total amount of derivatized MscL in the presence of FtsY was set to 100 %. For several repeated experiments the standard deviations (error bars) were calculated.*

Taken together, these data indicate that the membrane targeting and the subsequent insertion of MscL in the absence of FtsY can be mediated by the C-terminal domain of the marine YidC homolog of *R. baltica* and partially also by the C-terminal domain of the mitochondrial YidC-homolog Oxa1.

3.3.2 Localization of MscL-GFP in the absence of Ffh or FtsY

To visualize the cellular localization of MscL, the protein was expressed as an MscL-GFP fusion protein (Maier *et al*., 2008). The localization of MscL-GFP was analyzed in the FtsY depletion strain IY26 and in MC-Ffh cells. The cells were grown in arabinose containing media to allow and analyze normal membrane targeting or in glucose to deplete FtsY or Ffh, respectively. The YidC proteins were coexpressed and the cells were then inspected for the localization of MscL-GFP by fluorescence microscopy (2.8). In the presence of Ffh and FtsY, the fluorescence was evenly distributed at the membrane surface (Figs. 3.26 A and 3.27 A, respectively). However, when the cells were grown in the presence of glucose to deplete Ffh, the MscL-GFP aggregated at the cell poles (Fig. 3.26 B). Under FtsY-depleted conditions, the MscL-GFP protein was found in patches, also mostly at the cell poles (Fig. 3.27 B). This is similar to the phenotype when YidC is depleted (Fig. 3.26 C) in MK6 cells. Remarkably, coexpression of YidC-Rb in the absence of Ffh (Fig. 3.26 D) restored the mislocalization of MscL-GFP and showed a distribution of the fluorescent signal similar to the coexpression of wild type Ffh encoded on a plasmid (Fig. 3.26 F).

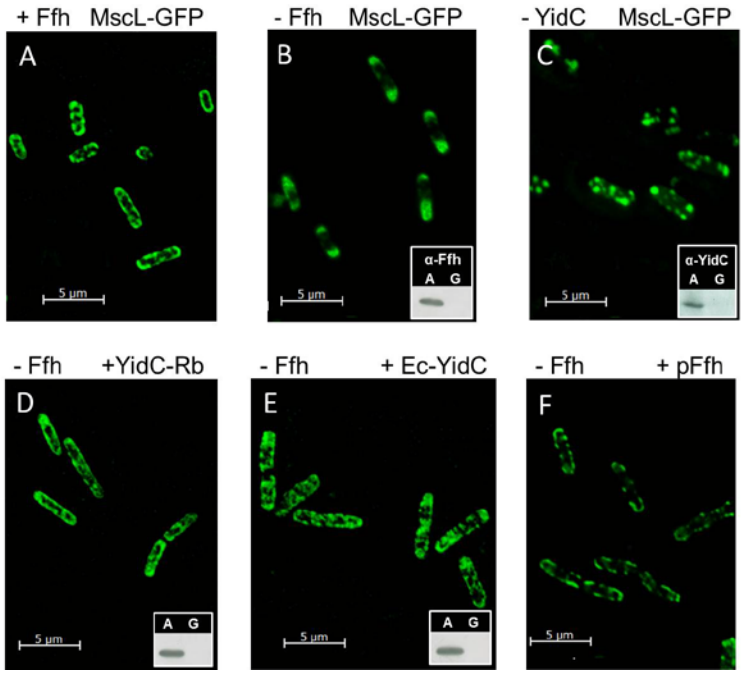

Fig. 3.26 ***Localization of MscL-GFP in the absence of Ffh.*** *Localization of MscL-GFP was studied in vivo by fluorescence microscopy. MC-Ffh cells bearing the MscL-GFP fusion plasmid were grown in LB medium either in the presence of arabinose* ***(A)*** *or in the presence of glucose to deplete Ffh* ***(B, D, E and F)****. Cells were induced with 1 mM IPTG for 2 h at 30 °C and inspected by fluorescence microscopy. The coexpression of YidC-Rb under Ffh depletion conditions (D) showed a distribution of the fluorescent signal similar to the positive control of the plasmid-encoded expression of wild type Ffh (F). Coexpression of Ec-YidC (E) showed more MscL-GFP patches, but also a different cell localization compared to Ffh-depleted cells expressing MscL-GFP with no other coexpressing plasmid (B).* ***(C)*** *Localization of MscL-GFP in YidC depleted MK6 cells.*

Targeting of the MscL-protein to the *E.* coli inner membrane is clearly dependent on the SRP-receptor FtsY (Fig. 3.27, compare A and B). Strikingly, the missing proper localization of MscL-GFP at the membrane in the absence of FtsY in IY26 cells (Fig. 3.27 B) was restored by the coexpression of YidC-Rb (Fig. 3.27 C). Expression of YidC-Rb together with MscL-GFP allowed a cellular distribution of MscL-GFP similar to wild type conditions (Fig. 3.27 A) despite depletion of FtsY.

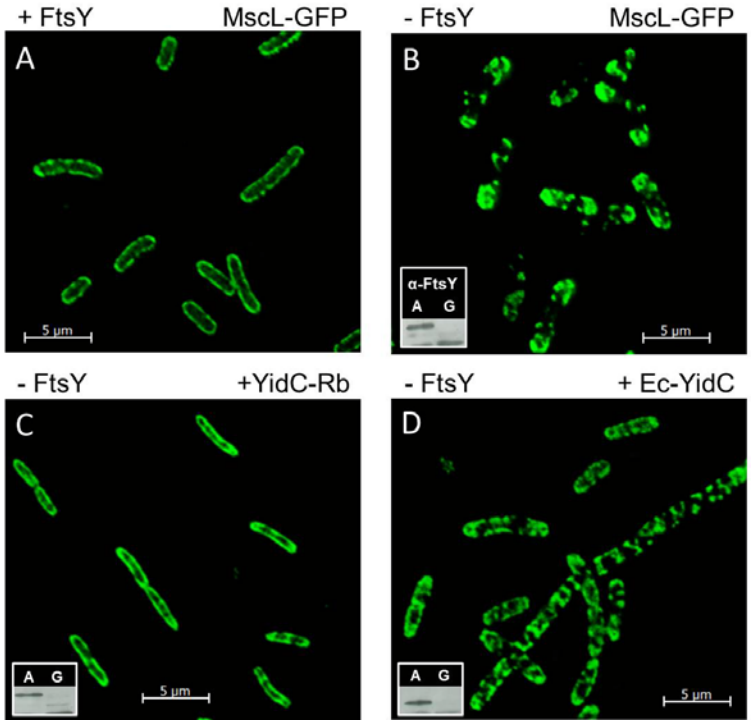

Fig. 3.27 ***YidC-Rb restores the mislocalization of MscL-GFP in the absence of FtsY.*** *Localization of MscL-GFP in the E. coli strain IY26 in the presence* ***(A)*** *or absence* ***(B-D)*** *of FtsY monitored in vivo by fluorescence microscopy as described for MC-Ffh. Mislocalization of MscL-GFP in the absence of FtsY (B) is prevented by coexpressing YidC-Rb (C), but not by Ec-YidC (D).*

These results, together with the data from the AMS derivatization assays (3.3.1) indicate that YidC-Rb supports membrane targeting of MscL also in the absence of Ffh or FtsY, while the correct insertion and membrane topology of MscL still requires Ffh. Thus the charged C-terminal ribosome-binding moiety of YidC-Rb can function as a membrane targeting factor.

3.4 Binding studies of SRP and the SRP signal sequence of KdpD

Similar to MscL, the KdpD protein of *E. coli* is targeted via SRP to the membrane but it does not require SecYEG nor YidC for its membrane insertion (Facey and Kuhn, 2003). This chapter focuses on the interaction of the signal recognition particle with SRP signal sequences to determine the specificity of SRP recognition in proteins.

The sensor protein KdpD of *E. coli* is composed of a large N-terminal hydrophilic region (aa 1-400), four transmembrane regions (aa 401-498) and a large hydrophilic region (aa 499-894) at the C-terminus (Fig. 3.28 A). Both termini are facing the cytoplasm. As in *E. coli* nearly all inner membrane proteins have N-terminal uncleaved signal sequences, the region that interacts with SRP is most likely the first transmembrane region. This provides that early after the translation start, SRP interacts with the nascent peptide chain at the ribosome and mediates its co-translational targeting to the membrane (Luirink and Sinning, 2004). Due to the long N-terminal hydrophilic region of KdpD, the first transmembrane region starts at amino acid residue 401, preventing an early membrane targeting of the protein. Therefore, an additional signal element might be present in the N-terminal region that is recognized by SRP and allows early co-translational membrane targeting of KdpD. *In vivo* studies of N-terminal KdpD-GFP fusion proteins revealed that residues 22-48 of KdpD (N22-48) contain a signal element that is capable to bind SRP and to target the GFP-fusion protein to the membrane (Maier *et al*., 2008) (Fig. 3.28 B). This peptide contains five positively charged residues, three of which are closely spaced (aa 22-26), as well as a stretch of 10 hydrophobic residues (aa 27-36) followed by a lysine residue an then another six hydrophobic residues (aa 38-43). Within this peptide, also a Walker A motif was identified ranging from residues 30-38 (Jung and Altendorf, 1998) (Fig. 3.28 B, boxed region).

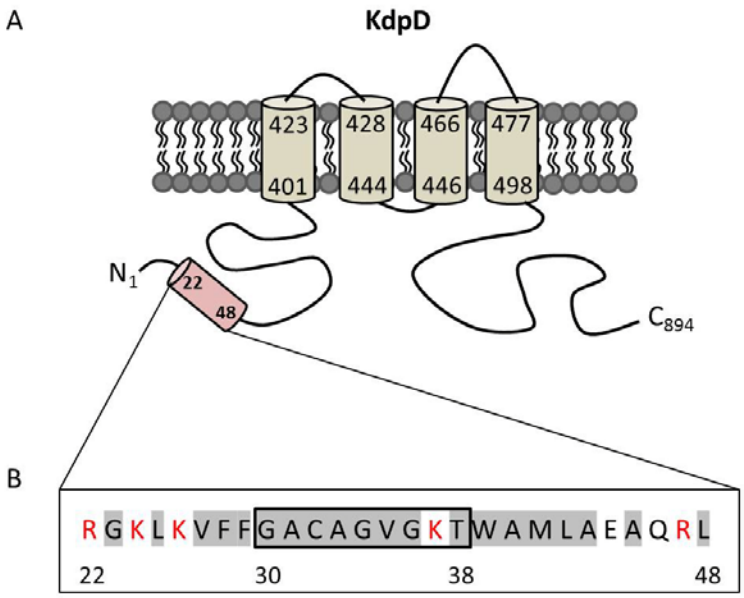

Fig. 3.28 ***The SRP dependent integral sensor protein KdpD.*** ***(A)*** *Membrane topology of KdpD. The E. coli inner membrane protein KdpD consists of a large N-terminal domain (1-400), four closely spaced transmembrane regions (401-498), and an extended cytoplasmic C-terminal domain (499-894).* ***(B)*** *The amino acid sequence of the minimal peptide (aa 22-48) that is required to target KdpD to the inner membrane. Positively charged residues are displayed in red; hydrophobic amino acids are shaded dark. The sequence of the Walker A motif is marked with a box.*

To explore the function of the N22-48 sequence of KdpD, two SRP signal mutants therein were generated (Fig. 3.29). Since basic amino acid residues are discussed to promote binding of SRP to a signal peptide (Peterson *et al*., 2003), the positively charged residues at positions 22, 24 and 26 were substituted by glutamine (Q) resulting in the 3Q mutant in which the net charge of the peptide is lowered from + 5 to + 2. Influence of the Walker A motif on SRP recognition of the KdpD signal element was investigated by mutating the conserved glycine residues at positions 30, 34 and 36 to alanine, respectively, resulting in the W3A mutant.

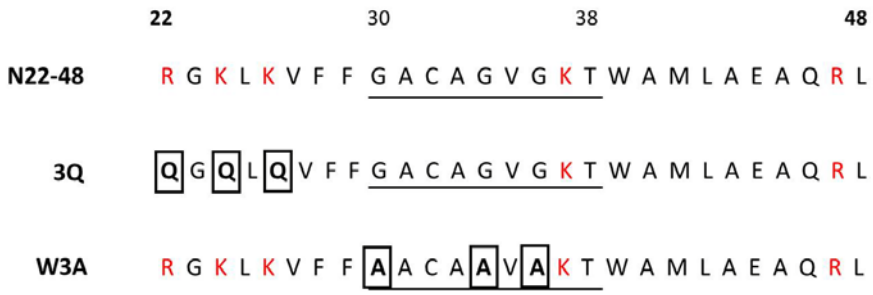

Fig. 3.29 ***SRP signal mutants of KdpD N22-48****. To investigate the influence of the positively charged residues at the beginning of the N22-48 peptide, the 3Q mutant was generated, resulting in a reduced net charge of the peptide (+2). In the W3A mutant (+5), three conserved glycine residues in the Walker A motif were exchanged with alanine residues. The mutated amino acid residues are marked with boxes. The Walker A motif is underlined and the positively charged residues are displayed in red.*

To investigate the involvement of the positively charged residues and the Walker A motif in binding of the signal sequence to SRP, the binding affinities of the wild type KdpD N22-48 fragment and the mutant peptides 3Q and W3A to SRP were determined via microscale thermophoresis (MST) measurements (2.17). The MST refers to the motion of molecules in microscopic temperature gradients and allows the quantification of biomolecule interactions by thermophoretic detection of even minute changes in conformation, charge and physical size of a molecule as they are induced by a binding event (Jerabek-Willemsen *et al*., 2011). The thermophoretical movement is monitored via a fluorescently labeled target molecule whose concentration is kept constant and low (1 – 100 nM), while the unlabeled binding partner (ligand) is titrated in a serial dilution (12 - 16 steps) with concentrations ranging from approximately 20 fold above the expected dissociation constant (K_d) down to sub-stoichiometric concentrations with respect to the labeled molecule.

For this approach the SRP protein was labeled, while the unlabeled KdpD signal peptides N22-48, 3Q and W3A were titrated. Since the KdpD peptides are too small (2951 Da) to purify them efficiently from *E. coli* cells, the peptides were synthesized *in vitro* by the Custom peptide synthesis services from GENOSPHERE Biotechnologies (France) (2.5). The purification, labeling and reconstitution of SRP will be discussed in detail in the next chapter.

3.4.1 Purification and labeling of Ffh from *E. coli*

The *E. coli* wild type *ffh* gene was amplified from the *E. coli* MC1061 chromosome by PCR using primers coding for a C-terminal Strep-tag (WSHPQFEK) sequence and flanking NcoI / EcoR1 restriction sites. The *ffh* gene was cloned into the pMS119HE vector and the wild type cysteine residue at position 406 was mutated to serine. A single cysteine residue was introduced at position 423 resulting in the construct Ffh_{Cstrep}C406S/M423C by site-directed mutagenesis (2.6.9). The recombinant protein expression was induced in a 4L LB culture of *E. coli* BL21 cells for 3 h at 37 °C and the Ffh_{M423C} mutant was purified as described in the method section 2.10.3 by strep-tag affinity chromatography. The Ffh_{M423C} protein was eluted in 2 ml fractions from the Strep-Tactin matrix in buffer E_{Ffh} (20 mM Hepes pH 8, 350 mM NaCl, 10 mM $MgCl_2$, 10 mM KCl, 10 % glycerol, 2,5 mM desthiobiotin) in sufficient amounts with only few contaminants (Fig. 3.30).

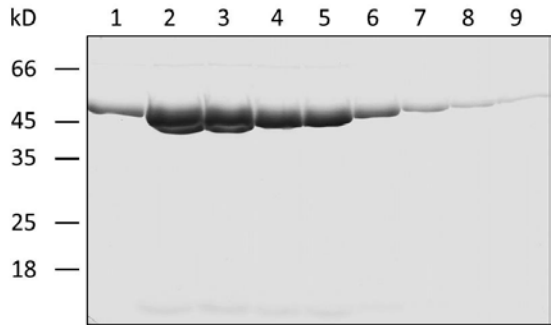

Fig. 3.30 ***Strep-tag elution fractions of Ffh_{M423C}.*** *10 µl of each elution fraction (1-9) were analyzed on a 12 % SDS-gel and visualized by Coomassie staining. The Ffh_{M423C} protein was eluted by gravity flow in 2 ml fractions from the Strep-Tactin matrix (IBA) with 2,5 mM desthiobiotin in the elution buffer.*

The main fractions 2 – 4 (Fig. 3.30) were further purified on a Superdex 75 16/60 gel filtration column with buffer GF_{Ffh} (20 mM Hepes pH 8, 200 mM NaCl, 20 mM $MgCl_2$, 10 mM KCl, 10 % glycerol). The SEC was monitored by tracking the UV absorptions at 280 nm and 260 nm and 2 ml fractions were collected (Fig. 3.31 A). The peak fractions were analyzed by a 12 % SDS-gel and Coomassie staining (Fig. 3.31 B). Two main peaks were detected during SEC, one representing the void volume at 45 ml and a second peak at an elution volume of 60 ml, corresponding to a molecular weight of ~ 50 kDa (Fig. 3.31 A). Presumably, the second peak contained the monomeric Ffh protein (48 kDa) with proper amount and purity (Fig. 3.31 B). The void volume peak showed a strong absorption at 260 nm (Fig. 3.31 A, red curve), indicating the presence of RNA or DNA. Indeed, the SDS-gel analysis of the void fractions 3 and 4 showed only minor amounts of Ffh protein (Fig. 3.31 B). Electrophoretic RNA analysis of these fractions revealed the presence of ribosomal 23S rRNA (2904 nt) and 16S rRNA (1540 nt) in the void volume, but not in the Ffh peak fraction 11 (Fig. 3.31 C). The assumption that the 260 nm peak contains 4.5S RNA (113 nt) was not confirmed since no RNA fragment at this size was visible on the RNA gel. Therefore, it is proposed that the Strep-Tactin matrix binds RNA unspecifically from the cell lysate during the purification process.

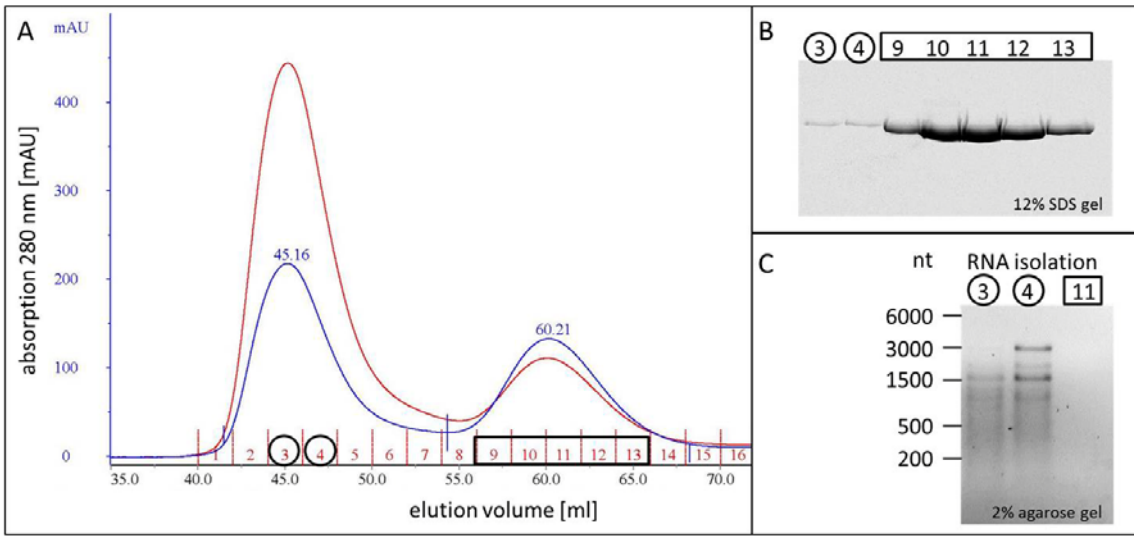

Fig. 3.31 ***SD75 16/60 SEC of Ffh$_{M423C}$strep. (A)*** *Chromatographic separation of the Ffh$_{M423C}$strep elution fractions. The absorption was detected at 260 nm (red curve) and 280 nm (blue curve), monitoring 2 peaks at 45 ml (V_0) and 60 ml (Ffh monomer; ~ 50 kDa).* ***(B)*** *SDS-gel analysis of the peak fractions 3+4 and 9-13. 10 µl of each fraction was loaded and analyzed by Coomassie staining.* ***(C)*** *RNA isolation of fractions 3, 4 and 11, analyzed on a 2 % agarose gel and visualized by ethidium bromide UV fluorescence, indicated the presence of ribosomal RNA at a size of ~ 3000 nt and ~ 1500 nt in the void volume (black circles, fraction 3 and 4), but not in the Ffh elution peak (black box, fraction 11). nt: nucleotides*

The gel filtration fraction 11 (Fig. 3.31) was used for the subsequent labeling reaction. Ffh$_{M423C}$strep was labeled using the NT-647-MALEIMIDE fluorescent dye and the RED-Maleimide labeling kit from NanoTemper Technologies (2.17.1). Prior to the labeling reaction, a buffer exchange had to be performed to remove the glycerol from the Ffh sample buffer since glycerol reduces the labeling efficiency drastically (Fig. 3.32, compare L1 with L2). L2 in figure 3.32 shows the Ffh protein from the labeling reaction with the same Ffh concentration in a buffer without glycerol demonstrating increased label efficiency. In the purification step removing the free dye from the reaction, the labeled Ffh protein eluted in fractions 3 and 4. The in gel fluorescence was measured by an ImageQuant^{TM} LAS400 system using a filter for Cy5 fluorescence (670 nm), detecting a distinct signal at the expected molecular weight of the Ffh protein in the SDS-gel without unspecifically labeled contaminants or free dye in the elution fractions (Fig. 3.32 E3 + E4).

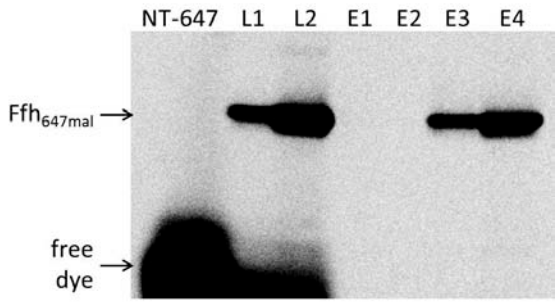

Fig. 3.32 ***In gel fluorescence measurement of the Ffh_{647mal} labeling procedure****. The first lane shows the fluorescent signal of the free dye (NT-647mal). L1 and L2 represent labeling reactions 1 (with 10 % glycerol) and 2 (without glycerol), respectively. E1-E4: elution fractions of Ffh_{647mal} after removal of the free dye. ImageQuant settings: Fluorescence: Cy5; Light: Red (RGB); Filter: 670 nm; Iris: F 0.85; exposure time: 1 sec.*

Concentration determination and calculation of the DOL (degree of labeling) was performed by measuring the absorbance at 280 nm and 650 nm using an UV-Vis spectrophotometer (2.17.1). For fraction 4 (Fig. 3.32) a protein concentration of 2,5 µM and a labeling efficiency of ~ 47 % was calculated. The Ffh protein was stored protected from light in aliquots at – 80 °C and thawed on ice just prior to 4.5S RNA reconstitution.

3.4.2 Reconstitution of a functional SRP protein

At this point of the SRP preparation only the protein component Ffh was present (Fig. 3.31 C fraction 11) but for a functional signal recognition particle, the 4.5S RNA is indispensable. Therefore, the 114 nt long 4.5S RNA was synthesized *in vitro* (2.6.12) and reconstituted with the Ffh protein to a functional SRP (2.17.2). For the *in vitro* transcription of the 4.5S RNA, the template DNA had to be linearized by restriction digestion downstream of the insert. The pUC18-4.5S RNA plasmid (2.3.5) was therefore linearized by BamHI and gel purified using a DNA gel extraction kit. A phenol / chloroform extraction of the template DNA was performed to end up in an A260/280 ratio of 1.8 – 2. The *in vitro* transcription reaction was incubated for 3 h at 37 °C, the RNA was purified (RNA clean & concentrator-25 Kit) and analyzed on a 2 % native agarose gel stained with ethidium bromide (Fig. 3.33).

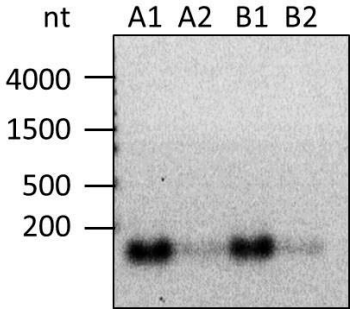

Fig. 3.33 ***In vitro transcription of 4.5S RNA.*** *After the in vitro transcription the RNA was matrix-isolated and step wise eluted in 50 µl (A) and 25 µl (B) RNAse free water. A total amount of 1,8 µg (A1 and B1) and 0,4 µg (A2 and B2) RNA was loaded onto a 2 % native agarose gel and detected by ethidium bromide fluorescence. UV exposure time: 0.2 sec. nt: nucleotides. Both elution fractions showed a single band <200 nt that corresponds to the 114 nt 4.5S RNA.*

The *in vitro* transcription produced a defined RNA fragment with a nucleotide length of < 200 nt that was assigned to the 114 nt comprising 4.5S RNA. A molecular weight of 36,7 kDa was calculated and the UV absorbance measurement at 260 nm determined a RNA concentration of ~ 48 µM for both elution fractions.

Prior to the studies on the interaction of the SRP holo-particle with the N-terminal KdpD peptides by MST, it was necessary to establish conditions that ensure a stably reconstituted SRP protein and to exclude that the labeling affected the interaction between Ffh and its RNA. Therefore a molecular interaction experiment was performed between Ffh and the 4.5S RNA to determine the dissociation coefficient (K_d). A titration series of up to 16 dilutions was prepared, where the concentration of the fluorescent Ffh_{647mal} protein is kept constant and the concentration of the unlabeled 4.5S RNA is varied. For best and reliable performance, the concentration of the labeled component should be close to the expected K_d or less and should yield a range of 200 – 1500 fluorescence counts (typically equivalent to 1 – 200 nM). The unlabeled binding partner was prepared in a 16-step dilution series around the expected K_d, starting from a concentration of > 20-fold of the expected K_d down to sub-stoichiometric concentrations. 10 µl of each sample of the dilution series was mixed with 10 µl of the stock solution of the labeled binding partner by pipetting up and down 10 times and the samples were incubated in the dark. Incubation times and temperatures differed between different binding assays. To design an appropriate MST experiment and find a proper concentration distribution, the concentration finder tool software from NanoTemper was used.

Published data for the binding affinity of the 4.5S RNA to Ffh ranges from K_d values of 7 pM (Siu *et al.,* 2007) to 3 nM (Jagath *et al*., 2001), depending on the used methods and concentrations of monovalent and bivalent cations in the binding buffer (Batey and Doudna, 2002). I decided to use binding conditions as described for a filter binding assay (Batey *et al.,* 2000) where a K_d of ~ 40 pM for the wild type 4.5S RNA binding to the *E. coli* Ffh protein was determined under physiological buffer conditions (20 mM Hepes-KOH pH 7.5, 100 mM KCl, 10 mM $MgCl_2$, 0,5 mM EDTA). First the lowest possible concentration of Ffh_{647mal} that gives an adequate fluorescence signal (> 200 counts) was determined, since the labeled binding partner should be used in a concentration range around the expected K_d. Solutions of Ffh with final concentrations of 2, 4 and 8 nM were tested, respectively (Fig. 3.34). The raw fluorescence counts of the different Ffh solutions were measured by the cap scan tool in premium coated capillaries (NanoTemper), without adjacent MST measurement.

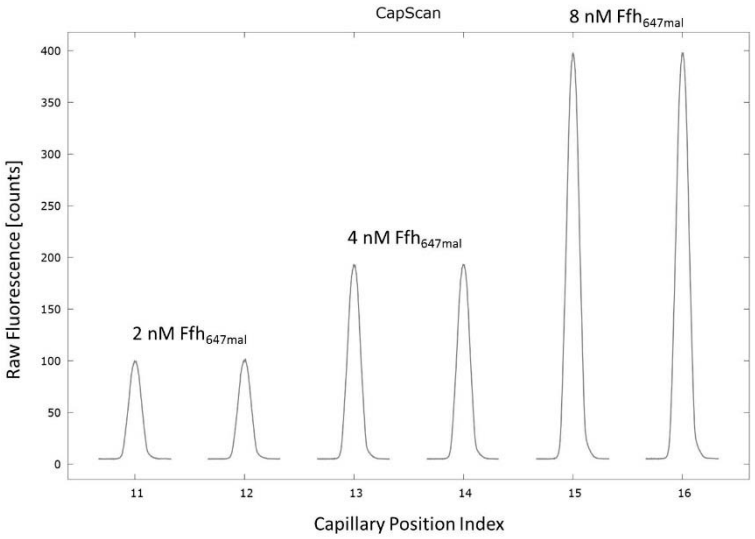

Fig. 3.34 ***Cap scan of Ffh$_{647mal}$.*** *Raw fluorescence signals for Ffh were measured with concentrations of 2 nM (capillary positions 11+12), 4 nM (13+14) and 8 nM (15+16) in premium treated capillaries. All samples showed symmetric peaks and a concentration - dependent fluorescence increase. The minimum of 200 counts was reached in the 4 nM Ffh sample.*

The Ffh_{647mal} protein in MST_{RNA} buffer (20 mM Hepes-KOH pH 7.5, 100 mM KCl, 10 mM $MgCl_2$, 0,5 mM EDTA, 0,05% Tween-20) showed a symmetric peak and a linear, concentration-dependent fluorescence signal increase (Fig. 3.34). This demonstrates that the protein was stable in this buffer and did not stick to the capillary surface. A 4 nM Ffh_{647mal} sample had a raw fluorescence intensity of 200 counts and represents the lowest possible concentration to measure MST. Consequently, the labeled Ffh stock solution for the binding assay was adjusted to 8 nM with MST_{RNA} buffer, resulting in a final concentration of 4 nM Ffh in the dilution series. Computer generated simulation (NanoTemper concentration-finder: K_d-fit) of the binding curve with 4 nM labeled molecule and a K_d of 40 pM suggested a ligand concentration of 200 nM for the dilution series. According to that, a stock solution of 400 nM 4.5S RNA in MST_{RNA} buffer was prepared, producing final ligand concentrations ranging from 6,1 pM to 200 nM after mixing with one volume of the Ffh_{647mal} stock solution. The mixed two binding partners were incubated for 20 min at room temperature, loaded into premium coated capillaries and analysis of their thermophoretic mobility was performed. Thermophoresis was measured using a Monolith NT.115 instrument (2.17.3) and data of two independent experiments were analyzed using the signals from Thermophoresis and T Jump. A significant change in MST response of the labeled Ffh in the presence of 4.5S RNA was observed that was attributed to the assembled SRP complex (Fig. 3.35). The dissociation constant was calculated to be 0.56 nM with a K_d confidence of 0.17 and a proper response amplitude of 14.3 (2.17.5). The standard error of regression was calculated to 0.55.

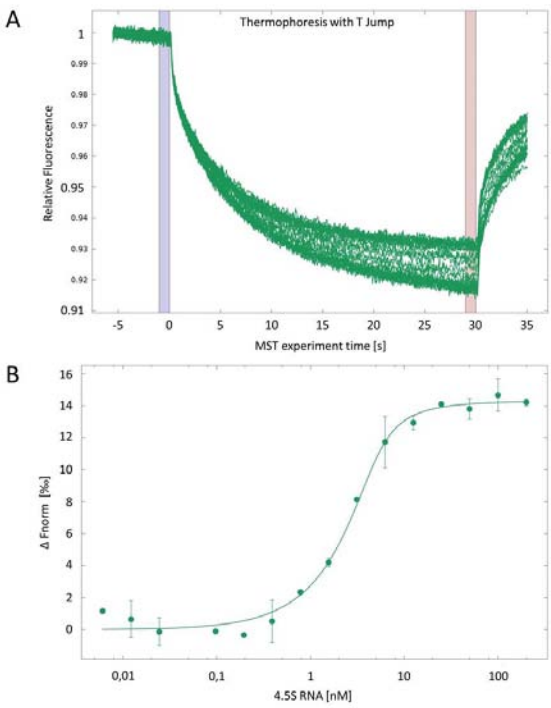

Fig. 3.35 ***Ffh-4.5S RNA assembly.*** *In the MST experiment the concentration of the Ffh-labeled molecule was kept constant (4 nM), while the concentration of the non-labeled binding partner (4.5S RNA) was titrated between 6,1 pM and 200 nM. Thermophoresis was measured with 95 % LED and 20 % MST power in premium coated caps.* ***(A)*** *Original time traces display the affected thermophoretical mobility of labeled Ffh upon binding of 4.5S RNA.* ***(B)*** *A K_d of 0.56 nM +/- 0.17 nM was determined for this interaction employing the Thermophoresis + T Jump signal for data analysis (2 independent measurements, error bars represent the standard deviation).*

From a comparison of various interaction techniques, it is known that surface-based methods tend to overestimate the affinity of an interaction (Jecklin *et al*., 2009). With this in mind, the affinity of a K_d = 0.56 nM determined with MST for the 4.5S RNA binding to Ffh is in good agreement with previous studies. Additionally, it has to be mentioned that strong binding affinities in the pM range, as this is the case for SRP reconstitution, could not be exactly measured with the Monolith NT.115 instrument due to the required high fluorescence intensity. Thus, the observed K_d of ~ 500 pM in this study, being about 10-fold higher than the expected dissociation constant (Batey *et al*., 2000), seems to represent a properly reconstituted SRP ribonucleoparticle under the assay conditions used in this study. Thus, the reconstituted SRP is suitable for further binding studies with the SRP signal sequence peptides.

3.4.3 Binding studies of SRP signal sequences to SRP using microscale thermophoresis

To explore the affinity of the wild type KdpD signal sequence N22-48 and the two mutant peptides W3A and 3Q (Fig. 3.29) to SRP, MST measurements were performed using the reconstituted SRP (Fig. 3.35) as the fluorescent binding partner at a constant concentration of 20 nM. The 27 amino acid comprising KdpD peptides with molecular weights of ~ 3 kDa were synthesized with a purity of > 95 % by GENOSPHERE Biotechnologies (2.5) and modified with an N-terminal amidation and a C-terminal acetylation. Prior to MST the lyophilized peptides were dissolved in $_{dd}H_2O$ by sonication to

a final concentration of about 1 mM. Based on fluorescence anisotropy measurements with SRP and the ΔEspP signal sequence (Bradshaw *et al*., 2009) a moderate, not too strong binding affinity of SRP to the signal peptides in the lower µM K_d range was expected. Therefore, the starting concentration of the KdpD peptides was set to 40 µM in the first titration step and was serially diluted to a lowest concentration of 1,2 nM.

First, the binding of N22-48 to SRP was tested in three different buffers whereas the SRP sample constantly was kept in RNA buffer (20 mM Hepes-KOH pH 7.5, 100 mM KCl, 10 mM $MgCl_2$, 0,5 mM EDTA, 0,05% Tween-20) that was also used for the SRP reconstitution measurements. The N22-48 peptide stock solutions were prepared in RNA-buffer, $MST_{optimized}$ buffer (50 mM Tris pH 7.4, 150 mM NaCl, 10 mM $MgCl_2$, 0,05 % Tween-20) and Ffh- buffer (20 mM Hepes pH 7.4, 200 mM NaCl, 10 mM $MgCl_2$, 10 mM KCl, 0,05% Tween), respectively. The binding components were mixed, incubated for 20 min on ice and loaded into premium treated capillaries and analysis of their thermophoretic mobility was performed. A significant change in the MST response of the labeled SRP in the presence of the N22-48 peptide was observed in all three buffer types (Fig. 3. 36 A). However, the calculated dissociation constants differ between the single K_d fitted curves (Fig. 3.36 B). The binding affinities of N22-48 to SRP in RNA- and MST-buffer (green and orange data points) were in the same range with calculated K_d values of ~ 320 nM and ~ 480 nM, whereas the binding in Ffh- buffer was reduced significantly with a 3 fold higher K_d of ~ 1200 nM (purple data points). Comparison of the three fitting results showed that the highest binding affinity for N22-48 to SRP in RNA- buffer is represented also by the largest response amplitude, while with increasing K_d values, the response amplitudes decrease (Fig. 3.36 C). Nevertheless it was possible to perform a K_d fit of the averaged measurements resulting in a calculated dissociation constant around 390 nM with a K_d confidence of +/- 140 nM and a proper response amplitude of 9 (Fig. 3.36 D).

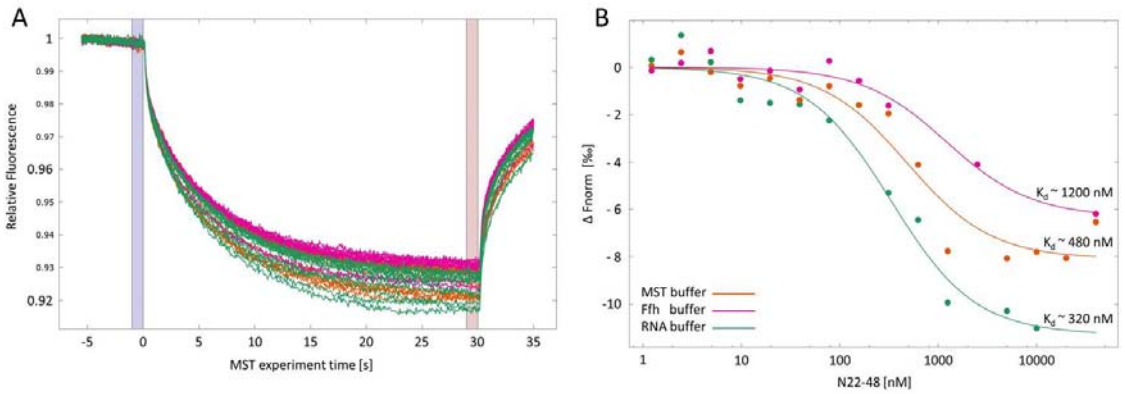

C

	RNA buffer	MST buffer	Ffh buffer
Graph color	●	●	●
Target	SRP_{647mal}	SRP_{647mal}	SRP_{647mal}
Ligand	N22-48	N22-48	N22-48
K_d [nM]	**321**	**473**	**1210**
K_d confidence [+/- nM]	92	162	449
Response amplitude	11	8	6
Target concentration [nM]	20	20	20
Unbound [fluor. counts]	929	930	932
Bound [fluor. counts]	918	922	926
Std. error of regression	0.85	0.9	0.49

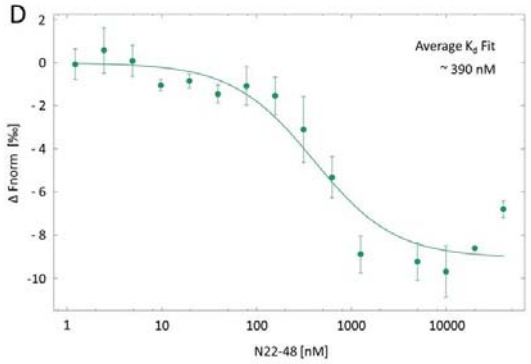

Fig. 3.36 ***SRP binding to KdpD N22-48 in MST measurements.*** *Concentration of the fluorescently labeled SRP- molecule was kept constant at 20 nM and the concentrations of the titrated N22-48 peptides were varied between 1,2 nM to 40 µM. Thermophoresis was measured with an excitation power of 50 % and 20 % MST power.* ***(A)*** *Original time traces of three independent MST measurements of SRP:N22-48 binding in different buffer systems, showing some bumpy regions in the curves at higher ligand concentrations.* ***(B)*** *Single K_d fitted curves of N22-48 titration in RNA- buffer (green), MST_{opt}- buffer (orange) and Ffh- buffer (purple).* ***(C)*** *Overview of the fitting results of the binding events in different buffer systems. Detailed explanation is given in chapter 0.* ***(D)*** *K_d of 388 nM +/- 142 nM was determined for the averaged K_d fit of the SRP:N22-48 interaction in different buffer compositions using the Thermophoresis + T Jump signal for data analysis (3 independent measurements, error bars represents the standard deviations).*

The lower the standard error of regression or root mean square error (RMSE) is, the better the experimental data are represented by the fitted curve. For the averaged fitting result the RMSE constituted 1.1, indicating that the calculated K_d only roughly represents the actual binding affinity. Of course this could be due to the use of different buffer compositions of the averaged measurements, but the deviation between the signals in the low ligand concentration samples (1-100 nM N22-48) showed a good agreement of the independent measurements in the unbound state of the SRP protein. Therefore it is assumed that the bumpy signals in the bound state curves are caused by the high ligand concentrations, presumably inducing the aggregation of the SRP protein during the binding event to some extent. To define an exact K_d for this binding event, further assay optimization would be necessary. However, a distinct and specific binding of SRP to the N-terminal KdpD wild type peptide N22-48 was detected in all MST measurements under

these conditions. Also, the binding affinity of ~ 400 nM calculated by the MST measurements are in good agreement with recent equilibrium measurements of SRP binding to RNCs stalled with nascent protein chains of 35 or more amino acid residues in length of the leader peptidase, indicating a very tight binding of ~ 1 nM, while K_d values around 50 nM were observed for vacant 70S ribosomes (Bornemann *et al*., 2008). Since I did not use ribosomes carrying the nascent peptide chain but used the free signal sequence peptide, it was expected that the binding affinity was lower due to the absence of the SRP binding sites on the ribosome. My data are therefore more comparable to the calculated binding affinity of ~ 1,5 µM of the ΔEspP signal peptide to SRP by fluorescence anisotropy (Bradshaw *et al*., 2009).

A crucial question is how the signal sequence is recognized and bound by SRP as no obvious consensus motifs are known for this process. SRP-dependent N-terminal signal sequences are highly diverse in amino-acid composition and length, but they all contain a core of at least eight consecutive hydrophobic amino acids that act as the major determinant for recognition by SRP (Valent *et al*., 1997 & 1998; Martoglio and Dobberstein 1998; Hegde and Bernstein 2006, Janda *et al*., 2010). In addition, the N-terminal region of a signal sequence typically contains positively charged residues with an as yet unknown function, suggesting a combination of hydrophobic interactions and electrostatic contacts during recognition and binding of SRP to signal sequences. To investigate the specificity of the SRP signal sequence of KdpD, the mutant W3A and 3Q peptides were tested of their ability to bind SRP under the same conditions as described for the wild type peptide, respectively. For the dilution series, 80 µM stock solutions of W3A and 3Q in MST_{opt} buffer (50 mM Tris pH 7.4, 150 mM NaCl, 10 mM $MgCl_2$, 0,05 % Tween-20) were prepared and mixed with 40 nM reconstituted SRP. The mixed binding components were incubated for 20 min on ice and MST measurements were performed in premium coated capillaries. Since the MST curves started to get bumpy after 10 s of thermophoretic movement, the affinity analysis was performed using the early MST signal of manually evaluated settings with start and end positions -1 s and 0 s for the cold region and 4.51 s / 5.51 s for start / end of the hot region (Fig. 3.37 A). This approach raised the K_d of the triplicate N22-48 measurement from ~ 390 nM (Fig. 3.36 D) to ~ 472 nM (Fig. 3.37 B) and also reduced the standard error of regression from 1.1 to 0.57 (Fig. 3.37 C), indicating that the manual K_d fitting represents more reliable affinity data for this assays than the Thermophoresis + T Jump evaluation. Both mutant peptides showed a change in MST response upon binding to SRP similar to the wild type peptide N22-48, however with reduced binding affinities. The calculation revealed a K_d of ~ 1,2 µM for 3Q binding and a

10-fold higher dissociation constant of ~ 5,4 µM, compared to the wild type peptide K_d, for the W3A mutant (Fig. 3.37 B).

A

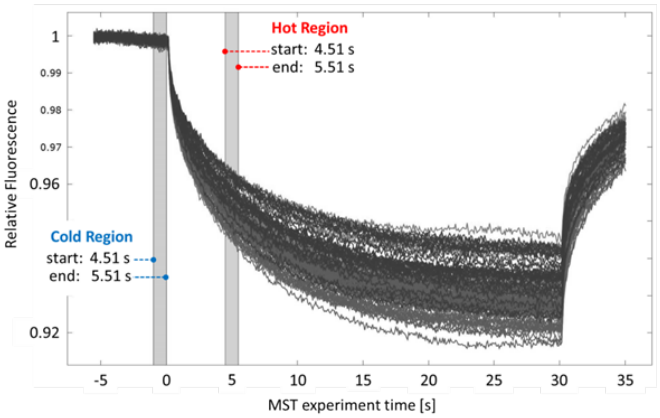

B

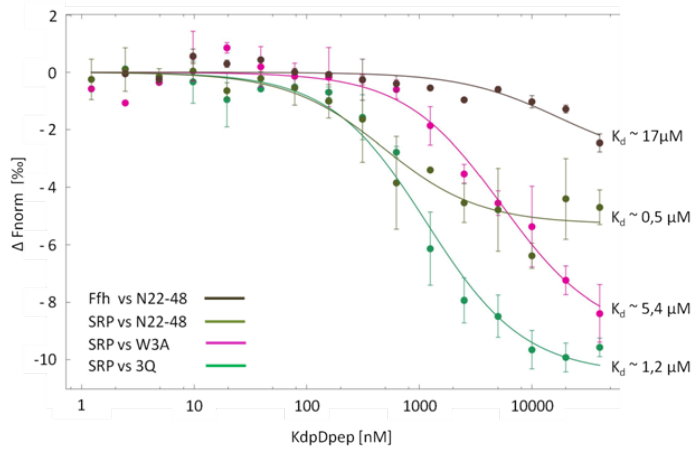

C

	N22-48	3Q	W3A	N22-48
Graph color	●	●	●	●
Target	SRP_{647mal}	SRP_{647mal}	SRP_{647mal}	Ffh_{647mal}
Ligand	N22-48	3Q	W3A	N22-48
K_d [nM]	**472**	**1156**	**5361**	**17006**
K_d confidence [+/- nM]	156	217	1307	13177
Response amplitude	5	10	9	3
Target concentration [nM]	20	20	20	20
Std. error of regression	0.57	0.59	0.54	0.35

Fig. 3.37 ***Interaction of SRP with KdpD signal sequence mutants.*** *Concentration of the SRP-labeled molecule was kept constant at 20 nM and the concentration of the titrated KdpD peptides varied between 1,2 nM to 40 µM. Thermophoresis was measured with an excitation power of 50 % and 20 % MST power.* ***(A)*** *Original time traces monitor a total of 9 independent MST measurements of SRP:N22-48 (n=3); SRP:W3A (n=2); SRP:3Q (n=2); Ffh:N22-48 (n=2). All traces gave bumpy curves after 10 s of thermophoresis. Manual cursor settings for K_d evaluation are indicated.* ***(B)*** *Reduced binding affinities were measured for 3Q (K_d ~ 1,2 µM) and W3A (K_d ~ 5,4 µM) compared to the wild type N22-48 peptide (K_d ~ 0,5 µM). Additionally, MST was measured for N22-48 binding to labeled Ffh protein without 4.5S RNA reconstitution (brown curve), demonstrating the loss of binding ability to the SRP signal peptide. The error bars represent the s.d. of each data point.* ***(C)*** *Overview of the fitted binding events of the different KdpD peptides in MST_{opt} buffer.*

Strikingly, substitution of the three positive amino acid residues in the N-terminal part of the signal peptide with glutamine in the 3Q mutant increased the K_d value for SRP binding only two fold. Also, it did not affect the binding of SRP as much as for the W3A mutant exhibiting an altered Walker A motif in the core region. This observation is in good agreement with earlier *in vivo* studies with ΔEspP signal sequence mutants, indicating that single point mutations that slightly change the hydrophobicity of the core region profoundly affect SRP recognition, whereas mutations that alter the charge of the N- region have only marginal effects (Lee and Bernstein, 2001; Peterson *et al*., 2003).

To ensure that the interaction detected between SRP and the various signal peptides truly represents specific binding, the labeled Ffh protein was used instead of reconstituted SRP to further analyze the binding to N22-48. The absence of the 4.5S RNA leads to an inactive signal recognition particle and raised the calculated K_d from ~ 0,5 µM to more than 17 µM, without reaching a saturated bound state within the peptide concentration range that was used for this assay (Fig. 3.37 B). This demonstrates the importance of a functional, fully assembled SRP and hence strongly suggests a specific SRP – substrate interaction in these measurements. Interestingly, the response amplitude changed from 5 to 10 for N22-48 and the 3Q mutant (R22Q, K24Q, K26Q), respectively. This is due to the fact that the thermophoretic amplitude not only depends on the size of the complex but contains contributions from both charge and structure. By replacing 3 charged arginine / lysine residues with structurally different and uncharged glutamine residues, a strong influence on the biophysical and thermodynamic features of the complex is very likely and can consequently be observed in the thermophoretic amplitude. Another explanation for the differing amplitudes could be that the conformational changes of SRP induced by binding of a proper signal sequence (Janda *et al*., 2010; Hainzl *et al*., 2011) are altered due to the mutant signal peptides and result in incorrect folded SRP:signal-peptide complexes.

In conclusion, it was shown that the SRP recognition sequence of KdpD encompasses the amino acid residues 22 – 48 at the very N-terminal region of the large cytoplasmic domain of the KdpD protein since a direct interaction of the isolated peptide N22-48 with purified SRP was demonstrated via microscale thermophoresis. A dissociation constant of ~ 500 nM was calculated for this binding event (Fig. 3.36). In addition, MST measurements of the SRP signal sequence mutants 3Q and W3A revealed a two-fold and 10-fold reduced binding affinity to SRP (Fig. 3.37), respectively. This suggests a direct influence of the amino acid composition in the signal peptide on its SRP binding affinity, whereby the detailed analyses of additional signal sequence mutants are required to understand the importance of particular amino acid residues and their position within the sequence.

4 DISCUSSION

In this study, the molecular mechanisms of co-translational membrane insertion of inner membrane proteins in *E. coli* were investigated in detail. Membrane proteins comprise about one third of the bacterial proteome, many of them being involved in essential physiological processes such as the membrane-located electron transport in the respiratory chain, generation of ATP and the proton motive force, uptake of nutrients or sensory mechanisms. To functionally assemble the wide variety of membrane-located proteins and protein complexes, bacterial cells have evolved several different pathways using various membrane insertion and translocation machineries. For the insertion of inner membrane proteins in eubacteria, the membrane translocase SecYEG and the membrane insertase YidC, as well as the signal recognition particle (SRP) targeting system are of central importance. Insertion of integral membrane proteins into the lipid bilayer usually takes place co-translationally at membrane-associated ribosomes (Luirink and Sinning, 2004; Egea *et al*., 2005; Halic and Beckmann, 2005). Not fully clear, however is, how SRP recognizes the specific features of nascent chains of hydrophobic substrate proteins and how the ribosome nascent chain complexes (RNCs) are transferred to the adequate translocase or insertase, especially in the YidC-only insertion pathway. YidC is the prokaryotic member of the YidC/Oxa1/Alb3 protein family (Dalbey and Kuhn, 2004) and works either independently inserting a subset of specific inner membrane proteins or it functions cooperatively with the Sec translocon (Dalbey *et al*., 2011).

In the first, main part of this thesis, the function of the prolonged C-terminal putative ribosome-binding domain in certain YidC proteins and its actual role in ribosome-interaction and in SRP-mediated membrane insertion in Gram-negative bacteria was analyzed. Evidence is provided for a possible (ancestral) function of this extended tail by biochemical as well as structural approaches. The second part focuses on the interaction of the signal recognition particle with the signal sequences. Isolated mutant signal sequence peptides were used to determine the specificity of SRP recognition in proteins. The interaction studies were established in an *in vitro* system with purified SRP and binding affinities were determined via microscale thermophoresis (MST), a new technique that enables immobilization-free, in-solution kinetic measurements of biomolecular interactions. Taken together, this study contributes to the understanding of the molecular mechanisms of co-translational membrane protein biogenesis in bacteria and also highlights evolutionary aspects of this complex vital cellular process.

4.1 C-terminally extended YidC variants complement *E. coli* YidC *in vivo*

The fundamental findings of this thesis are provided by analyzing the engineered YidC chimera, comprised of the insertase core domain of *E. coli* YidC and the C-terminal putative ribosome binding domains (CTDs) of marine, Gram-negative YidC homologs (Fig. 3.2), resulting in the C-terminally extended YidC variants YidC-Rb (CTD of *R. baltica* YidC) and YidC-Oa (CTD of *O. alexandrii* YidC). The C-terminal regions of YidC from *Rhodopirellula baltica* (80 aa; +20), a bacterium belonging to the planctomycetes, and from the α-proteobacterium *Oceanicaulis alexandrii* (99 aa; +18), are extended compared to the *E.* coli YidC insertase. The marine CTDs have numerous positively charged amino acid residues and show similarities to the C-terminal region of the mitochondrial Oxa1 protein (Fig. 3.1), as well as to the homologous Alb proteins in chloroplasts and YidC2 found in Gram-positive bacteria. In contrast to that, the C-terminus of *E. coli* YidC (Ec-YidC) is substantially shorter and only moderately positively charged (16 residues; +8).

At first, the ability of the chimeric YidC-Rb and YidC-Oa proteins to complement the *E. coli* YidC was tested *in vivo* (Fig. 3.3 C). Both YidC chimera promoted growth of *E. coli* MK6 cells when the wild type chromosomal YidC was depleted, with the same efficiency as the positive control (Fig. 3.3 A). Accordingly, this leads to the assumption that the elongated C-terminal tail on YidC does not interfere with its insertase function both in the YidC-only and in the Sec-YidC pathways of *E. coli.* This is consistent with the finding that Oxa1 of *Saccharomyces cerevisiae* (van Bloois *et al*., 2005) as well as YidC2 of *Streptococcus mutants* (Dong *et al*., 2008) and *Arabidopsis thaliana* Alb3 (Jiang *et al*., 2002), all containing alike C-terminally extended tails, are also able to rescue a YidC deficient phenotype in *E. coli*. However, it was shown that Oxa1 is unable to take over the Sec-associated function of YidC, while a direct association of Alb3 with SecY has been demonstrated in *A. thaliana* and a functional complementation for both pathways was observed (van Bloois *et al*., 2005). Importantly, the substitution of *E. coli* YidC was only successful when parts of its N-terminal region (aa 1-57 fused to Alb3; aa 1-247 fused to Oxa1 and YidC2), that contains an uncleaved signal sequence, had been fused to the respective homologous proteins. Hence, while the C-terminally extended YidC chimera used in this study could almost fully replace the *E. coli* protein, the mitochondrial and chloroplast, as well as the Gram-positive insertase homologs show differences in their activity and efficiency of complementation depending on growth and species background. This suggests that the complete functional spectrum of each insertase is optimized for the specific organism and environment in which they reside. A striking and explicit example

for this differentiation is the finding that Oxa1 cannot facilitate Sec-associated insertion, probably due to the fact that mitochondria lack a Sec translocon (Glick and van Heijne, 1996) but instead Oxa1 itself most likely forms an intricate homo-oligomeric insertion complex in the inner mitochondrial membrane (Nargang *et al*., 2002). The property of Oxa1 to interact directly with the Sec translocon might have been lost, concomitantly with the Sec-translocase, during evolution of mitochondria from endosymbiotic bacteria. In reciprocal experiments published by Preuss *et al*. (2005) it was shown that YidC expressed in mitochondria can functionally replace Oxa1, only when the C-terminal ribosome-binding domain of Oxa1 had been appended onto YidC. It would be interesting to test whether the C-terminally added ribosome-binding domains of the marine YidC homologs of the chimeric proteins YidC-Rb and YidC-Oa could substitute for Oxa1 in mitochondria.

4.2 The C-terminal tails of marine YidC homologs facilitate ribosome-binding independently of a nascent polypeptide chain

The YidC homolog Oxa1 of *S. cerevisiae* binds via its C-terminal domain to the large subunit of the mitochondrial ribosome in proximity to the protein exit tunnel (Szyrach *et al*., 2003; Jia *et al.,* 2003; Gruschke *et al*., 2010). Besides, the C-terminal tail of *S. mutants* YidC2 has been shown to be crucial for direct ribosome interaction (Funes *et al*., 2009; Wu *et al*., 2013). Therefore, the two C-terminal YidC extensions from marine Gram-negative bacteria (*R. baltica & O. alexandrii*) were tested for their ability to function also as ribosome binding domains. Ribosome binding was analyzed by *in vitro* ribosomal pull down assays (2.12) with purified YidC proteins and isolated *E. coli* ribosomes (Seitl, 2010; Maguire *et al*., 2008). A purification protocol for the YidC-chimera YidC-Rb and YidC-Oa, as well as for the *O. alexandrii* YidC homolog Oa-YidC, was successfully established (2.10.2), resulting in sufficient protein amounts and purity for the ribosome-binding assays (Fig. 3.8, input). Both chimeras with the hydrophilic C-tails of the marine YidC homologs fused to the *E. coli* YidC moiety (YidC-Rb and YidC-Oa) as well as the *O. alexandrii* YidC homolog Oa-YidC efficiently bound to *E. coli* ribosomes (Fig. 3.8 B-D). The results also verify that *E. coli* YidC (Ec-YidC), without an extended C-terminal tail, binds very poorly to empty ribosomes (Fig. 3.8 A).

However, contradictory data are published for the ribosome binding activity of Ec-YidC and the role of its short C-terminal tail in this regard. A cross-linking study published by the group of Koch in 2012 suggested that Ec-YidC interacts with both, empty and

translating ribosomes, while the interaction sites appear to be distributed over the large and the small subunits (Welte *et al*., 2012). However, the affinity of YidC to purified ribosomes was very low and the specificity could not be clearly shown in the study by Welte *et al*. (2012). On the other hand, in binding studies of a detergent-solubilized Ec-YidC to translating ribosomes, visualized by cryo-EM, the C-terminal region of YidC was assigned to be crucial for this interaction (Kohler *et al*., 2009). Corroborating the results presented in this thesis, the detailed analysis of the interaction between Ec-YidC and ribosomes by fluorescence correlation spectroscopy (FCS) delineated by Kedrov *et al*., demonstrated that under physiological buffer conditions (pH 7.4) Ec-YidC does not bind to non-programmed, so called empty, ribosomes (Kedrov *et al*., 2013). Furthermore, they showed that the addition of just six histidine residues to the C-terminus of YidC is sufficient to bind YidC to ribosomes particularly upon low pH (pH 6.2) when the histidine residues are positively charged. Since C-terminally histidine-tagged YidC protein was used by Kohler *et al*. (2009) for the cryo-EM reconstitution of the Ec-YidC:ribosome complex under acidic conditions, this would be an explanation for their observation of a strong and C-terminal tail-dependent binding of Ec-YidC to empty and translating ribosomes. Thus, these experiments may not reflect naturally occurring interactions. Hence, the binding assays in this present study were performed under physiological buffer conditions (pH 7.4) with N-terminally histidine-tagged YidC proteins and empty ribosomes, confirming the results of Kedrov *et al*. (2013) with YidC not binding empty ribosomes. Interestingly, membrane-reconstituted Ec-YidC without any artificial affinity tag was able to bind to ribosome nascent chain complexes that expose the N-terminal transmembrane segment of F_Oc, a natural substrate of Ec-YidC, at physiological pH (Kedrov *et al*., 2013). While the mitochondrial Oxa1 protein binds permanently to ribosomes even in the absence of nascent chains and therefore tethers mitochondrial ribosomes perpetually to the membrane (Szyrach *et al*., 2003; Jia *et al*., 2003), the lack of an interaction between Ec-YidC and non-programmed ribosomes probably provides a more flexible targeting of RNCs to the membrane insertase, depending on the emerging nascent substrate chain. Further studies are necessary to elucidate the specificity of YidC to nascent chains and the involvement of additional factors, particularly the signal recognition particle and its receptor. The SRP components might further contribute to the YidC-nascent chain interaction and support the discrimination between YidC-dependent and -independent substrates *in vivo*. The C-terminal region of Ec-YidC is not essential for its activity as a truncated variant fully complements the insertase function *in vivo* (Jiang *et al*., 2003). Concordantly, Kedrov *et al*. (2013) showed that the Ec-YidC:RNC binding is not completely abolished upon removal of the YidC C-terminal tail, suggesting that additional docking sites on Ec-YidC also contribute to ribosome binding. Recently Gen *et al*. (2015)

stated that the cytosolic loop C2 of Ec-YidC ensures stable docking of a translating ribosome to YidC while modifications in this regions lead to enhanced ribosome dissociation. Remarkably, simultaneous dual deletions within the C2 loop and at the C-terminus of Ec-YidC abolished the insertion of the YidC-only substrates F_Oc and MscL, underlining the important role of a direct YidC:RNC interaction for co-translational protein insertion.

Notably, the *in vitro* binding studies with empty 70S ribosomes in this study here clearly showed a strong affinity of the YidC hybrid protein with C-terminal extension sequences from the marine bacteria to *E. coli* ribosomes without the need of an emerging polypeptide chain, in contrast to the wild type Ec-YidC. Consequently, this leads to the assumption that the elongated, charged C-terminal tails of the marine YidC homologs from *R. baltica* and *O. alexandrii* functions as ribosome binding domains. This specific binding is therefore crucial for permanent association of the YidC homologs to ribosomes independent of their translational state and similar to the essential binding function of the C-terminal Oxa1 domain to mitochondrial ribosomes.

4.3 Visualization of the ribosome-bound insertase complex

In order to understand and accurately depict how YidC inserts proteins in a co-translational manner into the inner membrane of *E. coli*, it is essential to solve the structure of YidC bound to substrate specific RNCs at high resolution. The structural information for Ec-YidC was then limited to an X-ray structure of the large periplasmic domain (Oliver and Paetzel, 2008; Ravaud *et al*., 2008), a 10 Å 2D projection map of the membrane-integrated Ec-YidC dimer (Lotz *et al*., 2008) and a low-resolution (14,4 Å) cryo-EM reconstruction of an Ec-YidC:RNC complex (Kohler *et al*., 2009). None of those structures, though, had enough performance to answer for instance the question about the functional oligomeric state or to give further insights how YidC acts at a molecular level. To address these questions, we performed an advanced structural analysis of YidC-ribosome complexes using high-resolution cryo-EM with the C-terminally elongated YidC-chimera YidC-Rb. Due to the extension of Ec-YidC with the C-terminal ribosome binding domain, that drastically increases the ribosome affinity *in vitro* (Fig. 3.8), we were able to isolate stable YidC-Rb:RNC complexes (2.13). Those complexes were visualized using high-performance cryo-EM and the reconstruction of the complex could be refined to 8,6 Å (2.14). This improved resolution now allows a more detailed interpretation of the structural and functional features of the YidC-insertase complex. The TnaC-stalled ribosomes carried nascent polypeptide chains encompassing the first two TM segments of MscL, a

native YidC substrate in *E. coli* (Fig. 3.10). The path and position of the nascent chain within and at the ribosome can be traced from the peptidyl transferase center (PTC) through the ribosomal exit tunnel into an extra density at the tunnel exit representing YidC-Rb (Fig. 3.13). Although our overall resolution was in the subnanometer range, the alpha-helical secondary structures were barely resolved in the YidC density, most probably due to some flexibility in this region (Fig. 3.12). Interestingly, the presence of the C-terminal extension increases the affinity of YidC to the ribosome without changing its overall ribosome interaction mode. The spatial position and topology of the YidC-Rb chimera in this study agreed well with the position of Ec-YidC observed in the cryo-EM structure from an earlier study of ribosome-bound *E. coli* YidC (Kohler *et al*., 2009). Moreover, we observed a similar interaction pattern between our C-terminally extended YidC-Rb and the ribosome. We could resolve in molecular detail the contact sites of YidC-Rb to the ribosome: The helix H59 of the 23S rRNA showed the strongest contact to YidC-Rb followed by close interaction with the two ribosomal proteins L24 and L29. Surprisingly, we observed a relatively weak connecting density with L23, the main contact site for SRP and TF, and also for a proposed contact derived from the lower resolution structure of the Ec-YidC-RNC with a F_Oc nascent chain (Kohler *et al*., 2009). However, the ribosomal proteins L24 and L29, together with L23, also surround the ribosomal tunnel exit and provide binding sites for diverse factors involved in co-translational processing, folding, targeting and membrane insertion of nascent chains (Fig. 1.3). Since an enhanced interaction interface of YidC-Rb to the ribosomal protein L29 was observed (Fig. 3.11 C and D), compared to the Kohler *et al*. (2009) structure, the YidC-Rb protein as well as the Ec-YidC were tested for their ability to interact directly with isolated ribosomal proteins in *in vitro* pull down assays (2.15). Indeed, L29 only co-eluted with YidC-Rb (Fig. 3.16, lower panels), whereas L24 co-eluted both with Ec-YidC and in similar amounts as with YidC-Rb (Fig. 3.16, upper panels). Thus, L24 seems to be a major contact site for the YidC-insertase core domain, while the enhanced affinity of YidC-Rb to the ribosome is at least partially caused by the interaction between the C-terminal *R. baltica* YidC tail domain with the ribosomal protein L29, suggesting that the C-tail of YidC-Rb faces towards the L29 moiety of the ribosome.

Recently, Wickles *et al*. (2014) reconstituted YidC-Rb with RNCs exposing the first TM helix of F_Oc and subjected the purified complex to cryo-EM and single particle analysis to a resolution of ~ 8 Å. In contrast to our first cryo-EM structure of ribosome-bound YidC-Rb (Seitl *et al*., 2014), it was now possible to separate the weaker electron density of the detergent micelle from that of the YidC-Rb protein moiety (Fig. 4.1 B). Furthermore, Wickles *et al*. (2014) calculated a structural model of *E. coli* YidC via the intramolecular

co-variation analysis that could be docked in a distinct orientation into the cryo-EM structure of the YidC-Rb:RNC complex (Fig. 4.1 B and C). Shortly after, the X-ray structure of Ec-YidC was published and confirmed that the built Ec-YidC model (Wickles *et al.,* 2014) appeared in good agreement with the experimentally solved molecular structure (Kumazaki *et al*., 2014-b). Interestingly, in both YidC-Rb:RNC densities an additional density which is aligned with the ribosomal exit tunnel, neighboring TM3, was found that could be attributed to the TM helix of the nascent MscL- or F_OC- chain, respectively (Fig. 4.1 A and C). This hypothesis is supported by data from several independent studies which show that YidC substrates, and also nascent F_OC chains (Wickles *et al*., 2014), can be crosslinked to TM3 (Klenner *et al*., 2008; Yu *et al*., 2008; Neugebauer *et al*., 2012; Klenner and Kuhn, 2012). Strikingly, at the same relative position nascent chains have been observed inside the SecY channel (Frauenfeld *et al*., 2011; Wickles *et al*., 2014). Independently of the nascent chain substrate used in our experiments, YidC-Rb revealed an almost identical interaction pattern on the ribosomal exit site (Fig. 4.1) for both cryo-EM reconstructions (Seitl *et al*., 2014; Wickles *et al*., 2014).

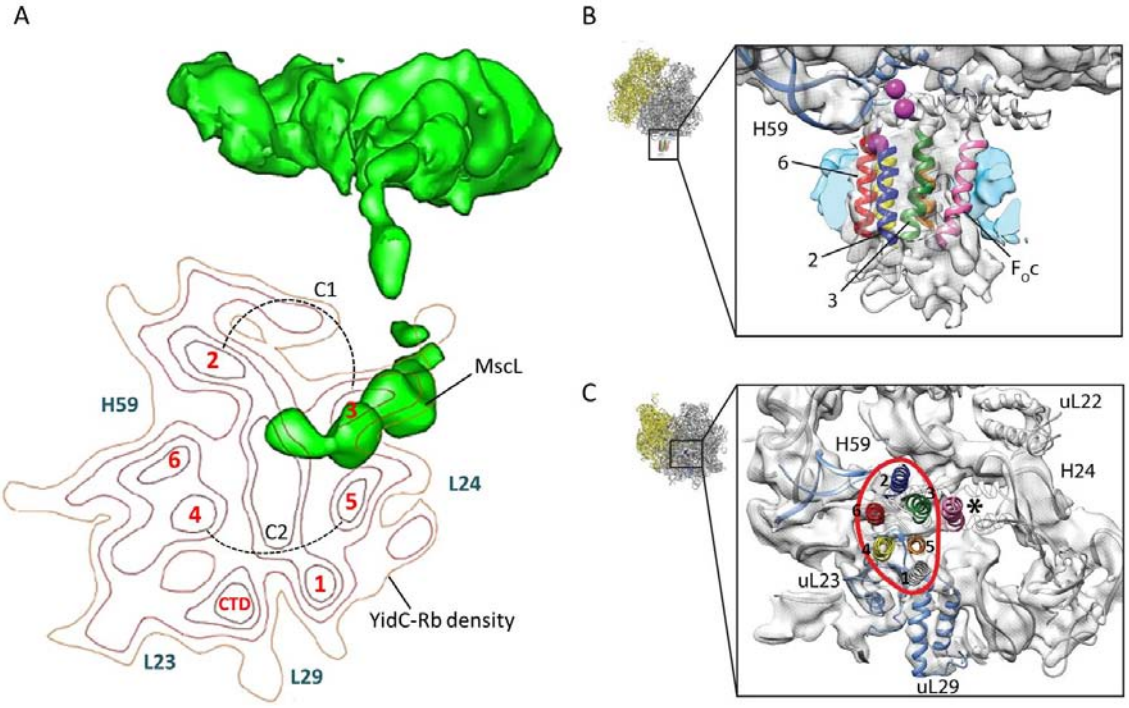

Fig. 4.1 ***Comparison of two YidC-Rb structures bound to RNCs carrying MscL (8.6 Å) – and F_OC (8 Å) nascent chains, respectively.*** *YidC-Rb revealed an almost identical interaction pattern on the ribosomal exit site for both cryo-EM reconstructions and both nascent chains enter the insertase core within particular proximity of TM3.* ***(A)*** *Density blot (bottom view) of YidC-Rb shows the entering of the nascent MscL chain (green) in the center of the YidC-Rb density (red) and the proposed TM domain arrangement (1-6; red), relative to the indicated ribosomal proteins L23, L24, L29 and the rRNA helix H59 (blue). The assumed position of the C-terminal ribosome-binding*

domain (CTD) was assigned to an additional density near L29. Cytoplasmic loops C1 (47aa) and C2 (13aa) are schematically (dotted lines) included in the figure for orientation. ***(B)*** *Close up view from within the membrane region of YidC-Rb bound to F_Oc-RNC, highlighting the predicted contacts between the C1 and C2 loops of YidC and the ribosome, indicated by magenta spheres. The detergent micelle is shown in blue and the F_Oc TM helix in pink.* ***(C)*** *Periplasmic view of the active ribosome-bound YidC model, with the YidC contour outlined in red. The polypeptide exit tunnel is indicated with an asterisk. Structure (A) was adapted from Seitl et al., 2014 and structure (B/C) from Wickles et al., 2014.*

Although the C-terminally extended domain of YidC-Rb was excluded in the built Ec-YidC model (Fig. 4.1 B and C), we suggest that the additional density, located between the ribosomal proteins L23 and L29, accounts for the C-terminal ribosome-binding domain (CTD) of the marine *Rhodopirellula* YidC homolog (Fig. 4.1 A). As discussed above, YidC-Rb shows a much higher affinity to L29 than Ec-YidC in pull down assays (Fig. 3.16). Therefore, we assume that the C-tail of YidC-Rb faces the ribosomal rRNA helix H59, which is located next to TM6, up to the opposite site of the exit tunnel. There it contacts the ribosomal protein L29 next to TM1, stabilizing the whole insertase-ribosome complex. This model also explains why we observed in both YidC-Rb structures only weak contacts to the ribosomal protein L23, compared to the Ec-YidC:RNC structure (Kohler *et al*., 2009). It is possible that the large CTD, positioned by the high affinity to L29, shields the L23 majority and therefore prevents to a large extent the interaction with the YidC-insertase core. As additional contacts to the ribosome, Wickles *et al*. (2014) suggested residues in the positively charged C1 (Y370; Y377, contacts to rRNA helix H59) and C2 (D488, contact to L23) loops of YidC (Fig. 4.1 B). Indeed, mutations in these residues compromised the growth of YidC-depleted *E. coli* cells, emphasizing their functional significance. However, as discussed in chapter 4.2, Geng *et al*. (2015) probed the influence of the C1 and C2 loop regions in direct ribosome-binding efficiency and showed that only C2 contributes to YidC:RNC assembly, while the C1 loop is involved in other vital functions. Due to the local proximity of the C1 region to the nascent chain portal site in the YidC-Rb density (Fig. 4.1 A), it is feasible that the C1 loop directly contacts the emerging polypeptide chain and assists the correct folding of inserting membrane proteins into the lipid bilayer.

Another striking finding of the cryo-EM YidC-Rb:RNC structures was that only a single monomer of YidC was bound to the translating ribosome (Fig. 4.1; Seitl *et al.,* 2014; Wickles *et al*., 2014). Until then, results from the early studies on YidC extracted from bacterial membranes suggested that the protein is present in both monomeric and dimeric forms (van der Laan *et al*., 2001; Heuberger *et al*., 2002). Also crystallographic analysis showed that YidC forms symmetric dimers in the membrane (Lotz *et al*., 2008). Additionally, the low resolution cryo-EM structure on a YidC:RNC-F_Oc complex also

suggested that two copies of YidC bind to the ribosomal tunnel exit (Kohler *et al*., 2009). However, this view changed during the last years due to the YidC-Rb:RNC structures and also by the recently published X-ray structures of both Gram-positive and Gram-negative YidC proteins, clearly showing YidC to be in a monomeric state (Kumazaki *et al*., 2014-a & 2014-b). Kedrov *et al*. (2013) probed the oligomeric state of Ec-YidC in its free form and bound at the ribosome via fluorescence cross-correlation spectroscopy (FCCS). In this study it was shown that a single membrane-embedded YidC copy is sufficient to bind a substrate-translating ribosome and YidC only oligomerizes on the ribosome when YidC was applied in excess, non-physiological concentrations, compared to the amount of applied RNCs. Since a 10-fold excess of YidC was used to form YidC:RNC complexes in the previously cryo-EM reconstitution (Kohler *et al*., 2009), the corresponding structure likely represented a concentration-dependent oligomer of YidC. Taken together our observation of a single YidC-Rb protein bound to a 70S *E. coli* ribosome is in agreement with the recent literature, showing clearly that a single YidC copy is fully active as monomer, thus being the minimal and probably true-to-life functional unit for YidC-dependent, co-translational insertion of membrane proteins.

4.4 The C-terminal ribosome-binding domains of marine YidC homologs are intrinsically disordered

Since the C-terminal domain (CTD) of YidC-Rb was not resolved in the cryo-EM structure (Fig. 3.13), the native architecture of the CTDs from *R. baltica* YidC (RbCT) and *O. alexandrii* YidC (OaCT) without their insertase core domains was further investigated by CD-spectroscopy (2.16). Therefore, RbCT and OaCT encompassing 80 and 99 amino acid residues, respectively, were separately cloned and purified via an N-terminal His_{10}-tag to near homogeneity by Ni-NTA affinity and strong cation exchange chromatography (2.10.5). Similar to the isolated CTDs of Alb3 (A3CT; Falk *et al*., 2009), yeast Oxa1p (O1CT; Szyrach *et al*., 2003) and human Oxa1L (Haque *et al*., 2010), both RbCT and OaCT revealed far-UV CD spectra typical for unfolded proteins (Fig. 3.22) in aqueous solution under low salt conditions. The results obtained by CD-spectroscopy are consistent with the prediction of the intrinsically disordered nature of RbCT and OaCT. The computer models identified unstructured regions in both protein domains (Fig. 3.21 A and B), similar to the Alb3 C-terminal segment (Fig. 3.21 D). However, formation of an α-helical conformation was induced by the addition of trifluoroethanol (TFE) for all C-terminal insertase domains (Fig. 3.22 A and B; Szyrach *et al*., 2003, Falk *et al*., 2009; Haque *et al*., 2010). TFE is a co-solvent that is known to disrupt coiled-coil interactions in proteins leading to non-interacting single helices, but also stabilizes the helices in single

α-helical segments (Lau *et al*., 1984; Frère *et al*., 1995). In accordance, secondary structure prediction of the CTDs from various organisms using the PSIRED server, confirmed the presence of regions in these domains that could potentially form α-helices (Fig. 4.2 A), but they show differences in lengths and numbers of the predicted helical regions as well as in the structural motifs these regions are predicted to form. However, all CTDs compromise helices within the first 20 amino acid residues of the extended regions, followed by another second, larger α-helical region, starting approximately at the position of amino acid residue 40, expect in the case of the *S. mutans* YidC2 CTD (Fig. 4.2 A; Y2CT). For the most extended A3CT, the C-tail of the chloroplast insertase homolog, two more regions were predicted to adopt a helical conformation. Alternative prediction analyses revealed coiled-coil interaction domains (COILS; Lupas *et al.*, 1991) almost certainly in O1CT and in A3CT (Fig. 4.2 A; dark green boxes) and with less probability for the second helical motif in OaCT (Fig. 4.2 A; light green boxes). RbCT and Y2CT analyses rendered no bias to form coiled-coil motifs. However, helical wheel projections (RZ lab) of the predicted α-helical regions suggested the formation of single amphipathic helices in RbCT (aa 42-52), Y2CT (aa 10-20) and also for the first putative helical domain (5-19) in OaCT (Fig. 4.1 B).

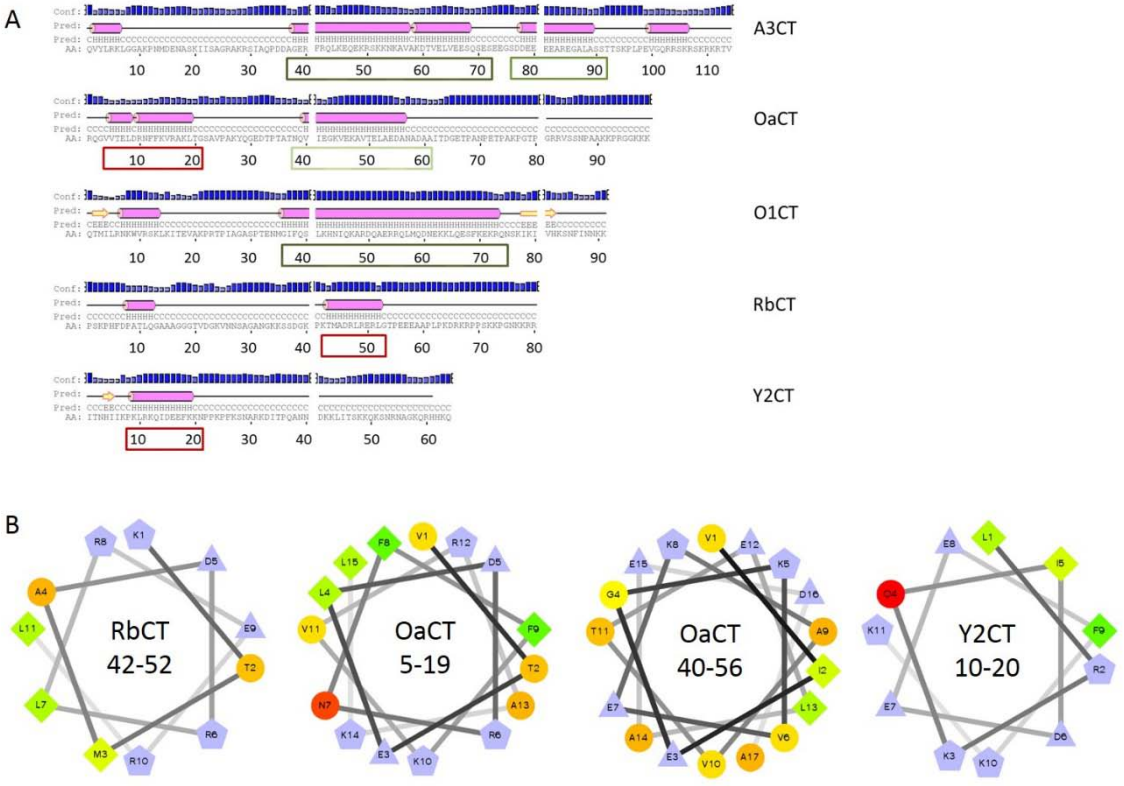

Fig. 4.2 ***Secondary structure predictions of C-terminally extended insertase domains (CTDs).*** ***(A)*** *Secondary structure prediction was generated computationally using the PSIRED server.*

Several α-helices of diverse lengths are predicted for all CTDs, but the number and length of the α-helical regions vary among the different organisms (A3CT: CTD of Alb3 from A. thaliana; OaCT: CTD of YidC from O. alexandrii; O1CT: CTD of Oxa1 from S. cerevisiae; RbCT: CTD of YidC from R. baltica; Y2CT: CTD of YidC2 from S. mutans). Pink bars indicate putative helical regions and yellow arrows predict strand motifs. Amino acid residues predicted to form coiled-coil motifs (Lupas et al., 1991) are boxed in green (dark green: most likely; light green: less likely). Regions predicted to form amphipathic helices are boxed in red. ***(B)*** *Helical wheel projections (RZ-lab) of the bacterial helical CTD regions suggest the formation of amphipathic helices for the second helix in RbCT, the first helix in OaCT (aa 5-19) and the sole helical region in Y2CT. The region encompassing amino acid residues 40-56 in OaCT is more likely to form a coiled-coil motif. Hydrophilic residues are presented as circles, hydrophobic residues as diamonds, potentially negatively charged as triangles, and potentially positively charged residues as pentagons. Hydrophobicity is color coded: the most hydrophobic residue is green, and the portion of green is decreasing proportionally to the declining hydrophobicity, with zero hydrophobicity coded as yellow. Hydrophilic residues are coded red with pure red being the most hydrophilic (polar) residue, and the amount of red decreasing proportionally to the hydrophilicity. The charged residues are marked in light blue.*

Despite the low primary sequence homology observed for all CTDs (Fig. 3.17 B), it seems that the organellar insertase homologs favor a coiled-coil formation in their C-terminal extended domains, whereas the prokaryotic ribosome-binding domains generally encompass only shorter helical regions, presumably forming single amphipathic helices for their interaction with the ribosomes or the membrane environment. It is likely that the differences between the organellar and the prokaryotic ribosomes lead to significant alterations in the interaction of ribosomes from different organisms with the respective insertase homologs. These differences may reflect the individual paths trodden in evolving the distinct eukaryotic and the prokaryotic membrane translocase systems, respectively. Although mitochondrial ribosomes developed from those of their bacterial ancestors, over the long period of eukaryotic evolution, the translational system in the organelle changed considerably (Smits *et al*., 2007). The catalytic core of the mitochondrial ribosome and the region around the polypeptide exit tunnel of the large subunit still resembles those of bacterial ribosomes, but many mitochondria-specific proteins have been added through the eras of evolution (Gruschke *et al*., 2010). Particularly in animals, the rRNA content has considerably decreased (Sharma *et al*., 2003; O'Brien, 2003). Interestingly, differences in the C-terminal domains of Oxa1 homologs from higher and lower eukaryotes, studied by Haque *et al.* (2010), revealed structural differences in the CTD from mammalian Oxa1L compared to the yeast Oxa1p. Also an alternative interaction pattern of the Oxa-homolog on mammalian mitochondrial ribosomes was found. However, even though these structural features may be organism specific, they obviously have sufficient relatedness to mediate the binding for example of yeast Oxa1 to *E. coli* ribosomes (Kohler *et al*., 2009), indicating an accommodative and conserved binding mode to some extent.

Interestingly, as demonstrated by Falk *et al*. (2009) via CD-spectroscopy, the intrinsically disordered C-terminal region of Alb3 folds upon binding to cpSRP43, its native chaperone-

like interaction partner in chloroplasts. In a similar experiment, it was investigated whether the isolated C-terminal ribosome binding domain of YidC-Rb (RbCT) adopts an α-helical conformation upon binding to the ribosomal protein L29, since a direct interaction of L29 with the C-terminal domain of YidC-Rb has been shown (Fig. 3.16 A). However, we did not observe any conformational change and RbCT remained in its disordered formation upon addition of the putative ribosomal binding partner L29 (Fig. 3.23 B). Alternative explanations are possible for this observation: (I) the ribosomal protein L29 is not the sole determinant for folding of the YidC-Rb C-tail, and other ribosomal components like the rRNA helix 59 may induce instead or in cooperation with L29 the conformational change of the C-terminal insertase domain. (II) The context of the full-length insertase protein as well as (III) the membrane, particularly lipid interaction might also influence the structure of the C-terminal domain. Especially for the formation of an amphipathic helix the presence and binding of lipids may be important. In general, the intrinsic disorder of these domains might be advantageous to provide orientational freedom and flexibility in scanning for and binding to RNCs at the crammed cytoplasmic surface of the inner bacterial membrane. Intrinsically disordered regions are associated with a broad repertoire of biological functions including cellular control mechanisms and signaling. It is proposed for the C-terminal domain of a potassium channel, that its disordered structure might modulate the kinetics of channel activation (Magidovich *et al*., 2007). Similar modulating functions are also proposed for the A3CT-cpSRP interaction (Falk *et al*., 2009). Triggered folding of intrinsically disordered regions upon binding to their interaction partners has been described for a number of physiologically relevant protein-protein interactions and it is suggested to be a general regulatory mechanism (Wright and Dyson, 2009). At present it is unclear whether such a mechanism can also be featured for the YidC:RNC assembly and further studies will be necessary to evaluate the binding-induced conformational changes of the intrinsically disordered C-terminal ribosome binding domains of the Gram-negative YidC homologs. Particularly a possible functional role of this trigger yet stays to be elucidated.

4.5 Stable ribosome:YidC association can partially substitute for an SRP-mediated targeting process in *E. coli*

Since the *in vitro* studies clearly showed an enhanced interaction of C-terminally elongated YidC proteins with empty ribosomes (Fig. 3.8) and likewise a stable complex formation with programmed RNCs (Fig. 3.11), I wanted to test a possible functional role of the C-terminal YidC extensions in co-translational protein targeting *in vivo*. For that purpose the membrane targeting of the SRP-dependent YidC-substrate protein MscL

(Facey *et al*., 2007) was analyzed as a GFP fusion protein by fluorescence microscopy (2.8). In addition, the proper membrane insertion of MscL was probed in radioactive pulse chase experiments via AMS gel shift assays (2.9) in the absence of a functional SRP pathway. To investigate whether an extended C-terminal region of YidC can compensate for a loss of SRP function, either the protein component of the signal recognition ribonucleoparticle Ffh or the SRP receptor protein FtsY was depleted (2.9.1) in MscL-plasmid transformed *E. coli* strains.

The AMS gel shift assays demonstrated that insertion of MscL in *E. coli* depends on the *R. baltica* tail of YidC when FtsY is depleted (Fig. 3.25, YidC-Rb). Similarly, coexpression of a YidC chimera extended by the C-terminal tail of Oxa1 resulted in an enhanced membrane insertion efficiency under FtsY-depleted conditions (Fig. 3.25, YidC-Oxa). Cellular localization of MscL as a GFP fusion protein showed that it accumulated as fluorescent patches mostly close to the cell poles when the receptor protein FtsY was depleted (Fig. 3.27 B). In accordance with results from the AMS assay, coexpression of YidC-Rb prevented the formation of these MscL-GFP aggregates and the fluorescence was found at the membrane (Fig. 3.27 C). In contrast, coexpression of Ec-YidC (Fig. 3.27 D) had no effect on the localization of MscL-GFP, indicating that only the C-terminal tail of YidC-Rb (or of Oxa1) can restore membrane targeting of MscL in the absence of FtsY. It should be kept in mind that under FtsY depletion conditions, Ffh is still present and possibly required under these conditions. When Ffh was depleted, the MscL-GFP fusion protein clearly aggregated at the cell poles (Fig. 3.26 B) and coexpression of YidC-Rb only partially restored membrane targeting (Fig. 3.26 D). Similar results were observed for the membrane insertion of MscL assayed by AMS derivatization in which coexpression of YidC-Rb or YidC-Oxa only marginally stimulated MscL insertion in Ffh-depleted cells (Fig. 3.24). Taken together, the extended C-tails of the YidC derivatives can replace mainly the FtsY receptor function but not the Ffh function. It is assumed that the presence of Ffh might still be required to keep the newly synthesized MscL protein in an insertion-competent form, a function that obviously cannot be fulfilled by YidC. Without a functional SRP-system the hydrophobic non-inserted MscL protein molecules most likely aggregate in the cytoplasm and are then prone to proteolytic degradation, which mostly occurs at the cell poles. In summary, I could show that the C-terminal ribosome-binding domain of YidC found in the marine Gram-negative bacterium *R. baltica* can partially substitute for the SRP receptor protein FtsY, in contrast to the native *E. coli* YidC but comparable to YidC-Oxa. Therefore, it is suggested that the C-terminally extended YidC-tail putatively acts as an adaptor for a specialized membrane-targeting function during the co-translational insertion of the YidC-only pathway.

This is in accordance with recent data that show a functional overlap of the SRP-machinery and the elongated C-terminal tails of YidC/Oxa1/Alb3 family members in co-translational protein insertion (Funes *et al*., 2009). However, also in post-translational insertion processes, a functional and spatial proximity of FtsY and YidC seems to be important for an efficient SRP-dependent membrane insertion of hydrophobic substrates (Robinson and Woolhead, 2013). The SRP pathway thus allows a dynamic, substrate-triggered membrane association of cytosolic ribosomes with the translocation machinery at the endoplasmic reticulum of eukaryotic cells as well as with translocases and insertases at the cytoplasmic inner membrane surface of prokaryotes. In addition to its role in ribosome recruitment to the membrane, the SRP ribonucleoprotein might shield hydrophobic sectors on nascent chains from adverse interactions, and thereby improve and regulate the ongoing synthesis of membrane proteins. Genome analyses of fully sequenced eukaryotes revealed that mitochondria generally lack an SRP system. Comparison of the different translational systems suggests that, during evolution of mitochondria, the universal SRP-mediated co-translational insertion system was replaced by an SRP-independent machinery that relies on direct binding of ribosomes to the membrane-embedded insertase Oxa1 (Preuss *et al*., 2005; Funes *et al*., 2009). This development was favored by the small number (13 polypeptides in humans / animals; 8 in yeast) of almost exclusively very hydrophobic membrane proteins that are synthesized by the mitochondrial translation apparatus. Presumably as a consequence of its specialization for the synthesis of hydrophobic membrane proteins, the translation machinery of mitochondria is closely coupled to the inner membrane (Liu and Spremulli, 2000; Ott and Herrmann, 2010). Permanent association of mitochondrial ribosomes to the inner membrane surface is manly mediated by the C-terminal domain of Oxa1 (Jia *et al*., 2003; Gruschke *et al.*, 2010) and by the ribosome receptor Mba1. Presumably, Mba1 does not mechanistically contribute to membrane insertion of the hydrophobic substrates, but ensures the positioning of the ribosomal polypeptide exit tunnel to the membrane-embedded insertase (Preuss *et al*., 2001; Ott *et al*., 2006). Mutants lacking both Mba1 and the CTD of Oxa1 show severe defects in the assembly of the respiratory chain (Ott *et al*., 2006). Similar to the observation that C-terminal ribosome binding domains on YidC can partially but significantly substitute an SRP-mediated targeting pathway in *E. coli*, Funes *et al.* (2013) showed that *E. coli* Ffh binds to the large subunit of mitochondrial ribosomes and could relieve, to some degree, the defect during double-depletion of the Mba1 ribosome receptor and the C-terminal ribosome-binding domain of Oxa1. Since yeast Mrp20, the homolog of L23 in bacterial ribosomes that is critical for the contact to Ffh, was identified as an interaction partner of Oxa1 (Jia *et al*., 2009) it is conceivable that Oxa1 and Ffh employ similar ribosomal binding sites that are in direct proximity to the

polypeptide exit tunnel. As Funes and co-workers were unable to detect direct contacts between Ffh and FtsY during their rescue experiments expressing the bacterial SRP components in mitochondria, it is assumed that prokaryotic Ffh and FtsY are not able to form a complex in mitochondria, presumably due to the absence of the functionally important 4.5S RNA (1.2.1). Therefore, it is suggested that expression of Ffh in mutant mitochondria lacking Mba1 and the Oxa1 C-tail, might reduce the risk of newly synthesized proteins aggregating irreversibly and increase the time window during which nascent chains can be productively integrated into the inner membrane (Funes *et al*., 2013). This conclusion is in good agreement with the observation that in Ffh-depleted *E. coli* cells MscL aggregated predominantly at the membrane, for the most part unaffected by the introduction of an additional ribosome-binding domain in YidC (Fig. 3.26 B and D). Yet, in presence of Ffh, but under FtsY depletion, the targeting defect was rescued by the YidC C-terminal ribosome-binding domain for targeting (Fig. 3.27 C) and insertion (Fig. 3.25) of MscL. This underlines the importance of a chaperone-like function of the free, cytosolic SRP in addition to its targeting function in cooperation with its receptor FtsY.

Another important evidence for the specialized co-translational functions of particular members of the YidC/Oxa1/Alb3 family is that the development of C-terminal ribosome binding domains does not only occur in mitochondria, but also during evolution in different prokaryotic systems. In Gram-positive bacteria usually two YidC homologs coexist. The oral pathogen *Streptococcus mutans* for example, possesses one homolog with a ribosome-binding domain (YidC2) while the other one lacks it (Funes *et al*., 2009). Both paralogs have certain overlapping functions (Hasona *et al*., 2005; Funes *et al*., 2009), but also reveal strong differences conferred by the presence or absence of the C-terminal domain (Palmer *et al*., 2012). Interestingly, the phenotype of the deletion of YidC2 in this organism is strikingly similar to that of SRP pathway mutants, including stress-sensitivity and diminished genetic competence. Deletion of SRP is tolerated when YidC2 is present, while double mutants lacking both YidC2 and SRP components are not viable, even in the absence of environmental stressors. This suggests that YidC2 overlaps functionally with the SRP pathway and supports a co-translational membrane insertion pathway that does not rely on the SRP only (Hasona *et al*., 2005). Furthermore, it was shown that YidC2 expressed in yeast binds to mitochondrial ribosomes and promotes co-translational integration of proteins into the inner mitochondrial membrane in the absence of Oxa1. Reciprocally YidC2 can be functionally replaced by Oxa1 in *S. mutans* (Funes *et al*., 2009). Interestingly, *E. coli* YidC was not able to complement Oxa1 until the C-terminal tail of YidC2 had been appended to it.

The studies employed in mitochondria provide detailed, yet specialized knowledge for a system that lacks an SRP pathway, whereas my *in vivo* studies in *E. coli* gave new insights also on the molecular level on how C-terminal ribosome binding domains in general can assist co-translational protein insertion in an organism in which the SRP components are essential for viability. Depletion of the essential SRP components in *E. coli* bears drastic physiological consequences for a wide range of synthesized proteins, especially for the SRP-mediated insertion/translocation of proteins via the SecYEG translocase. Since targeting of by far the most inner membrane proteins to the Sec-translocase is mediated by the SRP pathway, it was not surprising that the C-terminally elongated YidC proteins were only able to compensate partially for the loss of the SRP components in *E. coli* cells. To evade this complexity the assays in this study were focused on the targeting and insertion of the MscL protein, a native SRP-dependent, but SecYEG-independent YidC substrate in *E. coli.*

Based on the current structural (4.3 and 4.4) and biochemical (4.1, 4.2 and 4.5) data a combined targeting and insertion model of YidC-substrates (e.g. MscL) is proposed involving the SRP, the nascent ribosome and the C-terminally extended YidC making the SRP-receptor FtsY dispensable (Fig. 4.3). For the initial step it is assumed that the nascent chain is recognized by SRP, either on free cytosolic RNCs **(1a)** or on membrane-associated ribosomes **(1b)**. Possibly, a stable association of a certain pool of ribosomes at the membrane, irrespective of their translational state, is mediated by the C-terminally extended YidC due to additional contacts of its C-terminal ribosome binding domain and the flexible binding platform at the ribosomal exit tunnel (H59, L24 and L29). For both initial stages **(1ab)**, the ribosomal protein L23 offers a transient binding site for the N-domain of SRP while the M-domain binds the emerging nascent chain, preventing the aggregation or misfolding of the growing polypeptide. The binding of SRP to an RNC with a proper SRP signal sequence repositions the NG domain and thereby clears the ribosomal protein L29 (Estrozi *et al*., 2011). This then allows an enhanced YidC:RNC interaction probably due to the expanded contact-interface of the C-terminally extended YidC domain to L29. As a result the proper positioning of the RNC onto the YidC insertase is promoted and SRP can be displaced from the RNC:insertase complex **(2)**. Finally, the nascent chain is directly and co-translationally inserted by YidC-Rb into the inner membrane of *E. coli* **(3)**, alike it is proposed for the SRP-FtsY pathway for Sec-independent YidC-substrates such as MscL.

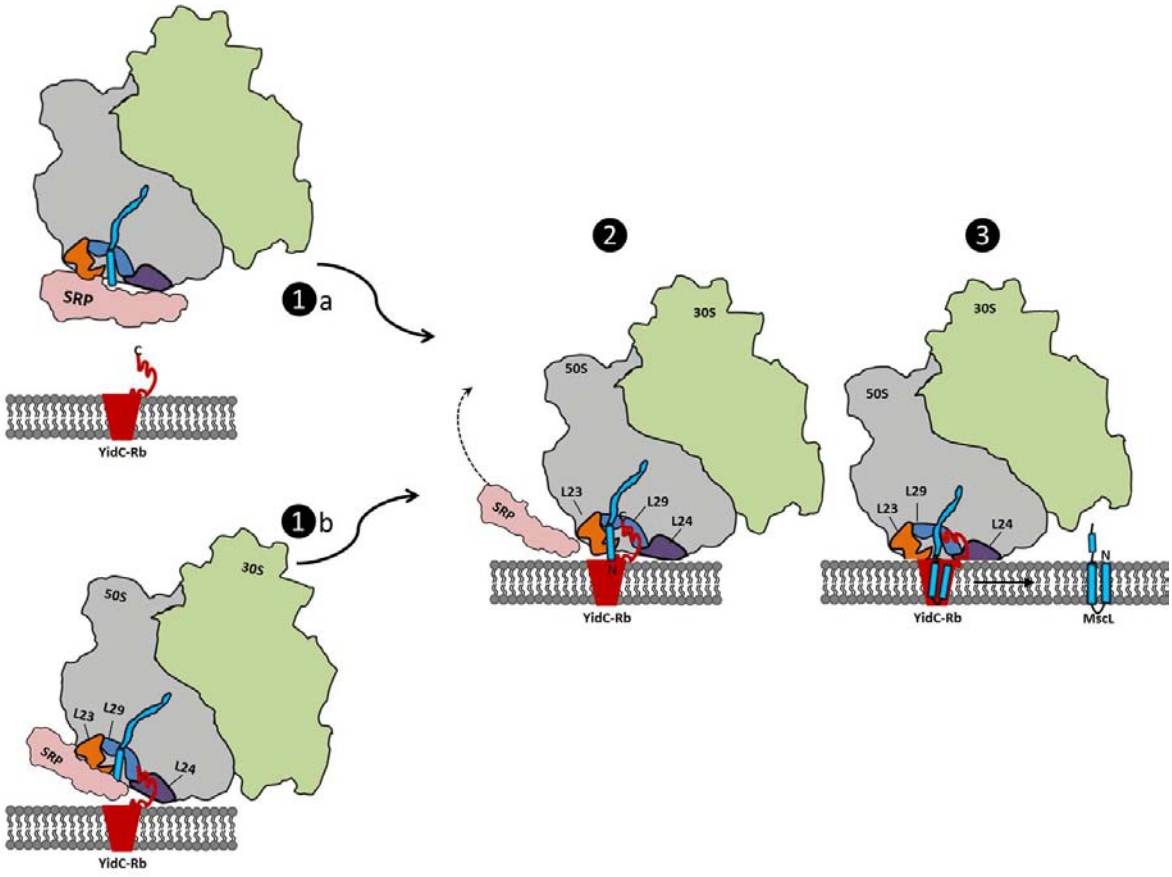

Fig. 4.3 ***Cartoon model of co-translational targeting and insertion via a C-terminally elongated YidC in the absence of the SRP-receptor FtsY.*** *SRP (light pink) binds to cytosolic (1a) or membrane-associated (1b) RNCs and prevents aggregation and misfolding of the nascent chain (MscL-moiety: turquois). (2) The ribosomal complex is positioned onto the membrane located YidC-Rb insertase (red) by its C-terminal extension due to the interaction with L29 (blue) and SRP is probably displaced from the ribosome. (3) This results in a co-translational membrane insertion of MscL through YidC-Rb.*

Further studies are required to explicitly analyze a possible tripartite complex of RNC:SRP:YidC-Rb and also to dissect at which stage SRP is displaced from the ribosome. It also would be interesting to analyze if YidC insertases with an extended C-terminal tail in prokaryotes are predominantly occupied by ribosomes, similar to their mitochondrial homologs, or if the transfer of the RNC to the YidC insertase occurs mainly co-translationally from free cytosolic ribosomes in cooperation with other components, such as SRP.

4.6 Evolutionary aspects of the accessory YidC domains

The combination of a conserved membrane-spanning core domain with subtype-specific flanking regions makes the YidC/Oxa1/Alb3 protein family an interesting example to study the evolution of membrane proteins (Fig. 1.12; Yen *et al*., 2001; Funes *et al*., 2009; Zhang

et al., 2009). Phylogenetic tree analysis reveal three separate clades corresponding to mitochondrial Oxa proteins, bacterial YidC proteins including chloroplast Alb3 family members, and the more distantly related archaeal DUF106 proteins (Borowska et al., 2015), respectively. These clades are further divided into several subbranches: YidC/YidC1/SpoIIIJ and YidC2/YqjG in bacteria, Oxa1 and Cox18/Oxa2 in mitochondria, Alb3 and Alb4 in plastids (Funes *et al*., 2011) and the highly divergent archaeal DUF106 proteins (Borowska *et al*., 2015). These subbranches presumably represent monophyletic subgroups of common ancestry and it is suggested that the different subgroups have been evolutionarily developed through three independent gene duplication events that occurred in Gram-positive bacteria, mitochondria and chloroplasts coincidently. Specialization then shaped the different subgroups and allowed the diverse insertase variants to acquire specific flanking regions, individual functional properties and their particular substrate specificities (Funes *et al*., 2009).

Among eubacteria, there is a clear structural and topological distinction between Gram-negative and Gram-positive YidC homologs. The Gram-positives have only 5 TM domains, similar to the organellar homologs and all the bacteria with two YidC homologs genes are generally Gram-positive bacteria. However not every Gram-positive bacterial species possesses two YidC genes (Zhang *et al*., 2009). There are some *Streptomyces* and *Frankia* genera where only one YidC gene is found on the genomes (Zhang *et al.*, 2009). The YidC homologs within the group of the Gram-negative bacteria are easily recognized by the additional N-terminal TM domain and a large periplasmic loop P1 connecting TM1 and TM2. Thus, only these YidC proteins feature six transmembrane segments. The P1 domain varies in size from 232 residues in *Thermotoga maritima* to 500 in *Rhodopirellula baltica*. Intriguingly, the C-terminal regions of many marine Gram-negative bacteria are extended and show unique similarities to the C-terminal region of Oxa1 (Kiefer and Kuhn, 2007). One important question that arose during this work is why solely the marine prokaryotes, among them the model organisms of this thesis, *R. baltica* and *O. alexandrii,* exhibit C-terminal extensions on their YidC homologs in contrast to all the other Gram-negative bacteria. *R. baltica* and *O. alexandrii* both have homologous Ffh and FtsY genes on their chromosome, which most likely operate in a similar mode as the *E. coli* SRP components. However, particularly in the A-domain of the marine SRP receptor protein, there are some striking differences, compared to the *E. coli* homolog. Sequence alignments reveal that in contrast to the strongly conserved N and G domains of FtsY (Fig. 4.4 B), the A domain is poorly conserved (Pohlschröder *et al*., 2004). Moreover, several bacterial and archaeal FtsY homologs lack an A domain (Egea *et al*., 2004; Eitan and Bibi 2004; Focia *et al*., 2004). For the FtsY protein of *Haloferax volcanii*,

the N-terminal A-domain, a typically prokaryotic feature of the SRP receptor homolog, is namely present in this archaeon, but is not essential for growth (Haddad *et al*., 2005). In *E. coli*, two conserved helical stretches were identified which are proposed to constitute the lipid-binding sites of FtsY. One is located in the very N-terminal segment of the A-domain (aa 1-14) (Weiche *et al*., 2008), and a second one near the N-terminal end of the conserved N-domain of FtsY (aa 195-207), which has been shown to form an amphipathic helix (Fig. 4.4 A) (Parlitz *et al*., 2007).

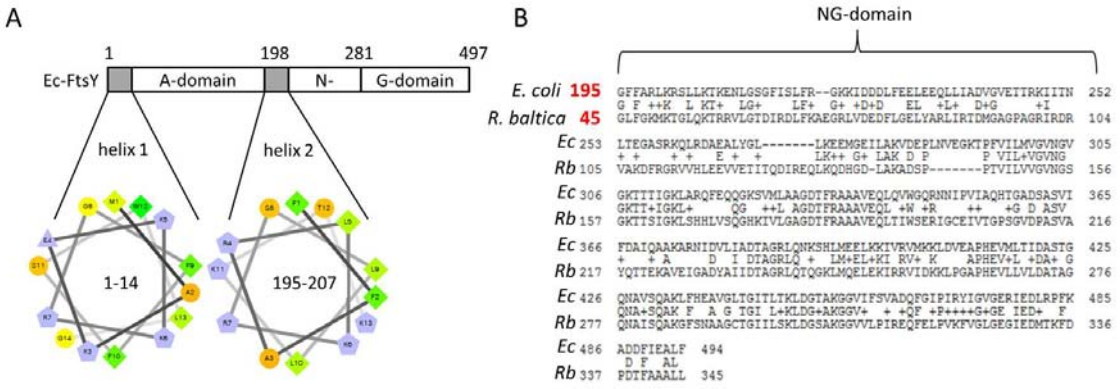

Fig. 4.4 ***Comparison of Gram-negative FtsY homologs. (A)*** *Domain structure of E. coli FtsY. The two conserved helices are indicated by their amino acid position (1-14; 195-207). Helical wheel representation shows a typically amphipathic conformation for helix 2. Residues are color coded like in Fig. 4.2.* ***(B)*** *Sequence alignment of the NG domains of the FtsY homologs from E. coli and R. baltica shows a moderate conservation, while the N-terminal A-domain of R. baltica is strikingly truncated (aa 1-45 in Rb-FtsY; aa 1-195 in Ec-FtsY).*

Both helices together allow FtsY to execute an exceptionally stable interaction with the membrane (Braig *et al*., 2009). Additionally, the first-14-amino acid residues comprising region of the A-domain was shown to stabilizes the FtsY:SecYEG interaction. It has a highly positive net charge, compared to the remainder of the acidic A-domain (Weiche *et al*., 2008). Interestingly, sequence comparison of *E. coli* FtsY (Ec-FtsY) with the *R. baltica* homolog revealed an identity score of 43 % for their NG-domains, but the sequence alignment also revealed that the NG-domain of *R. baltica* FtsY (Rb-FtsY) already starts at amino acid position 45, compared to the nearly 200 amino acid residues long A domains of Ec-FtsY (Fig. 4.4 B) or the *H. volcanii* archaeal homolog. Secondary structure prediction of the first 45 amino acid residues of Rb-FtsY revealed a coil-conformation without exhibition of helical features. Conclusively, the A-domain of Rb-FtsY is either very small, operating without helical motifs or even is basically nonexistent.

Due to the fact that the C-terminal ribosome binding domain of the *R. baltica* YidC homolog (Rb-YidC) fused to Ec-YidC can mediate the co-translational insertion of an inner membrane YidC substrate protein even in the absence of FtsY (Fig. 4.3) and the Rb-FtsY seems to be an N-terminally truncated version of the SRP receptor, I hypothesize that the accessory C-terminal YidC domain of Rb-YidC possibly fulfills similar functions in the marine prokaryote as does the FtsY A domain during co-translation protein biogenesis in other organisms. Particularly, the local targeting and arrangement of RNCs at the membrane and the subsequent selective delivery of the nascent chain to the respective translocation or insertion machineries. This may be promoted and quality-controlled by involving either the A-domain or alternatively the C-terminal YidC domains in marine bacteria. Interestingly, *in vitro* experiments suggested that the A-domain of FtsY may also be involved in recruiting the SRP to the haloarchaeal cytoplasmic membrane (Lichi *et al*., 2004). This is also in accordance with the observation that SRP apparently plays an important role during the co-translational membrane insertion of MscL via the C-terminally extended YidC in the absence of FtsY (Fig. 4.3), underlining the functional similarities of the FtsY A domain and the C-terminally extended YidC domain. The marine planctomycete *Rhodopirellula* shows some unique features concerning the overall nature of its proteins and particularly its membrane proteins (Kiefer and Kuhn, 2007). The extraordinary features of exhibiting intracellular organelle-like compartments with sterol ladderane lipids like e.g. the anammoxosomes and the strikingly complex and huge membrane proteins puts the planctomycetes more close to eukaryotes as any other group of bacteria. Especially the anammoxosomes are suggested to be functional and structural homologs to mitochondria (Fuerst and Sagulenko, 2011). If the C-terminally elongated YidC of marine bacteria has a higher affinity to ribosomes, more ribosomes should be firmly bound to the membrane surface. This could be an advantage for cells that synthesize a large number of hydrophobic membrane proteins, similar to the specialized translation and insertion machineries in mitochondria. Marine prokaryotic organisms are, in many cases, unique in their genomic organization (Serres *et al*., 2009). Particularly in the planctomycete group, several gene duplications and protein motifs are found that only have counterparts in the archaeal or eukaryotic phyla (Studholme *et al*., 2004). Thus, the C-terminally extended tail of YidC in marine bacteria may be an ancestral remnant of a primordial translocation system operating without a SRP receptor or a truncated, minimal version of it. Later in evolution this system might have shifted to the mitochondria. Possibly, the phylogenetically ancient function of the SRP was mainly chaperone-like rather than having a targeting function. The targeting function may first have been acquired by an ancestral YidC protein with an extended C-terminal tail mediating membrane binding of ribosome-associated substrates. Later on in evolution the SRP

receptor became more efficient in membrane targeting and thus also allowed interaction with the Sec translocase. At this evolutionary stage, the C-terminal extensions of the YidC proteins were dispensable. Above all, marine bacterial groups may be a key to understanding how complex cellular processes like membrane targeting and protein translocation may have evolved and spread over the whole organismic world.

4.7 Deciphering the SRP signal sequence of KdpD

The aim of the second part of this study was to determine the specificity of SRP recognition in substrate proteins. In *E. coli*, the ribonucleoprotein SRP is essential for cell viability (Phillips and Silhavy, 1992) and comprises a single protein, Ffh, bound to the 4.5S RNA (Poritz *et al*., 1990; Ribes *et al*., 1990). During protein synthesis, the SRP binds to a hydrophobic signal sequence of the emerging polypeptide at the ribosomal exit tunnel of RNCs and targets the whole ribosome-associated complex in a GTP-dependent process to the inner membrane (de Gier *et al.*, 1996; Ulbrandt *et al*., 1997). Two functional domains in SRP contribute to this activity: the NG domain of the Ffh protein, containing a Ras-like GTPase motif (Freymann *et al*., 1997), and the 4.5S RNA-Ffh M domain complex, which is responsible for signal sequence recognition (Zopf *et al*., 1990).

In earlier studies of our group the SRP-dependent membrane targeting of the sensor protein KdpD of *E. coli* was analyzed. KdpD had been shown to insert into the inner membrane independently both of Sec and YidC (Facey and Kuhn, 2003; Rothenbücher *et al*., 2006; Maier *et al*., 2008). The four-spanning membrane topology of KdpD provides an interesting aspect of signal sequence recognition by SRP. As in *E. coli* nearly all inner membrane proteins contain an N-terminal uncleaved signal sequence, the region that interacts with SRP is most likely the first transmembrane region, ensuring that early after the translation start, SRP mediates the co-translational targeting to the membrane. However, this is not possible for KdpD, since the protein encompasses a huge N-terminal hydrophilic region of 400 amino acid residues (Fig. 3.28 A) and recognition of a signal sequence in the first TM domain following that long hydrophilic region would prevent an early membrane targeting of the protein. Maier *et al*. (2008) identified via GFP-localization studies of N-terminal KdpD-GFP fusion proteins, a minimal peptide of residues 22-48 (N22-48) that is required to target KdpD to the membrane. This peptide contains three positively charged residues at its very N-terminus (aa 22-26), a stretch of 10 hydrophobic residues (aa 27-36), followed by a lysine residue and then another 6 hydrophobic residues (aa 38-43) and accessorily a predicted Walker A motif (aa 30-38) (Fig. 3.28 B). A crucial question is how the KdpD signal sequence is recognized by SRP as no obvious

consensus motifs are known for this interaction. SRP-dependent N-terminal signal sequences are highly diverse in their amino-acid composition and length, but they all contain a core of at least eight consecutive hydrophobic amino acid residues that act as the major determinant for recognition by SRP (Valent *et al*., 1997 & 1998; Martoglio and Dobberstein 1998; Hegde and Bernstein 2006, Janda *et al*., 2010). In addition, the N-terminal tail of a signal sequence typically contains positively charged residues with yet unknown function, suggesting a combination of hydrophobic interactions and electrostatic contacts during recognition and binding of SRP to signal sequences. Optionally, the positively charged residues may also interact with the negatively charged head groups of the membrane phospholipids.

To investigate the involvement of the positively charged residues and the Walker A motif in binding of SRP to the signal sequence, the binding affinities of the wild type KdpD N22-48 fragment and the mutant peptides 3Q (reduced net charge from +5 to +2) as well as the W3A mutant signal sequence (destroyed Walker A motif) to *E. coli* SRP were determined via microscale thermophoresis (MST) (2.17). I established purification (2.10.3) and labeling (2.17.1) protocols for the Ffh protein and stably reconstituted SRP (2.17.2) by the addition of *in vitro* synthesized 4.5S RNA (2.6.12). To ensure a properly reconstituted SRP under the assay conditions, MST measurements were performed to analyze the correct binding of labeled Ffh to the synthesized 4.5S RNA. A dissociation constant (K_d) of ~ 0.56 nM was determined for the Ffh:4.5S RNA holo SRP assembly (Fig. 3.35), which is in good agreement with the values cited in the relevant literature. Published data for the *in vitro* SRP assembly ranges from K_d values of 7 pM (Siu *et al*., 2007) to 3 nM (Jagath *et al*., 2001), depending on the method and on buffer components (Batey and Doudna, 2002; Jecklin *et al*., 2009). Thus, the reconstituted SRP here is highly suitable for the projected binding studies with the variant KdpD SRP signal sequence peptides. As expected, the wild type KdpD peptide N22-48 revealed the highest affinity to SRP with calculated K_d of ~ 500 nM, while the signal sequence mutants 3Q and W3A showed two-fold and 10-fold reduced binding affinities to SRP (Fig. 3.37), respectively. To ensure that the measured binding affinities truly represent specific binding of the signal sequence peptides to the 4.5S RNA-Ffh M domain complex, the interaction of the wild type N22-48 peptide with labeled Ffh protein, without the 4.5S RNA, was tested. When using this RNA-free SRP the calculated K_d raised from ~ 0,5 µM to more than 17 µM. This demonstrates the importance of using a functional, fully assembled SRP and hence strongly suggests the specificity of the SRP-substrate recognition in these *in vitro* MST-measurements.

In general, it is obviously very difficult to estimate a universally valid affinity of SRP to signal sequences since several previous studies already revealed contradictory results of

this highly dynamic process. Nearly all of the studies investigating the SRP:substrate interaction, were performed with ribosome nascent chain complexes. This is due to the physiological significance of the ribosome during substrate recognition of SRP. On the other hand, this bears difficulties concerning the translationally stalled state of the RNCs and especially the influence of the nascent chain length is discussed controversially (Flanagan *et al*., 2003; Bornemann *et al*., 2008; Holtkamp *et al*., 2012; Noriega *et al*., 2014-1) compared to SRP binding to actively translating ribosomes (Noriega *et al*., 2014-2). Considerably influenced by the applied method, binding affinities of SRP to RNCs displaying hydrophobic signal sequences range from 0,1 nM – 10 nM (Flanagan *et al*., 2003; Bornemann *et al*., 2008; Zhang *et al*., 2010; Saraogi *et al*., 2011; Holtkamp *et al*., 2012; Noriega *et al*., 2014-1), in all cases indicating a very tight binding. Interestingly, SRP still binds to vacant, non-translating ribosomes with a K_d around 50 nM, while over long nascent chains, especially from SRP-independent proteins, weaken the binding affinity of SRP to the RNCs down to a K_d value of > 200 nM (Bornemann *et al.,* 2008). Since I did not use RNCs in the MST measurements but instead analyzed the direct SRP:signal sequence interaction with isolated components, it was expected that the binding affinities were lower due to the absence of the stabilizing SRP binding sites on the ribosome. Indeed, the MST-data are in good agreement to the calculated binding affinity of ~ 1,5 µM of an isolated ΔEspP signal peptide to SRP, measured by fluorescence anisotropy (Bradshaw *et al*., 2009). These observed binding affinities are likely due to multiple hydrophobic interactions between the SRP M domain and the signal sequence (Janda *et al*., 2010), but they cannot account for the high affinity of SRP to RNCs by only adding the SRP:signal sequence interactions to the SRP:ribosome interaction. This suggests that the tight binding of SRP to RNCs displaying a proper signal sequence is mainly caused by the conformational changes of SRP upon binding to a nascent chain (Hainzl *et al*., 2011), changing the interaction mode of SRP on the ribosome (Estrozi *et al*., 2011). These structural changes of SRP seems to be an important feature of SRP:substrate discrimination, since it is supposed that SRP also binds to RNCs displaying an incorrect cargo with moderate K_d values of around 13 nM, but resulting in an falsely assembled SRP:FtsY targeting complex (von Loeffelholz *et al*., 2013). However, whether these observations represents the native mechanisms *in vivo* remains still unclear since recent interaction studies with actively translating ribosomes and dynamic single-molecule measurements at physiologically relevant substrate concentrations showed that SRP only engages translating RNCs that expose a functional signal sequence (Noriega *et al*., 2014-2). Further studies will be necessary to answer the question how a limited, sub-stoichiometric pool of cellular SRP (~ 400 nM in *E. coli,*

compared to 40 – 50 µM ribosomes) effectively distinguishes RNCs that display a proper signal sequence from those that do not.

Surprisingly, the measurements of the SRP interaction with isolated signal sequence peptides in this work revealed striking differences in the binding affinities of the wild type sequence compared to both, only slightly changed, mutant peptides. Substitution of the three positively charged amino acid residues in the N-terminal part of the signal peptide with glutamine residues in the 3Q mutant decreased the binding affinity for SRP two-fold. Initially, it had been proposed that the SRP 4.5S RNA interacts with the positively charged residues in the N-region of a signal peptide via electrostatic interactions (Batey *et al*., 2000; Wild *et al*., 2004), but crystal structures of SRP and cryo-EM structures of SRP:RNC complexes elucidated that the N-region is presumably too far away from the SRP RNA to make direct contacts (Janda *et al*., 2010). The positively charged residues in the N-region of the signal sequences may be conserved for other reasons, for example for its interaction with the phospholipid head groups of the membrane lipids during protein translocation (van den Berg *et al*., 2004). This is also consistent with preliminary results of localization studies with GFP fused to the KdpD-peptides, analyzed by fluorescence microscopy (data not shown). It was observed that the 3Q:GFP construct, although the isolated peptide showed direct interaction with SRP *in vitro* in the MST measurements, was distributed mainly in patches over the whole cell *in vivo*, probably due to a reduced interaction ability with the membrane. In contrast, the N22-48 (wild type) and W3A peptides fused to GFP were localized mainly at the inner membrane of *E. coli*. This also demonstrates that, although a 10-fold higher K_d for SRP:W3A interaction was observed *in vitro*, SRP efficiently targets the W3A:GFP fusion to the membrane *in vivo*, emphasizing the difficulty of direct conclusions from SRP:signal sequence affinities to proper targeting via SRP. For instance, there is no conclusive explanation for the strongly reduced binding affinity of the W3A mutant to SRP in the MST measurements, although *in vivo* studies showed that single point mutants that slightly change the hydrophobicity of the core region profoundly affect SRP recognition, while an altered charge in the N-region only has weak influence (Lee and Bernstein, 2001; Peterson *et al*., 2003). Since the grand average of hydropathicity (GRAVY) actually showed a slightly increased hydrophobicity of the W3A mutant (0,3 N22-48; 0,36 3Q; 0,54 W3A), in which three glycine residues were substituted for alanine residues, hydrophobicity alone could not account for the different binding affinities. One possible explanation could be that the destroyed Walker A motif in this mutant causes an altered conformation of the peptide, which is then disadvantaged in the direct interaction with the hydrophobic groove of the signal sequence binding cavity of SRP. It is proposed that the exclusion of the N- and C-terminal regions of the signal

sequence from the hydrophobic groove likewise restricts the longitudinal position of the signal peptide with respect to the groove (Janda *et al*., 2010). Secondary structure prediction of the three KdpD-signal sequence peptides confirm a presumable structural change of the signal sequence conformation due to the substitution of the three glycine residues in the W3A mutant, compared to the wild type N22-48 and 3Q peptides (Fig. 4.5).

Fig. 4.5 ***Secondary structure prediction of the KdpD-signal sequence peptides.*** *The wild type peptide N22-48 and the 3Q mutant show the same predicted conformation, while the structure prediction of W3A shows an enhanced tendency for helix formation (purple boxes). Yellow boxes indicate sheet formation. Structure prediction was performed by the PSIRED server.*

Therefore, it can be assumed that the alterations in the helical stretch of the hydrophobic core region of the signal sequence in W3A mainly causes the low binding affinity to SRP in the *in vitro* MST assays, which is in agreement with the observation that hydrophobicity may not be the sole factor for SRP recognition (Huber *et al*., 2005). Taken together, my results confirm that the SRP recognition sequence of KdpD encompasses the amino acid residues 22-48 at the very N-terminal tail of the large cytoplasmic domain of KdpD since a direct interaction of the isolated peptide with purified SRP was demonstrated via MST. A direct influence of the amino acid composition in the signal peptide on its SRP binding affinity *in vitro* was also shown, thereby confirming a minor influence of an altered charge in the N-terminal region while mutations in the hydrophobic core region cause strongly reduced binding affinities. These, however, probably are not due to the changed hydrophobicity but conformational changes in the helical region. However, more detailed analyses of additional signal sequence mutants and their SRP affinity, in combination with *in vivo* localization studies are required to understand the importance of particular amino acid residues and their position within the sequence.

SUMMARY

Members of the YidC/Oxa1/Alb3 protein family catalyze the insertion of integral membrane proteins into the lipid bilayer of the bacterial plasma membrane (YidC), the inner mitochondrial membrane (Oxa1), and the chloroplast thylakoid membrane (Alb3) (Saller *et al*., 2012; Dalbey *et al*., 2014). The insertase homologs are comprised of a conserved core region of 5 transmembrane domains, but are provided with additionally flanking N- and C-terminal regions of variable lengths and functions. The Gram-negative YidC is characterized by an additional N-terminal domain, while Gram-positive bacteria, mitochondria and plastids developed C-terminally extended insertase-domains. These domains are involved e.g. in direct interaction with ribosomes and facilitate a functional overlap with the co-translational SRP-targeting pathway. An extended C-terminal highly positively charged tail region was also found in the YidC homologs of the Gram-negative marine bacteria *Rhodopirellula baltica* and *Oceanicaulis alexandrii*, but not in *Escherichia coli.*

The primary subject of this work was to characterize and analyze in detail the C-terminally extended YidC chimera, composed of the *E. coli* YidC and the C-terminally extended domains of the marine YidC homologs. Biochemical binding assays with the purified YidC proteins and isolated, vacant *E. coli* 70S ribosomes showed that the C-tails mediate specific binding to ribosomes independently of the translational state of the ribosome. Furthermore, a ribosome-bound insertase complex was visualized by cryo-electron microscopy. The enhanced affinity of the C-terminally extended YidC was used to isolate stable complexes with stalled ribosomes, carrying a nascent polypeptide chain of a YidC substrate protein (MscL). The cryo-EM structure of a YidC-ribosome nascent chain complex (RNC) was solved to a 8,6 Å resolution and allowed the visualization of the nascent chain from the peptidyl transferase center through the ribosomal exit tunnel into the YidC density. The structure revealed the helix H59 of the 23S rRNA and the two ribosomal proteins L24 and L29 as the major contacts sites of YidC at the ribosomal tunnel exit. Pull down assays confirmed a significantly interaction of the C-terminal ribosome binding domain and the ribosomal protein L29, while L24 seems to be a universal contact site for the YidC-insertase core domain. Strikingly, the cryo-EM structure clearly showed a single monomer of YidC bound to the translating ribosome. This suggests that monomeric YidC might be the minimal functional unit for YidC-dependent, co-translational insertion of inner membrane proteins.

In addition to the *in vitro* tests, a possible role of the C-terminal YidC extensions in co-translational protein targeting was tested *in vivo* in *E. coli*. For that purpose the targeting and localization of the SRP-dependent YidC-substrate protein MscL (Facey *et al.,* 2007) was investigated as a GFP fusion protein via fluorescence microscopy. In addition, the proper membrane insertion of MscL was analyzed in radioactive pulse chase experiments via AMS gel shift assays, either in the absence of a functional SRP or SRP receptor (FtsY). Both *in vivo* assays clearly showed that the C-terminal ribosome binding domain of the *R. baltica* YidC homolog can partially substitute for the SRP receptor function in *E. coli*, while the cytosolic signal recognition particle is still required for correct insertion of the MscL protein. Therefore, a new co-translational targeting and insertion model of YidC-only substrates was proposed. This model includes the binding of SRP to the ribosome nascent chain complex (RNC), preventing the aggregation and misfolding of the polypeptide chain. Together with the C-terminal ribosome binding domain that stably positions the RNC:SRP complex on the YidC insertase due to the interaction with the ribosomal protein L29, the SRP-receptor became dispensable. This works also highlights evolutionary aspects of the accessory YidC domains and indicates that the C-terminal extended tail of YidC in the planctomycete group may be an ancestral remnant of a primordial translocation system operating without a typical SRP receptor.

The second part focuses on the interaction of the signal recognition particle with SRP signal sequences. Isolated mutant signal sequence peptides were used to determine the specificity of SRP recognition in proteins. The interaction studies were established in an *in vitro* system and binding affinities of purified SRP to the isolated signal sequence peptides were determined via microscale thermophoresis (MST). A short sequence of 27 amino acid residues at the very N-terminal tail of the large cytoplasmic domain of KdpD was identified as a SRP signal sequence. Furthermore, a direct influence of the amino acid composition in the signal peptide on its SRP binding affinity *in vitro* was demonstrated. This confirms a low influence of an altered charge in the N-terminal region while mutations in the hydrophobic core region causes significantly reduced binding affinities to SRP.

Taken together, this study contributes to the understanding of the molecular mechanisms of co-translational membrane protein biogenesis in bacteria.

ZUSAMMENFASSUNG

Proteine aus der YidC/Oxa1/Alb3-Famile vermitteln die direkte Insertion von integralen Membranproteinen in den Lipid-Bilayer der bakteriellen Plasmamembran (YidC), in die innere Mitochondrien-Matrix (Oxa1) und in die Thylakoidmembran von Chloroplasten (Alb3) (Saller *et al*., 2012; Dalbey *et al*., 2014). Die Homologe dieser Insertase-Familie besitzen eine konservierte Kernregion aus 5 Transmembrandomänen und zusätzliche N- und C-terminale Regionen, die sich in ihrer Länge und Funktion stark voneinander unterscheiden. Charakteristisch für das YidC aus Gram-negativen Bakterien ist eine zusätzliche N-terminale Transmembrandomäne, während Mitochondrien und Plastide C-terminal verlängerte, hydrophile Domänen an ihren Insertasen besitzen. Diese C-terminalen Domänen sind zum Beispiel an der direkten Bindung von Ribosomen beteiligt und verleihen der Insertase co-translationale Funktionen die sich mit dem SRP-Targetingmechanismus überschneiden. Im Gegensatz zur YidC-Insertase aus *E. coli*, besitzen die Gram-negativen, marinen Bakterien *Rhodopirellula baltica* und *Oceanicaulis alexandrii* YidC Homologe mit C-terminal erweiterten, positiv geladenen, hydrophilen Domänen.

Ziel dieser Arbeit war die detaillierte Charakterisierung und Analyse von C-terminal erweiterten YidC-Chimären. Die YidC-Chimären bestehen aus Fusionen des *E. coli* YidC Proteins und den C-terminalen Domänen der marinen YidC Homologe. Biochemische Bindungsstudien mit den gereinigten YidC-Proteinen und isolierten *E. coli* 70S Ribosomen zeigten, dass die C-terminalen Domänen eine spezifische Bindung an die Ribosomen vermitteln. Ähnlich zu der essentiellen Funktion der C-terminalen Domäne von Oxa1 war die Ribosomenbindung der YidC-Chimären unabhängig von einer translatierten Polypeptidkette am Ribosom. Des Weiteren, wurde ein Komplex aus naszierendem Ribosom (RNC) und gebundener YidC-Chimäre mittels Kryo-Elektronenmikroskopie auf 8,6 Å gelöst. In der Struktur konnte man den Weg der wachsenden Polypeptidkette vom Peptidyltransferase-Zentrum, durch den Ausgangstunnel des Ribosoms bis hinein in das YidC Protein verfolgen. Mit Hilfe der Kryo-EM Struktur wurde die Helix H59 der 23S rRNA und die beiden ribosomalen Proteine L24 und L29 als Hauptkontakte des YidCs am Ribosom identifiziert. Durch Pull-Down Versuche konnte eine signifikante Interaktion der C-terminalen Domäne mit L29 gezeigt werden, wohingegen L24 vermutlich eine Interaktion mit der YidC-Kerndomäne eingeht. Außerdem lieferte die Struktur des YidC:RNC Komplexes den Beweis, dass ein einzelnes YidC-Molekül an translatierende Ribosomen bindet und somit vermutlich die minimalste, funktionelle Einheit für die YidC-abhängige, co-translationale Insertion von Membranproteinen darstellt.

Um die *in vivo*-Funktion der C-terminalen YidC Domänen während des co-translationalen Targetings in *E. coli* zu untersuchen, wurde das Membrantargeting des SRP-abhängigen YidC-Substratproteins MscL (Facey *et al.,* 2007) als GFP-Fusionsprotein mittels Fluoreszenzmikroskopie untersucht. Parallel dazu wurde die korrekte Membraninsertion von MscL über eine AMS-Modifizierung in radioaktiven pulse-chase Experimenten analysiert. Beide *in vivo* Untersuchungen zeigten, dass die C-terminale Ribosomenbindedomäne des *R. baltica* YidC Homologs zu einem gewissen Teil die Funktion des SRP-Rezeptors in *E. coli* übernehmen kann. Dabei wird jedoch SRP weiterhin für die korrekte Insertion von MscL benötigt. Aufgrund der Erkenntnisse dieser Arbeit kann ein neues Modell der co-translationalen Insertion von YidC-abhängigen Proteinen, wie z.B. MscL, postuliert werden. Daran beteiligt ist das SRP, welches durch die Bindung an RNC-Komplexe die Aggregation und Missfaltung der Polypeptidkette verhindert. Zusammen mit der C-terminalen Ribosomenbindedomäne, kann in Abwesenheit des SRP-Rezeptors der RNC:SRP-Komplex an der YidC-Insertase durch die Interaktion mit dem ribosomalen Protein L29 positioniert und stabilisiert werden. In dieser Arbeit werden ebenfalls evolutionäre Aspekte der akzessorischen YidC-Domänen behandelt, die darauf schließen lassen, dass die C-terminale YidC-Domäne in der Gruppe der Planktomyceten eine Art Überbleibsel eines Vorfahren mit primitivem Translokationssystem ohne klassischem SRP-Rezeptor ist.

Der zweite Teil dieser Arbeit behandelt die Interaktion des Signal-Erkennungs-Partikel (SRP) mit SRP-Signalsequenzen. Um die Spezifität der SRP-Erkennung von Proteinen zu bestimmen wurden isolierte Peptide mit verschiedenen Signalsequenzmutationen verwendet. Die Bindungsaffinitäten der *in vitro* Interaktionsstudien von SRP und den Signalsequenz-peptiden wurden mittels Microscale Thermophorese (MST) bestimmt. Eine Sequenz von 27 Aminosäureresten am Anfang der großen N-terminalen, cytoplasmatischen Domäne des KdpD Proteins wurde als SRP-Signalsequenz identifiziert. Darüber hinaus konnte ein direkter Einfluss der Aminosäurekomposition im Signalpeptid auf die Bindungsaffinität zu SRP *in vitro* gezeigt werden. Während die Ladungsänderung in der N-terminalen Region des Signalpeptids nur einen geringen Einfluss auf die Interaktion mit SRP hatte, zeigten Mutationen in der hydrophoben Kernregion des Peptids eine deutlich verringerte Bindeaffinität zu SRP.

Beide Teilaspekte dieser Arbeit tragen zum Verständnis des molekularen Mechanismus der co-translationalen Biogenese von integralen Membran-proteinen in Bakterien bei.

5 REFERENCES

Adams J.M. (1968) On the release of the formyl group from nascent protein. *J Mol Biol* 33(3):571-589

Agashe V.R., Guha S., Chang H.C., Genevaux P., Hayer-Hartl M., Stemp M., Georgopoulos C., Hartl F.U. and Barral J.M. (2004) Function of trigger factor and DnaK in multidomain protein folding: increase in yield at the expense of folding speed. *Cell* 117(2):199-209

Agmon I., Bashan A. and Yonath A. (2006) On Ribosome Conservation and Evolution. *Israel Journal of Ecology & Evolution* 52:3-4, 359-374

Akopian D., Dalal K., Shen K., Duong F. and Shan S.O. (2013-b) SecYEG activates GTPases to drive the completion of cotranslational protein targeting. *J Cell Biol* 200(4):397-405

Akopian D., Shen K., Zhang X. and Shan S.O. (2013-a) Signal recognition particle: an essential protein-targeting machine. *Annu Rev Biochem* 82:693-721

Angelini S., Boy D., Schiltz E. and Koch H.G. (2006) Membrane binding of the bacterial signal recognition particle receptor involves two distinct binding sites. *J Cell Biol* 174(5):715-724

Angelini S., Deitermann S. and Koch H.G. (2005) FtsY, the bacterial signal-recognition particle receptor, interacts functionally and physically with the SecYEG translocon. *EMBO Rep* 6(5):476-481

Aschtgen M.S., Zoued A., Lloubès R., Journet L. and Cascales E. (2012) The C-tail anchored TssL subunit, an essential protein of the enteroaggregative Escherichia coli Sci-1 Type VI secretion system, is inserted by YidC. *Microbiologyopen* 1(1):71-82

Ataide S.F., Schmitz N., Shen K., Ke A., Shan S.O., Doudna J.A. and Ban N. (2011) The crystal structure of the signal recognition particle in complex with its receptor. *Science* 331(6019):881-886

Baars L., Ytterberg A.J., Drew D., Wagner S., Thilo C., van Wijk K.J. and de Gier J.W. (2006) Defining the role of the Escherichia coli chaperone SecB using comparative proteomics. *J Biol Chem* 281(15):10024-10034

Ban N., Nissen P., Hansen J., Moore P.B. and Steitz T.A. (2000) The complete atomic structure of the large ribosomal subunit at 2.4 A resolution. *Science* 289(5481):905-920

Bashan A. and Yonath A. (2008) Correlating ribosome function with high-resolution structures. *Trends Microbiol* 16(7):326-335

Batey R.T. and Doudna J.A. (2002) Structural and energetic analysis of metal ions essential to SRP signal recognition domain assembly. *Biochemistry* 41(39):11703-11710

Batey R.T., Rambo R.P., Lucast L., Rha B. and Doudna J.A. (2000) Crystal structure of the ribonucleoprotein core of the signal recognition particle. *Science* 287(5456):1232-1239

Beck K., Eisner G., Trescher D., Dalbey R.E., Brunner J. and Müller M. (2001) YidC, an assembly site for polytopic Escherichia coli membrane proteins located in immediate proximity to the SecYE translocon and lipids. *EMBO Rep* 2(8):709-714

Becker T., Bhushan S., Jarasch A., Armache J.P., Funes S., Jossinet F., Gumbart J., Mielke T., Berninghausen O., Schulten K., Westhof E., Gilmore R., Mandon E.C. and Beckmann R. (2009) Structure of monomeric yeast and mammalian Sec61 complexes interacting with the translating ribosome. *Science* 326(5958):1369-1373

Beckert B., Kedrov A., Sohmen D., Kempf G., Wild K., Sinning I., Stahlberg H., Wilson D.N. and Beckmann R. (2015) Translational arrest by a prokaryotic signal recognition particle is mediated by RNA interactions. *Nat Struct Mol Biol* doi: 10.1038/nsmb.3086

Beckmann R., Spahn C.M., Eswar N., Helmers J., Penczek P.A., Sali A., Frank J. and Blobel G. (2001) Architecture of the protein-conducting channel associated with the translating 80S ribosome. *Cell* 107(3):361-372

Bellafiore S., Ferris P., Naver H., Göhre V. and Rochaix J.D. (2002) Loss of Albino3 leads to the specific depletion of the light-harvesting system. *Plant Cell* 14(9):2303-2314

Benz M., Bals T., Gügel I.L., Piotrowski M., Kuhn A., Schünemann D., Soll J. and Ankele E. (2009) Alb4 of Arabidopsis promotes assembly and stabilization of a non-chlorophyll-binding photosynthetic complex, the CF1CF0-ATP synthase. *Mol Plant* 2(6):1410-1424

Benz M., Soll J. and Ankele E. (2013) Arabidopsis thaliana Oxa proteins locate to mitochondria and fulfill essential roles during embryo development. *Planta* 237(2):573-588

Bernstein H.D., Poritz M.A., Strub K., Hoben P.J., Brenner S. and Walter P. (1989) Model for signal sequence recognition from amino-acid sequence of 54K subunit of signal recognition particle. *Nature* 340(6233):482-486

Bernstein H.D., Zopf D., Freymann D.M. and Walter P. (1993) Functional substitution of the signal recognition particle 54-kDa subunit by its Escherichia coli homolog. *Proc Natl Acad Sci USA* 90(11):5229-5233

Bibi E. (2011) Early targeting events during membrane protein biogenesis in Escherichia coli. *Biochim Biophys Acta* 1808(3):841-850

Bienvenut W.V., Giglione C. and Meinnel T. (2015) Proteome-wide analysis of the amino terminal status of Escherichia coli proteins at the steady-state and upon deformylation inhibition. *Proteomics* 15(14):2503-2518

Bingel-Erlenmeyer R., Kohler R., Kramer G., Sandikci A., Antolić S., Maier T., Schaffitzel C., Wiedmann B., Bukau B. and Ban N. (2008) A peptide deformylase-ribosome complex reveals mechanism of nascent chain processing. *Nature* 452(7183):108-111

Bischoff L., Berninghausen O. and Beckmann R. (2014-2) Molecular basis for the ribosome functioning as an L-tryptophan sensor. *Cell Rep* 9(2):469-475

Bischoff L., Wickles S., Berninghausen O., van der Sluis E.O. and Beckmann R. (2014-1) Visualization of a polytopic membrane protein during SecY-mediated membrane insertion. *Nat Commun* 5:4103

Blobel G. (1980) Intracellular protein topogenesis. *Proc Natl Acad Sci USA* 77(3):1496-1500

Blobel G. and Sabatini D.D. (1971) Ribosome-Membrane Interaction in Eukaryotic Cells. *Biomembranes* pp 193-195

Bohnert M., Rehling P., Guiard B., Herrmann J.M., Pfanner N. and van der Laan M. (2010) Cooperation of stop-transfer and conservative sorting mechanisms in mitochondrial protein transport. *Curr Biol* 20(13):1227-1232

Bornemann T., Jöckel J., Rodnina M.V. and Wintermeyer W. (2008) Signal sequence-independent membrane targeting of ribosomes containing short nascent peptides within the exit tunnel. *Nat Struct Mol Biol* 15(5):494-499

Borowska M.T., Dominik P.K., Anghel S.A., Kossiakoff A.A. and Keenan R.J. (2015) A YidC-like Protein in the Archaeal Plasma Membrane. *Structure* 23:1-10

Bradshaw N., Neher S.B., Booth D.S. and Walter P. (2009) Signal sequences activate the catalytic switch of SRP RNA. *Science* 323(5910):127-130

Braig D., Mircheva M., Sachelaru I., van der Sluis E.O., Sturm L., Beckmann R. and Koch H.G. (2011) Signal sequence-independent SRP-SR complex formation at the membrane suggests an alternative targeting pathway within the SRP cycle. *Mol Biol Cell* 22(13):2309-2323

Buskiewicz I., Deuerling E., Gu S.Q., Jöckel J., Rodnina M.V., Bukau B. and Wintermeyer W. (2004) Trigger factor binds to ribosome-signal-recognition particle (SRP) complexes and is excluded by binding of the SRP receptor. *Proc Natl Acad Sci USA* 101(21):7902-7906

Buskiewicz I., Kubarenko A., Peske F., Rodnina M.V. and Wintermeyer W. (2005-1) Domain rearrangement of SRP protein Ffh upon binding 4.5S RNA and the SRP receptor FtsY. *RNA* 11(6):947-957

Buskiewicz I., Peske F., Wieden H.J., Gryczynski I., Rodnina M.V. and Wintermeyer W. (2005-2) Conformations of the signal recognition particle protein Ffh from Escherichia coli as determined by FRET. *J Mol Biol* 351(2):417-430

Cabelli R.J., Chen L., Tai P.C. and Oliver D.B. (1988) SecA protein is required for secretory protein translocation into E. coli membrane vesicles. *Cell* 55(4):683-692

Casadaban, M. J. and Cohen, S. N. (1980). Analysis of gene control signals by DNA fusion and cloning in Escherichia coli. *J Mol Biol* 138(2): 179-207

Celebi N., Yi L., Facey S.J., Kuhn A. and Dalbey R.E. (2006) Membrane biogenesis of subunit II of cytochrome bo oxidase: contrasting requirements for insertion of N-terminal and C-terminal domains. *J Mol Biol* 357(5):1428-1436

Chen M., Samuelson J.C., Jiang F., Muller M., Kuhn A. and Dalbey R.E. (2002) Direct interaction of YidC with the Sec-independent Pf3 coat protein during its membrane protein insertion*. J Biol Chem* 277(10):7670-7675

Chen Y., Soman R., Shanmugam S.K., Kuhn A. and Dalbey R.E. (2014) The role of the strictly conserved positively charged residue differs among the Gram-positive, Gram-negative, and chloroplast YidC homologs. *J Biol Chem* 289(51):35656-35667

Chen, J.Z., and Grigorieff, N. (2007) SIGNATURE: a single-particle selection system for molecular electron microscopy. *J Struct Biol* 157: 168-173

Cheng Z., Jiang Y., Mandon E.C. and Gilmore R. (2005) Identification of cytoplasmic residues of Sec61p involved in ribosome binding and cotranslational translocation*. J Cell Biol* 168(1):67-77

Chiba S., Lamsa A. and Pogliano K. (2009) A ribosome-nascent chain sensor of membrane protein biogenesis in Bacillus subtilis. *EMBO J* 28(22):3461-3475

Clarke T.F. 4th and Clark P.L. (2008) Rare codons cluster. *PLoS One* 3(10):e3412

Connolly T., Rapiejko P.J. and Gilmore R. (1991) Requirement of GTP hydrolysis for dissociation of the signal recognition particle from its receptor. *Science* 252(5009):1171-1173

Cross B.C., Sinning I., Luirink J. and High S. (2009) Delivering proteins for export from the cytosol*. Nat Rev Mol Cell Biol* 10(4):255-264

Dalbey R.E. and Kuhn A. (2014) How YidC inserts and folds proteins across a membrane. *Nat Struct Mol Biol* 21(5):435-436

Dalbey R.E. and Kuhn A. (2015) Membrane Insertases Are Present in All Three Domains of Life. *Structure* 23(9):1559-1560

Dalbey R.E. and von Heijne G. (2002) Protein targeting, transport and translocation. *Academic Press*, London

Dalbey R.E., Kuhn A., Zhu L. and Kiefer D. (2014) The membrane insertase YidC. *Biochim Biophys Acta* 1843(8):1489-1496

Dalbey R.E., Wang P. and Kuhn A. (2011) Assembly of bacterial inner membrane proteins. *Annu Rev Biochem* 80:161-187

Datsenko, K. A. and Wanner B. L. (2000) One-step inactivation of chromosomal genes in Escherichia coli K-12 using PCR products. *Proc Natl Acad Sci USA* 97(12): 6640-6645

de Gier J.W. and Luirink J. (2003) The ribosome and YidC. New insights into the biogenesis of Escherichia coli inner membrane proteins. *EMBO Rep* 4(10):939-943

de Gier J.W., Mansournia P., Valent Q.A., Phillips G.J., Luirink J. and von Heijne G. (1996) Assembly of a cytoplasmic membrane protein in Escherichia coli is dependent on the signal recognition particle. *FEBS Lett* 399(3):307-309

de Leeuw E., te Kaat K., Moser C., Menestrina G., Demel R., de Kruijff B., Oudega B., Luirink J. and Sinning I. (2000) Anionic phospholipids are involved in membrane association of FtsY and stimulate its GTPase activity. *EMBO J* 19(4):531-541

Demeshkina N., Jenner L., Westhof E., Yusupov M. and Yusupova G. (2012) A new understanding of the decoding principle on the ribosome. *Nature* 484(7393):256-259

Denks K., Vogt A., Sachelaru I., Petriman N.A., Kudva R. and Koch H.G. (2014) The Sec translocon mediated protein transport in prokaryotes and eukaryotes. *Mol Membr Biol* 31(2-3):58-84

Deuerling E., Schulze-Specking A., Tomoyasu T., Mogk A. and Bukau B. (1999) Trigger factor and DnaK cooperate in folding of newly synthesized proteins. *Nature* 400(6745):693-696

Dong Y., Palmer S.R., Hasona A., Nagamori S., Kaback H.R., Dalbey R.E. and Brady L.J. (2008) Functional overlap but lack of complete cross-complementation of Streptococcus mutans and Escherichia coli YidC orthologs. *J Bacteriol* 190(7):2458-2469

Driessen A.J. and Nouwen N. (2008) Protein translocation across the bacterial cytoplasmic membrane. *Annu Rev Biochem* 77:643-667

du Plessis D.J., Nouwen N. and Driessen A.J. (2006) Subunit a of cytochrome o oxidase requires both YidC and SecYEG for membrane insertion. *J Biol Chem* 281(18):12248-12252

Egea P.F., Shan S.O., Napetschnig J., Savage D.F., Walter P. and Stroud R.M. (2004) Substrate twinning activates the signal recognition particle and its receptor. *Nature* 427(6971):215-221

Eisner G., Koch H.G., Beck K., Brunner J. and Muller M. (2003) Ligand crowding at a nascent signal sequence. *J Cell Biol* 163(1):35-44

Eitan A. and Bibi E. (2004) The core Escherichia coli signal recognition particle receptor contains only the N and G domains of FtsY. *J Bacteriol* 186(8):2492-2494

Emanuelsson O. and von Heijne G. (2001) Prediction of organellar targeting signals. *Biochim Biophys Acta* 1541(1-2):114-119

Estrozi L.F., Boehringer D., Shan S.O., Ban N. and Schaffitzel C. (2011) Cryo-EM structure of the E. coli translating ribosome in complex with SRP and its receptor. *Nat Struct Mol Biol* 18(1):88-90

Facey S.J. and Kuhn A. (2003) The sensor protein KdpD inserts into the Escherichia coli membrane independent of the Sec translocase and YidC. *Eur J Biochem* 270(8):1724-1734

Facey, S. J., Neugebauer S. A., et al. (2007). The mechanosensitive channel protein MscL is targeted by the SRP to the novel YidC membrane insertion pathway of Escherichia coli. *J Mol Biol* 365(4): 995-1004

Falk S., Ravaud S., Koch J. and Sinning I. (2010) The C terminus of the Alb3 membrane insertase recruits cpSRP43 to the thylakoid membrane. *J Biol Chem* 285(8):5954-5962

Fedyukina D.V. and Cavagnero S. (2011) Protein folding at the exit tunnel. *Annu Rev Biophys* 40:337-359

Fekkes P. and Driessen A.J. (1999) Protein targeting to the bacterial cytoplasmic membrane. *Microbiol Mol Biol Rev* 63(1):161-173

Ferbitz L., Maier T., Patzelt H., Bukau B., Deuerling E. and Ban N. (2004) Trigger factor in complex with the ribosome forms a molecular cradle for nascent proteins. *Nature* 431(7008):590-596

Flanagan J.J., Chen J.C., Miao Y., Shao Y., Lin J., Bock P.E. and Johnson A.E. (2003) Signal recognition particle binds to ribosome-bound signal sequences with fluorescence-detected subnanomolar affinity that does not diminish as the nascent chain lengthens. *J Biol Chem* 278(20):18628-18637

Focia P.J., Shepotinovskaya I.V., Seidler J.A. and Freymann D.M. (2004) Heterodimeric GTPase core of the SRP targeting complex. *Science* 303(5656):373-377

Frank, J., Radermacher, M., Penczek, P., Zhu, J., Li, Y., Ladjadj, M., and Leith, A. (1996) SPIDER and WEB: processing and visualization of images in 3D electron microscopy and related fields. *J Struct Biol* 116: 190-199

Frauenfeld J., Gumbart J., Sluis E.O., Funes S., Gartmann M., Beatrix B., Mielke T., Berninghausen O., Becker T., Schulten K. and Beckmann R. (2011) Cryo-EM structure of the ribosome-SecYE complex in the membrane environment. *Nat Struct Mol Biol* 18(5):614-621

Frère V., Sourgen F., Monnot M., Troalen F. and Fermandjian S. (1995) A peptide fragment of human DNA topoisomerase II alpha forms a stable coiled-coil structure in solution. *J Biol Chem* 270(29):17502-17507

Freymann D.M., Keenan R.J., Stroud R.M. and Walter P. (1997) Structure of the conserved GTPase domain of the signal recognition particle. *Nature* 385(6614):361-364

Freymann D.M., Keenan R.J., Stroud R.M. and Walter P. (1999) Functional changes in the structure of the SRP GTPase on binding GDP and Mg2+GDP*. Nat Struct Biol* 6(8):793-801

Fry K.T. and Lamborg M.R. (1967) Amidohydrolase activity of Escherichia coli extracts with formylated amino acids and dipeptides as substrates. *J Mol Biol* 28(3):423-433

Fuerst J.A. and Sagulenko E. (2011) Beyond the bacterium: planctomycetes challenge our concepts of microbial structure and function. *Nat Rev Microbiol* 9(6):403-413

Funes S., Gerdes L., Inaba M., Soll J. and Herrmann J.M. (2004-2) The Arabidopsis thaliana chloroplast inner envelope protein ARTEMIS is a functional member of the Alb3/Oxa1/YidC family of proteins. *FEBS Lett* 569(1-3):89-93

Funes S., Hasona A., Bauerschmitt H., Grubbauer C., Kauff F., Collins R., Crowley P.J., Palmer S.R., Brady L.J. and Herrmann J.M. (2009) Independent gene duplications of the YidC/Oxa/Alb3 family enabled a specialized cotranslational function. *Proc Natl Acad Sci USA* 106(16):6656-6661

Funes S., Kauff F., van der Sluis E.O., Ott M. and Herrmann J.M. (2011) Evolution of YidC/Oxa1/Alb3 insertases: three independent gene duplications followed by functional specialization in bacteria, mitochondria and chloroplasts. *Biol Chem* 392(1-2):13-19

Funes S., Nargang F.E., Neupert W. and Herrmann J.M. (2004-1) The Oxa2 protein of Neurospora crassa plays a critical role in the biogenesis of cytochrome oxidase and defines a ubiquitous subbranch of the Oxa1/YidC/Alb3 protein family. *Mol Biol Cell* 15(4):1853-1861

Funes S., Westerburg H., Jaimes-Miranda F., Woellhaf M.W., Aguilar-Lopez J.L., Janßen L., Bonnefoy N., Kauff F. and Herrmann J.M. (2013) Partial suppression of Oxa1 mutants by mitochondria-targeted signal recognition particle provides insights into the evolution of the cotranslational insertion systems. *FEBS J* 280(3):904-915

Gasper R., Meyer S., Gotthardt K., Sirajuddin M. and Wittinghofer A. (2009) It takes two to tango: regulation of G proteins by dimerization. *Nat Rev Mol Cell Biol* 10(6):423-429

Gawronski-Salerno J. and Freymann D.M. (2007) Structure of the GMPPNP-stabilized NG domain complex of the SRP GTPases Ffh and FtsY. *J Struct Biol* 158(1):122-128

Genevaux P., Georgopoulos C. and Kelley W.L. (2007) The Hsp70 chaperone machines of Escherichia coli: a paradigm for the repartition of chaperone functions. *Mol Microbiol* 66(4):840-857

Geng Y., Kedrov A., Caumanns J.J., Crevenna A.H., Lamb D.C., Beckmann R. and Driessen A.J. (2015) Role of the Cytosolic Loop C2 and the C Terminus of YidC in Ribosome Binding and Insertion Activity. *J Biol Chem* 290(28):17250-17261

Gerdes L., Bals T., Klostermann E., Karl M., Philippar K., Hünken M., Soll J. and Schünemann D. (2006) A second thylakoid membrane-localized Alb3/OxaI/YidC homologue is involved in proper chloroplast biogenesis in Arabidopsis thaliana. *J Biol Chem* 281(24):16632-16642

Gerken U., Erhardt D., Bär G., Ghosh R. and Kuhn A. (2008) Initial binding process of the membrane insertase YidC with its substrate Pf3 coat protein is reversible. *Biochemistry* 47(22):6052-6058

Gierasch L.M. (1989) Signal sequences. *Biochemistry* 28(3):923-930

Glick B.S. and Von Heijne G. (1996) Saccharomyces cerevisiae mitochondria lack a bacterial-type sec machinery. *Protein Sci* 5(12):2651-2652

Glöckner F.O., Kube M., Bauer M., Teeling H., Lombardot T., Ludwig W., Gade D., Beck A., Borzym K., Heitmann K., Rabus R., Schlesner H., Amann R. and Reinhardt R.

(2003) Complete genome sequence of the marine planctomycete Pirellula sp. strain 1. *Proc Natl Acad Sci USA* 100(14):8298-8303

Gold V.A., Whitehouse S., Robson A. and Collinson I. (2013) The dynamic action of SecA during the initiation of protein translocation. *Biochem J* 449(3):695-705

Goldman D.H., Kaiser C.M., Milin A., Righini M., Tinoco I. Jr. and Bustamante C. (2015) Ribosome. Mechanical force releases nascent chain-mediated ribosome arrest in vitro and in vivo. *Science* 348(6233):457-460

Gong F. and Yanofsky C. (2001) Reproducing tna operon regulation in vitro in an S-30 system. Tryptophan induction inhibits cleavage of TnaC peptidyl-tRNA. *J Biol Chem* 276(3):1974-1983

Gong F. and Yanofsky C. (2002) Instruction of translating ribosome by nascent peptide. *Science* 297(5588):1864-1867

Gowda K. and Zwieb C. (1997) Determinants of a protein-induced RNA switch in the large domain of signal recognition particle identified by systematic-site directed mutagenesis. *Nucleic Acids Res* 25(14):2835-2840

Graubner W., Schierhorn A. and Brüser T. (2007) DnaK plays a pivotal role in Tat targeting of CueO and functions beside SlyD as a general Tat signal binding chaperone. *J Biol Chem* 282(10):7116-7124

Gray A.N., Henderson-Frost J.M., Boyd D., Sharafi S., Niki H. and Goldberg M.B. (2011) Unbalanced charge distribution as a determinant for dependence of a subset of Escherichia coli membrane proteins on the membrane insertase YidC. *MBio* 2(6) pii: e00238-11

Grenz S. (2008) Funktionelle und strukturelle Analyse des YidC-Homologs Aq-175 in Aquifex aeolicus. *Institute of Microbiology, University of Hohenheim*: Diploma Thesis

Grudnik P., Bange G. and Sinning I. (2009) Protein targeting by the signal recognition particle. *Biol Chem* 390(8):775-782

Gruschke S., Gröne K., Heublein M., Hölz S., Israel L., Imhof A., Herrmann J.M. and Ott M. (2010) Proteins at the polypeptide tunnel exit of the yeast mitochondrial ribosome. *J Biol Chem* 285(25):19022-19028

Gu S.Q., Peske F., Wieden H.J., Rodnina M.V. and Wintermeyer W. (2003) The signal recognition particle binds to protein L23 at the peptide exit of the Escherichia coli ribosome. *RNA* 9(5):566-573

Gualerzi C.O. and Pon C.L. (1990) Initiation of mRNA translation in prokaryotes. *Biochemistry* 29(25):5881-5889

Haddad A., Rose R.W. and Pohlschröder M. (2005) The Haloferax volcanii FtsY homolog is critical for haloarchaeal growth but does not require the A domain. *J Bacteriol* 187(12):4015-4022

Hainzl T., Huang S. and Sauer-Eriksson A.E. (2007) Interaction of signal-recognition particle 54 GTPase domain and signal-recognition particle RNA in the free signal-recognition particle. *Proc Natl Acad Sci USA* 104(38):14911-14916

Hainzl T., Huang S., Meriläinen G., Brännström K. and Sauer-Eriksson A.E. (2011) Structural basis of signal-sequence recognition by the signal recognition particle. *Nat Struct Mol Biol* 18(3):389-391

Halic M., Becker T., Pool M.R., Spahn C.M., Grassucci R.A., Frank J. and Beckmann R. (2004) Structure of the signal recognition particle interacting with the elongation-arrested ribosome. *Nature* 427(6977):808-814

Halic M., Blau M., Becker T., Mielke T., Pool M.R., Wild K., Sinning I. and Beckmann R. (2006) Following the signal sequence from ribosomal tunnel exit to signal recognition particle. *Nature* 444(7118):507-511

Haque M.E., Spremulli L.L. and Fecko C.J. (2010) Identification of protein-protein and protein-ribosome interacting regions of the C-terminal tail of human mitochondrial inner membrane protein Oxa1L. *J Biol Chem* 285(45):34991-8

Hardy S.J. and Randall L.L. (1991) A kinetic partitioning model of selective binding of nonnative proteins by the bacterial chaperone SecB. *Science*. 251(4992):439-443

Harms J., Schluenzen F., Zarivach R., Bashan A., Gat S., Agmon I., Bartels H., Franceschi F. and Yonath A. (2001) High resolution structure of the large ribosomal subunit from a mesophilic eubacterium. *Cell* 2001 107(5):679-688

Hartl F.U., Bracher A. and Hayer-Hartl M. (2011) Molecular chaperones in protein folding and proteostasis. *Nature* 475(7356):324-332

Hasona A., Crowley P.J., Levesque C.M., Mair R.W., Cvitkovitch D.G., Bleiweis A.S. and Brady L.J. (2005) Streptococcal viability and diminished stress tolerance in mutants lacking the signal recognition particle pathway or YidC2. *Proc Natl Acad Sci USA* 102(48):17466-17471

Hegde R.S. and Bernstein H.D. (2006) The surprising complexity of signal sequences. *Trends Biochem Sci* 31(10):563-571

Hell K., Herrmann J., Pratje E., Neupert W. and Stuart R.A. (1997) Oxa1p mediates the export of the N- and C-termini of pCoxII from the mitochondrial matrix to the intermembrane space*. FEBS Lett* 418(3):367-370

Hell K., Herrmann J.M., Pratje E., Neupert W. and Stuart R.A. (1998) Oxa1p, an essential component of the N-tail protein export machinery in mitochondria. *Proc Natl Acad Sci USA* 95(5):2250-2255

Hell K., Neupert W. and Stuart R.A. (2001) Oxa1p acts as a general membrane insertion machinery for proteins encoded by mitochondrial DNA. *EMBO J* 20(6):1281-1288

Hennon S.W., Soman R., Zhu L. and Dalbey R.E. (2015) YidC/Alb3/Oxa1 Family of Insertases. *J Biol Chem* 290(24):14866-14874

Herrmann J.M. and Bonnefoy N. (2004) Protein export across the inner membrane of mitochondria: the nature of translocated domains determines the dependence on the Oxa1 translocase. *J Biol Chem* 279(4):2507-2512

Heuberger E.H., Veenhoff L.M., Duurkens R.H., Friesen R.H. and Poolman B. (2002) Oligomeric state of membrane transport proteins analyzed with blue native electrophoresis and analytical ultracentrifugation. *J Mol Biol* 317(4):591-600

Hildenbeutel M., Theis M., Geier M., Haferkamp I., Neuhaus H.E., Herrmann J.M. and Ott M. (2012) The membrane insertase Oxa1 is required for efficient import of carrier proteins into mitochondria. *J Mol Biol* 423(4):590-599

Hinttala R., Sasarman F., Nishimura T., Antonicka H., Brunel-Guitton C., Schwartzentruber J., Fahiminiya S., Majewski J., Faubert D., Ostergaard E., Smeitink J.A. and Shoubridge E.A. (2015) An N-terminal formyl methionine on COX 1 is required for the assembly of cytochrome c oxidase. *Hum Mol Genet* 24(14):4103-1413

Hoffmann A., Becker A.H., Zachmann-Brand B., Deuerling E., Bukau B. and Kramer G. (2012) Concerted action of the ribosome and the associated chaperone trigger factor confines nascent polypeptide folding. *Mol Cell* 48(1):63-74

Holtkamp W., Lee S., Bornemann T., Senyushkina T., Rodnina M.V. and Wintermeyer W. (2012) Dynamic switch of the signal recognition particle from scanning to targeting. *Nat Struct Mol Biol* 19(12):1332-1337

Huber D., Boyd D., Xia Y., Olma M.H., Gerstein M. and Beckwith J. (2005) Use of thioredoxin as a reporter to identify a subset of Escherichia coli signal sequences that promote signal recognition particle-dependent translocation. *J Bacteriol* 187(9):2983-2991

Huber D., Rajagopalan N., Preissler S., Rocco M.A., Merz F., Kramer G. and Bukau B. (2011) SecA interacts with ribosomes in order to facilitate posttranslational translocation in bacteria. *Mol Cell* 41(3):343-353

Ito K., Chiba S. and Pogliano K. (2010) Divergent stalling sequences sense and control cellular physiology. *Biochem Biophys Res Commun* 393(1):1-5

Jagath J.R., Matassova N.B., de Leeuw E., Warnecke J.M., Lentzen G., Rodnina M.V., Luirink J. and Wintermeyer W. (2001) Important role of the tetraloop region of 4.5S RNA in SRP binding to its receptor FtsY. *RNA* 7(2):293-301

Janda C.Y., Li J., Oubridge C., Hernández H., Robinson C.V. and Nagai K. (2010) Recognition of a signal peptide by the signal recognition particle. *Nature* 465(7297):507-510

Jecklin M.C., Schauer S., Dumelin C.E. and Zenobi R. (2009) Label-free determination of protein-ligand binding constants using mass spectrometry and validation using surface plasmon resonance and isothermal titration calorimetry. *J Mol Recognit* 22(4):319-329

Jenner L., Melnikov S., Garreau de Loubresse N., Ben-Shem A., Iskakova M., Urzhumtsev A., Meskauskas A., Dinman J., Yusupova G. and Yusupov M. (2012) Crystal structure of the 80S yeast ribosome. *Curr Opin Struct Biol* 22(6):759-767

Jenner L., Starosta A.L., Terry D.S., Mikolajka A., Filonava L., Yusupov M., Blanchard S.C., Wilson D.N. and Yusupova G. (2013) Structural basis for potent inhibitory activity of the antibiotic tigecycline during protein synthesis*. Proc Natl Acad Sci USA* 110(10):3812-3816

Jerabek-Willemsen M., Wienken C.J., Braun D., Baaske P. and Duhr S. (2011) Molecular interaction studies using microscale thermophoresis. *Assay Drug Dev Technol* 9(4):342-353

Jia L., Dienhart M.K. and Stuart R.A. (2007) Oxa1 directly interacts with Atp9 and mediates its assembly into the mitochondrial F1Fo-ATP synthase complex. *Mol Biol Cell* 18(5):1897-1908

Jia L., Kaur J. and Stuart R.A. (2009) Mapping of the Saccharomyces cerevisiae Oxa1-mitochondrial ribosome interface and identification of MrpL40, a ribosomal protein in close proximity to Oxa1 and critical for oxidative phosphorylation complex assembly. *Eukaryot Cell* 8(11):1792-1802

Jia, L., Dienhart, M., Schramp, M., McCauley, M., Hell, K. and Stuart, R.A. (2003) Yeast Oxa1 interacts with mitochondrial ribosomes: the importance of the C-terminal region of Oxa1. *EMBO J* 22(24):6438-6447

Jiang F., Chen M., Yi L., de Gier J.W., Kuhn A. and Dalbey R.E. (2003) Defining the regions of Escherichia coli YidC that contribute to activity. *J Biol Chem* 278(49):48965-48972

Jiang F., Yi L., Moore M., Chen M., Rohl T., Van Wijk K.J., De Gier J.W., Henry R. and Dalbey R.E. (2002) Chloroplast YidC homolog Albino3 can functionally complement the bacterial YidC depletion strain and promote membrane insertion of both bacterial and chloroplast thylakoid proteins. *J Biol Chem* 277(22):19281-19288

Johnson, W. C. (1999). Analyzing protein circular dichroism spectra for accurate secondary structures. *Proteins* 35(3): 307–312

Jung K. and Altendorf K. (1998) Truncation of amino acids 12-128 causes deregulation of the phosphatase activity of the sensor kinase KdpD of Escherichia coli. *J Biol Chem* 273(28):17406-17410

Karamyshev A.L. and Johnson A.E. (2005) Selective SecA association with signal sequences in ribosome-bound nascent chains: a potential role for SecA in ribosome targeting to the bacterial membrane. *J Biol Chem* 280(45):37930-37940

Karimi R., Pavlov M.Y., Buckingham R.H. and Ehrenberg M. (1999) Novel roles for classical factors at the interface between translation termination and initiation. *Mol Cell* 3(5):601-609

Kedrov A., Sustarsic M., de Keyzer J., Caumanns J.J., Wu Z.C. and Driessen A.J. (2013) Elucidating the native architecture of the YidC: ribosome complex. *J Mol Biol* 425(22):4112-4124

Keenan R.J., Freymann D.M., Stroud R.M. and Walter P. (2001) The signal recognition particle. *Annu Rev Biochem* 70:755-775

Keenan R.J., Freymann D.M., Walter P. and Stroud R.M. (1998) Crystal structure of the signal sequence binding subunit of the signal recognition particle. *Cell* 94(2):181-191

Kiefer D. and Kuhn A. (2007) YidC as an essential and multifunctional component in membrane protein assembly. *Int Rev Cytol* 259:113-138

Klenner C. and Kuhn A. (2012) Dynamic disulfide scanning of the membrane-inserting Pf3 coat protein reveals multiple YidC substrate contacts. *J Biol Chem* 287(6):3769-3776

Klenner C., Yuan J., Dalbey R.E. and Kuhn A. (2008) The Pf3 coat protein contacts TM1 and TM3 of YidC during membrane biogenesis. *FEBS Lett* 582(29):3967-3972

Koch H.G., Moser M., Schimz K.L. and Muller M. (2002) The integration of YidC into the cytoplasmic membrane of Escherichia coli requires the signal recognition particle, SecA and SecYEG. *J Biol Chem* 277(8):5715-5718

Kohler R., Boehringer D., Greber B., Bingel-Erlenmeyer R., Collinson I., Schaffitzel C. and Ban N. (2009) YidC and Oxa1 form dimeric insertion pores on the translating ribosome. *Mol Cell* 2009 34(3):344-353

Kol S., Majczak W., Heerlien R., van der Berg J.P., Nouwen N. and Driessen A.J. (2009) Subunit a of the F(1)F(0) ATP synthase requires YidC and SecYEG for membrane insertion. *J Mol Biol* 390(5):893-901

Kramer G., Boehringer D., Ban N. and Bukau B. (2009) The ribosome as a platform for co-translational processing, folding and targeting of newly synthesized proteins. *Nat Struct Mol Biol* 16(6):589-597

Kramer G., Rauch T., Rist W., Vorderwülbecke S., Patzelt H., Schulze-Specking A., Ban N., Deuerling E. and Bukau B. (2002) L23 protein functions as a chaperone docking site on the ribosome. *Nature* 419(6903):171-174

Krüger V., Deckers M., Hildenbeutel M., van der Laan M., Hellmers M., Dreker C., Preuss M., Herrmann J.M., Rehling P., Wagner R. and Meinecke M. (2012) The mitochondrial oxidase assembly protein1 (Oxa1) insertase forms a membrane pore in lipid bilayers. *J Biol Chem* 287(40):33314-33326

Kuhn A., Stuart R., Henry R. and Dalbey R.E. (2003) The Alb3/Oxa1/YidC protein family: membrane-localized chaperones facilitating membrane protein insertion? *Trends Cell Biol* 13(10):510-516

Kuhn P., Weiche B., Sturm L., Sommer E., Drepper F., Warscheid B., Sourjik V. and Koch H.G. (2011) The bacterial SRP receptor, SecA and the ribosome use overlapping binding sites on the SecY translocon. *Traffic* 12(5):563-578

Kumazaki K., Chiba S., Takemoto M., Furukawa A., Nishiyama K., Sugano Y., Mori T., Dohmae N., Hirata K., Nakada-Nakura Y., Maturana A.D., Tanaka Y., Mori H., Sugita Y., Arisaka F., Ito K., Ishitani R., Tsukazaki T. and Nureki O. (2014-a) Structural basis of Sec-independent membrane protein insertion by YidC. *Nature* 509(7501):516-520

Kumazaki K., Kishimoto T., Furukawa A., Mori H., Tanaka Y., Dohmae N., Ishitani R., Tsukazaki T. and Nureki O. (2014-b) Crystal structure of Escherichia coli YidC, a membrane protein chaperone and insertase. *Sci Rep* 4:7299

Lam V.Q., Akopian D., Rome M., Henningsen D. and Shan S.O. (2010) Lipid activation of the signal recognition particle receptor provides spatial coordination of protein targeting. *J Cell Biol* 190(4):623-635

Lau S.Y., Taneja A.K. and Hodges R.S. (1984) Synthesis of a model protein of defined secondary and quaternary structure. Effect of chain length on the stabilization and formation of two-stranded alpha-helical coiled-coils. *J Biol Chem* 259(21):13253-13261

Lentzen G., Moine H., Ehresmann C., Ehresmann B. and Wintermeyer W. (1996) Structure of 4.5S RNA in the signal recognition particle of Escherichia coli as studied by enzymatic and chemical probing. *RNA* 2(3):244-253

Li Z., Boyd D., Reindl M. and Goldberg M.B. (2014) Identification of YidC residues that define interactions with the Sec Apparatus. *J Bacteriol* 196(2):367-377

Lichi T., Ring G. and Eichler J. (2004) Membrane binding of SRP pathway components in the halophilic archaea Haloferax volcanii. *Eur J Biochem* 271(7):1382-1390

Liu M. and Spremulli L. (2000) Interaction of mammalian mitochondrial ribosomes with the inner membrane. *J Biol Chem* 275(38):29400-29406

Lotz M., Haase W., Kühlbrandt W. and Collinson I. (2008) Projection structure of yidC: a conserved mediator of membrane protein assembly. *J Mol Biol* 375(4):901-907

Luirink J. and Sinning I. (2004) SRP-mediated protein targeting: structure and function revisited. *Biochim Biophys Acta* 1694(1-3):17-35

Luirink J., Samuelsson T. and de Gier J.W. (2001) YidC/Oxa1p/Alb3: evolutionarily conserved mediators of membrane protein assembly. *FEBS Lett* 501(1):1-5

Luirink J., ten Hagen-Jongman C.M., van der Weijden C.C., Oudega B., High S., Dobberstein B. and Kusters R. (1994) An alternative protein targeting pathway in Escherichia coli: studies on the role of FtsY. *EMBO J* 13(10):2289-2296

Luirink J., von Heijne G., Houben E. and de Gier J.W. (2005) Biogenesis of inner membrane proteins in Escherichia coli. *Annu Rev Microbiol* 59:329-355

Lupas A., Van Dyke M. and Stock J. (1991) Predicting coiled coils from protein sequences. *Science* 252(5009):1162-1164

Lycklama A Nijeholt J.A. and Driessen A.J. (2012) The bacterial Sec-translocase: structure and mechanism. *Philos Trans R Soc Lond B Biol Sci* 367(1592):1016-1028

Magidovich E., Orr I., Fass D., Abdu U. and Yifrach O. (2007) Intrinsic disorder in the C-terminal domain of the Shaker voltage-activated K+ channel modulates its interaction with scaffold proteins. *Proc Natl Acad Sci USA* 104(32):13022-13027

Maguire B.A., Wondrack L.M., Contillo L.G. and Xu Z. (2008) A novel chromatography system to isolate active ribosomes from pathogenic bacteria. *RNA* 14(1):188-195

Maier K.S., Hubich S., Liebhart H., Krauss S., Kuhn A. and Facey S.J. (2008) An amphiphilic region in the cytoplasmic domain of KdpD is recognized by the signal recognition particle and targeted to the Escherichia coli membrane. *Mol Microbiol* 68(6):1471-1484

Mainprize I.L., Beniac D.R., Falkovskaia E., Cleverley R.M., Gierasch L.M., Ottensmeyer F.P. and Andrews D.W. (2006) The structure of Escherichia coli signal recognition particle revealed by scanning transmission electron microscopy. *Mol Biol Cell* 17(12):5063-5074

Malkin L.I. and Rich A. (1967) Partial resistance of nascent polypeptide chains to proteolytic digestion due to ribosomal shielding. *J Mol Biol* 26(2):329-346

Martoglio B. and Dobberstein B. (1998) Signal sequences: more than just greasy peptides. *Trends Cell Biol* 8(10):410-415

Mboubi Kouaga, E. (2013) Strukturelle Dynamik der ribosomalen Proteinen L23, L24 und L29 bei der Interaktion mit Membraninsertasen. *Institute of Microbiology, University of Hohenheim*: Master Thesis

McGuffin L.J., Bryson K. and Jones D.T. (2000) The PSIPRED protein structure prediction server. *Bioinformatics* 16(4):404-405

Ménétret J.F., Schaletzky J., Clemons W.M. Jr, Osborne A.R., Skånland S.S., Denison C., Gygi S.P., Kirkpatrick D.S., Park E., Ludtke S.J., Rapoport T.A. and Akey C.W. (2007) Ribosome binding of a single copy of the SecY complex: implications for protein translocation. *Mol Cell* 28(6):1083-1092

Merz F., Boehringer D., Schaffitzel C., Preissler S., Hoffmann A., Maier T., Rutkowska A., Lozza J., Ban N., Bukau B. and Deuerling E. (2008) Molecular mechanism and structure of Trigger Factor bound to the translating ribosome. *EMBO J* 27(11):1622-32

Milligan D.L. and Koshland D.E. Jr. (1990) The amino terminus of the aspartate chemoreceptor is formylmethionine. *J Biol Chem* 265(8):4455-4460

Milligan R.A. and Unwin P.N. (1982) In vitro crystallization of ribosomes from chick embryos. *J Cell Biol* 95(2 Pt 1):648-653

Mircheva M., Boy D., Weiche B., Hucke F., Graumann P. and Koch H.G. (2009) Predominant membrane localization is an essential feature of the bacterial signal recognition particle receptor. *BMC Biol* 7:76

Miroux, B. and Walker J. E. (1996). Over-production of proteins in Escherichia coli: mutant hosts that allow synthesis of some membrane proteins and globular proteins at high levels. *J Mol Biol* 260(3): 289-298

Mitra K., Schaffitzel C., Shaikh T., Tama F., Jenni S., Brooks C.L. 3rd, Ban N. and Frank J. (2005) Structure of the E. coli protein-conducting channel bound to a translating ribosome. *Nature* 438(7066):318-324

Monro R.E. (1967) Catalysis of peptide bond formation by 50 S ribosomal subunits from Escherichia coli. *J Mol Biol* 26(1):147-151

Monro R.E., Staehelin T., Celma ML. and Vazquez D. (1969) The peptidyl transferase activity of ribosomes. *Cold Spring Harb Symp Quant Biol* 34:357-368

Montoya G., Svensson C., Luirink J. and Sinning I. (1997) Crystal structure of the NG domain from the signal-recognition particle receptor FtsY. *Nature* 385(6614):365-368

Moore M., Goforth R.L., Mori H. and Henry R. (2003) Functional interaction of chloroplast SRP/FtsY with the ALB3 translocase in thylakoids: substrate not required. *J Cell Biol* 162(7):1245-1254

Moore M., Harrison M.S., Peterson E.C. and Henry R. (2000) Chloroplast Oxa1p homolog albino3 is required for post-translational integration of the light harvesting chlorophyll-binding protein into thylakoid membranes. *J Biol Chem* 275(3):1529-1532

Moore P.B. (2012) How should we think about the ribosome? *Annu Rev Biophys* 41:1-19

Murakami T., Haga K., Takeuchi M. and Sato T. (2002) Analysis of the Bacillus subtilis spoIIIJ gene and its Paralogue gene, yqjG. *J Bacteriol* 184(7):1998-2004

Nagamori S., Smirnova I.N. and Kaback H.R. (2004) Role of YidC in folding of polytopic membrane proteins. *J Cell Biol* 165(1):53-62

Nakatogawa H. and Ito K. (2002) The ribosomal exit tunnel functions as a discriminating gate. *Cell* 108(5):629-636

Nargang F.E., Preuss M., Neupert W. and Herrmann J.M. (2002) The Oxa1 protein forms a homooligomeric complex and is an essential part of the mitochondrial export translocase in Neurospora crassa. *J Biol Chem* 277(15):12846-12853

Neher S.B., Bradshaw N., Floor S.N., Gross J.D. and Walter P. (2008) SRP RNA controls a conformational switch regulating the SRP-SRP receptor interaction. *Nat Struct Mol Biol* 15(9):916-923

Neugebauer S.A., Baulig A., Kuhn A. and Facey S.J. (2012) Membrane protein insertion of variant MscL proteins occurs at YidC and SecYEG of Escherichia coli. *J Mol Biol* 417(4):375-386

Nirenberg M. and Leder P. (1964) RNA codewords and protein synthesis. The effect of Trinucleotides upon the binding of sRNA to ribosomes. *Science* 145(3639):1399-1407

Noeske J., Wasserman M.R., Terry D.S., Altman R.B., Blanchard S.C. and Cate J.H. (2015) High-resolution structure of the Escherichia coli ribosome. *Nat Struct Mol Biol* 22(4):336-341

Noriega T.R., Chen J., Walter P. and Puglisi J.D. (2014-2) Real-time observation of signal recognition particle binding to actively translating ribosomes. *Elife* 3. doi: 10.7554/eLife.04418

Noriega T.R., Tsai A., Elvekrog M.M., Petrov A., Neher S.B., Chen J., Bradshaw N., Puglisi J.D. and Walter P. (2014-1) Signal recognition particle-ribosome binding is sensitive to nascent chain length. *J Biol Chem* 289(28):19294-19305

Nouwen N. and Driessen A.J. (2002) SecDFyajC forms a heterotetrameric complex with YidC. *Mol Microbiol* 44(5):1397-1405

O'Brien T.W. (2003) Properties of human mitochondrial ribosomes. *IUBMB Life* 55(9):505-513

Oh E., Becker A.H., Sandikci A., Huber D., Chaba R., Gloge F., Nichols R.J., Typas A., Gross C.A., Kramer G., Weissman J.S. and Bukau B. (2011) Selective ribosome profiling reveals the cotranslational chaperone action of trigger factor in vivo. *Cell* 147(6):1295-1308

Oliver D., Norman J. and Sarker S. (1998) Regulation of Escherichia coli secA by cellular protein secretion proficiency requires an intact gene X signal sequence and an active translocon. *J Bacteriol* 180(19):5240-5242

Oliver D.C. and Paetzel M. (2007) Crystal structure of the major periplasmic domain of the bacterial membrane protein assembly facilitator YidC. *J Biol Chem* 283(8):5208-5216

Ott M. and Herrmann J.M. (2010) Co-translational membrane insertion of mitochondrially encoded proteins. *Biochim Biophys Acta* 1803(6):767-775

Ott M., Prestele M., Bauerschmitt H., Funes S., Bonnefoy N. and Herrmann J.M. (2006) Mba1, a membrane-associated ribosome receptor in mitochondria. *EMBO J* 25(8):1603-1610

Palmer S.R., Crowley P.J., Oli M.W., Ruelf M.A., Michalek S.M. and Brady L.J. (2012) YidC1 and YidC2 are functionally distinct proteins involved in protein secretion, biofilm formation and cariogenicity of Streptococcus mutans. *Microbiology* 158(Pt 7):1702-1712

Palmer T. and Berks B.C. (2012) The twin-arginine translocation (Tat) protein export pathway. *Nat Rev Microbiol* 10(7):483-496

Parlitz R., Eitan A., Stjepanovic G., Bahari L., Bange G., Bibi E. and Sinning I. (2007) Escherichia coli signal recognition particle receptor FtsY contains an essential and autonomous membrane-binding amphipathic helix. *J Biol Chem* 282(44):32176-32184

Peluso P., Herschlag D., Nock S., Freymann D.M., Johnson A.E. and Walter P. (2000) Role of 4.5S RNA in assembly of the bacterial signal recognition particle with its receptor. *Science* 288(5471):1640-1643

Peluso P., Shan S.O., Nock S., Herschlag D. and Walter P. (2001) Role of SRP RNA in the GTPase cycles of Ffh and FtsY. *Biochemistry* 40(50):15224-15233

Penczek, P.A., Frank, J., and Spahn, C.M. (2006) A method of focused classification, based on the bootstrap 3D variance analysis, and its application to EFG-dependent translocation. *J Struct Biol* 154: 184–194

Pérez-Rodríguez R., Fisher A.C., Perlmutter J.D., Hicks M.G., Chanal A., Santini C.L., Wu L.F., Palmer T. and DeLisa M.P. (2007) An essential role for the DnaK molecular chaperone in stabilizing over-expressed substrate proteins of the bacterial twin-arginine translocation pathway. *J Mol Biol* 367(3):715-730

Pestka S. (1968) Studies on the formation of transfer ribonucleic acid-ribosome complexes -3- The formation of peptide bonds by ribosomes in the absence of supernatant enzymes. *J Biol Chem* 243(10):2810-2820

Peterson J.H., Woolhead C.A. and Bernstein H.D. (2003) Basic amino acids in a distinct subset of signal peptides promote interaction with the signal recognition particle. *J Biol Chem* 278(46):46155-46162

Phillips G.J. and Silhavy T.J. (1992) The E. coli ffh gene is necessary for viability and efficient protein export. *Nature* 359(6397):744-746

Picking W.D., Picking W.L., Odom O.W. and Hardesty B. (1992) Fluorescence characterization of the environment encountered by nascent polyalanine and polyserine as they exit Escherichia coli ribosomes during translation. *Biochemistry* 31(8):2368-2375

Pine M.J. (1969) Kinetics of maturation of the amino termini of the cell proteins of Escherichia coli. *Biochim Biophys Acta* 174(1):359-372

Poetsch A. and Wolters D. (2008) Bacterial membrane proteomics. *Proteomics* 8(19):4100-4122

Pohlschröder M., Dilks K., Hand N.J. and Wesley Rose R. (2004) Translocation of proteins across archaeal cytoplasmic membranes. *FEMS Microbiol Rev* 28(1):3-24

Pohlschröder M., Hartmann E., Hand N.J., Dilks K. and Haddad A. (2005) Diversity and evolution of protein translocation. *Annu Rev Microbiol* 59:91-111

Pool M.R., Stumm J., Fulga T.A., Sinning I. and Dobberstein B. (2002) Distinct modes of signal recognition particle interaction with the ribosome. *Science* 297(5585):1345-1348

Poritz M.A., Bernstein H.D., Strub K., Zopf D., Wilhelm H. and Walter P. (1990) An E. coli ribonucleoprotein containing 4.5S RNA resembles mammalian signal recognition particle. *Science* 250(4984):1111-1117

Poritz M.A., Strub K. and Walter P. (1988) Human SRP RNA and E. coli 4.5S RNA contain a highly homologous structural domain. *Cell* 55(1):4-6

Powers E.T., Morimoto R.I., Dillin A., Kelly J.W. and Balch W.E. (2009) Biological and chemical approaches to diseases of proteostasis deficiency. *Annu Rev Biochem* 78:959-991

Powers T. and Walter P. (1997) Co-translational protein targeting catalyzed by the Escherichia coli signal recognition particle and its receptor. *EMBO J* 16(16):4880-4886

Preissler S. and Deuerling E. (2012) Ribosome-associated chaperones as key players in proteostasis. *Trends Biochem Sci* 37(7):274-283

Preuss M., Leonhard K., Hell K., Stuart R.A., Neupert W. and Herrmann J.M. (2001) Mba1, a novel component of the mitochondrial protein export machinery of the yeast Saccharomyces cerevisiae. *J Cell Biol* 153(5):1085-1096

Preuss M., Ott M., Funes S., Luirink J. and Herrmann J.M. (2005) Evolution of mitochondrial oxa proteins from bacterial YidC. Inherited and acquired functions of a conserved protein insertion machinery. *J Biol Chem* 280(13):13004-13011

Price C.E. and Driessen A.J. (2010) Conserved negative charges in the transmembrane segments of subunit K of the NADH:ubiquinone oxidoreductase determine its dependence on YidC for membrane insertion. *J Biol Chem* 285(6):3575-3581

Qi H.Y., Hyndman J.B. and Bernstein H.D. (2002) DnaK promotes the selective export of outer membrane protein precursors in SecA-deficient Escherichia coli. *J Biol Chem* 277(52):51077-51083

Ramakrishnan V. (2002) Ribosome structure and the mechanism of translation. *Cell* 108(4):557-572

Ravaud S., Stjepanovic G., Wild K. and Sinning I. (2008) The crystal structure of the periplasmic domain of the Escherichia coli membrane protein insertase YidC contains a substrate binding cleft. *J Biol Chem* 283(14):9350-9358

Rheinberger H.J. and Nierhaus K.H. (1983) Testing an alternative model for the ribosomal peptide elongation cycle. *Proc Natl Acad Sci USA* 80(14):4213-4217

Ribes V., Römisch K., Giner A., Dobberstein B. and Tollervey D. (1990) E. coli 4.5S RNA is part of a ribonucleoprotein particle that has properties related to signal recognition particle. *Cell* 63(3):591-600

Robinson P.J. and Woolhead C.A. (2013) Post-translational membrane insertion of an endogenous YidC substrate. *Biochim Biophys Acta* 1833(12):2781-2788

Rosendal K.R., Wild K., Montoya G. and Sinning I. (2003) Crystal structure of the complete core of archaeal signal recognition particle and implications for interdomain communication. *Proc Natl Acad Sci USA* 100(25):14701-14706

Rothenbücher M.C., Facey S.J., Kiefer D., Kossmann M. and Kuhn A. (2006) The cytoplasmic C-terminal domain of the Escherichia coli KdpD protein functions as a K+ sensor. *J Bacteriol* 188(5):1950-1958

Rubio A., Jiang X. and Pogliano K. (2005) Localization of translocation complex components in Bacillus subtilis: enrichment of the signal recognition particle receptor at early sporulation septa. *J Bacteriol* 187(14):5000-5002

Rutkowska A., Mayer M.P., Hoffmann A., Merz F., Zachmann-Brand B., Schaffitzel C., Ban N., Deuerling E. and Bukau B. (2008) Dynamics of trigger factor interaction with translating ribosomes. *J Biol Chem* 283(7):4124-4132

Sääf A., Monné M., de Gier J.W. and von Heijne G. (1998) Membrane topology of the 60-kDa Oxa1p homologue from Escherichia coli. *J Biol Chem* 273(46):30415-30418

Sachelaru I., Petriman N.A., Kudva R., Kuhn P., Welte T., Knapp B., Drepper F., Warscheid B. and Koch H.G. (2013) YidC occupies the lateral gate of the SecYEG translocon and is sequentially displaced by a nascent membrane protein. *J Biol Chem* 288(23):16295-16307

Saller M.J., Fusetti F. and Driessen A.J. (2009) Bacillus subtilis SpoIIIJ and YqjG function in membrane protein biogenesis. *J Bacteriol* 191(21):6749-6757

Saller M.J., Wu Z.C., de Keyzer J. and Driessen A.J. (2012) The YidC/Oxa1/Alb3 protein family: common principles and distinct features. *Biol Chem* 393(11):1279-1290

Samuelson J.C., Chen M., Jiang F., Möller I., Wiedmann M., Kuhn A., Phillips G.J. and Dalbey R.E. (2000) YidC mediates membrane protein insertion in bacteria. *Nature* 406(6796):637-641

Samuelson J.C., Jiang F., Yi L., Chen M., de Gier J.W., Kuhn A. and Dalbey R.E. (2001) Function of YidC for the insertion of M13 procoat protein in Escherichia coli: translocation of mutants that show differences in their membrane potential dependence and Sec requirement. *J Biol Chem* 276(37):34847-34852

Samuelsson T. and Zwieb C. (1999) The Signal Recognition Particle Database (SRPDB). *Nucleic Acids Res* 27(1):169-170

Sandikci A., Gloge F., Martinez M., Mayer M.P., Wade R., Bukau B. and Kramer G. (2013) Dynamic enzyme docking to the ribosome coordinates N-terminal processing with polypeptide folding. *Nat Struct Mol Biol* 20(7):843-850

Sanger, F., Nicklen S., et al. (1977). DNA sequencing with chain-terminating inhibitors. *Proc Natl Acad Sci USA* 74(12): 5463-5467

Saracco S.A. and Fox T.D. (2002) Cox18p is required for export of the mitochondrially encoded Saccharomyces cerevisiae Cox2p C-tail and interacts with Pnt1p and Mss2p in the inner membrane. *Mol Biol Cell* 13(4):1122-1131

Saraogi I., Zhang D., Chandrasekaran S. and Shan S.O. (2011) Site-specific fluorescent labeling of nascent proteins on the translating ribosome*. J Am Chem Soc* 133(38):14936-14939

Sargent F. (2007) Constructing the wonders of the bacterial world: biosynthesis of complex enzymes. *Microbiology* 153(Pt 3):633-651

Schaffitzel C., Oswald M., Berger I., Ishikawa T., Abrahams J.P., Koerten H.K., Koning R.I. and Ban N. (2006) Structure of the E. coli signal recognition particle bound to a translating ribosome*. Nature* 444(7118):503-506

Schlesner H., Rensmann C., Tindall B.J., Gade D., Rabus R., Pfeiffer S. and Hirsch P. (2004) Taxonomic heterogeneity within the Planctomycetales as derived by DNA-DNA hybridization, description of Rhodopirellula baltica gen. nov., sp. nov., transfer of Pirellula marina to the genus Blastopirellula gen. nov. as Blastopirellula marina comb. nov. and emended description of the genus Pirellula. *Int J Syst Evol Microbiol* 54(Pt 5):1567-1580

Schneider, C. A., Rasband W. S., et al. (2012). NIH Image to ImageJ: 25 years of image analysis. *Nat Methods* 9(7): 671-675

Schuenemann D., Gupta S., Persello-Cartieaux F., Klimyuk V.I., Jones J.D., Nussaume L. and Hoffman N.E. (1998) A novel signal recognition particle targets light-harvesting proteins to the thylakoid membranes. *Proc Natl Acad Sci USA* 95(17):10312-10316

Schulze R.J., Komar J., Botte M., Allen W.J., Whitehouse S., Gold V.A., Lycklama A Nijeholt J.A., Huard K., Berger I., Schaffitzel C. and Collinson I. (2014) Membrane protein insertion and proton-motive-force-dependent secretion through the bacterial holo-translocon SecYEG-SecDF-YajC-YidC. *Proc Natl Acad Sci USA* 111(13):4844-4849

Schuwirth, B.S., Borovinskaya, M.A., Hau, C.W., Zhang, W., Vila-Sanjurjo, A., Holton, J.M., and Cate, J.H. (2005) Structures of the bacterial ribosome at 3.5 A resolution. *Science* 310: 827-834

Scopes R.K. (1974) Measurement of protein by spectrophotometry at 205 nm. *Anal Biochem* 59(1):277-282

Scotti P.A., Urbanus M.L., Brunner J., de Gier J.W., von Heijne G., van der Does C., Driessen A.J., Oudega B. and Luirink J. (2000) YidC, the Escherichia coli homologue of mitochondrial Oxa1p, is a component of the Sec translocase. *EMBO J* 19(4):542-549

Seidelt B., Innis C.A., Wilson D.N., Gartmann M., Armache J.P., Villa E., Trabuco L.G., Becker T., Mielke T., Schulten K., Steitz T.A. and Beckmann R. (2009) Structural insight into nascent polypeptide chain-mediated translational stalling. *Science* 326(5958):1412-1415

Seitl, I. (2010) Charakterisierung der Ribosomenbindedomäne von Membraninsertasen mariner Bakterien. *Institute of Microbiology, University of Hohenheim*: Diploma Thesis

Seitl I., Wickles S., Beckmann R., Kuhn A. and Kiefer D. (2014) The C-terminal regions of YidC from Rhodopirellula baltica and Oceanicaulis alexandrii bind to ribosomes and partially substitute for SRP receptor function in Escherichia coli. *Mol Microbiol* 91(2):408-421

Serek J., Bauer-Manz G., Struhalla G., van den Berg L., Kiefer D., Dalbey R. and Kuhn A. (2004) Escherichia coli YidC is a membrane insertase for Sec-independent proteins. *EMBO J* 23(2):294-301

Serres M.H., Kerr A.R., McCormack T.J. and Riley M. (2009) Evolution by leaps: gene duplication in bacteria. *Biol Direct* 4:46

Shan S.O. and Walter P. (2003) Induced nucleotide specificity in a GTPase. *Proc Natl Acad Sci USA* 100(8):4480-4485

Shan S.O., Stroud R.M. and Walter P. (2004) Mechanism of association and reciprocal activation of two GTPases. *PLoS Biol* 2(10):e320

Sharma M.R., Koc E.C., Datta P.P., Booth T.M., Spremulli L.L. and Agrawal R.K. (2003) Structure of the mammalian mitochondrial ribosome reveals an expanded functional role for its component proteins. *Cell* 115(1):97-108

Shen K., Arslan S., Akopian D., Ha T. and Shan S.O. (2012) Activated GTPase movement on an RNA scaffold drives co-translational protein targeting. *Nature* 492(7428):271-275

Shepotinovskaya I.V. and Freymann D.M. (2002) Conformational change of the N-domain on formation of the complex between the GTPase domains of Thermus aquaticus Ffh and FtsY. *Biochim Biophys Acta* 1597(1):107-114

Siller E., DeZwaan D.C., Anderson J.F., Freeman B.C. and Barral J.M. (2010) Slowing bacterial translation speed enhances eukaryotic protein folding efficiency. *J Mol Biol* 396(5):1310-1318

Singh R., Kraft C., Jaiswal R., Sejwal K., Kasaragod V.B., Kuper J., Bürger J., Mielke T., Luirink J. and Bhushan S. (2014) Cryo-electron microscopic structure of SecA protein bound to the 70S ribosome. *J Biol Chem* 289(10):7190-7199

Siu F.Y., Spanggord R.J. and Doudna J.A. (2007) SRP RNA provides the physiologically essential GTPase activation function in cotranslational protein targeting. *RNA* 13(2):240-250

Smits P., Smeitink J.A., van den Heuvel L.P., Huynen M.A. and Ettema T.J. (2007) Reconstructing the evolution of the mitochondrial ribosomal proteome. *Nucleic Acids Res* 35(14):4686-4703

Solbiati J., Chapman-Smith A., Miller J.L., Miller C.G. and Cronan J.E. Jr. (1999) Processing of the N termini of nascent polypeptide chains requires deformylation prior to methionine removal. *J Mol Biol* 290(3):607-614

Soman R., Yuan J., Kuhn A. and Dalbey R.E. (2014) Polarity and charge of the periplasmic loop determine the YidC and sec translocase requirement for the M13 procoat lep protein. *J Biol Chem* 289(2):1023-1032

Souza R.L., Green-Willms N.S., Fox T.D., Tzagoloff A. and Nobrega F.G. (2000) Cloning and characterization of COX18, a Saccharomyces cerevisiae PET gene required for the assembly of cytochrome oxidase. *J Biol Chem* 275(20):14898-14902

Sreerama, N. and Woody, R.W. (2000). Estimation of protein secondary structure from circular dichroism spectra: comparison of CONTIN, SELCON, and CDSSTR methods with an expanded reference set. *Anal Biochem* 287(2):252-60

Strömpl C., Hold G.L., Lünsdorf H., Graham J., Gallacher S., Abraham W.R., Moore E.R. and Timmis K.N. (2003) Oceanicaulis alexandrii gen. nov., sp. nov., a novel stalked bacterium isolated from a culture of the dinoflagellate Alexandrium tamarense (Lebour) Balech. *Int J Syst Evol Microbiol* 53(Pt 6):1901-1906

Studholme D.J., Fuerst J.A. and Bateman A. (2004) Novel protein domains and motifs in the marine planctomycete Rhodopirellula baltica. *FEMS Microbiol Lett* 236(2):333-340

Sundberg E., Slagter J.G., Fridborg I., Cleary S.P., Robinson C. and Coupland G. (1997) ALBINO3, an Arabidopsis nuclear gene essential for chloroplast differentiation, encodes a chloroplast protein that shows homology to proteins present in bacterial membranes and yeast mitochondria. *Plant Cell* 9(5):717-730

Szyrach G., Ott M., Bonnefoy N., Neupert W. and Herrmann J.M. (2003) Ribosome binding to the Oxa1 complex facilitates co-translational protein insertion in mitochondria. *EMBO J* 22(24):6448-6457

Teter S.A., Houry W.A., Ang D., Tradler T., Rockabrand D., Fischer G., Blum P., Georgopoulos C. and Hartl F.U. (1999) Polypeptide flux through bacterial Hsp70: DnaK cooperates with trigger factor in chaperoning nascent chains. *Cell* 97(6):755-765

Tjalsma H., Bron S. and van Dijl J.M. (2003) Complementary impact of paralogous Oxa1-like proteins of Bacillus subtilis on post-translocational stages in protein secretion. *J Biol Chem* 278(18):15622-15632

Ulbrandt N.D., Newitt J.A. and Bernstein H.D. (1997) The E. coli signal recognition particle is required for the insertion of a subset of inner membrane proteins. *Cell* 88(2):187-196

Ullers R.S., Houben E.N., Raine A., ten Hagen-Jongman C.M., Ehrenberg M., Brunner J., Oudega B., Harms N. and Luirink J. (2003) Interplay of signal recognition particle and trigger factor at L23 near the nascent chain exit site on the Escherichia coli ribosome. *J Cell Biol* 161(4):679-684

UniProt Consortium. (2015) UniProt: a hub for protein information. *Nucleic Acids Res*. 43(Database issue):D204-212

Urbanus M.L., Fröderberg L., Drew D., Björk P., de Gier J.W., Brunner J., Oudega B. and Luirink J. (2002) Targeting, insertion, and localization of Escherichia coli YidC. *J Biol Chem* 277(15):12718-12723

Urbanus M.L., Scotti P.A., Froderberg L., Saaf A., de Gier J.W., Brunner J., Samuelson J.C., Dalbey R.E., Oudega B. and Luirink J. (2001) Sec-dependent membrane protein insertion: sequential interaction of nascent FtsQ with SecY and YidC. *EMBO Rep* 2(6):524-529

Valent Q.A., de Gier J.W., von Heijne G., Kendall D.A., ten Hagen-Jongman C.M., Oudega B. and Luirink J. (1997) Nascent membrane and presecretory proteins synthesized in Escherichia coli associate with signal recognition particle and trigger factor. *Mol Microbiol* 25(1):53-64

Valent Q.A., Scotti P.A., High S., de Gier J.W., von Heijne G., Lentzen G., Wintermeyer W., Oudega B. and Luirink J. (1998) The Escherichia coli SRP and SecB targeting pathways converge at the translocon. *EMBO J* 17(9):2504-2512

van Bloois E., Haan G.J., de Gier J.W., Oudega B. and Luirink J. (2006) Distinct requirements for translocation of the N-tail and C-tail of the Escherichia coli inner membrane protein CyoA. *J Biol Chem* 281(15):10002-10009

van Bloois E., Jan Haan G., de Gier J.W., Oudega B. and Luirink J. (2004) F(1)F(0) ATP synthase subunit c is targeted by the SRP to YidC in the E. coli inner membrane. *FEBS Lett* 576(1-2):97-100

van Bloois E., Koningstein G., Bauerschmitt H., Herrmann J.M. and Luirink J. (2007) Saccharomyces cerevisiae Cox18 complements the essential Sec-independent function of Escherichia coli YidC. *FEBS J* 274(21):5704-5713

Van den Berg B., Clemons W.M. Jr, Collinson I., Modis Y., Hartmann E., Harrison S.C. and Rapoport T.A. (2004) X-ray structure of a protein-conducting channel. *Nature* 427(6969):36-44

van der Laan M., Bechtluft P., Kol S., Nouwen N. and Driessen A.J. (2004) F1F0 ATP synthase subunit c is a substrate of the novel YidC pathway for membrane protein biogenesis. *J Cell Biol* 165(2):213-222

van der Laan M., Houben E.N., Nouwen N., Luirink J. and Driessen A.J. (2001) Reconstitution of Sec-dependent membrane protein insertion: nascent FtsQ interacts with YidC in a SecYEG-dependent manner. *EMBO Rep* 2(6):519-523

van der Laan M., Urbanus M.L., Ten Hagen-Jongman C.M., Nouwen N., Oudega B., Harms N., Driessen A.J. and Luirink J. (2003) A conserved function of YidC in the biogenesis of respiratory chain complexes. *Proc Natl Acad Sci USA* 100(10):5801-5806

von Heijne G. (1985) Signal sequences. The limits of variation. *J Mol Biol* 184(1):99-105

von Heijne G. (1989) Control of topology and mode of assembly of a polytopic membrane protein by positively charged residues. *Nature* 341(6241):456-458

von Loeffelholz O., Jiang Q., Ariosa A., Karuppasamy M., Huard K., Berger I., Shan S.O. and Schaffitzel C. (2015) Ribosome-SRP-FtsY cotranslational targeting complex in the closed state. *Proc Natl Acad Sci USA* 112(13):3943-3948

von Loeffelholz O., Knoops K., Ariosa A., Zhang X., Karuppasamy M., Huard K., Schoehn G., Berger I., Shan S.O. and Schaffitzel C. (2013) Structural basis of signal sequence surveillance and selection by the SRP-FtsY complex. *Nat Struct Mol Biol* 20(5):604-610

Voss N.R., Gerstein M., Steitz T.A. and Moore P.B. (2006) The geometry of the ribosomal polypeptide exit tunnel. *J Mol Biol* 360(4):893-906

Wagner S., Pop O.I., Haan G.J., Baars L., Koningstein G., Klepsch M.M., Genevaux P., Luirink J. and de Gier J.W. (2008) Biogenesis of MalF and the MalFGK(2) maltose transport complex in Escherichia coli requires YidC. *J Biol Chem* 283(26):17881-17890

Walter P and Blobel G. (1982) Signal recognition particle contains a 7S RNA essential for protein translocation across the endoplasmic reticulum. *Nature* 299(5885):691-698

Walter P. and Johnson A.E. (1994) Signal sequence recognition and protein targeting to the endoplasmic reticulum membrane*. Annu Rev Cell Biol* 10:87-119

Weiche B., Bürk J., Angelini S., Schiltz E., Thumfart J.O. and Koch H.G. (2008) A cleavable N-terminal membrane anchor is involved in membrane binding of the Escherichia coli SRP receptor. *J Mol Biol* 377(3):761-773

Welte T., Kudva R., Kuhn P., Sturm L., Braig D., Müller M., Warscheid B., Drepper F. and Koch H.G. (2012) Promiscuous targeting of polytopic membrane proteins to SecYEG or YidC by the Escherichia coli signal recognition particle. *Mol Biol Cell* 23(3):464-479

Whitmore, L. and Wallace, B.A. (2004). DICHROWEB, an online server for protein secondary structure analyses from circular dichroism spectroscopic data. *Nucleic Acids Res* 32(Web Server issue): W668–W673

Whitmore, L. and Wallace, B.A. (2008). Protein secondary structure analyses from circular dichroism spectroscopy: methods and reference databases. *Biopolymers* 89(5): 392–400

Wickles S., Singharoy A., Andreani J., Seemayer S., Bischoff L., Berninghausen O., Soeding J., Schulten K., van der Sluis E.O. and Beckmann R. (2014) A structural model of the active ribosome-bound membrane protein insertase YidC. *Elife* 3:e03035

Wild J., Altman E., Yura T. and Gross C.A. (1992) DnaK and DnaJ heat shock proteins participate in protein export in Escherichia coli. *Genes Dev* 6(7):1165-1172

Wild K., Halic M., Sinning I. and Beckmann R. (2004) SRP meets the ribosome. *Nat Struct Mol Biol* 11(11):1049-1053

Wood H., Luirink J. and Tollervey D. (1992) Evolutionary conserved nucleotides within the E.coli 4.5S RNA are required for association with P48 in vitro and for optimal function in vivo. *Nucleic Acids Res* 20(22):5919-5925

Wright P.E. and Dyson H.J. (2009) Linking folding and binding. *Curr Opin Struct Biol* 19(1):31-38

Wu Z.C., de Keyzer J., Berrelkamp-Lahpor G.A. and Driessen A.J. (2013) Interaction of Streptococcus mutans YidC1 and YidC2 with translating and nontranslating ribosomes. *J Bacteriol* 195(19):4545-4551

Xie K., Kiefer D., Nagler G., Dalbey R.E. and Kuhn A. (2006) Different regions of the nonconserved large periplasmic domain of Escherichia coli YidC are involved in the SecF interaction and membrane insertase activity. *Biochemistry* 45(44):13401-13408

Yang M.J. and Zhang X. (2011) Molecular dynamics simulations reveal structural coordination of Ffh-FtsY heterodimer toward GTPase activation. *Proteins* 79(6):1774-1785

Yen M.R., Harley K.T., Tseng Y.H. and Saier M.H. Jr. (2001) Phylogenetic and structural analyses of the oxa1 family of protein translocases. *FEMS Microbiol Lett* 204(2):223-231

Yi L., Celebi N., Chen M. and Dalbey R.E. (2004) Sec/SRP requirements and energetics of membrane insertion of subunits a, b, and c of the Escherichia coli F1F0 ATP synthase. *J Biol Chem* 279(38):39260-39267

Yi L., Jiang F., Chen M., Cain B., Bolhuis A. and Dalbey R.E. (2003) YidC is strictly required for membrane insertion of subunits a and c of the F(1)F(0)ATP synthase and SecE of the SecYEG translocase. *Biochemistry* 42(35):10537-10544

Youngman E.M., McDonald M.E. and Green R. (2008) Peptide release on the ribosome: mechanism and implications for translational control. *Annu Rev Microbiol* 62:353-373

Yu Z., Koningstein G., Pop A. and Luirink J. (2008) The conserved third transmembrane segment of YidC contacts nascent Escherichia coli inner membrane proteins. *J Biol Chem* 283(50):34635-34642

Yusupov M.M., Yusupova G.Z., Baucom A., Lieberman K., Earnest T.N., Cate J.H. and Noller H.F. (2001) Crystal structure of the ribosome at 5.5 A resolution. *Science* 292(5518):883-896

Yusupova G.Z. and Yusupov M.M. (2014) High-resolution structure of the eukaryotic 80S ribosome. *Annu Rev Biochem* 83:467-486

Zhang G. and Ignatova Z. (2010) Folding at the birth of the nascent chain: coordinating translation with co-translational folding. *Curr Opin Struct Biol* 21(1):25-31

Zhang G., Hubalewska M. and Ignatova Z. (2009) Transient ribosomal attenuation coordinates protein synthesis and co-translational folding. *Nat Struct Mol Biol* 16(3):274-280

Zhang X. and Shan S.O. (2014) Fidelity of cotranslational protein targeting by the signal recognition particle. *Annu Rev Biophys* 43:381-408

Zhang X., Lam V.Q., Mou Y., Kimura T., Chung J., Chandrasekar S., Winkler J.R., Mayo S.L. and Shan S.O. (2011) Direct visualization reveals dynamics of a transient intermediate during protein assembly. *Proc Natl Acad Sci USA* 108(16):6450-6455

Zhang X., Rashid R., Wang K. and Shan S.O. (2010) Sequential checkpoints govern substrate selection during cotranslational protein targeting. *Science* 328(5979):757-760

Zhang X., Schaffitzel C., Ban N. and Shan S.O. (2009) Multiple conformational switches in a GTPase complex control co-translational protein targeting. *Proc Natl Acad Sci USA* 106(6):1754-1759

Zhang Y.J., Tian H.F. and Wen J.F. (2009) The evolution of YidC/Oxa/Alb3 family in the three domains of life: a phylogenomic analysis. *BMC Evol Biol* 9:137

Zheng N. and Gierasch L.M. (1996) Signal sequences: the same yet different. *Cell*. 86(6):849-852

Zheng N. and Gierasch L.M. (1997) Domain interactions in E. coli SRP: stabilization of M domain by RNA is required for effective signal sequence modulation of NG domain. *Mol Cell* 1(1):79-87

Zhu L., Kaback H.R. and Dalbey R.E. (2013) YidC protein, a molecular chaperone for LacY protein folding via the SecYEG protein machinery. *J Biol Chem* 288(39):28180-28194

Zhu L., Klenner C., Kuhn A. and Dalbey R.E. (2012) Both YidC and SecYEG are required for translocation of the periplasmic loops 1 and 2 of the multispanning membrane protein TatC. *J Mol Biol* 424(5):354-367

Zhu L., Wasey A., White S.H. and Dalbey R.E. (2013) Charge composition features of model single-span membrane proteins that determine selection of YidC and SecYEG translocase pathways in Escherichia coli. *J Biol Chem* 288(11):7704-7716

Zimmer J., Nam Y. and Rapoport T.A. (2008) Structure of a complex of the ATPase SecA and the protein-translocation channel. *Nature* 455(7215):936-943

Zopf D., Bernstein H.D., Johnson A.E. and Walter P. (1990) The methionine-rich domain of the 54 kd protein subunit of the signal recognition particle contains an RNA binding site and can be crosslinked to a signal sequence. *EMBO J* 9(13):4511-4517

6 ABBREVATIONS

µM	micromolar
Å	Ångstroem
A. thaliana	*Arabidopsis thaliana*
A3CT	C-terminal domain of *A. thaliana* Alb3
aa	amino acid
aa-tRNA	aminoacyl-tRNA
AC	affinity chromatography
Alb3	Albino-3, chloroplast insertase homolog
amp	ampicillin
AMS	4-acetamido-4´-maleimidylstilbene-2,2´-disulfonic acid
ara	arabinose
A-site	acceptor-site of the ribosome
ATP	adenosine triphosphate
bp	base pairs
CD	circular dichroism
cpSRP	chloroplast signal recognition particle
cryo-EM	cryo-electron microscopy
CTD	C-terminal domain
C-terminal	carboxyl-terminal
cV	column volume
Da	dalton
DDM	n-dodecyl-β-d-maltoside
DMSO	dimethylsulfoxide
DNA	deoxyribonucleic acid
DTT	dithiothreitol
DUF	archaeal insertase homolog
E. coli	*Escherichia coli*
EcYidC	*E. coli* YidC
EDTA	ethylenediaminotetraacetic acid
EF	elongation factor
ER	endoplasmic reticulum

E-site	exit-site of the ribosome
et al.,	*et alii*; and others
EtOH	ethanol
Ffh	fifty-four-homolog, SRP54-homolog
FSC	fourier shell correlation
FtsY	filamentous temperature sensitive Y, prokaryotic SRP-receptor
g	acceleration of gravity (9,81 m/s^2)
GFP	green fluorescent protein
glc	glucose
GTP	guanosine triphosphate
h	hour
H_2O_{dd}	double-deionized water
HCl	hydrochloric acid
HEPES	4-(2-hydroxyethyl)-1-piperazineethanesulfonic acid
His-tag	histidine-tag
IEC	ion exchange chromatography
IF	initiation factor
IMAC	immobilized metal ion affinity chromatography
IMV	inner membrane vesicle
Inc.	incorporated
IPTG	isopropyl-β-D-thiogalactoside
kDa	kilodalton
LB	Luria-Bertani
LDAO	lauryldimethylamine oxide
min	minute
mM	millimolar
mRNA	messenger ribonucleic acid
MscL	mechanosensitive channel of large conductance
MST	microscale thermophoresis
MW	molecular weight
MWCO	molecular weight cut-off
NaCl	natriumchloride
Ni^{2+}	nickel

nm	nanometer
nM	nanomolar
N-terminal	amino-terminal
O. alexandrii	*Oceanicaulis alexandrii*
O1CT	C-terminal domain of *S. cerevisiae* Oxa1
OaCT	C-terminal domain of *O. alexandrii* YidC
Oa-YidC	YidC homolog of *O. alexandrii*
OD	optical density
Oxa1	oxidase assembly protein 1, mitochondrial insertase homolog
PAGE	polyacrylamide gel electrophoresis
PBS	phosphate buffered saline
PCR	polymerase chain reaction
pH	potential hydrogen
PMF	proton motive force
PMSF	phenylmethylsulfonyl fluoride
P-site	peptidyl-site of the ribosome
PTC	peptidyl transferase center
R. baltica	*Rhodopirellula baltica*
RbCl	rubidium chloride
RbCT	C-terminal domain of *R. baltica* YidC
Rb-YidC	YidC homolog of *R. baltica*
RNA	ribonucleic acid
RNC	ribosome nascent chain
rpm	revolutions per minute
RRF	ribosome recycling factor
rRNA	ribosomal ribonucleic acid
RT	room temperature
S	sedimentation coefficient (Svedberg)
S. cerevisiae	*Saccharomyces cerevisiae*
S. mutans	*Streptococcus mutans*
SDS	sodium dodecyl sulfate
Sec	secretion
SEC	size exclusion chromatography

SRP	signal recognition particle
Staph A	*Staphylococcus aureus* protein A
Strep-tag	streptavidin-tag
TAE	tris-acetate-EDTA buffer
TAT	twin arginine translocation
TCA	trichloroacetic acid
TF	trigger factor
TM	transmembrane (segment)
Tris	trishydroxymethylaminomethane
tRNA	transfer ribonucleic acid
UV	ultraviolet
wt	wild type
YidC	bacterial membrane insertase
YidC-Oa	*E. coli* YidC with the C-terminal domain of *O. alexandrii* YidC
YidC-Oxa	*E. coli* YidC with the C-terminal domain of *S. cerevisiae* Oxa1
YidC-Rb	*E. coli* YidC with the C-terminal domain of *R. baltica* YidC
α	anti, alpha

ACKNOWLEDGMENTS

First of all, I would like to thank Prof. Andreas Kuhn for the possibility to perform my PhD thesis in his laboratory and to work on fascinating and also challenging projects in an excellent research environment. Especially, I want to thank Prof. Kuhn for giving me the opportunity and the support to present my work on many national and international conferences.

Exceptionally, I want to express my deep gratitude to Dr. Dorothee Kiefer for supervising this work, thereby giving me all the freedom and support I needed to conduct my research. Thank you for all the help, proof-reading of this work, enriching discussions and for sharing the passion of C-terminal tails!

Special thanks also to the whole “Doro-Lab” for the great time and excellent teamwork. Lutz and Renate, it was a pleasure of working with you. Furthermore, I want to thank my Master students Emanuelle, Markus and Paul for their outstanding work, contributing to this thesis.

I would like to thank all past and present members of the entire Institute of Microbiology for providing such a great working atmosphere during my time in the lab. Special thanks go to Chris, Dirk and Eva for the funny times in the lab and also for critical discussions, great support and motivation throughout the past 5 years. Domenico and Sebastian, thank you for all the answered biochemical and biophysical questions, sharing protocols and critical proof-reading of my application. I also want to thank Andrea for the help in all important things beyond the scientific stuff.

Additionally, I want to thank the Beckmann group for the great collaboration with special thanks to Stephan for the excellent work in pushing the YidC:RNC complexes to a successful cryo-EM structure.

Schließlich möchte ich mich noch ganz herzlich bei meinen Eltern für die bedingungslose Unterstützung in all den Jahren bedanken, ebenso bei meiner Schwester, die einfach immer an mich glaubt! Vielen Dank Andy, dass du immer für mich da bist und die ganzen Jahre über mein Ausgleich warst.

ERKLÄRUNG

Eidesstattliche Versicherung gemäß §7 Absatz 7 der Promotionsordnung der Universität Hohenheim zum Dr. rer. nat.

Hiermit erkläre ich, dass es sich bei der eingereichten Dissertation zum Thema *Functional and structural studies of a C-terminally extended YidC* um meine eigenständig erbrachte Leistung handelt. Ich habe nur die angegebenen Quellen und Hilfsmittel verwendet. Wörtlich oder sinngemäß übernommene Inhalte sind als solche gekennzeichnet. Außerdem wurde keine kommerzielle Promotionsvermittlung oder –Beratung in Anspruch genommen.

Ich versichere an Eides Statt, dass ich nach bestem Wissen die reine Wahrheit erklärt und nichts verschwiegen habe.

_____ _____

Ort, Datum Unterschrift

CURRICULUM VITAE

Personal data

Name	Ines Seitl
Date of birth	17.06.1985
Place of birth	Esslingen a.N., Germany
Nationality	German

Education

2015 / 10 – to date	Post Doc at the University of Hohenheim, Institute of Food Science and Biotechnology, Prof. Dr. rer. nat. Lutz Fischer
2015 / 09 – 2010 / 03	PhD student at the University of Hohenheim, Institute of Microbiology, Prof. Dr. rer. nat. Andreas Kuhn
2010 / 01 – 2009 / 03	Diploma thesis “Charakterisierung der Ribosomenbindedomäne von Membraninsertasen mariner Bakterien“, University of Hohenheim, Institute of Microbiology, Prof. Dr. rer. nat. Andreas Kuhn
2010 / 03 – 2004 / 10	Studies of Biology, Dipl. Biol., University of Hohenheim
2004 / 07 – 1995 / 09	Abitur at Otto-Hahn Gymnasium Ostfildern, Nellingen

Publication

Seitl I., Wickles S., Beckmann R., Kuhn A. and Kiefer D. (2014) The C-terminal regions of YidC from Rhodopirellula baltica and Oceanicaulis alexandrii bind to ribosomes and partially substitute for SRP receptor function in Escherichia coli. *Mol Microbiol* 91(2):408-421